INFORMATION TO USERS

This manuscript has been reproduced from the microfilm master. UMI films the text directly from the original or copy submitted. Thus, some thesis and dissertation copies are in typewriter face, while others may be from any type of computer printer.

The quality of this reproduction is dependent upon the quality of the copy submitted. Broken or indistinct print, colored or poor quality illustrations and photographs, print bleedthrough, substandard margins, and improper alignment can adversely affect reproduction.

In the unlikely event that the author did not send UMI a complete manuscript and there are missing pages, these will be noted. Also, if unauthorized copyright material had to be removed, a note will indicate the deletion.

Oversize materials (e.g., maps, drawings, charts) are reproduced by sectioning the original, beginning at the upper left-hand corner and continuing from left to right in equal sections with small overlaps.

Photographs included in the original manuscript have been reproduced xerographically in this copy. Higher quality 6" x 9" black and white photographic prints are available for any photographs or illustrations appearing in this copy for an additional charge. Contact UMI directly to order.

Bell & Howell Information and Learning
300 North Zeeb Road, Ann Arbor, MI 48106-1346 USA
800-521-0600

UMI®

Application of High-pressure Spectroscopic and Powder X-ray Diffraction Techniques to Inorganic Materials

By

Clare M. Edwards

A thesis submitted to the Faculty of Graduate Studies and Research of McGill University in partial fulfillment of the requirements for the degree of Doctor of Philosophy

March 1998
Department of Chemistry
McGill University
Montréal, Québéc
Canada

0-612-44419-8

Abstract

The vibrational spectra (IR, Raman) of $(\eta^6\text{-}C_6H_5CO_2CH_3)Cr(CO)_3$, $(\eta^6\text{-}C_6H_5CO_2CH_3)Cr(CO)_2(CS)$, $[Pt(NH_3)_4][PtCl_4]$ (MGS), $[Pt(ND_3)_4][PtCl_4]$ (MGS-D), $[Pt(NH_3)_4][PtBr_4]$ (MGS-Br), $ReH_7(dppe)$ (dppe = 1,2-bis(diphenylphosphino)ethane) and $CpCo(C_{64}H_4)$ (Cp = cyclopentadiene) have been studied under pressures up to ~45 kbar. The magnitude and direction of the pressure-induced shift of the Raman-active ν(CO) and ν(CS) vibrational modes of $(\eta^6\text{-}C_6H_5CO_2CH_3)Cr(CO)_3$ and $(\eta^6\text{-}C_6H_5CO_2CH_3)Cr(CO)_2(CS)$ indicate an increase in the amount of π-backbonding to the CO and CS ligands under pressure, the increase being greater to the CO ligand than to the CS ligand. Wavenumber *vs.* pressure plots revealed a phase transition in both the tricarbonyl and thiocarbonyl complexes between 10-15 kbar. For $CpCo(C_{64}H_4)$, discontinuities in the wavenumber *vs.* pressure plots at 10 kbar indicate a phase transition at this pressure, most likely involving rotation of the Cp ring. Insertion of the Co atom into the cage does not occur under compression; a shift to higher wavenumbers was observed for all the Raman and IR vibrational modes of $CpCo(C_{64}H_4)$ and the parent fulleride, $C_{64}H_4$. Phenyl ring rotation is thought to occur in $ReH_7(dppe)$ under compression. Three pressure regions, from ambient pressure to ~16 kbar, between 16 and 29 kbar and above 29 kbar, were identified from the wavenumber *vs.* pressure plots. A broad, weak feature in the IR spectrum appears from 5 kbar, increasing in intensity with increasing pressure. This peak has been assigned to the ν(HH) mode of a coordinated dihydrogen ligand, $Re(\eta^2\text{-}H_2)$. Ring rotation may assist the pressure-induced dihydride-dihydrogen interconversion. The pressure-tuning IR study of MGS and its derivatives probed the intermolecular interactions, in particular the interactions of the NH_3 groups and investigated the hypothesis that hydrogen bonding of the type N-H···Cl exists in MGS. Splitting of the IR bands at ambient pressure, and a negative pressure shift of the bending $\delta_s(NH_3)$ mode under compression, indicates hindered motion of the NH_3 groups. Finally, powder X-ray diffraction patterns of the pseudoscheelite salt potassium chromate, K_2CrO_4, have been recorded up to 52 GPa (520 kbar). A gradual decrease in the

relative intensity of several diffraction peaks is consistent with disordering of the chromate tetrahedra under compression. Since the tetrahedra are small compared to the cavity in which they are located, pressure-induced orientational disordering can occur initially without disruption of the metal sub-lattice. Pressure-induced disordering of the BX_4-tetrahedra is the first step in the amorphization of A_2BX_4 compounds.

Résumé

Les spectres vibrationnels (IR, Raman) des complexes $(\eta^6\text{-}C_6H_5CO_2CH_3)Cr(CO)_3$, $(\eta^6\text{-}C_6H_5CO_2CH_3)Cr(CO)_2(CS)$, $[Pt(NH_3)_4][PtCl_4]$ (MGS), $[Pt(ND_3)_4][PtCl_4]$ (MGS-D), $[Pt(NH_3)_4][PtBr_4]$ (MGS-Br), $ReH_7(dppe)$ (dppe = 1,2-bis(diphénylphosphino)éthane) et $CpCo(C_{64}H_4)$ (Cp = cyclopentadiène) ont été étudiés sous pression jusqu'à ~45 kbar. L'amplitude et la direction des déplacements des modes vibrationnels actifs en Raman $\nu(CO)$ et $\nu(CS)$ des complexes $(\eta^6\text{-}C_6H_5CO_2CH_3)Cr(CO)_3$ et $(\eta^6\text{-}C_6H_5CO_2CH_3)Cr(CO)_2(CS)$ sous pression, montrent une augmentation de l'effet retour du métal aux ligands CO et CS $d_{Cr} \rightarrow \pi^*_{CO,CS}$ sous haute pression. L'augmentation est plus importante pour le ligand CO que pour le ligand CS. Les courbes de dépendance des nombres d'ondes en fonction de la pression révèlent une transition de phase à la fois dans le cas des complexes tricarbonyles et thiocarbonyles située entre 10-15 kbar. En ce qui concerne le complexe $CpCo(C_{64}H_4)$, des discontinuités, observées au niveau des courbes de dépendance des nombres d'ondes en fonction de la pression, à 10 kbar indiquent une transition de phase à cette pression. Cette transition met certainement en jeu la rotation du ligand Cp. L'insertion de l'atome de Cobalt dans la cage n'a pas eu lieu sous l'effet de la pression; tous les modes vibrationnels Raman et IR du complexe $CpCo(C_{64}H_4)$ et de son dérivé $C_{64}H_4$ ont été déplacés vers les hautes fréquences. Une rotation des ligands phényles semble avoir lieu dans le complexe $ReH_7(dppe)$ sous haute pression. Trois domaines de pression ont été délimités à partir des courbes de dépendance des nombres d'ondes en fonction de la pression; de la pression ambiante à ~16 kbar, entre 16 et 29 kbar et au-dessus de 29 kbar. Une large bande de faible intensité est visible sur les spectres IR à partir de 5 kbar. L'intensité de ce pic augmente avec la pression. Il a été attribué au mode $\nu(HH)$ d'un ligand dihydrogène, $Re(\eta^2\text{-}H_2)$. Il se peut que la rotation des groupements phényles favorise la conversion induite par la pression du ligand dihydrure en ligand dihydrogène. Les études IR sous haute pression du sel de Magnus et de ses dérivés ont mis l'accent sur les intéractions intermoléculaires, en particulier les intéractions liées au groupements NH_3, et ont permis d'approfondir l'hypothèse de l'existence de liaisons hydrogènes du type $N\text{-}H\cdots Cl$. Un dédoublement des bandes IR à pression ambiante ainsi qu'un déplacement vers les basses fréquences du mode de déformation $\delta_s(NH_3)$ sous haute pression, suggèrent une rotation encombrée des groupements NH_3. Enfin, les digrammes de diffraction X du sel de chromate de potassium, K_2CrO_4, ont été enregistrés jusqu'à 52 GPa (520 kbar). Une diminution graduelle de l'intensité relative de plusieurs pics de diffraction est significatif d'une diminution de l'ordre dans les tétrahèdres du chromate sous pression. Du fait de la petite taille des tétrahèdres par rapport à la cavité dans laquelle ils se trouvent, ils peuvent de désordonner sous l'effet de la pression sans influencer au début la sous-maille du métal. Le désordonnement des tétrahèdres du type BX_4 induit par la pression, est la première étape vers l'amorphisation de composés du type A_2BX_4.

Acknowledgments

I would first like to thank my supervisor, Professor Ian Butler, for his support, encouragement and enthusiasm throughout the course of this work.

I would also like to acknowledge:

Drs. Andrew Vreugdenhil and Ross Markwell, for their help with the spectroscopy and computers, and many helpful discussions;
Drs. Julian Haines and Jean-Michel Léger at CNRS Laboratoire de Physico-Chimie des Matériaux, Meudon, France, for giving me the opportunity to work in their laboratory. Their experience in the field of high-pressure, X-ray diffraction was fundemental to the success of the project;
Dr. Yves Rubin and Wenyuan Qian, of the University of California, Los Angeles, for providing the fulleride samples and for helpful discussions;
Mr. Michel Boulay for technical assistance with the IR and Raman spectrometers;
Ms. Renee Charon and all the other office staff for taking care of the administration, and
Pierre Lesté-Lasserre for help with translation of the abstract.

Many thanks to all those, past and present, from lab 335 and Otto Maass, who have helped to make my time at McGill and in Montreal a very memorable experience.

Note on Units

The following units have been used in this thesis for historical reasons. Their definitions and SI equivalents are given below:

Physical Quantity	Symbol	SI Unit	Unit Used
wavenumber	$\bar{\nu}$	m^{-1}	cm^{-1} (= 100 m^{-1})
pressure	p	Pa (Nm^{-2})	kbar (= 10^8 Pa)
force constant	k	Nm^{-1}	dyne cm^{-1} (= $10^3 Nm^{-1}$)
bond length,	r,	m	Å (= 10^{-10} m)
cell constants	*a*, *b*, *c*	m	Å (= 10^{-10} m)

In the text of this thesis, the unit of vibrational wavenumber is often referred to as vibrational frequency (ν). These quantities are directly proportional to one another, $\bar{\nu} = c\nu$, where c is the speed of light.

Chapters 3-6 use the pressure unit kbar. Chapter 7 uses the pressure unit GPa, the SI unit. This difference comes about from tradition, where 1 GPa ≅ 10 kbar. In the literature, the unit GPa is more often used in high-pressure X-ray studies, particularly where the pressures used exceed 100 kbar or 10 GPa. Furthermore, in France, the SI pressure unit is much more widely used than kbar.

Contributions of Authors

This thesis represents a collection of papers, which are to be submitted for publication. All the work has been completed as part of the requirements for the Ph.D. degree. The common theme is that all the papers are concerned with the use of high-pressure experiments in the diamond-anvil cell, in conjunction with infrared, Raman or powder X-ray diffraction techniques. The work has been presented in this manner since each chapter is an individual subject, requiring its own introduction and conclusions. The introductory Chapter 1, is a review article, which summarizes much of the work published in the literature over the last 15 years and provides a solid introduction to the new work presented in Chapters 3 to 7.

Co-authors

As my supervisor, I. S. Butler is a co-author for each publication.

Chapter 3: R. J. Moore was involved in the preparation of the carbonyl and thiocarbonyl complexes as part of her honours project. She was also involved in some of the initial pressure studies.

Chapter 6: Y. Rubin and W. Qian, at UCLA, were the first to prepare the $CpCo(C_{64}H_4)$ and $C_{64}H_4$ materials. They provided us with samples for the high pressure experiments.

Chapter 7. The high-pressure X-ray powder diffractin experiments were performed in collaboration with Drs. J. Haines and J. M. Léger at CNRS Meudon, France. Their experience in this field was critical in the full interpretation and discussion of the data collected.

Contents

Chapter 1. Pressure-tuning Spectroscopy of Inorganic Compounds: A Summary of the Past 15 Years

Chapter 2. Theory and Experiment

Chapter 3. **High-Pressure Vibrational Study of (η^6-arene)Cr(CO)$_2$(CX) Complexes (X=O, S); π-Backbonding to CX ligands and The Effect of Variation in the Arene Ligand.**

Chapter 4. **Pressure-Tuning FT-IR Spectroscopy of Magnus' Green Salt and its Derivatives.**

Chapter 5. Pressure-Induced Solid-State Isomerisation: The Dihydride-Dihydrogen Interconversion.

Chapter 6. Pressure-Tuning Spectroscopic Study of $(\eta^5\text{-}C_5H_5)Co(C_{64}H_4)$: Can Endohedral Fullerenes Be Formed Under Pressure?

Chapter 7. High-Pressure X-ray Diffraction Study of Potassium Chromate: Pressure-induced Orientational Disorder and its Implications for Amorphization in A_2BX_4 Compounds.

Chapter 8. Conclusions

Chapter 1

Pressure-tuning Spectroscopy of Inorganic Compounds: A Summary of the Past 15 Years[1]

1.1 Introduction

Compared to temperature, pressure is a much less explored physical variable. The diamond-anvil cell (DAC) is probably the most widely known high-pressure device for scientific studies. Although the DAC offers only a tiny sample volume, the simplicity of its design, the range of attainable pressures, and the wide variety of experiments possible make the DAC very attractive for the study of all kinds of materials under compression. After nearly forty years since its development by Alvin Van Valkenburg and Charles Weir, then at the National Bureau of Standards in Washington D.C. [1], the DAC has found its way into many areas of research and scientific analysis ranging from Physics and Chemistry to Geology, Biochemistry and Forensic Science. Diamond-anvil cells, capable of achieving pressures of the order of 500 kbar to 1 Mbar, have allowed geologists to determine the high-pressure structures of minerals and to relate geophysical phenomena to pressure-induced phase transitions in minerals [2]. In Materials Science, the use of more modest pressures, up to 200 kbar, has afforded insight into structure-property relationships of solids, for example, of magnetic materials, and in the pressure-tuning of the band-gaps in semiconductor materials [3]. More recently, high hydrostatic pressures produced in DACs have led to the synthesis of new compounds. e.g., the solid state polymerization of acetylene at ~142 kbar, and the synthesis of sp^2-bonded carbon nitrides [4].

Compression of a material results in a decrease in sample volume, a decrease in inter- and intramolecular and atomic distances and so an increase in orbital overlap. The perturbation of the orbitals will depend on the type of orbital involved. Pressure-

---

[1] C. M. Edwards and I. S. Butler, Coord. Chem. Rev., in preparation.

tuning studies of the vibrational and electronic levels of a material permit an examination of its optical, electrical, magnetic and chemical properties.

In 1984, Ferraro published his classic book entitled "Vibrational Spectroscopy at High External Pressures: The Diamond-anvil Cell" [5], in which he describes the effect of high, external pressures on a wide variety of inorganic, coordination, and organic and biological compounds. Since then, a number of concise reviews have appeared, notably by Drickamer [6], who has focused his attention on pressure-tuning electronic spectroscopy. The construction and techniques associated with high-pressure devices have also been reviewed, e.g., see refs. [7] and [8].

The present review is directed towards a summary of pressure-tuning IR, Raman and electronic spectroscopic studies of selected coordination and organometallic compounds, which have afforded some particularly interesting results. The review is by no means exhaustive, but offers an overview of the work done in this area over the past 15 years and the type of results that can be obtained. Many coordination compounds have been studied by high-pressure X-ray diffraction techniques as well, but these results are not included here.

1.2 The Diamond-anvil Cell

The opposed-anvil, lever arm design consists of two polished diamonds with flat faces, between which the sample is placed in a gasket. Pressure is applied by simply turning a screw which forces the diamond anvils together. There are several commercially available DACs. One of the most commonly used is that built by High Pressure Diamond Optics, Tucson, Arizona. The P-II type DAC is suitable for pressure-tuning Raman and FT-IR measurements up to ~70 kbar. Figure 1.1 shows a schematic of the design of the cell. The diamond anvils are mounted on hardened steel and held in alignment in a cylinder as pressure is applied. The Super pressure cell can achieve much higher pressures, up to 700 kbar; its design is based on a piston-cylinder arrangement, with the diamond-anvils on tungsten carbide mounts.

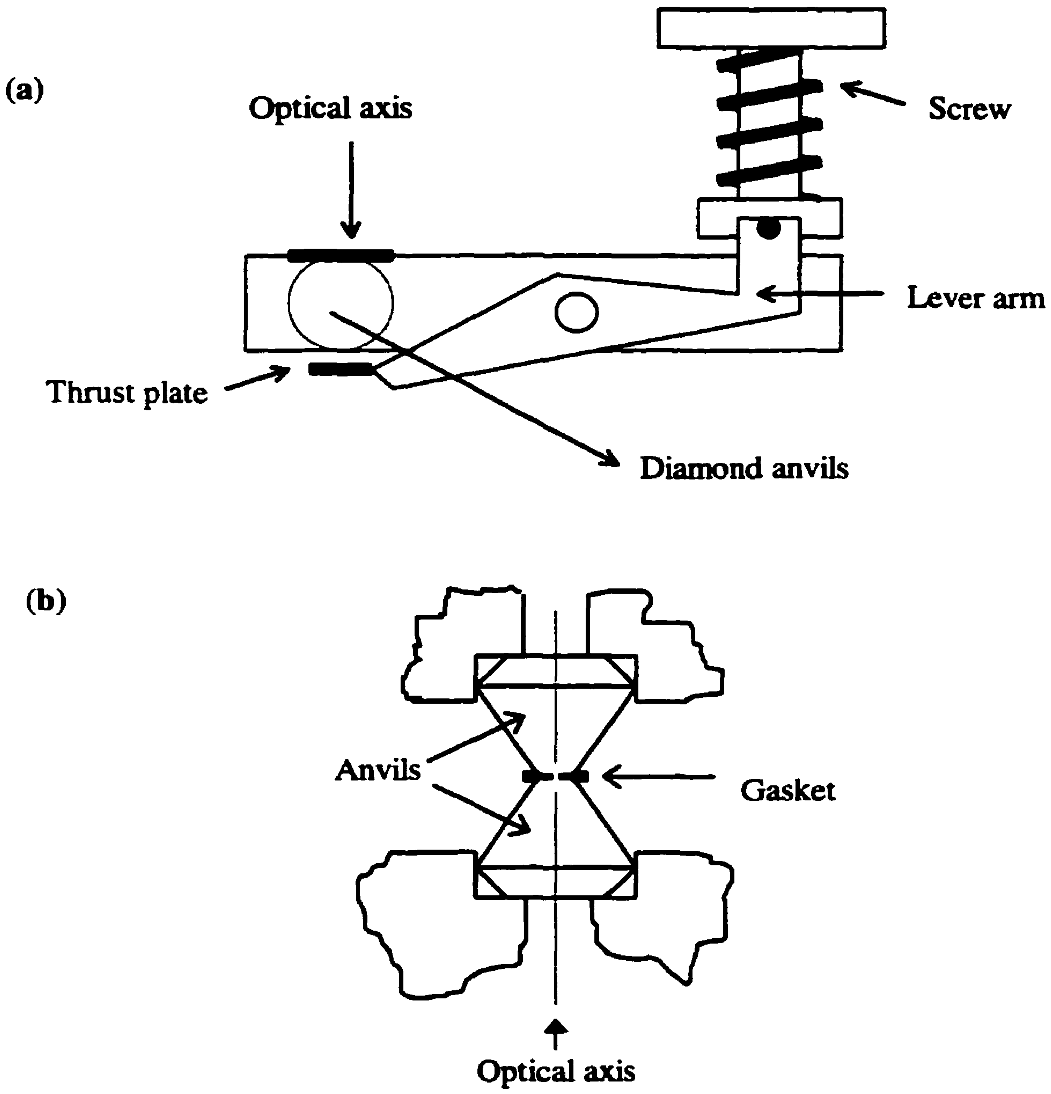

Figure 1.1. Schematic of the diamond-anvil cell from High Pressure Diamond Optics. (a) Side view. (b) The diamond-anvils and gasket.

In the DAC, the diamonds act as both the pressure bearing medium and the optical window. The transparency of diamonds over the whole range of the eletro-magnetic spectrum, except vacuum UV, allows the study of materials directly in the DAC at high, static pressures, not only through visual techniques and refractive index measurements, but by scattering techniques, e.g., X-ray diffraction, Brilloiun scattering, and by various spectroscopies including IR absorption and reflection, fluorescence and Raman. For FT-IR and FT-Raman work, the selection of the diamonds is particularly important. In the case of IR, the purest diamonds with no nitrogen impurities, type IIa, are preferred. Unfortunately, these diamonds have a tendency to cleave easily and so do not always make the best high-pressure anvils. The strongest anvils seem to contain a reasonable amount of evenly dispersed, nitrogen platelet impurity, type I, but this impurity causes considerable absorption in the mid-IR region. Even type II diamonds absorb in the mid-IR, in the 2000-1900 cm^{-1} region, as shown in Figure 1.2. Cell designs, which use just one diamond anvil, and/or 180° scattering geometry, can minimize the amount of absorption. For Raman studies, the diamond anvils are often screened for low fluorescence. Type IIb diamonds, the most expensive, have been shown to be better in some cases, but generally it is more a case of luck! Another high-pressure window material that has been examined is sapphire. Compared to type II diamonds, sapphire windows show much less fluorescence over a range of laser excitation lines. However, the use of sapphire anvils is limited to a maximum pressure of ~12 kbar. Gem-cut single crystal cubic zirconia anvils have recently been investigated for high-pressure optical cells [9]. A maximum pressure of 132 kbar was achieved, which was dependent on the pressure transmitting medium and the gasket material employed. Background florescence and Raman scattering from the anvils was eliminated and IR spectra could be recorded between 4000 and 1500 cm^{-1} without interference.

The introduction of gaskets has permitted the study of single crystals and fluids, since it has provided a sample chamber. The gasket also creates more hydrostatic conditions, minimizing pressure gradients across the sample area [10]. Gaskets, made from stainless steel or inconel, for example, are often pre-indented

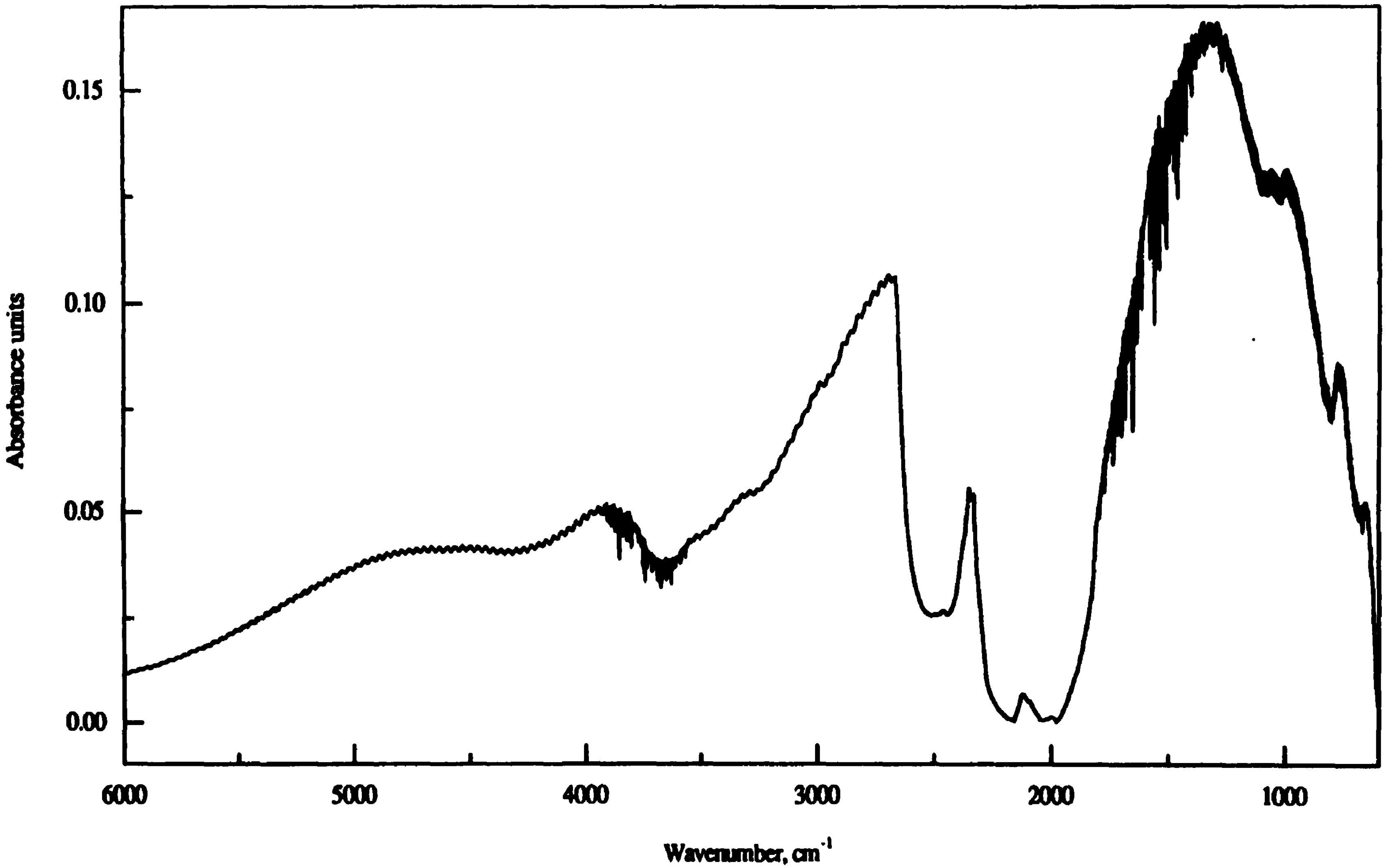

Figure 1.2. Mid-IR absorption spectrum of type IIa diamond anvils in a DAC, showing the strong absorption band in the 2400-1900 cm^{-1} region.

before drilling the central sample hole. The thickness of the gasket and the size of the drilled hole will determine, in part, the maximum pressure that can be achieved. As DACs are pushed to reach ever increasing pressures, the culet face of the diamond anvil becomes smaller and so does the gasket hole. For instance, diamond anvils with 50 μm faces are required for multi-megabar experiments, requiring gasket hole diameters as small as 25 μm.

In most high-pressure devices, the pressures are generated in the uni-axial sense, and pressure transmitting mediums are required to translate the pressure into a stress that is distributed uniformly. Pressure-transmitting media are especially important for experiments above 100 kbar, where significant pressure gradients can develop. Pressure-transmitting media can be gases, fluids or solids. They need to be chemically inert, have zero penetration into the sample or construction materials, have zero compressibility and be easy to handle and contained within the high-pressure enclosure. Gases are the most difficult to work with since more excessive technical design of the high-pressure device is required. They are, however, advantageous because of their low viscosity. Fluids are the most practical choice for pressure-transmitting media in the DAC. Pure, single component liquids tend to crystallize at relatively modest pressures, whereas a mixture of liquids can be taken to pressures well above the freezing pressure of the individual components. Under compression, the viscosity of such mixtures tends to rise exponentially, eventually forming a glass. The viscosity of the mixture is important - if too low, the sample will flow in the DAC during analysis while, if too large, other problems can arise. A damp mixture of ethanol and methanol in a 4:1 ratio is one of the most common pressure-transmitting media used. At room temperature, the glass transition point is ~104 kbar, but in some cases the viscosity can become very large by ~70 kbar. Other fluids used in the DAC are Nujol and silicones. The choice of pressure-transmitting medium will depend on the pressure range being investigated. For example, silicone fluid can be used to create hydrostatic conditions up to 150 kbar, after which broadening of the R_1 fluorescence line of the ruby calibrant (see below) has been reported, probably as a result of distributions in stresses [11]. Above 225 kbar, the R_1 and R_2 ruby fluorescence peaks are difficult to distinguish as they are broadened and overlap.

1.3 Pressure Calibration

The need for a secondary pressure gauge in the determination of the internal pressures in DACs and other high-pressure devices became evident when it was realized that the usual way in which pressure was determined, i.e. force-over-area, became unreliable at high pressures. High pressures are considered to be those above 1 kbar (1000 atm). Ideally, the pressure gauge must show a fairly linear response of some property under high static pressures, and not require a large sample volume, since the sample chamber of the DAC is obviously very small already. The precision of the gauge depends on both the precision with which the physical property can be measured and the rate at which this property changes under compression.

One of the first reliable methods of pressure calibration in the 100-300 kbar range was an X-ray pressure gauge. NaCl is a high symmetry solid, which shows a continuous volume change under compression up to its phase transition to the CsCl structure at 294 kbar. The lattice spacing of NaCl can be used to the determine the pressure by making use of the Decker equation of state for NaCl [12].

For pressure-tuning vibrational spectroscopy, an optical pressure gauge is obviously more convenient and perhaps the most well known is the ruby fluorescence R_1 line. At ambient pressures, the R_1 and R_2 ruby fluorescence lines lie at 694.1 and 692.6 nm, respectively. A continuous calibration of the ruby R_1 fluorescence gauge from 0.06 to 1 Mbar has been made, and the generally accepted equation for the pressure dependence is $P(\mathrm{Mbar}) = (19.04/5)\{[(\lambda_o + \Delta\lambda)/\lambda_o]^5 - 1\}$, where λ_o is the wavelength measured at 1 bar [13]. Pressure differences or strain in the DAC can be monitored by looking at the ruby R_1-R_2 doublet, which will broaden at high pressures as a result of pressure gradients and/or strain.

The ruby fluorescence gauge is suitable for measurements with a visible laser system. For pressure-tuning FT-Raman spectroscopy, however, the NIR Nd^{3+}:YAG laser emitting at 1064.1 nm is too far removed to excite the ruby fluorescence and hence two Raman measurements would be required. For this reason, the development of a new secondary pressure gauge for use in FT-Raman measurements was needed. A second drawback to the pressure-tuning FT-Raman spectroscopic technique is the need for a high-sample loading. Therefore, the possibility of using the 1332.5 cm^{-1} Raman-active t_{2g} phonon band of the diamond windows in the DAC was investigated as a potential *in-situ* pressure calibrant. This method obviously does not require the addition of material to the sample chamber and so a maximum loading of sample is still possible. The Raman-active diamond line has been shown to have a linear response to pressure over the 50-200 kbar range [14], and several mathematical models have been proposed to relate the effects of the pressure dependence of the normal modes of vibration of solids to the pressure shift of the diamond line [15]. The shift of the Raman-active t_{2g} phonon line of the diamond, as a possible internal calibrant for FT-Raman studies, has recently been investigated [16]. Under compression, the stress in the diamond-anvil is concentrated in the region near the sample-diamond interface, for the 0.001- ~70 kbar range. As pressure discontinuities in the diamond-anvil form perpendicular to the pressure axis, the diamond band at the sample-diamond interface shifts with a linear response with increasing pressure. Since Raman scatter is collected in a 180° geometry from the DAC, scattering from all depths of the diamond-anvil contributes to the diamond line and a band envelope is observed. It is the wavenumber of the band half-front which is measured to determine the pressure (Fig. 1.3); a linear least-squares fit was used to derive an equation to relate the band half-front and the pressure. The pressure dependence of the line shift is specific for each DAC.

For pressure-tuning IR spectroscopy, the frequency shift of the antisymmetric N-O stretching bands of dilute solutions of sodium nitrite and sodium nitrate ions in sodium bromide are used to calculate the internal pressure [17]. The band positions at ambient pressure are 1279.0 and 1403.1 cm^{-1}, respectively. The pressure is related to the shift, $\Delta\nu$/cm^{-1}, of the wavenumber of the nitrite ion from zero pressure by

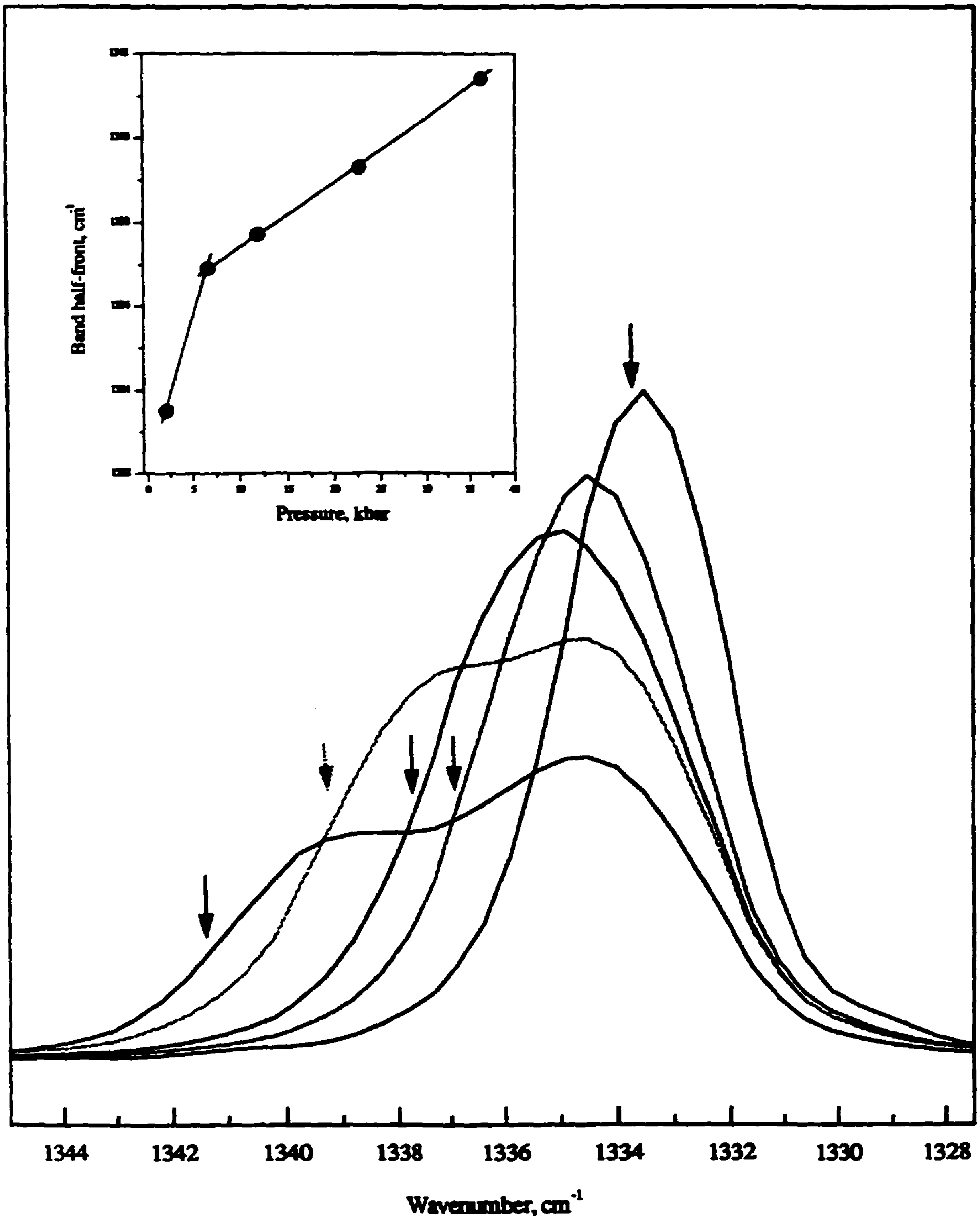

Figure 1.3. FT-Raman (Nd^{3+}:YAG) spectrum of the Raman-active t_{2g} phonon mode of the diamond-anvil. The arrows indicate the band half-front used to calculate the applied pressure (inset).

P/kbar = 2.356($\Delta\nu$) - [1.334($\Delta\nu$)exp($\Delta\nu$/92)] and to the shift, $\Delta\nu$/cm^{-1}, of the frequency of the nitrate ion by P/kbar = 1.775($\Delta\nu$) - [0.7495($\Delta\nu$)exp($\Delta\nu$/78)].

1.4 Effects of Pressure on Vibrational and Electronic Spectra

1.4.1 Metal-Carbonyls and Other Complexes with π-Backbonding Ligands

The bonding between a metal and carbonyl ligand has dual character. A metal ← carbonyl σ-bond is formed by using an unshared pair of electrons on the carbon (Fig. 1.4a) and the formation of a metal → carbon π-bond results from donation of electrons from a filled metal orbital of suitable symmetry into the π-antibonding orbital of the carbonyl ligand (Fig. 1.4b). The bonding is synergic, which means that as the extent of σ-donation increases, this will tend to promote an increase in the π–backbonding, as the amount of electron density at the metal center becomes too high. The extent of σ-donation and π–backbonding can be monitored in metal carbonyl complexes by measuring the frequencies of the ν(CO) and ν(M-CO) stretching modes. Increased π–backbonding will give a stronger M-C bond but a weaker, longer C≡O bond as electrons move into the π*-orbital of CO. The metal-carbon bonds have much lower force constants than do CO groups and so, under pressure, an increase in the degree of π-backbonding from the metal is expected, increasing the population of the π*-orbitals of CO. This situation should manifest itself as a negative pressure dependence of the ν(CO) stretching frequency.

Adams and Ekejiuba first reported the effect of applied pressure on metal-carbonyl interactions in 1982 [18]. They were looking at the high-pressure Raman spectra of $Mn(CO)_5Br$ up to 50 kbar, as part of a broad study of the phase behavior of inorganic molecular crystals. Changes in the slopes of the wavenumber *vs.* pressure plots indicated a phase transition at 24 ± 3 kbar. All the internal and lattice modes showed a positive pressure dependence with the exception of ν_2, the a_1, axial ν(CO) mode, which exhibited a small negative pressure shift from ambient pressure to 23 kbar of -0.067 cm^{-1} kbar^{-1}. Above 23 kbar, the pressure dependence became positive,

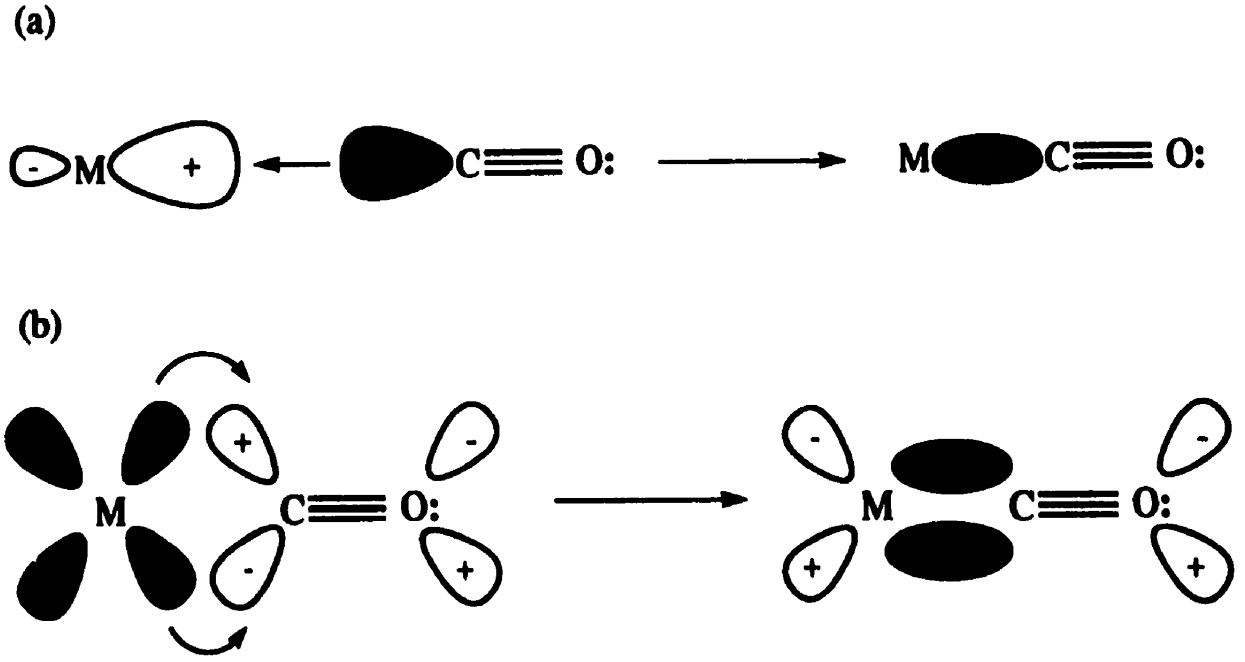

Figure 1.4. (a) The formation of the metal ← carbon σ-bond using an unshared pair on the carbon atom. (b) The formation of the metal → carbon π-bond.

0.239 cm^{-1} kbar^{-1}. The other ν(CO) modes showed continuous, but small, positive pressure dependences over the pressure range studied.

Very similar behavior was found for other pentacarbonyl halide and pentacarbonyl-methyl complexes, almost all of which are isomorphous with $Mn(CO)_5Br$. The micro-Raman spectra of pentacarbonyl(chloro)rhenium(I), $Re(CO)_5Cl$, from ambient pressure to ~60 kbar, showed discontinuities in several bands in the wavenumber *vs.* pressure plots [19]. These were accounted for by a second-order phase transition, as was observed for $Mn(CO)_5Br$. For $Re(CO)_5Cl$, it was shown that the a_1 ν(CO^{eq}) mode shifts steadily towards higher energies with increasing pressures and is insensitive to the phase transition. The a_1 ν(CO^{ax}) mode, on the other hand, has a small, negative dν/dp value in the low-pressure phase of -0.011 cm^{-1} kbar^{-1}.

In contrast, neither $Re(CO)_5Br$ nor $Re(CO)_5I$ undergo a phase change under compression to 43 kbar [20]. The latter crystallizes in a different space group (*Cmcm*) from its isostructural congeners (*Pnma*) due to a different mode of packing, linked presumably to the increase in halogen size from the bromide to iodide. All the modes showed a hardening (increasing wavenumber) with the increase of pressure.

The positive dν/dp value for the equatorial CO groups and the smaller, negative dν/dp value of the axial CO groups indicates that π-backbonding increases preferentially to the axial carbonyl, *trans* to the halide group, compared to the equatorial carbonyl groups. The pressure dependence of a ν(CO) frequency is a combination of two effects. First, the amount of π-backbonding can increase, which causes a lowering of the CO stretching frequency. Secondly, the general effect of compression is to decrease all intramolecular distances, resulting in an increase in the force constant and hence a positive shift in the CO mode frequency. When these two effects are combined, increases in π-backbonding are usually recognized as very small positive or negative pressure shifts. These observed results are summarized in Table 1.1.

$Re(CO)_5Cl$[c]				$Mn(CO)_5Br$[d]				$Re(CO)_5Br$[e]		$Re(CO)_5I$[e]		Assignment
low-pressure phase		high-pressure phase		low-pressure phase		high-pressure phase						
ν	dν/dp	ν	dν/dp	ν	dν/dp	ν	dν/dp	ν	dν/dp	ν	dν/dp	
2157	0.38	a	-	2139	0.139	a	-	2156	0.30	2150	0.43	$\nu(CO^{eq})$, a_1
2090	0.36	a	-	2088	0.328	a	-	2088	0.30	-	-	ν(CO), b_1
2073	0.16	2078	0.31	2074	0.171	a	-	2073	0.17	2074	0.28	ν(CO), e
2031	0.11	2035	0.22									"
1960	-0.01	1961	0.15	1988	-0.067		0.239	1964	0.11	1984	0	$\nu(CO^{ax})$, a_1
1954	-0.01	b	-									
1926	-0.11	b	-									$\nu(^{12}CO^{ax})$, a_1
289	1.15	b	-	218	0.702	-	0.239	218	0.20	163	0.34	ν(M-X)

Table 1.1. Wavenumber, ν (cm^{-1}) for the Raman-active ν(CO) modes and the ν(M-X) mode in $M(CO)_5X$, (M = Re, Mn; X = Cl, Br, I) and their pressure dependence, dν/dp (cm^{-1} $kbar^{-1}$). [a] Slope unchanged after phase transition. [b] Peak too weak to measure. [c]Ref. 22. [d]Ref. 21. [e]Ref. 23.

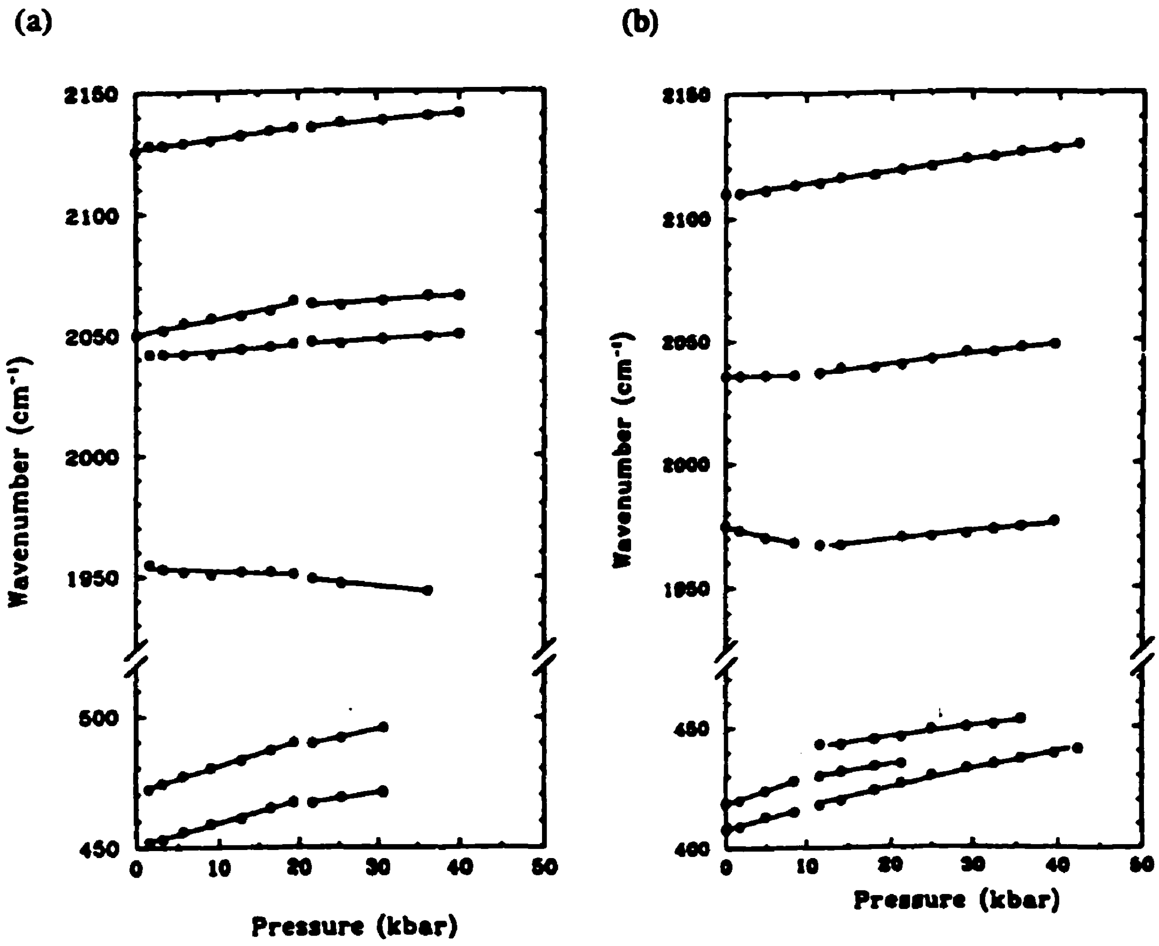

Figure 1.5. Pressure dependences of selected Raman bands of (a) $CH_3Mn(CO)_5$ and (b) $CH_3Re(CO)_5$. Reprinted with permission from Y. Huang, I. S. Butler, D. F. R. Gilson and D. Lafleur, Inorg. Chem., 30 (1991) 117-120. ©1991 American Chemical Society

The micro-Raman spectra of $CH_3Re(CO)_5$ and $CH_3Mn(CO)_5$ have been studied under pressures up to 40 kbar [21]. The vibrational data showed that both complexes undergo a second-order phase transition at ~9 kbar for $CH_3Mn(CO)_5$ and 22 kbar for $CH_3Re(CO)_5$ (Fig. 1.5). The pressure dependences of the ν(CO) modes show a similar pattern to those seen for the pentacarbonyl halides, but the pressure dependences of the modes appear to increase upon replacing an electron-withdrawing halide ligand with an electron-donating methyl ligand. Prior to the phase transition, the application of pressure increases the extent of π-backbonding preferentially to the axial CO ligand, but to different extents for the Mn and Re complexes. At higher pressures, the effect of pressure on the π-backbonding is different for $CH_3Mn(CO)_5$ and $CH_3Re(CO)_5$. The $\nu(CO^{eq})$ modes exhibit a positive shift with an increase in pressure for both complexes. For $CH_3Mn(CO)_5$, the $\nu(CO^{ax})$ mode shows a negative pressure dependence up to 9 kbar of -0.82 cm^{-1} $kbar^{-1}$. Following the phase transition, the pressure dependence becomes positive, 0.3 cm^{-1} $kbar^{-1}$. The $\nu(CO^{ax})$ mode of $CH_3Re(CO)_5$, on the other hand, shows a negative pressure response over the whole pressure range investigated, becoming more negative after the phase transition: $d\nu/dp = -0.15$ and -0.33 cm^{-1} $kbar^{-1}$. These effects are due to the *trans* effect of the methyl group. Furthermore, the application of external pressures preferentially enhances the π–effect of the methyl ligand, in which the $M\text{-}CO^{ax}$ bond length is increased by increasing the population of the axial carbonyl π*-orbitals through interaction with the metal d_{xz} and d_{yz} orbitals, over the σ–effect. The σ effect weakens the $M\text{-}CO^{ax}$ bond because of the presence of the inductive methyl group which increases the electron density on the metal atom through the σ-bond. All the $\nu(M\text{-}CO^{ax})$ modes exhibited high positive pressure dependences. These results are summarized in Table 1.2.

High-pressure studies on M_2CO_{10} (M = Re, Mn) [22] and $MnReCO_{10}$ [23] present further evidence that the effect of pressure on the axial carbonyl groups is dependent on the nature of the *trans* group. In Re_2CO_{10}, at the phase transition, which involves a change in geometry from staggered to eclipsed, the Raman-active axial

$CH_3Mn(CO)_5$[b]				$CH_3Re(CO)_5$[b]				Assignment
Low-pressure phase		High-pressure phase		Low-pressure phase		High-pressure phase		
ν, cm^{-1}	dν/dp, $cm^{-1}kbar^{-1}$	ν, cm^{-1}	dν/dp, $cm^{-1}kbar^{-1}$	ν, cm^{-1}	dν/dp, $cm^{-1}kbar^{-1}$	ν, cm^{-1}	dν/dp, $cm^{-1}kbar^{-1}$	
2110	0.46	a	-	2126	0.44	2135	0.31	ν_2, a_1, $\nu(CO^{eq})$
-	-	-	-	2050	0.69	2063	0.22	ν_{12}, b_1, $\nu(CO^{eq})$
2036	0.00	2037	0.40	2042	0.24	2047	0.19	"
1975	-0.82	1967	0.30	1955	-0.15	1949	-0.33	ν_3, a_1, $\nu(CO^{ax})$
419	1.09	430	0.51	452	0.85	467	0.44	ν_7, a_1, $\nu(MCH_3)$

Table 1.2. Pressure dependences of the Raman-active ν(CO) and ν(M-CH$_3$) modes for $CH_3M(CO)_5$, (M = Re, Mn). [a] Indicates no break in the slope at the phase transition. [b]Ref. 24.

ν(CO) mode drops by 8 cm^{-1}. Concurrently, the ν(Re-C^{ax}) mode shifts upward by 17 cm^{-1}. These changes imply that on becoming eclipsed the π-backbonding from the rhenium metal to the axial carbonyl is sharply enhanced. No such effect is observed for Mn_2CO_{10} or $MnReCO_{10}$.

A series of metal tricarbonyl complexes has also been investigated to determine the effect, if any, of changing the nature of the ancillary ligand on the metal and the pressure response of the carbonyl ligands. Tricarbonyl(η^5-cyclopentadienyl)rhenium(I), $CpRe(CO)_3$ [24] and the analogous η^5-pentamethylcyclopentadienyl complex, $Cp^*Re(CO)_3$ [25], were studied under applied pressures up to 40-60 kbar. Both complexes show a phase transition at ~9 kbar, although they are probably of a different nature since they crystallize in different space groups and the increase in intermolecular splitting is greater for the η^5-cyclopentadienyl complex than for the η^5-pentamethylcyclopentadienyl one, as seen from the increased factor group splitting in the former. For $CpRe(CO)_3$, two of the Raman-active e ν(CO) stretching modes at 1910 and 1904 cm^{-1} showed negative pressure responses in the low-pressure phase of -0.16 and -0.45 cm^{-1} $kbar^{-1}$, respectively. The third component of the e_1 ν(CO) mode at 1935 cm^{-1} was insensitive to pressure initially, but showed a high positive pressure dependence, 0.39 cm^{-1} $kbar^{-1}$, in the high-pressure phase. The pressure insensitivity and negative pressure dependence point to an increase in π-backbonding from the rhenium metal to CO, in the low-pressure phase. The other ν(CO) bands displayed positive pressure dependences. The effect of pressure on the ν(CO) modes of (η^5-Cp*)$Re(CO)_3$ was very similar. Only two components of the e_1 ν(CO) mode were clearly visible, the low frequency band showing a negative shift, dν/dp = -0.22 cm^{-1} $kbar^{-1}$ in the low-pressure phase but 0.07 cm^{-1} $kbar^{-1}$ in the high-pressure phase. The smaller pressure shifts for the ν(CO) modes for (η^5-Cp*)$Re(CO)_3$ compared to (η^5-Cp)$Re(CO)_3$ are interesting, because, *a priori*, it would be expected that the pentamethylcyclopentadienyl ligand would be capable of transferring greater electronic charge to the metal center than does the cyclopentadienyl ligand, thereby affording increased π-backbonding to the carbonyl ligands under pressure. These results imply a limitation to the extent of π-backbonding allowed between a metal and a carbonyl ligand.

The thiocarbonyl ligand is also a π-acid like carbonyl but, because of different relative energies of the HOMO and LUMO orbitals of the thiocarbonyl ligand compared to the carbonyl ligand, CS is both a better σ-donor and π-acceptor ligand. But like CO, the metal-CS interactions can be perturbed by the application of pressure and high-pressure studies have been conducted on several thiocarbonyl complexes in order to probe the bonding interactions and study the influence of the ancillary ligands. For example, $Cr(CO)_5(CS)$, $(\eta^6\text{-}C_6H_6)Cr(CO)_2(CS)$ [26] and $CpMn(CO)_2(CS)$ [27] have been examined under high-pressure by both FT-IR and Raman spectroscopy. The three complexes showed that the effect of pressure was a complicated balance between the effect of compression on the intramolecular distances, which results in a positive shift of all vibrational frequencies, and an increase in the π-backbonding from the metal to the carbonyl or thiocarbonyl ligand. Comparison of the results for $Cr(CO)_5(CS)$ and $(\eta^6\text{-}C_6H_6)Cr(CO)_2(CS)$ indicates that on replacing three carbonyl ligands with an electron donating ancillary ligand, a benzene ring, the extent of π-backbonding increases to all the carbonyl and thiocarbonyl ligands, but that under pressure the increase of π-backbonding to the carbonyls is greater than to the thiocarbonyl ligand (Table 1.3). Initially, the Cr-CS interactions are stronger than the Cr-CO interactions, but the results again demonstrate that there is a limit to the amount of electron donation possible through π-backbonding. We have recently measured the high-pressure Raman spectra of $(\eta^6\text{-}C_6H_5CO_2CH_3)Cr(CO)_3$ and $(\eta^6\text{-}C_6H_5CO_2CH_3)Cr(CO)_2(CS)$ in order to study the influence of replacing the benzene ligand with, $\text{-}C_6H_5CO_2CH_3$, which has an electron-withdrawing character. These results are presented in Chapter 3.

Another π-acid ligand is *tert*-butyl isocyanide (CNBu-*t*). NMR studies indicate that CNBu-*t* is a better σ-donor, but poorer π-acceptor ligand compared to the carbonyl ligand. Pressure-tuning infrared and Raman spectroscopy have been used to examine the relative π-backbonding capabilities of the CO and CNBu-*t* ligands in chromium(0) complexes [28]. Two complexes were studied, $Cr(CO)_5$(CNBu-*t*) and

$Cr(CO)_5(CS)$[a]		$(\eta^6\text{-}C_6H_6)Cr(CO)_2(CS)$[a]		$(\eta^6\text{-}C_6H_5CO_2CH_3)Cr(CO)_3$[b]		$(\eta^6\text{-}C_6H_5CO_2CH_3)Cr(CO)_2(CS)$[b]		Assignment
ν, cm^{-1}	dν/dp, cm^{-1} $kbar^{-1}$	ν, cm^{-1}	dν/dp, cm^{-1} $kbar^{-1}$	ν, cm^{-1}	dν/dp,[c] cm^{-1} $kbar^{-1}$	ν, cm^{-1}	dν/dp,[c] cm^{-1} $kbar^{-1}$	
2088^{eq}	0.18	1962	0 37	1970	0.03, 0.27	1962	0.01, 0.17	ν(CO)
2017^{eq}	0.22	1943	-0.59	1898	0.05, 0.19	1912	-0.03, -0.34	ν(CO)
2017^{ax}	-0.18	1908	0.59	1870	-0.03, -0.07			ν(CO)
1989^{eq}	-0.53	1856	-0.54	1855	0.08, -			ν(CO)
1289	-0.25	1211	0.85			1205	0.02, 0.63	ν(CS)
1260	-0.09	1192	0.37			1197	1.12	ν(CS)
427^{eq}	0.73	452	0.80	480	0, 0.69	452.1	0.017, 0.61	ν(CrCO)
422^{ax}	0.82			474	- ,0.34			ν(CrCO)
381^{eq}	0.78							ν(CrCO)
352	0.70	432	0.41			429	0.04, 0.3	ν(CrCS)
636	-0.46,0.33	646	0.17	663	0.04, 0.46			δ(CrCO)
512	0.16	611	0.33	632	0.05, -	640	0.04, 0.32	δ(CrCO)
487	0.21	600	0.12	623	-			δ(CrCO)
340	-	521	0.21			592.	-0.55, -	δ(CrCS)
		502	0.28			524	-0.16, 0.26	δ(CrCS)

Table 1.3. Pressure dependence of selected Raman-active modes. [a]Ref. 29. [b]Ref 30. [c]A phase transition was observed in the 10 to 15 kbar range. The pressure dependence is given for the low-presure phase and the high-pressure phase.

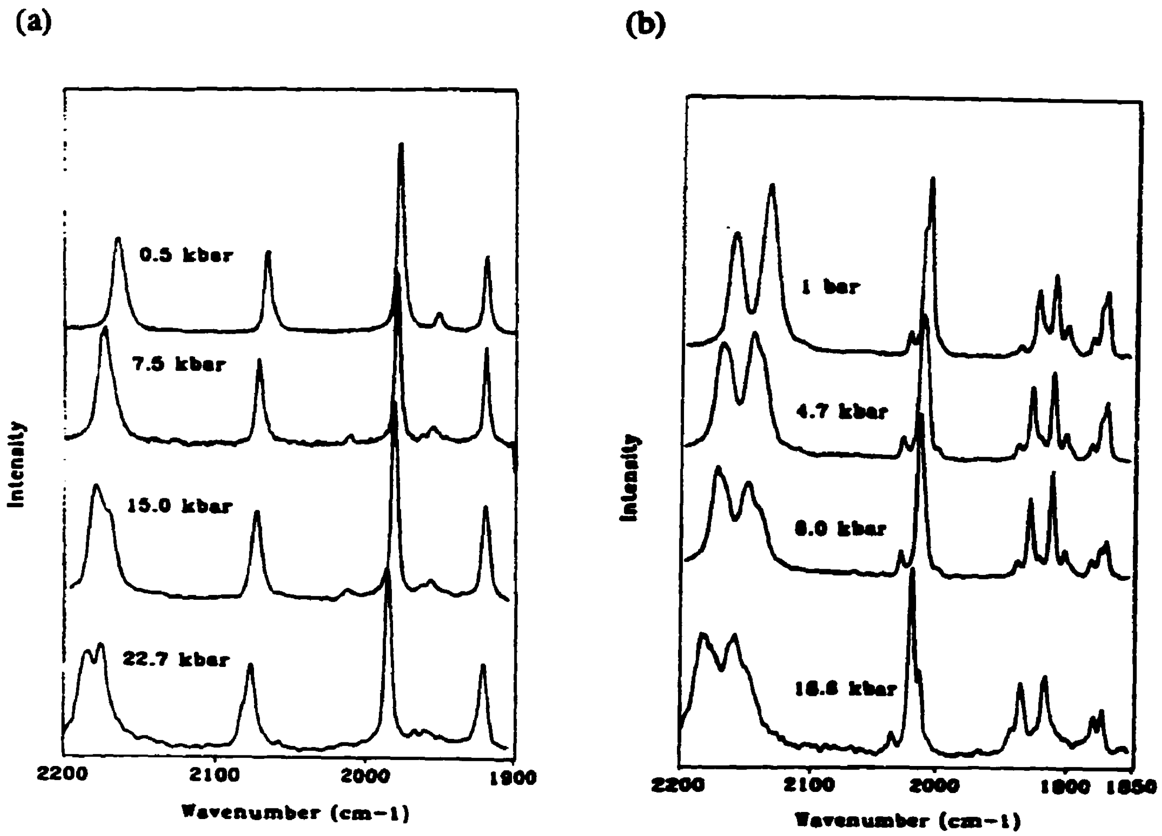

Figure 1.6. Raman spectra of $Cr(CO)_5(CNBu\text{-}t)$ (a) and $Cr(CO)_4(CNBu\text{-}t)_2$ (b) at four different pressures. Reprinted with permission from H. Li and I. S. Butler, Inorg. Chem., 34 (1995) 1193-1197. ©1995 American Chemical Society.

cis-$Cr(CO)_4(CNBu\text{-}t)_2$, both complexes showing a second-order phase transition at ~11 kbar and ~6 kbar, respectively (Fig. 1.6). For $Cr(CO)_5(CNBu\text{-}t)$, the equatorial ν(CO) mode was more pressure sensitive than was the axial ν(CO) mode, which was essentially independent of pressure below the transition pressure. After the phase change, all three modes (a_1^{ax}, a_1^{eq} and b_1) showed a positive pressure shift of about the same magnitude. ν(CN) was more compressible in both the low-pressure and high-pressure phases as a result of the greater anharmonicity of the CN vibration and the larger bulk of the ligand itself. The fact that dν/dp [ν(CN)] >> dν/dp [ν(CO)] in the low-pressure phase provides further evidence that CNBu-*t* has a lower π-acceptor capability. The results for *cis*-$Cr(CO)_4(CNBu\text{-}t)_2$ further demonstrate the geometrical dependence of the pressure sensitivities of the ν(CO^{eq}) and ν(CO^{ax}) modes. The CO groups *trans* to the CNBu-*t* ligands would be expected to exhibit greater π-backbonding effects and therefore have a smaller dν/dp value than do the ν(CO^{eq}) modes. This is exactly what was observed.

The phase behaviour of some metal-cyano complexes has been studied, and the results show that the metal π - CN π* interactions are increased under compression in a similar manner to those for metal-carbonyl interactions [29]. For instance, $K[Au(CN)_2]$ is one of the most stable and best characterized two coordinate complexes, with discrete, almost linear $[N{\equiv}C\text{-}Au\text{-}C{\equiv}N]^-$ ions. Phase transitions, indicated by large discontinuities in the pressure sensitivities of the Raman modes, were observed at 6.6 and 10.5 kbar. In phase II, between 6.6 and 10.5 kbar, the ν(CN) modes in the 2175-2165 cm^{-1} region showed very strong negative pressure shifts of -3.43, -3.85 and -3.7 cm^{-1} $kbar^{-1}$. Before and after the phase transition, these modes exhibit typical, positive pressure sensitivities. The first-order phase transition at 6.6 kbar leads to a phase in which the π-backbonding to the CN ligand has a controlling influence on the phase behaviour of the complex.

Metal-alkene bonding interactions are have dual character, the two bonding interactions being synergically related, as for carbonyl ligands. One particularly well-known example of metal-alkene coordination is in Zeise's salt, $K[Pt(\eta^2\text{-}C_2H_2)Cl_3]$. In order for π-backdonation of electrons from the platinum to the π*-orbital on the ethylene to occur, a perpendicular geometry of the ethylene to the $PtCl_3$ plane is required. High-pressure infrared and micro-Raman spectra were recorded for $K[Pt(\eta^2\text{-}C_2H_2)Cl_3]$, the dimer, $[Pt(\eta^2\text{-}C_2H_2)Cl_2]_2$, and dichloro(1,5-cyclooctadiene)platinum(II), $Pt(COD)Cl_2$ [30]. Under compression the extent of π-backbonding increased, as shown by the negative pressure dependences of the peaks assigned to the $\nu(C{=}C)$ stretching frequencies.

1.4.2 Isomerization and Piezochromism

When external pressure is applied, the unit cell volume of the system decreases and the intermolecular separations are reduced. The consequence of this is changes in the lattice packing forces, including cation-anion interactions, van der Waals forces and hydrogen-bonding, which determine the specific configuration of the molecule or ion. Under pressure, the delicate balance of the competing molecular forces is disrupted and, if a second configuration of comparable stability exists, solid-state isomerization can be induced.

Coffer *et al.* have shown that the green form of $[Au_9(PPh_3)_8][PF_6]_3$, which can be viewed as a D_{2h} fragment of an icosahedron **1**, could be transformed to the brown form, which has a D_{4d} centered-crown structure **2** [31]. Each form possesses its own distinct electronic absorption spectrum in the solid state and changes in the spectrum of the green form of $[Au_9(PPh_3)_8][PF_6]_3$ showed that, over the pressure range 45-60 kbar, isomerization to the brown form occurred. This piezochromic process was reversible and was favored by changing cation-cation and cation-anion intermolecular forces.

$Rh_2(\mu\text{-}Cl)_2(CNC_8H_9)_4(\mu\text{-}AuPPh_3)]_2(PF_6)_2$ (**3**) exists as two isomers, a red isomer, in which the two cluster fragments adopt a *trans*, eclipsed conformation about a central Rh-Rh bond, and a green isomer, which has a *gauche*, staggered conformation. Pressure-dependent electronic spectroscopy indicates that the two isomers become geometrically similar at high pressures, inducing a conformational change around the Rh-Rh bond [32].

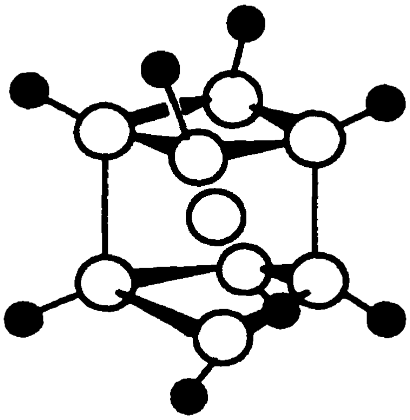

1

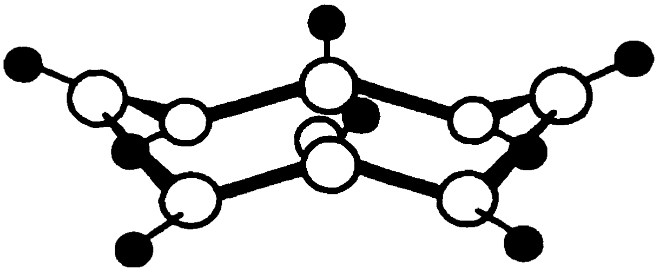

2

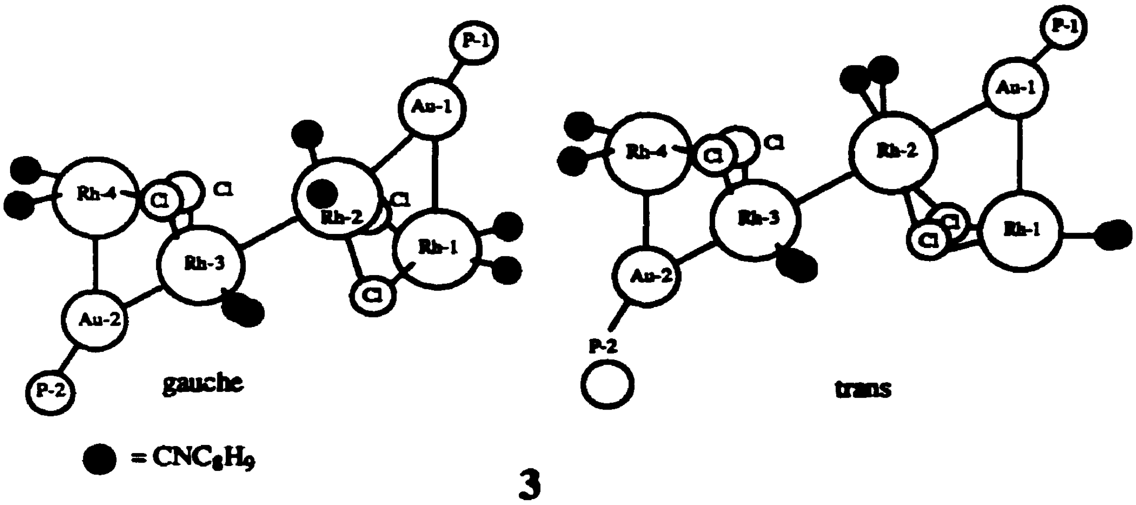
P-1
Au-1
Rh-4
Cl
Cl
Rh-2
Cl
Rh-3
Rh-1
Cl
Au-2
P-2
gauche
P-1
Au-1
Rh-4
Cl
Cl
Rh-2
Rh-3
Cl
Cl
Rh-1
Au-2
P-2
trans
● = CNC_8H_9

3

Piezochromism has been observed in a large number of Cu(II) complexes, containing a variety of ligands [33]. For example, complexes of the type $[CuL_2]X_2$ [L = N,Ndiethylethylenediamine (dieten), ethylenediamine (en), X = BF_4^-] adopt an elongated, tetragonal octahedral configuration with an approximately planar CuN_4 arrangement and the anions occupying symmetric sites above and below the CuN_4 plane (4). When L is en, the anions lie perpendicular to the plane passing through the copper cation. When L is dieten, the anions lie off this perpendicular. Under pressure, a molecular rearrangement in $[Cu(dieten)_2](BF_4)_2$ occurs, in which a marked decrease in the anion-molecular plane distance results together with a concomitant increase in the interaction between the anion and cation [34]. These changes appear as significant shifts of the bands in the electronic spectrum as the d_{z^2} orbital of copper interacts with the anion (Fig. 1.7), and changes in the IR spectra, which correspond to a lowering of the symmetry of the tetrahedral anion. At higher pressures, the structure of the dieten complex becomes more like the low-pressure structure of the en complexes.

Copper complexes of the type $[Cu(dien)(bipyam)]X_2.nH_2O$ (dien = diethylenetriamine, bipyam = 2,2′-dipyridylamine; X = Cl^-, ClO_4^-, NO_3^-) show continuous transformations from a distorted trigonal-bypyramidal structure to a regular square- pyramidal conformation under the application of pressure [35]. Again, the electronic and IR spectra provided evidence for the rearrangement. Other five-coordinate Cu^{2+} complexes show similar behavior under compression [36].

In the tetrachlorocuprate anion, $[CuCl_4]^{2-}$, the dihedral angle can vary such that geometries from nearly tetrahedral to square planar are possible, simply on changing the cation. Bray and Drickamer have studied the effect of compression on a range of $X^{2+}[CuCl_4]^{2-}$ complexes and their electronic spectra [37]. They found that complexes with a large dihedral angle at ambient pressure, e.g., $Cs_2[CuCl_4]$, tended to show an increase in dihedral angle under pressure, but a complex with a smaller dihedral angle, e.g., $[(nmpH)_2][CuCl_4]$ (nmpH = N-methylphenethylammonuim) showed an increase in dihedral angle. The general result was that, at higher pressures, there was a much smaller range of dihedral angles for the complexes.

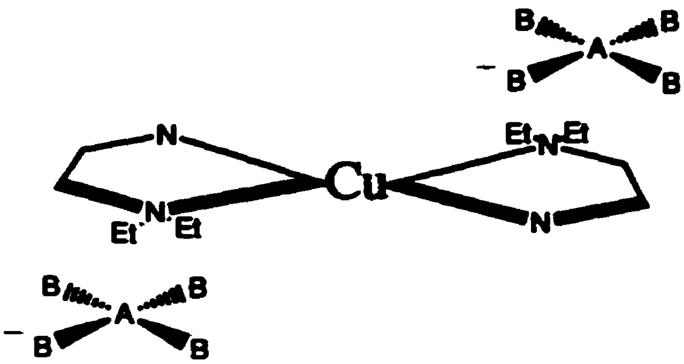

4

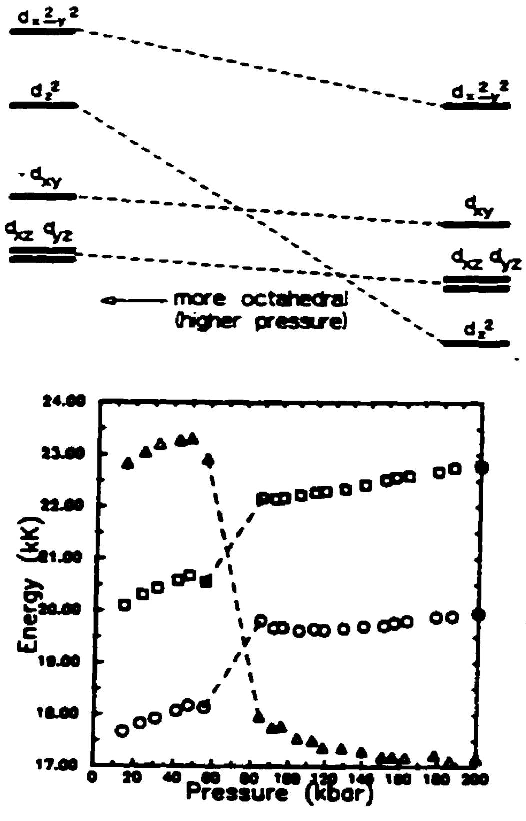

Figure 1.7. Splitting of the one-electron energy levels of the d^9 Cu^{2+} cation in D_{4h} symmetry and the pressure dependences of the energies of the $d_{z^2} \rightarrow d_{x^2-y^2}$ (Δ), d_{xz}, d_{yz} → $d_{x^2-y^2}$ (○), and d_{xy} → $d_{x^2-y^2}$ (□) electronic transitions in polycrystalline [Cu(dieten)$_2$](BF$_4$)$_2$. Reprinted with permission from K. L. Bray, H. G. Drickamer, E. A. Schmitt and D. N. Hendrickson, J. Am. Chem. Soc., 111 (1989) 2849-2856. ©1989 American chemical Society.

The interconversion of a metal-dihydride [M-(H)$_2$] to a metal-dihydrogen [M-(η^2-H$_2$)] occurs in several complexes in solution and has been demonstrated by ^{1}H NMR spectroscopy [38]. It has recently been shown that the dihydride to dihydrogen isomerization can be induced under compression at room temperature [39]. [(PP$_3$)Co(H)$_2$]X [PP$_3$ = P(C$_2$H$_4$PPh$_2$)$_3$] contains two hydride ligands when co-crystallized with the BPh$_4^-$ counterion, but shows the dihydrogen form when PF$_6^-$ is the counterion, Scheme 1.1. In solution, the dihydride is the stable form, regardless of anion. The dihydride complex is pale yellow while the dihydrogen complex is red. Under modest pressures of just 6-10 kbar, the pale yellow dihydride complex [(PP$_3$)Co(H)$_2$] BPh$_4$ is transformed into the red dihydrogen complex. The isomerization was seen visually by observing the colour change, in the visible spectrum (Fig. 1.8), and in the FT-IR spectrum. A disappearance of the ν(CoH) stretching mode was observed at the transition pressure. Chapter 5 focuses on the high-pressure dihydride-dihydrogen interconversion in a neutral rhenium heptahydride complex, ReH$_7$(dppe) [dppe = 1,2-bis(diphenylphosphino)ethane].

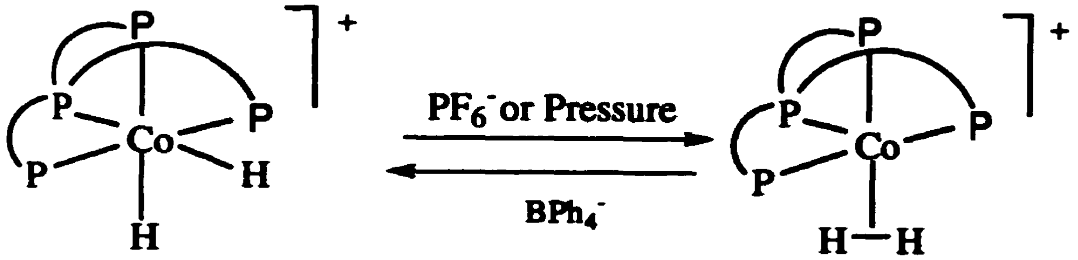

Scheme 1.1.

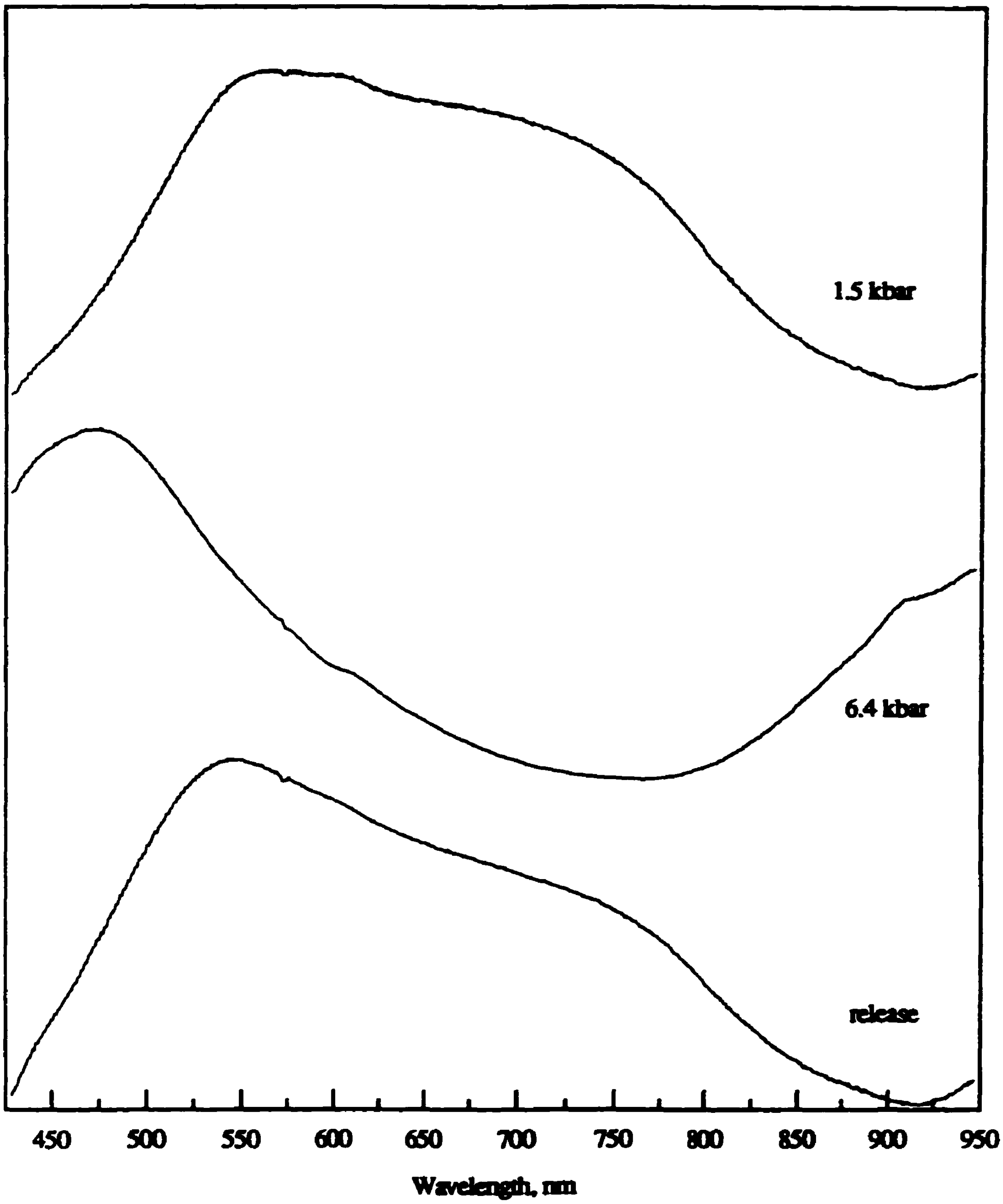

Figure 1.8. Compression and decompression visible absorption spectra of $[(PP_3)Co(H)_2]BPh_4$.

1.4.3 Binuclear Complexes and Clusters

The metal-metal quadruple bond is typified by the $[ReCl_8]^{2-}$ anion, which has an eclipsed conformation of the two $ReCl_4$ halves, despite the resulting steric effects. The application of high pressures to salts of both $[ReBr_8]^{2-}$ and $[ReI_8]^{2-}$ causes torsion from an eclipsed to a staggered conformation [40,41,42]. With increasing pressure, a new band appears in the visible spectrum, red-shifted from the well-known $\delta \rightarrow \delta^*$ transition of the eclipsed form. The new, low-energy peak is assigned to $\delta \rightarrow \delta^*$ transition of the staggered conformation. The transformation from eclipsed to staggered results in zero overlap of the d_{xy}-d_{xy} orbitals. Morris *et al.* have studied the electronic and resonance Raman spectra of eclipsed $[Re_2X_8]^{2-}$ (X = F, Cl, Br), as well as the complex $Mo_2Cl_4(PMe_3)_4$, whose D_{2d}-interlocked phosphine-ligand geometry contributes considerable torsional rigidity up to 15 kbar [43]. The $\nu(Re_2)$ mode for $[Re_2X_8]^{2-}$ in dichloromethane and $\nu(Mo_2)$ for $Mo_2Cl_4(PMe_3)_4$ in cyclohexane showed a continuous increase in frequency with increasing pressure. The shift in $\nu(Re_2)$ was dependent on X, with F > Cl > Br. The shortening of the metal-metal bond was significant in all the complexes. The change in Mo-Mo bond length was intermediate between the bond length change in the $[Re_2Cl_8]^{2-}$ and $[Re_2Br_8]^{2-}$ complexes. Although the PMe_3 ligands are larger than the halide ligands, the D_{2d}-interlocked phosphine geometry mitigates this effect. The electronic spectra in solution showed a continuous shift to lower wavenumbers. No new bands were observed as previously reported by Carrol *et al.* [40]. The bands did broaden and changes in intensity were noted. A pressure-induced torsional distortion was thought to occur in all three rhenium complexes, although $[Re_2Cl_8]^{2-}$ and $[Re_2Br_8]^{2-}$ had a greater tendency to distort. The molybdenum complex, on the other hand, did not undergo torsional distortion, presumably due to steric repulsion of the tertiary phosphine ligands.

The decacarbonyl complexes, Mn_2CO_{10} and Re_2CO_{10}, have a staggered conformation in the solid state, at ambient pressure. Under the application of pressure, the IR spectra show changes consistent with a change in symmetry from D_{4d}

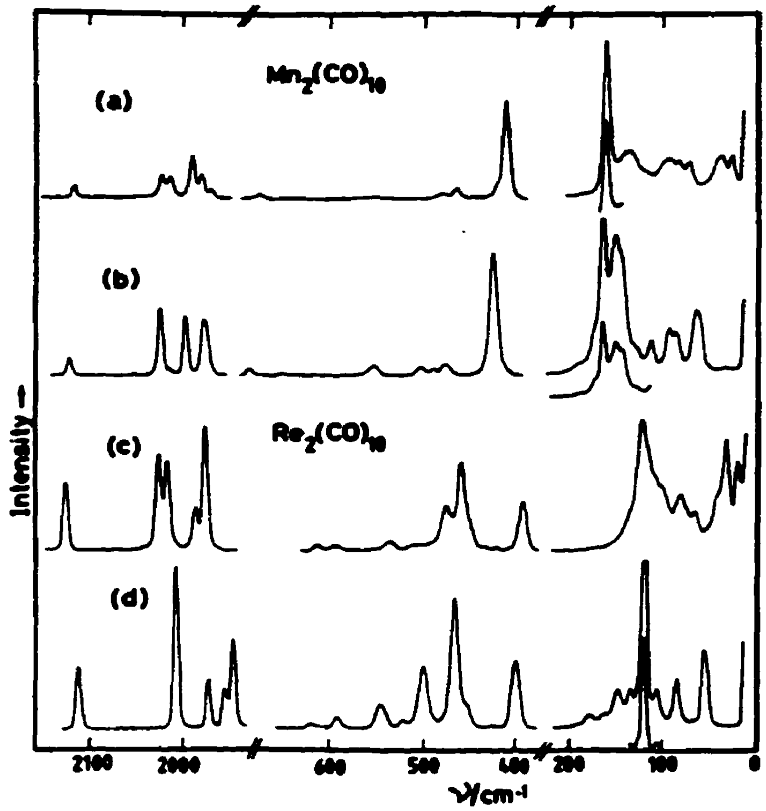

Figure 1.9. Raman spectrum of $Mn_2(CO)_{10}$ at (a) ambient pressure, (b) 16 kbar, and of $Re_2(CO)_{10}$ at (c) ambient pressure and (d) 16 kbar. Reprinted with permission from D. M. Adams, P. D. Hatton and A. C. Shaw, J. Phys., Condens. Matter, 3 (1991) 6145-6158. ©1991 American Chemical Society.

to D_{4h} (Fig. 1.9) [22]. The transition observed at ~5 kbar for Re_2CO_{10} and ~8 kbar for Mn_2CO_{10} is due to torsion about the M-M bond to the eclipsed conformation. Pressure-tuning of the electronic states of Mn_2CO_{10} and Re_2CO_{10} has also been investigated [44] but, since the electronic states have cylindrical symmetry, the phase transition from the staggered to eclipsed form was not detected. However, a change in the electronic spectrum was observed because of changes in the intramolecular distances, which lead to increased overlap of orbitals and stabilization of the bonding orbitals and a destabilization of the antibonding orbitals. The net result was a shift of the $\sigma \rightarrow \sigma^*$ and $\pi \rightarrow \pi^*$ bands towards higher energies, increasing to a maximum.

Breaks in the wavenumber *vs.* pressure plots for the IR modes of $MnReCO_{10}$ indicate two phase transitions at ~7 and ~13 kbar. The low and high-pressure phases have very similar spectra, while the middle phase, between 7-13 kbar, has a significantly different IR spectrum [23]. The ν(Mn-Re) mode was particularly sensitive to the phase transition, disappearing at 7 kbar, and a new band appearing at ~10 cm^{-1} lower. At 13 kbar, this band showed a discontinuous shift of +8 cm^{-1}. These changes suggest a transition from the staggered conformation to the eclipsed form at 7 kbar, reverting back to the staggered conformation at pressures above 13 kbar, with a shortening of the Mn-Re bond distance in the eclipsed conformation. The $M(CO)_5$ units have C_{4v} symmetry in both the staggered and eclipsed conformations and so the symmetry of the ν(CO) modes are insensitive to the transition.

Dihalotetrakis(pivalalto)dirhenium(III) contains a Re-Re quadruple bond. The electronic absorption spectra and high-pressure IR spectra in the 1800-700 cm^{-1} region of $Re_2(piv)_4Cl_2$ and $Re_2(piv)_4Br_2$ (piv = O_2CCMe_3) for both the crystalline solids and the complexes dispersed in a polymer matrix were recorded [45]. In the electronic spectra, a new band was observed to grow from ambient pressure on the low-energy side of the $\delta \rightarrow \delta^*$ excitation (Fig. 1.10). Only above 40 kbar was a decrease in the $\delta \rightarrow \delta^*$ excitation band noted. In the IR spectra, three new bands were observed at 1134, 1280 and 1697 cm^{-1} for X = Br and at 1142, 1286 and 1697 cm^{-1} for X = Cl. Since the results were the same for both the crystalline solids and the

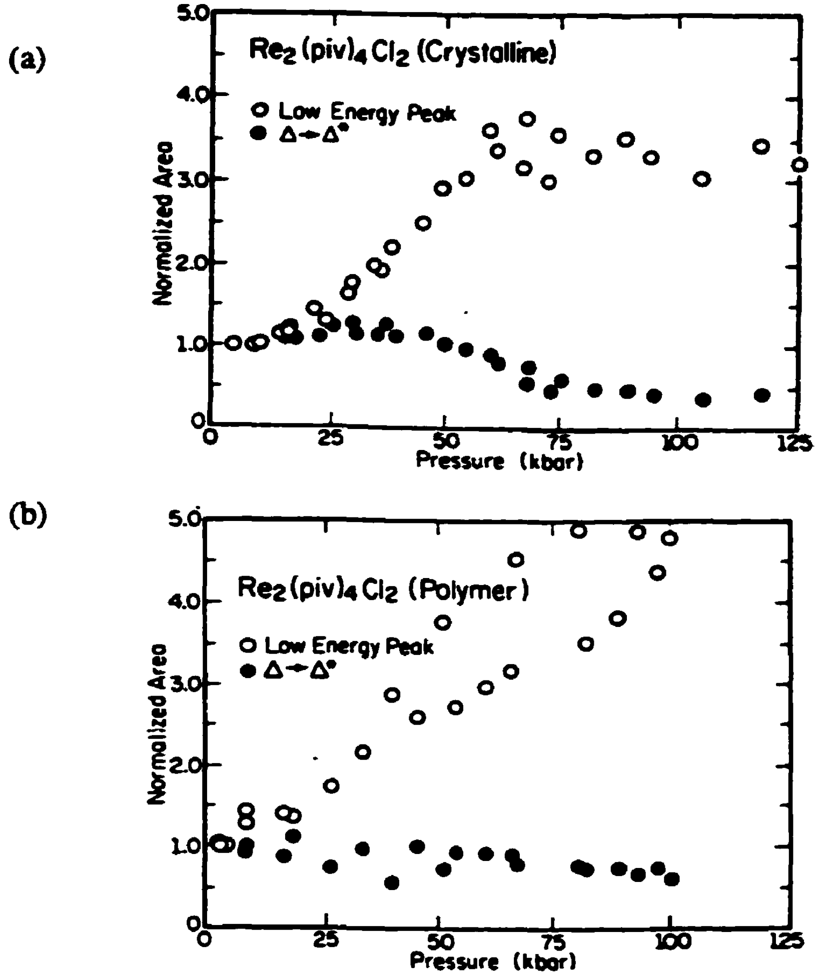

Figure 1.10. Area of the low-energy peak (normalized to 1 atm) and of the δ → δ* peak in polycrystalline $Re_2(piv)_4Cl_2$ (a) and of $Re_2(piv)_4Cl_2$ in a PMMA matrix (b). Reprinted with permission from R. T. Roginski, T. L. Carroll, A. Moroz, B. R. Whittlesey, J. R. Shapley and H. G. Drickamer, Inorg. Chem., 27 (1988) 3701-3709. ©1988 American Chemical Society.

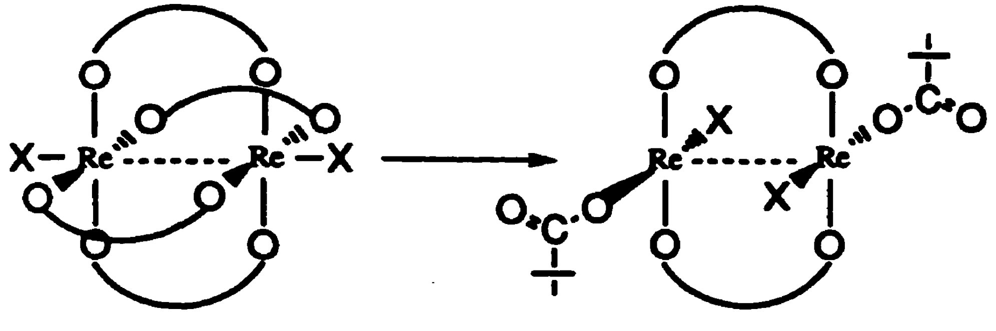

Scheme 1.2.

dispersed in polymer, the pressure-induced changes were due to intramolecular changes, probably being a change in the coordination of one of the pivalato ligands from bidentate to monodentate, as shown in Scheme 1.2. The new IR band at 1697 cm^{-1} is assigned to the $\nu(CO)$ vibration of the ketone. Other complexes have shown similar behaviour upon chemical changes.

Metal clusters, in particular organometallic carbonyl clusters, have been used as structural models for adsorbed organic species on metal surfaces. Infrared measurements of molecules adsorbed to metal surfaces have been used to complement data from other surface techniques. Pressure-tuning spectroscopy on clusters has been useful in the assignment of vibrational bands of adsorbed species. Coffer *et al.* [46] have studied a series of triosmium clusters with coordinated C_2 hydrocarbon ligands under high pressures up to 96 kbar. They found that for complex **5** the pressure dependences of the bands follow the order C-H stretch > C-C stretch > C-H bend, with all bands typically shifting to higher energy. For clusters **6** and **7**, the order changed to C-C stretch > C-H stretch > C-H bend, if the shifts were considered in terms of percent change. It was also found that the shift of the C-C stretch was proportional to the frequency of the mode at ambient pressure. A similar high-pressure IR study on the α-pyridyl moiety in $HOs_3(CO)_{10}(\mu,\eta^2\text{-}NC_5H_4)$ to 70 kbar also showed that the $d\nu/dp$ values varied as $\nu(CC) > \delta(CH)$ [47].

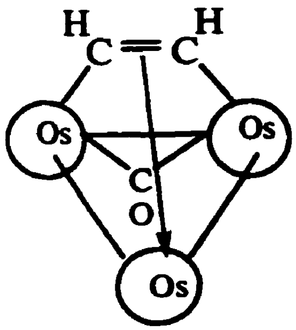

5

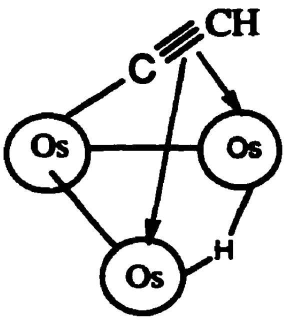

6

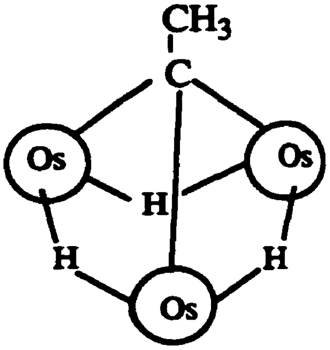

7

Metal-sulfido clusters are of interest, in particular $M_6(\mu_3\text{-}S)_8(PEt_3)_6^{n+}$ (M = Fe, n = 2; M = Co, n = 1, 0), due to their structural similarity to clusters present in the bulk metal sulfides known as Chevrel phases. The structural feature of Chevrel phases is that they contain Mo_6 clusters, and the origin of superconductivity is the Mo 4*d* electrons which are strongly localized in the Mo_6 clusters [48]. Pressure-tuning spectroscopy has been used to probe the electronic structure of the metal-sulfido clusters [49]. The large blue shifts of the observed peaks were due to intramolecular effects since the same shifts were observed for $Fe_6(\mu_3\text{-}S)_8(PEt_3)_6^{2+}$ dissolved in PMMA and as the crystalline form. Compared to the iron cluster, the cobalt cluster showed a much smaller pressure dependence, attributed to weaker M-M interactions and a more delocalized ligand character of the frontier orbitals.

1.4.4 Pressure-induced Order-disorder

Order-disorder transitions involving solids containing CH_3 or NH_3 groups can occur with temperature or pressure and involve molecular internal torsion. A Raman study of the phase behavior of CH_3HgX (X = Cl, Br, I) was carried out up to pressures of 40 kbar [50]. For CH_3HgCl, three phase transitions were observed from the Raman measurements at ~1.5, 5.9 and again at ~ 6 kbar. Above 8 kbar there was a single phase present which was stable up to 40 kbar (Fig. 1.11a). Three Becke lines were observed when viewed under a microscope, which confirm the transitions as first-order. Becke lines arise from the combination of reflected and refracted light rays at the junction of two materials whose refractive indices are close in magnitude. CH_3HgBr shows a single transition at 12.5 kbar, seen readily in plots of Raman wavenumber *vs*. pressure (Fig. 1.11b). Two Becke lines were observed for CH_3HgI, with the two phase transitions occurring at 5.0 and 11.5 kbar (Fig. 1.11c). In all three materials, the increase in pressure causes significant softening of the $\delta_s(CH_3)$ mode. For the chloride and bromide, in the high-pressure phases, this mode hardens with increasing pressures, while for the iodide the $\delta_s(CH_3)$ mode continues to soften under pressure. The crystal structure detrmined for CH_3HgCl has a tetragonal space

(a)

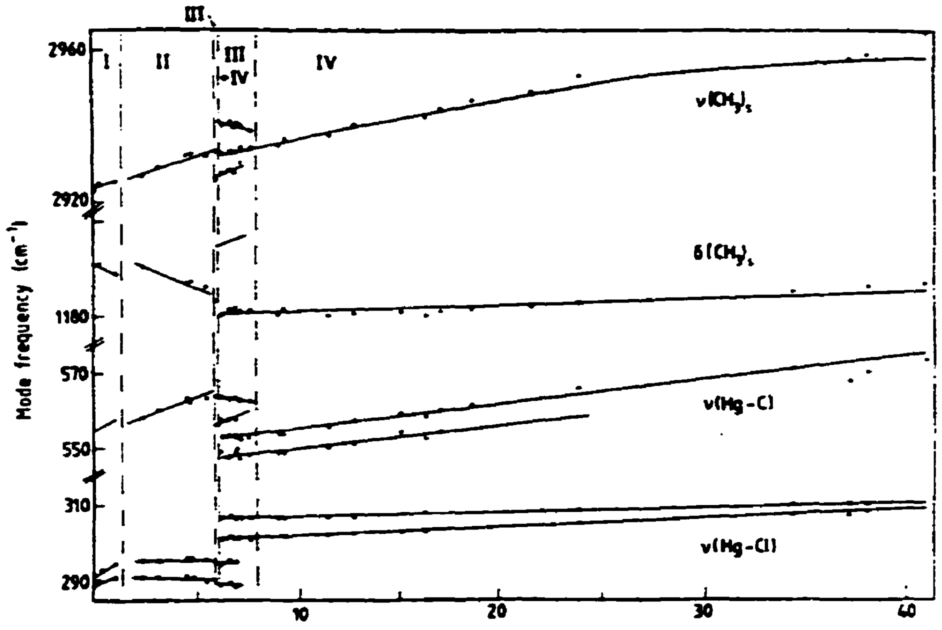
III
2960
I
II
III
→IV
IV
ν(CH3)s
2920
δ(CH3)s
1180
570
ν(Hg-C)
550
310
ν(Hg-Cl)
290
10
20
30
40
Mode frequency (cm⁻¹)

(b)

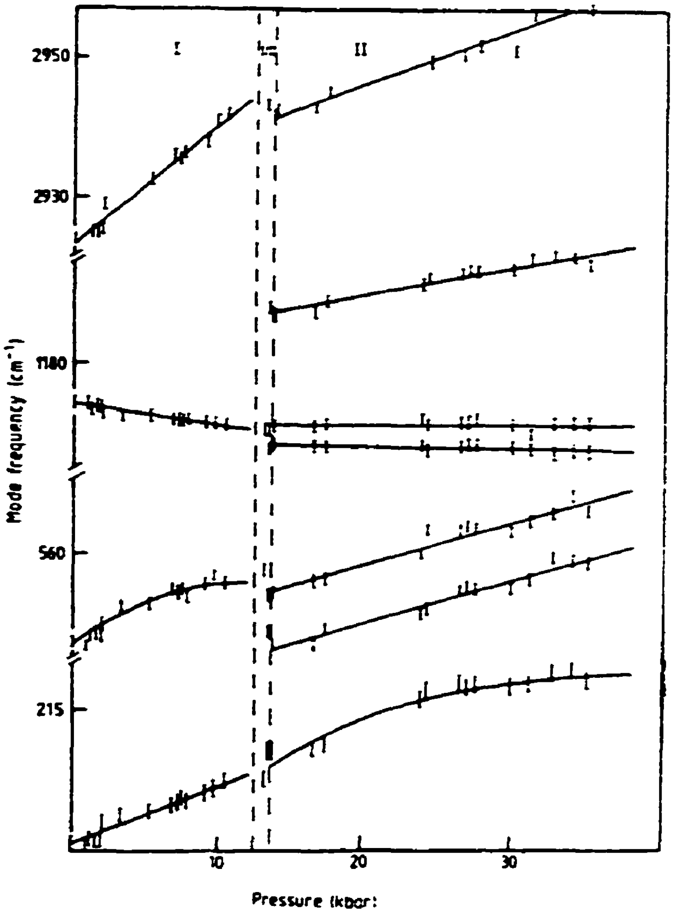
2950
I
II
2930
1180
560
215
10
20
30
Pressure (kbar)
Mode frequency (cm⁻¹)

(c)

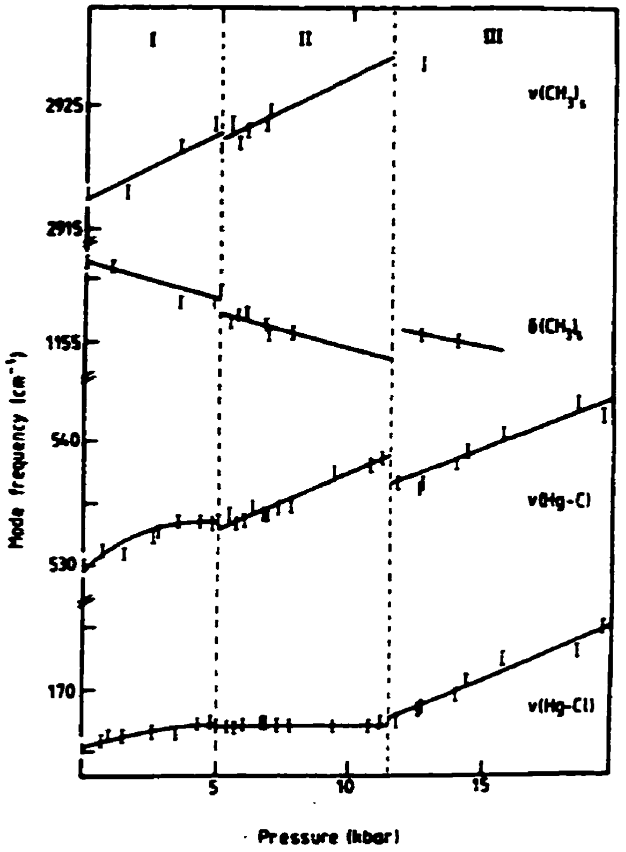

Figure 1.11. Wavenumber vs. pressure plots for the internal modes of (a) CH_3HgCl, (b) CH_3HgBr, and (c) CH_3HgI. Reprinted with permission from D. M. Adams and M. Pogson, J. Phys. C: Solid State Phys., 21 (1988) 1065-1079.

group, which is incompatible with the methyl groups and hence they must be disordered, i.e., there is unrestricted rotation about the Hg-C bond. The crystal structure of CH_3HgBr is similar but there is a definite departure from linearity of the C-Hg-Br skeleton. The methyl groups could be ordered or disordered. CH_3HgI has a crystal structure which is different again. The pronounced softening of the $\delta_s(CH_3)$ mode indicates that the methyl groups are implicated in the transition. In the high pressure phases, the spectral complexity increases, with new $\nu(CH)$, $\delta(CH_3)$ and $\nu(Hg\text{-}Cl)$ bands appearing. These results suggest that, on the transition to phase III of CH_3HgCl, the methyl groups cease to be in essentially free rotation and become fixed.

The methyl groups in dimethyltin difluoride, $(CH_3)_2SnF_2$, lie along the four-fold crystal axis and have been shown to be disordered by NMR and neutron scattering [51]. A phase transition at low-temperature (70.4 K) involves a change in the reorientational behavior of the methyl groups. All the IR and Raman modes harden under compression [52]. At ~40 kbar, the dv/dp values change quite significantly for the IR-active symmetric and antisymmetric $\delta(CH_3)$ modes, becoming essentially zero, which indicates that above the transition pressure the motion involved with this vibration is less restricted. A shoulder on the degenerate $\delta_{as}(CH_3)$ mode is resolved above the transition pressure. At higher pressures, restricted rotation of the methyl groups is limited and they become ordered, since the interactions between the methyl groups increase as the molecules are packed closer together.

The $(CH_3)_2TlX$ (X = Cl, Br, I) complexes have been similarly investigated at high pressures [53]. High-pressure IR and Raman spectra revealed a phase transition in all three complexes. The first transition, which again involves ordering of the methyl groups, occurred at ~15 kbar for the chloride and just below 10 kbar for the bromide and iodide. A second transition was observed at higher pressures, 25 kbar for the chloride, 27 kbar for the iodide, and 45 kbar for the bromide. This second transition involves a doubling of the unit cell and bending of the $[(CH_3)_2Tl]^+$ ions. The iodide and bromide also showed significant changes in the lattice region in the second phase indicating a disruption of the $(TlCl)_n$ layers.

The NH_3 groups in the hexaamminenickel(II) halides, $[Ni(NH_3)_6]X_2$ (X = Cl, Br, I), have considerable rotational freedom at ambient pressure. Several high-pressure investigations using a variety of methods have detected phase transitions in all three complexes. Electronic spectroscopy indicated a phase transition at ~70 kbar [54], while a phase transition at 27 K and 5.6 kbar was observed in $[Ni(NH_3)_6]I_2$ by inelastic neutron scattering [55]. Far-IR measurements for hexaamminenickel(II) and hexaamminecobalt(III) halides under compression also detected phase transitions, which involved a lowering of symmetry [56]. No explanation for the nature of these transitions was proposed.

A more recent high-pressure IR investigation of the $[Ni(NH_3)_6]X_2$ (X = Cl, Br, I) complexes were undertaken under hydrostatic conditions to obtain a better understanding of their phase-transition behavior [57]. In all three compounds, the $\nu_{as}(NH)$ and $\rho(NH)$ modes shifted to higher wavenumbers with increasing pressure, while the two NH_3 bending modes showed negative pressure dependences (Fig. 1.12). The magnitude of the pressure shift for the $\delta_s(NH_3)$ mode, -0.75 to -0.9 cm^{-1} $kbar^{-1}$, was much greater than is usually observed for bending modes under compression, indicating that this mode is strongly coupled to a soft mode. A phase transition, detected by the splitting of the vibrational bands, was observed close to 51 kbar for X = Cl and Br and 23 kbar for X = I. New bands were noticed, particularly on the high wavenumber side of the $\delta_s(NH_3)$ mode, which gained intensity with further increases in pressure. Less splitting in the iodide complex indicated a higher symmetry in the high-pressure phase of this complex compared to that for the chloride and bromide complexes. This splitting of the internal modes of the NH_3 group indicates that the transition involves an ordering of the NH_3 groups. A similar effect was observed at low temperatures, but the low-temperature phase and high-pressure phases are not the same.

Ferrocene and other metallocenes exhibit phase transitions with changes in temperature, generally of the order-disorder genre, involving rotational disorder of the π-cyclopentadienyl (Cp) ring and/or reorientational mechanisms. For example, at 169 K there is an order-disorder phase change in ferrocene, Cp_2Fe, followed at 163.9 K by

Figure 1.12. Infrared spectra at various pressures and the pressure dependence of selected IR modes of (a) $[Ni(NH_3)_6]Cl_2$ and (b) $[Ni(NH_3)_6]Br_2$. * = ν_3 of NO_3^-. Reprinted with permission from D. M. Adams and J. Haines, J. Phys. Chem., 95 (1991) 7068-7071. ©1991 American Chemical Society.

(a)

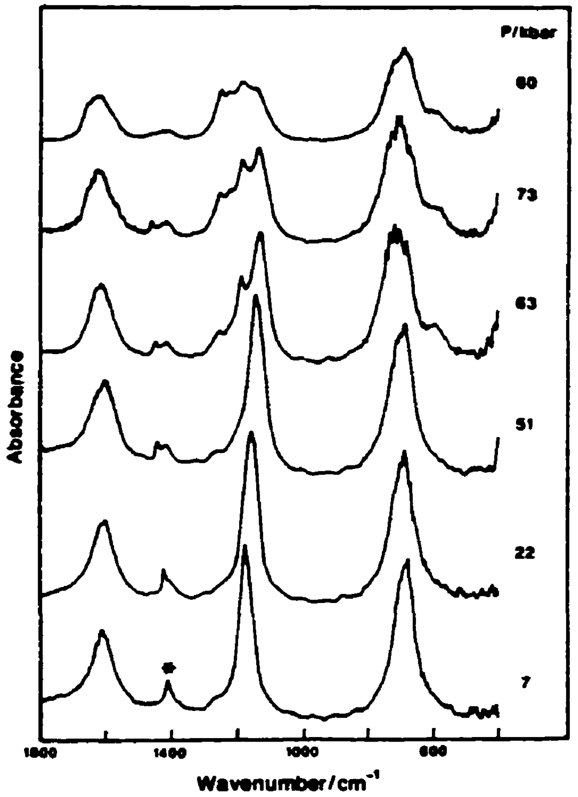
P/kbar
80
73
63
51
22
7
*
Absorbance
1800
1400
1000
600
Wavenumber/cm^{-1}

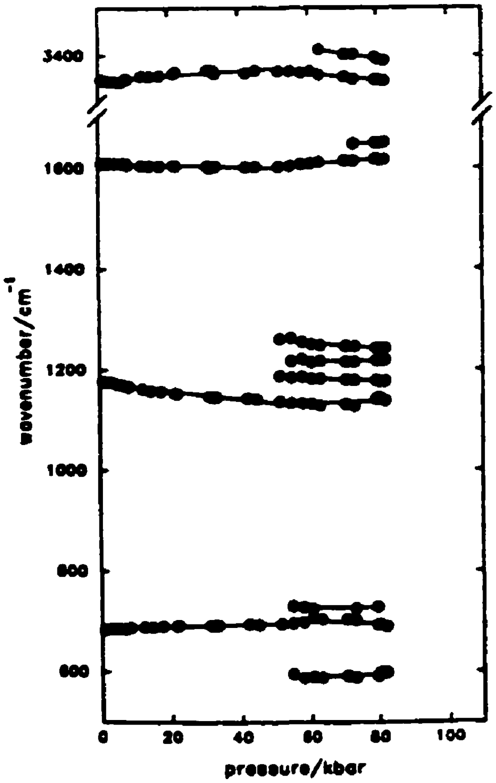
3400
1600
1400
1200
1000
800
600
wavenumber/cm^{-1}
0
20
40
60
80
100
pressure/kbar

(b)

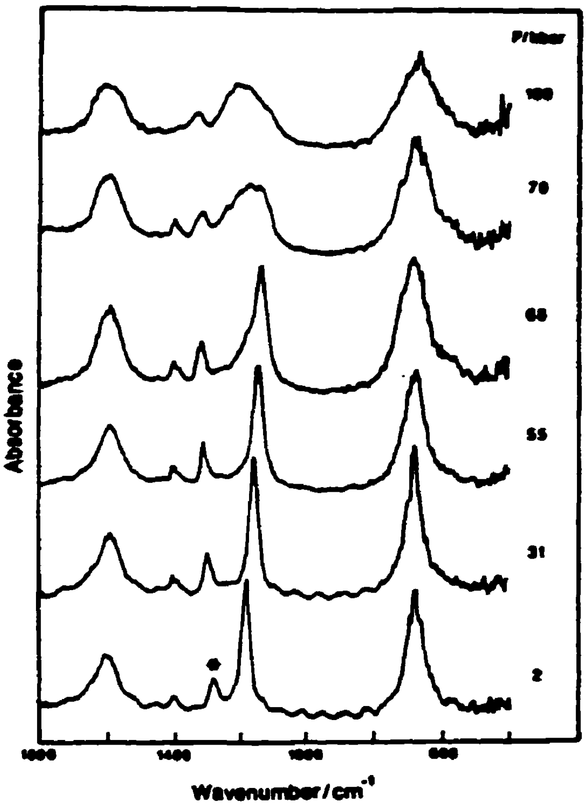
P/kbar
100
70
65
55
31
2
Absorbance
1800
1400
1000
600
Wavenumber/cm⁻¹

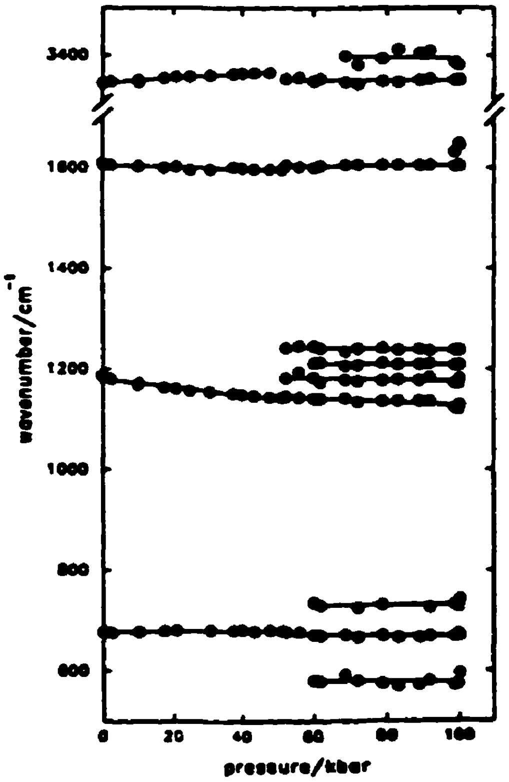
3400
1600
1400
1200
1000
800
600
wavenumber/cm⁻¹
0
20
40
60
80
100
pressure/kbar

a first-order structural phase change to ferrocene-II [58]. The initial IR spectrum of ferrocene at pressures up to 50 kbar showed a sluggish phase change between 10 and 16.5 kbar [59]. The most dramatic changes were observed for three bands normally inactive under strict D_{5h} symmetry, but which are permitted in the solid state. These bands show a continuous increase in intensity with increasing pressures. The infrared spectrum of $[Cp_2Fe]PF_6$ was recorded at various pressures up to 85 kbar [60]. Three modes in particular showed interesting behavior under pressure (Fig. 1.13). The CH bend, ν_5, displayed a discontinuous change between 4.8 and 5.5 kbar. The CH bend, ν_3, split into a doublet in the same pressure regime and a band at 1347 cm^{-1} showed a dramatic increase in intensity between 4.8 and 5.5 kbar, but changed very little above 5.5 kbar. Discontinuities in the pressure shift of the electronic transition bands were also observed below 10 kbar. The dramatic changes in the IR spectra suggest that the mechanism for this transition involved perhaps orientational order-disorder for the $[Cp_2Fe]^+$ cation. The solid-state IR spectra of ferrocene, Cp_2Fe, nickelocene, Cp_2Ni, and ruthenocene, Cp_2Ru, exhibit significant changes upon compression to 120 kbar [61]. The CH bend, ν_5, shows a large continuous increase in intensity with pressure, except for Cp_2Ru, in which a splitting of the band to a doublet is observed. The antisymmetric ring breathing mode broadens considerably, as does the CH bend, ν_{18}, the latter eventually splits into a doublet for Cp_2Fe and a triplet for Cp_2Ni and Cp_2Ru at high pressures. These observations have been explained by considering the result of increased intermolecular coupling, since there are at least two molecules per unit cell and there exist several coincidences between the IR and Raman frequencies. If there is an intermolecular interaction that couples vibrational motions of the two molecules a vibration, which is normally only Raman active, may become dipole allowed and appear in the IR. As the coupling increases, already dipole-allowed modes will be affected and increase in intensity. This model was used to explain the observed changes of the increasing intensity of certain bands and a broadening of others. New bands observed in the 900-800 cm^{-1} region at higher pressures are coincident with normally Raman-active modes at ambient pressure. The observed

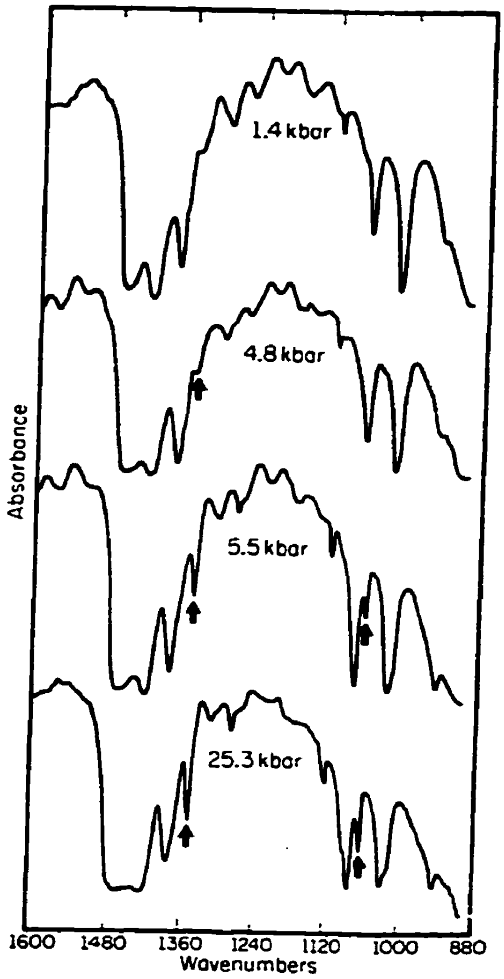

Figure 1.13. Portion of the IR spectrum of polycrystalline $[Cp_2Fe]PF_6$ at four different pressures. Reprinted from Chem. Phys. Lett., 143(6) R. T. Roginski, A. Moroz and H. G. Drickamer, "High Pressure Spectroscopic Study of Ferrocenium Hexafluorophosphate: Pressure-induced Order-disorder Transitions" (1988) 577-579, with kind permission of Elsevier Science-NL, Sara Burgerhartstraat 25, 1055 KV Amsterdam, The Netherlands.

changes for the $[Cp_2Fe]^+$ cation must then also involve an increase in intermolecular coupling.

Pressure-tuning of the electronic levels of Cp_2Fe, $[Cp_2Co]PF_6$ and Cp_2Ni showed that the ligand field parameters, Δ_1 and Δ_2, for these metallocenes change with pressure in a manner that increases the magnitude of the splitting between the core levels between 2 and 8% for a 100 kbar pressure change [62]. Simple ionic compounds show larger changes of the order 7 to 15% in 100 kbar. The Racah parameter, B, is almost independent of pressure for the metallocenes, while, for ionic compounds, B increases by 10-15% under compression up to 100 kbar. These differences have been attributed to the already very large covalent character of the metallocenes, the pressure not enhancing covalency. On the other hand, compression of ionic compounds increases the *d*-electron overlap with the ligand orbitals resulting in a greater *d*-electron shielding and a decreased electron-electron repulsion.

It appears that under compression, ligands, which normally exhibit free rotation under ambient conditions, become ordered most likely as a result of increased intermolecular interactions.

1.4.5 Pressure-Tuning of Quasi One-Dimensional Materials

In halogen-bridged mixed-valence complexes of the general composition, $[ML_4][MX_2L_4]Y_4$, a linear chain forms with alternating long and short metal-to-halogen bonds: $—Pt^{II}—Br\text{-}Pt^{IV}\text{-}Br—Pt^{II}—Br\text{-}Pt^{IV}\text{-}Br—Pt^{II}—Br\text{-}Pt^{IV}\text{-}Br—$. A network of ligands and ions forms a template to which the metal and X atoms tend to adjust to along the chain. The choice of L and Y will dramatically influence the separation between metal atoms, which appears to determine Peierls distortion, ρ (the ratio of the short-to-long M-X bond lengths) and the charge-density wave (CDW) state. The Raman-active chain mode, ν_1, associated with the symmetric M-X vibration of Pt^{IV} and the energy of the bandgap, E_g, increase monotonically as ρ decreases. The application of hydrostatic pressure is an ideal method for tuning ρ. A combination of absorption and Raman spectroscopies, and diffraction techniques have been used to study the structure and CDW state of these linear chain complexes under applied pressure. These materials are of interest because of their semi-conductor properties; the cyanoplatinate compounds possess nearly metallic electrical conductivities. These complexes have also aided in the development of the theory of the one-dimensional state, 1-D conduction properties, and associated phenomena such as Peierls distortions and CDW.

A series of complexes of the type $M(A)X_3$ [M = Pd, Pt; A = $(NH_3)_2$, $(C_2H_5NH_2)_4$, en, and X = Cl, Br, I] has been studied under compression over a wide range of pressures up to ~150 kbar [63]. Conductivity measurements under pressure showed an increase in conductivity, for all the different types of complex. The rate of increase, and a leveling off of the conductivity at higher pressures, was shown to be dependent on the metal, ligands and halide present. X-ray diffraction studies indicated that compression in the chain direction was occurring, increasing orbital overlap in the chain direction [62].

Spectral measurements revealed a red shift of the inter-valence, charge-transfer (IVCT) band for the mixed valence complex $[Pt(en)_2][Pt(en)_2Br_2](SO_4)_2{\cdot}6H_2O$ with increasing pressure [64]. These results indicate a decrease in the energy gap in the mixed valence Pt(II) and Pt(IV) states, leading to a system with essentially Pt(III) and the bromide lying at the midpoint of the platinum centers.

The Raman-active ν_1 chain modes for the complexes $[Pt(en)_2][Pt(en)_2Cl_2](ClO_4)$ [65] and $Pt(Br)_6(NH_3)_4$ [66] have negative pressure shifts with initial increases in pressure. These shifts are consistent with the template effect and a preferential shortening of the long, weaker Pt(II)-X bonds. For the ethyldiamine complex [65], a continuous shift of the ν_1 Pt-Cl stretch was observed to 30 kbar, at which pressure a shoulder on the high wavenumber side of the band appeared (Fig. 1.14). This shoulder steadily gained intensity with further increases in pressure, at the expense of the original band. The original phase was found to coexist with the new high-pressure phase up to at least 60 kbar, the maximum pressure attained. The new high-pressure phase was not identified. For the amine complex, three pressure

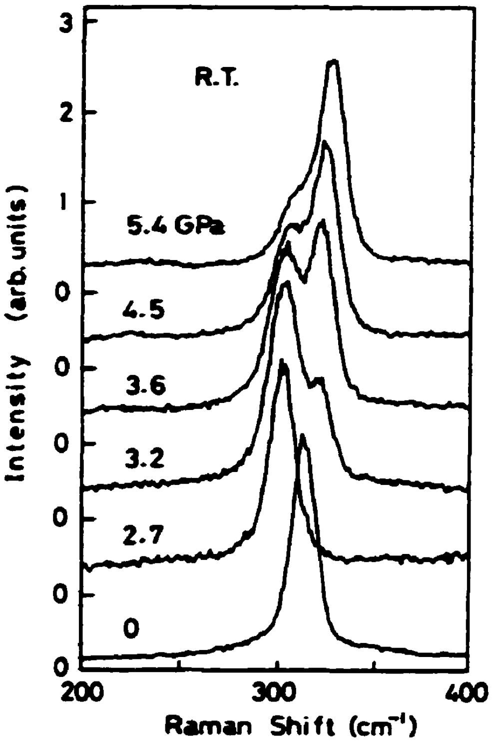

Figure 1.14. Raman spectra of the Pt-Cl stretch mode of $[Pt(en)_2][Pt(en)_2Cl_2](ClO_4)_4$ at various pressures. Reprinted with permission from N. Kuroda, M. Sakai, Y. Nishina and K. Sasaki, Phys. Rev. lett., 68 (1992) 3056-3059.

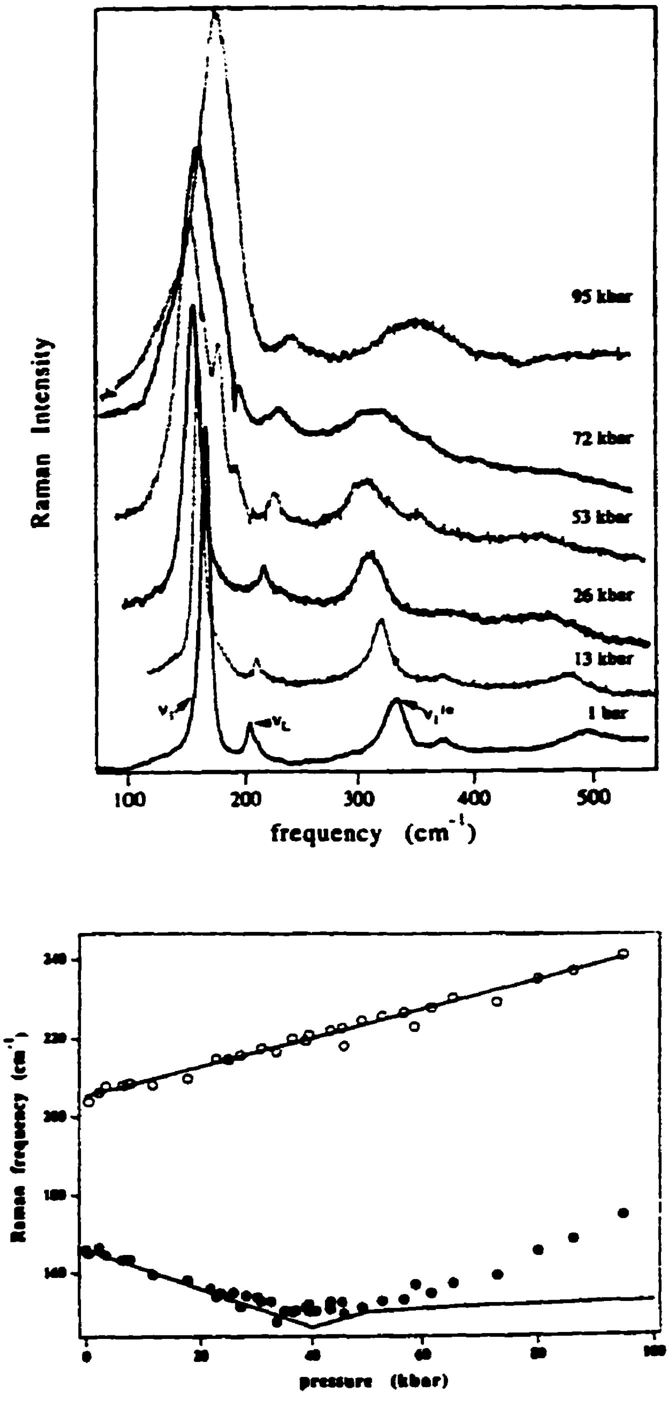

Figure 1.15. (a) Raman spectra of $Pt_2Br_6(NH_3)_4$ at various pressures. (b) The pressure dependence at 300 K of the Raman-active chain mode ν_l (solid circle) and ν_L (hollow circle), the symmetric stretch mode of the equatorial Br ligand in $Pt_2Br_6(NH_3)_4$. Reprinted with permission from G. S. Kanner, J. Tinka Gammel, S. P. Love, S. R. Johnson, B. Scott and B. I. Swanson, Phys. Rev. B, 50 (1994) 18682-18685.

domains were observed from ambient pressure to 95 kbar (Fig. 1.15) [66]. From 1 bar to 30 kbar, ν_1 decreased in frequency. Between 30 and 40 kbar, the slope was essentially zero as each bromide was now mid-point between the platinum atoms, these becoming equivalent. At even higher pressures, the sign of the slope changed such that, above 80 kbar, ν_1 exceeded the ambient pressure value. This result could be because at shorter distances there is a repulsion between the Pt and axial Br leading to a bending of the chains to afford a more zigzag structure, at high pressures. A positive shift of the ν_1 mode is observed in 3-D solids, in the absence of a phase transition.

High pressure absorption, luminescence and Raman spectroscopic studies of Wolframs' red salt, $[Pt(en)_4][Pt(en)_2Cl_4](Cl\cdot H_2O)_4$ (en = ethylamine) [67] up to 34 kbar showed a similar response to compression. A rapid decrease of the energy gap below 20 kbar was explained by the increase in $d(Pt^{IV}\text{-}Cl)$ as $d(Pt^{II}\text{-}Cl)$ decreases with increasing pressures.

A more extensive study of the pressure dependence of the electronic spectra of quasi 1-D semiconductors of the type $K_4[Pt_2(P_2O_5H_2)_4X]\cdot 3H_2O$, X = Cl, Br, ($Pt_2X$), has been made by Stroud *et al.* [68]. The electronic spectrum of these complexes includes bands attributable to the reduced complex, $[Bu_4N]_4[Pt_2(P_2O_5H_2)_4]$ (Pt_2), to the oxidized complex, $K_4[Pt_2(P_2O_5H_2)_4X_2]\cdot 2H_2O$ (Pt_2Cl_2), and an intense IVCT band. The IVCT band corresponds to $d\sigma^* \rightarrow d\sigma^*$ electron transfer along the chain axis from a Pt_2 dimer to an adjacent Pt_2X_2 dimer (Fig. 1.16(a)). For Pt_2Cl, the IVCT band is located at 18,600 cm^{-1}, while in the more delocalized Pt_2Br complex, it is found at lower energy at 16,100 cm^{-1}. As the pressure is increased, the IVCT band shifts to lower energy leveling off at ~40 kbar for both Pt_2Cl and Pt_2Br. The decrease was of the order of -75 and -100 cm^{-1} $kbar^{-1}$, respectively. These changes are consistent with a continuous change towards a more symmetric structure, with the halogen located equidistant between adjacent Pt_2 dimers, leading to a decrease in the energy difference of $d\sigma^*$ on adjacent Pt_2 dimers. Other spectral changes indicated a destabilization of the $d\sigma^*$ and $p\sigma$ levels through increased orbital overlap and *d*/*p* mixing, and a

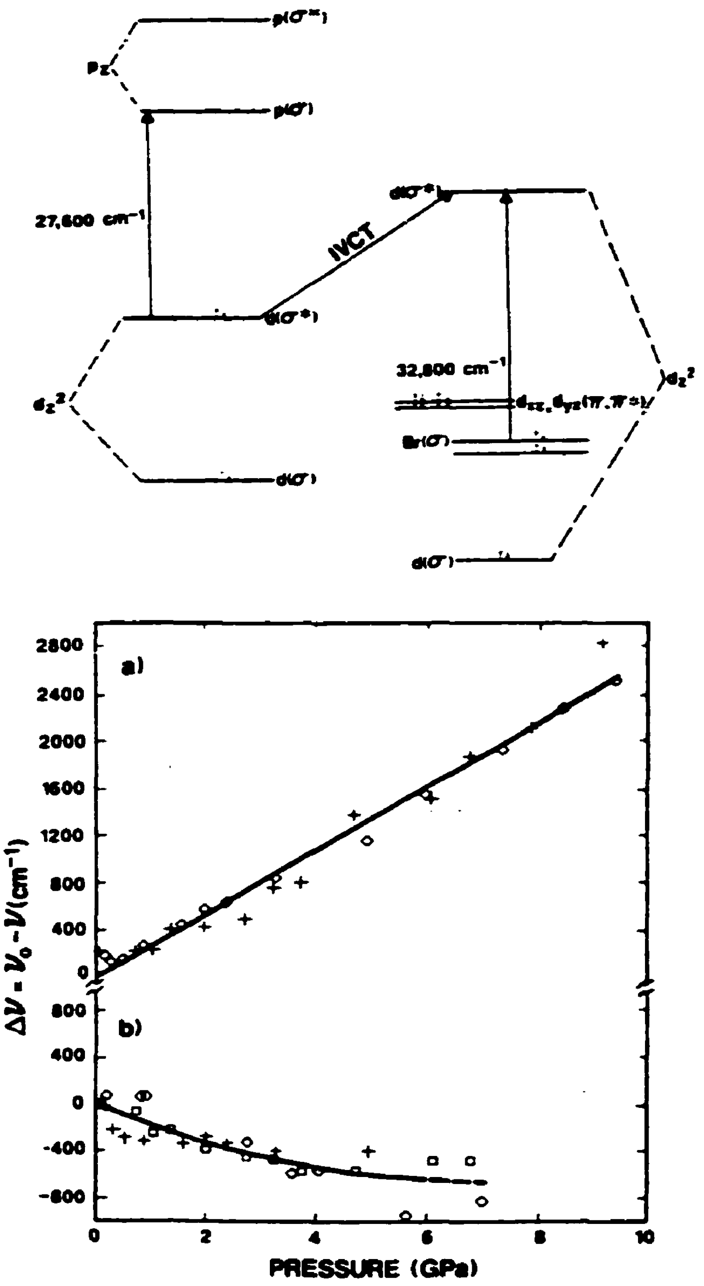

Figure 1.16. (a) Energy level diagram for Pt_2Br at ambient pressure. (b) Pressure shift of the σ(Br) $\rightarrow$ $d\sigma^*$ transition (top) and the $d\sigma^* \rightarrow p\sigma$ transition (bottom) in Pt_2Br. Reprinted with permission from M. A. Stroud, H. G. Drickamer, M. Heinrichs Zeitlow, H. B. Gray and B. I. Swanson, J. Am. Chem. Soc., 111 (1989) 66-72. ©1989 American Chemical Society.

destabilization of the $d_{x^2-y^2}$ level at high pressure through increased ligand field interactions (Fig. 1.16b).

The effect of pressure on the $\sigma \rightarrow \sigma^*$ ($\nu_o = 14.7 \times 10^3$ cm^{-1}) and $\pi \rightarrow \sigma^*$ ($\nu_o = 20.8 \times 10^3$ cm^{-1}) metal-metal charge transfer bands in the visible spectrum of $[Pt_2(NH_3)_4(C_5H_5NO)_2]_2(NO_3)_5$ (**8**) dispersed in a polystyrenesulfonic acid (PSSA) medium were measured up to 134 kbar [69]. Other platinum blue tetramers of this type have been synthesized and characterized from which a correlation between the average Pt_4 chain length and the location of the two absorption bands in the visible absorption spectrum was noted, the higher energy band showing a more significant shift with varying chain length. Pressure-tuning of the complex $[Pt_2(NH_3)_4(C_5H_5NO)_2]_2(NO_3)_5$ revealed a dramatic blue-shift of both the bands with increasing pressure: 1690 cm^{-1} and 2020 cm^{-1} for the 14.7×10^3 cm^{-1} and 20.8×10^3 cm^{-1} bands, respectively, over 120 kbar (Fig. 1.17). These results corroborate an electronic model proposed for these complexes and confirm that the change in Pt-Pt distance determines the shift of the absorption bands. A pressure-induced disproportionation, as seen for the tetramer in aqueous media, was observed in the polymeric medium; a significant decrease in the area of the 14.7×10^3 cm^{-1} band and a concomitant increase of the 20.8×10^3 cm^{-1} band with increasing pressure was observed. From calculations, the $\sigma \rightarrow \sigma^*$ transition (14.7×10^3 cm^{-1}) originates from an orbital which involves a net bonding interaction between the inner two platinum atoms and two antibonding interactions between the two sets of outer platinum atoms. The $\pi \rightarrow \sigma^*$ transition, (20.8×10^3 cm^{-1}) however, involves excitation from an orbital of two separate weak π interactions between the outer and inner Pt-atoms and an essentially non-bonding interaction between the inner Pt-atoms.

Earlier work on the partially oxidized tetracyanoplatinates, e.g. $K_2[Pt(CN)_4]Br_{0.3}\cdot 3H_2O$, showed the increasing conductivity parallel to the chain axis with increasing pressures, and a concomitant decrease in the Pt-Pt distance along the chain [70,71,72]. Magnus' green salt, $[Pt(NH_3)_4][PtCl_4]$, and related complexes, contain planar $[Pt(NH_3)_4]^{2+}$ and $[PtCl_4]^{2-}$ units which stack in columns in the crystal forming metal chains. The solid-state properties of these materials, e.g., anisotropic

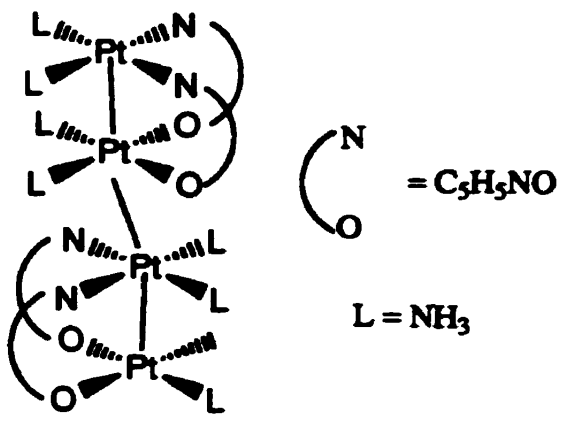

8

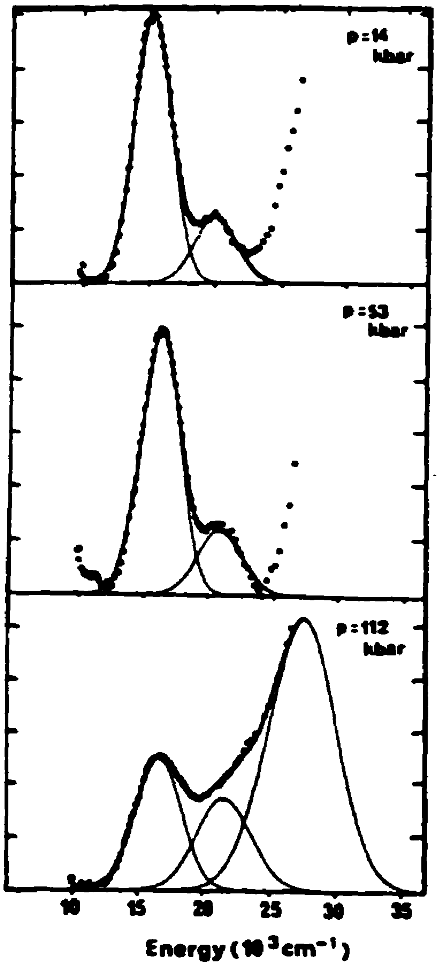

Figure 1.17. Visible spectrum of $[Pt_2(NH_3)_4(C_5H_5NO)_2]_2(NO_3)_5$ in PSSA at 14, 53 and 114 kbar. Reprinted with permission from Chem. Phys. Lett., 149() J. L. Coffer, J. R. Shapley and H. G. Drickamer, "A Pressure Tuning Spectroscopic Study of cis-Diammine α-Pyridone Platinum Blue" (1988) 487-490, with kind permission of Elsevier Science-NL, Sara Burgerhartstraat 25, 1055 KV Amsterdam, The Netherlands.

conductivity, are due to the direct interaction between the metal atoms. Electrical, spectral and X-ray diffraction measurements carried out at pressures up to ~17 kbar [73] show a continuous change in the lattice parameters and conductivities. The rate of change was dependent on the metal and the initial metal-metal distance in the chain.

Various metal-glyoxime complexes also stack to form one-dimensional systems with the associated optical and electrical properties. A sharp absorption band observed in the crystalline state has been assigned to the optical n*d* → (n+1)*p* interbond transition. This transition is intensified in the crystal by borrowing intensity from a metal-to-ligand charge-transfer excitation. A large, red shift of this band, -6×10^{-3} cm^{-1} over 100 kbar, and considerable broadening was observed [74]. This shift was originally ascribed to an electrostatic interaction. A rapid decrease in the electrical resistance of these complexes under pressure and the red shift of the absorption band, suggested a decreasing band-gap between the filled nd_{z^2} valence band and $(n + 1)p_z$ conduction band, as the inter-chain metal-metal distance decreased [75]. Resistance minima, as observed for many of the quasi 1-D complexes, are the consequence of a pressure-induced metal → ligand electron transfer. High-pressure IR spectroscopy [76] showed a negative pressure shift of one ν(CN) mode, with a second ν(CN) mode disappearing over 17 kbar. A negative pressure shift of the ν(CN) mode indicates an increase in π-backbonding from the metal into a π*-orbital of CN. A more recent high-pressure absorption study of Ni, Pd and Pt glyoximes confirmed the shift to lower energy with increasing pressure of the n*d* → (n+1)*p* interband transition [77]. For the Ni and Pd glyoximes, the shift tended to level at higher pressure, but for the Pt complex a reversal of the shift, at sufficiently high pressures, was observed. The initial response to pressure is to further stabilize the excited state, (n + 1)*p*, in the order Pt > Pd > Ni, due to the greater spatial extent of orbitals with larger n-values. At sufficiently high pressures, the overlap repulsion of the Pt *p* orbitals results in the observed blue shift. Intensity borrowing was thought to be the major cause of the dramatic changes in the peak intensities with increasing pressure.

1.4.6 Others

In the previous section, the pressure-tuning of the charge-transfer bands, or more specifically, the IVCT band, of the quasi one-dimensional platinum complexes and related complexes, was discussed. The effect of pressure on the charge-transfer band or intervalence-transfer (IT) band, corresponding to an inter-ionic electron transfer, has also been studied. A series of 1′,1‴-disubstituted biferrocenium cations with several different substituents and counterions was examined at pressures up to ~150 kbar [78]. The rates of electron transfer varied from relatively valence trapped for complex **9**, to complex **10**, which is valence detrapped. The influence of the anion can influence the rate of electron transfer, as can temperature. Complex **11** becomes valence detrapped at high enough temperatures. Three different types of pressure dependences of the energy of the IT band were seen, which reflected the different arrangement of the anions and cations with respect to one another; alternating anions and cations, cations located in the interlamellar region of clays and segregated cation stacks, in which each cation stack is surround by four stacks of anions. An initial blue shift of the IT band for complexes of alternating and intercalated cation structures results from enhanced intermolecular interactions under compression. At high pressures, a red shift of the IT band dominated in the complexes with alternating stacks, due to increased intramolecular interactions and a reduction in the vibronic coupling in the mixed-valence cation. For the salts with segregated cation stacks, a red shift was observed over the whole pressure range. Similar results were found for the IT bands of the bis(fulvalene)diiron monocation, in various media [crystal lattice, poly(methyl methacrylate) and a zeolite] [79]. The initial blue shift of the charge-transfer bands arose from increased intramolecular interactions and the increase in the energy separation of the bonding ground state and the antibonding excited states of the IT transition with increasing pressure. At higher pressures, but to varying degrees in the different media, intermolecular effects become dominant.

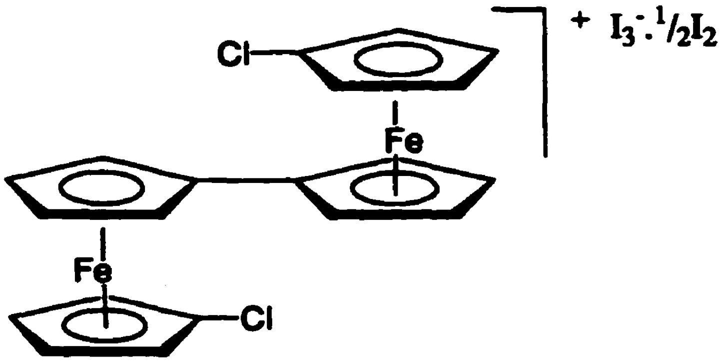

9

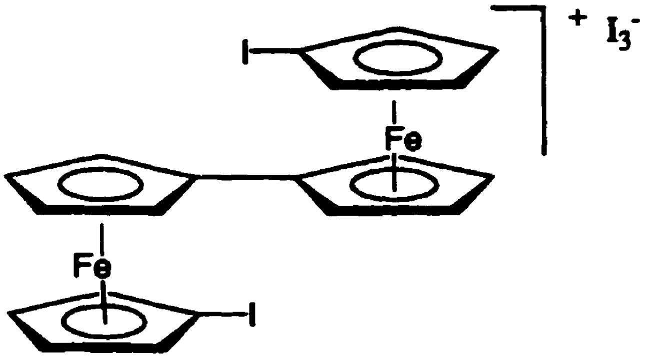

10

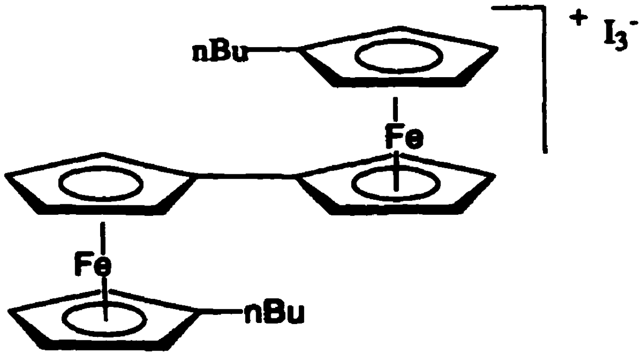

11

The charge-transfer salt, $[Cp_2Co]^+T$, shows a different response to pressure when in solution and dispersed in solid media [80]. The X-ray crystal structure indicates contact ion pairs for $[Cp_2Co]^+T$. In dichloromethane, a blue shift of the charge-transfer band was observed while, in three polymeric media, red shifts of the CT bands were observed. A blue shift can be accounted for as a result of increased intermolecular and inter-ionic interactions through compression. The red shift of the bands in polymeric media is in contrast to the blue shift observed for $[Cp_2Co]^+PF_6^-$ [62].

Although not recorded with a DAC, the charge-transfer band of the ion pair, $[Fe(CN)_6]^{4-}\cdot$DMV (DMV = dimethyl viologen), showed a red shift of ~1700 cm^{-1} over a 10-kbar pressure range [81], in accord with a vibronic coupling model used to describe mixed-valence compounds.

The use of luminescent d^6 transition metal complexes are of current interest as photosensitizers in a number of areas. For luminescent complexes of the general formula, *fac*-$[SRe(CO)_3L]^+$, the triplet excited state can be influenced by the ligands, solvent environment, temperature, and pressure effects. The pressure dependence of the emissions from some Re(I) complexes, *fac*-$[(py)Re(CO)_3(phen)]CF_3SO_3$ and *fac*-$[(QPVP)Re(CO)_3(phen)]CF_3SO_3$ [82], and $[Re(phen)_2(py)_2]^+$ and $[Re(phen)_3]^+$ [83] has been determined. The luminescence characters arise from MLCT [Re $\rightarrow$ π^* phen] phosphorescence at room temperature, the excited state being a triplet state. The emission peak maximum and relative intensity of the different Re(I) samples [81] were shown to decrease with increasing pressures up to 70 kbar, the sample dissolved in the polymer PVP (4-vinylpyridine) showing greater pressure sensitivity than did the same complex dissolved in the polymer PAA [poly (arylic acid)] (Fig 1.18). The increased polarizability of the excited state results in a decrease in the energy of the transition, the difference in the polarizability of the medium influencing the decrease. Thus, the lower polarizability of the polymer substrate resulted in a reduced pressure sensitivity of the emission. The close correlation between the change in peak energy and intensity with pressure was explained using the energy gap law, which shows a linear relation between $\ln K_{nr}$, the non-radioactive decay rate constant, and E_{em}, the

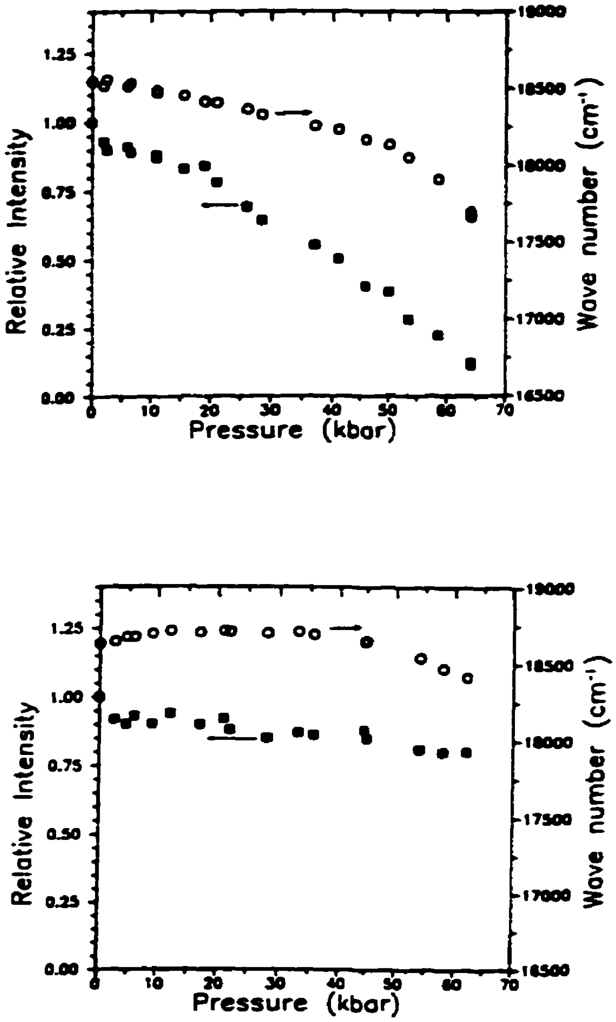

Figure 1.18. MLCT emission energy and relative intensity versus pressure for *fac*-[(py)Re(CO)$_3$(phen)]CF$_3$SO$_3$ dissolved in PVP (top) and PAA (bottom). Reprinted with permission from Chem. Phys. Lett., 192(), J. M. Lang, Z. A. Dreger and H. G. Drickamer, "Luminescence studies of rhenium (I) complexes under high pressure", (1992) 299-302, with kind permission of Elsevier Science-NL, Sara Burgerhartstraat 25, 1055 KV Amsterdam, The Netherlands.

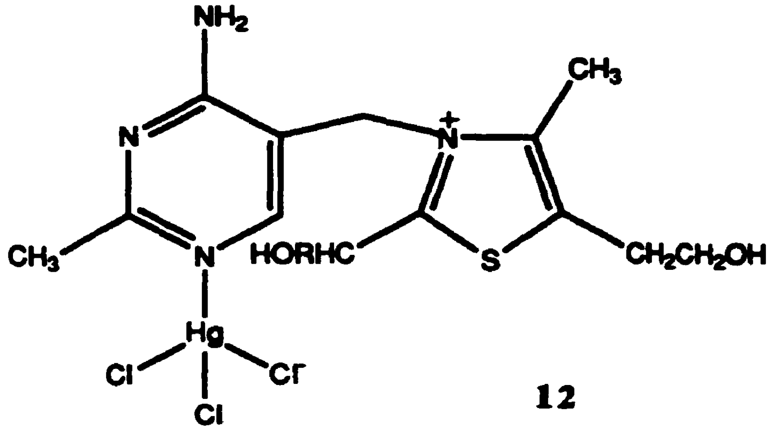

12

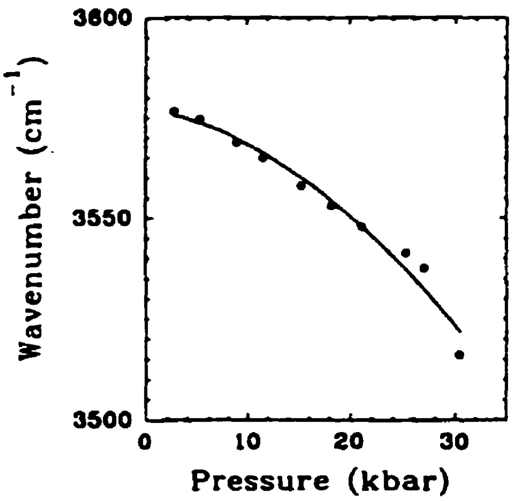

Figure 1.19. Pressure dependence of the ν(OH) stretch of the solid HBT-ligand. Reprinted with permission from I. S. Butler, N. T. Kawai, Y. Huang, M. Louloudi and N. Hadjiliadis, Inorg. Chim. Acta, 196 (1992) 119-122.

emission energy. As K_{nr} increases with pressure, I_{em}, the luminescence intensity, will decrease as E_{em} decreases.

In the biological field, the complexation of bio-ligands to a metal and the subsequent change in the vibrational spectrum have provided important information about the nature of the bonding involved, particularly in biological molecules where several potential ligating sites exist. High-pressure infrared studies up to 30 kbar of a thiamine enzyme intermediate HBT (2-(α-hydroxybenzyl)thiamine chloride) and a mercury(II) complex, Hg(HBT)Cl_3 (**12**), revealed that the S-conformation of the thiamine enzyme was retained under complexation, its rigidity most likely due to hydrogen bonding interactions [84]. The ν(OH) mode at 3577 cm^{-1} in the uncomplexed form showed a negative pressure shift, -0.39 cm^{-1} $kbar^{-1}$ (Fig. 1.19), indicative of an increased hydrogen bonding interaction under pressure.

Pressure-tuning IR and solution Raman studies of 17β-estradiol [85] have aided in the assignment of its vibrational spectrum. Furthermore, pressure-tuning studies revealed hydrogen bonding in 17α-ethynyl-estradiol, which is disrupted upon complexation of an α-[$Cr(CO)_3$] fragment on the arene A-ring. The effects of substitution appeared, however, to be localized to the ring of substitution, most likely because of the ridged nature of the estradiol backbone.

A high-pressure resonance Raman study of the metalloprotein azurin, a blue copper protein, showed that the structure of the protein was essentially independent of pressure up to 36 kbar [86]. The very small shifts of the bands in the 600-100 cm^{-1} region, assigned to the Cu-protein interactions indicated four significant Cu-ligand bonds. Above 36 kbar, a gradual decomposition of the protein occurred, when exposed to laser light. Without exposure to light, the pressure-incuded changes were reversible up to 70 kbar.

Pressure-tuning spectroscopy has been widely used in the study of hydrogen-bonding interactions in a large number of organic and ionic compounds. A negative pressure shift of the hydrogenic stretching frequency is observed as weak-medium hydrogen-bonding increases in strength with increasing pressure [87]. The results from a recent high-pressure FT-IR study on Magnus' green salt, $[Pt(NH_3)_4][PtCl_4]$, and two derivatives, $[Pt(ND_3)_4][PtCl_4]$ (MGS-D) and $[Pt(NH_3)_4][PtBr_4]$ (MGS-Br), are presented in Chapter 4. They indicate that weak hydrogen-bonds of the type N-H...Cl are present in MGS at ambient pressure.

The presence of a hydrogen-bonded hydroxide ion in hydroxyapatites has been a controversial subject for many years. In calcium hydroxyapatite, $Ca_{10}(PO_4)_6(OH)_2$, or HAP, the O...O distance between two OH^- ions in adjacent reticular planes is too large (3.44 Å) for hydrogen bond formation, but the O...O distance between hydroxide and phosphate oxygens is 3.068 Å. However, hydrogen bonding between negatively charged species is expected to be very weak. The low ν(OH) frequency in HAP compared to $Ca(OH)_2$ (3644 cm^{-1}), $Mg(OH)_2$ (3700 cm^{-1}) and a low-pressure phase of $Li(OH)_2$ (3676 cm^{-1}), for example, was used to argue that hydrogen bonding was in fact present in HAP. A recent high pressure vibrational study on HAP and the analogous calcium fluoroapatite, $Ca_{10}(PO_4)_6F_2$, of FAP, concluded that hydrogen bonding does not occur, or is very weak, in HAP [88]. The pressure-induced shift of the internal vibrations of FAP were continuous up to 30 kbar, indicating the absence of any pressure-induced structural transition. For HAP, a distinct break in the ν(cm^{-1}) *vs.* P(kbar) plots at ~20 kbar (IR and Raman) suggested the occurrence of a structural change at this pressure. The dν/dp values for all modes in HAP were positive, before and after the phase transition, with the exception of the OH librational mode, for which dν/dp = -0.15 and -0.02 cm^{-1} $kbar^{-1}$, below and above 20 kbar, respectively. This negative pressure shift of the OH librational mode is due to the rotational motion of the OH groups in apatites, the barrier to motion decreasing with increasing pressure.

A novel route to the formation of endohedral fullerenes has been proposed which involves insertion of an atom into the vacant cavity of the C_{60} fullerene *via* formation of a temporary hole within the fullerene cage while the sample is subjected to high temperatures and pressures. This approach has already proved successful for $^3He@C_{60}$, as well as Ne, Ar, Kr and even Xe. To allow insertion of a larger metal atom, however, a larger hole must first be cut in the C_{60} framework. Rubin and co-workers have recently succeeded in producing a 15-membered hole by the consecutive triple scission of a six-membered ring on the C_{60} surface *via* consecutive pericyclic reactions [89] (**13**). Subsequent oxidative cobalt insertion affords the Co(III) organometallic complex $CpCo(C_{64}H_4)$ ($Cp = \eta^5\text{-}C_5H_5$) (**14**), in which an ethylene bridge acts as a η^2-handle to the metal, Scheme 1.3. We felt that it would be interesting to ascertain whether, upon application of sufficient external pressures to $CpCo(C_{64}H_4)$, the cobalt atom might be encouraged to slip inside the fullerene cage through an 11-membered ring. The results of the high-pressure study are presented in Chapter 6.

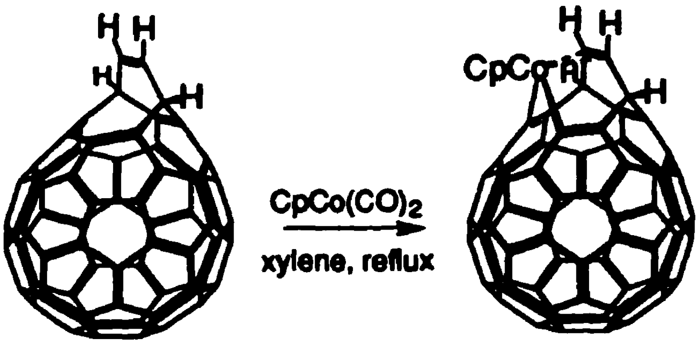

13

14

Ring rotation of a different kind was recently identified in the coordination compounds Ph_4M (M = Si, Ge, Sn, Pb) [90]. A phase transiton, starting at ~15 kbar, resulted in a curved response i.e., curved wavenumber vs. pressure plots, for many of the observed vibrational modes. The compounds have S_4 symmetry at ambient pressure, with the phenyl rings orientated as in a helicopter propeller. As pressure is applied above 15 kbar, the phenyl rings rotate continuously through all angles, about the M-C bond. These results parallel those for the free PPh_3 ligand, where in the ambient pressure form the three phenyl rings are orientated differently. Under pressure, changes in the vibrational mode frequencies are gradual and continuous, suggesting a rotation of the phenyl rings through all angles, resulting in a helical arrangement of the phenyl rings at 50 kbar [91].

1.5 Concluding Remarks

This review, although not exhaustive, covers much of the literature on pressure-tuning spectroscopic studies during the last 15 years. Although the review was limited to spectroscopic techniques (IR, Raman and absorption spectroscopy), it reflects the wide range of coordination compounds studied and the subsequent diversity of the results obtained. Following Chapter 2, in which the theory of pressure-induced vibrational shifts and those of electronic transitions is considered in more detail, Chapter 3 describes the high-pressure Raman study of two complexes $(\eta^6\text{-}C_6H_5CO_2CH_3)Cr(CO)_3$ and $(\eta^6\text{-}C_6H_5CO_2CH_3)Cr(CO)_2(CS)$. As discussed in Chapter 1, Section 1.4.1, under compression, the amount of π-backbonding form a metal to CO or CS ligand can be changed. This study was made to further consider the effect of the ancillary ligand, the arene ring, on the extent of π-backbonding.

1.7 References

---

[1] R. M. Hazen, in The New Alchemists, Times Books 1993.

[2] High-Pressure Research: Application to Earth and Planetary Science, M. H. Maghnani and Y. Syono (eds.), Geophys. Monograph 67, Min. Phys., 2, Terra Scientific Pub. Co. Tokyo, 1992.

[3] D. J. Dunstan, in High Pressure Chemistry, Biochemistry and Materials Science, R. Winter and J. Jonas (eds.) (1993) 101-119.

[4] (a) M. Sakashita, H. Yamawaki and K. Aoki, J. Phys. Chem., 100 (1996) 9943-9947; (b) D. C. Nesting and J. V. Badding, Chem. Mater., 8 (1996) 1535-1539.

[5] J. R. Ferraro, Vibrational Spectroscopy at High External pressures: The Diamond-anvil Cell, Wiley 1984.

[6] (a) H. G. Drickamer, Trends Phys. Chem., 3 (1992) 1-6; (b) H. G. Drickamer, Annu. Rev. Mater. Sci. 20 (1990) 1-17; (c) H. G. Drickamer, Chemtracts: Anal Phys. Chem., 1 (1989) 271-287; (d) H. G. Drickamer, Q. Rev. Biophys. 16 (1988) 89-112; (e) H. G. Drickamer, Acc. Chem. Res., 19 (1986) 329-334.

[7] W. F. Sherman and A. A. Stadtmuller, Experimental techniques in High Pressure Research, John Wiley & Sons 1987.

[8] D. M. Adams and A. G. Christy, High Temp.- High Pressures, 24 (1992) 1-11.

[9] T. P. Russell and G. J. Piermarini, Rev. Sci. Instrum. 68 (1997) 1835-1840.

[10] D. J. Dunstan, Rev. Sci. Instrum., 60 (1989) 3789-3795.

[11] D. D. Ragan, D. R. Clarke and D. Schiferl, Rev. Sci. Instrum., 67 (1996) 494-496.

[12] (a) D. L. Decker, J. Appl. Phys., 37 (1966) 5012-5014; (b) D. L. Decker, J. Appl. Phys., 42 (1971) 3239-3244.

[13] H. K. Mao, P. M. Bell, J. W. Shaner and D. J. Steinberg, J. Appl. Phys., 49(6) (1978) 3276-3283.

[14] S. K. Sharma, H. K. Mao, P. M. Bell and J. A. Xu, J. Raman Spectrosc., 16 (1985) 350-352.

---

[15] W. F. Sherman, J. Phys. C: Solid State Phys., 18 (1985) L973-L978.

[16] (a) R. D. Markwell and I. S. Butler, Can. J. Chem., 73 (1995) 1019-1022; (b) I. S. Butler, C. M. Edwards and R. D. Markwell, Spectrochim. Acta, A, 53 (1997) 2253-2259.

[17] D. D. Klug and E. Whally, Rev. Sci. Instrum., 54 (1983) 1205-1208.

[18] (a) D. M. Adams and I. O. C. Ekejiuba, J. Chem. Phys., 77 (1982) 4793-4795; (b) D. M. Adams, L. M. Davey, P. D. Hatton and A. C. Shaw, J. Mol. Struc., 79 (1982) 415-418.

[19] Y. Huang, I. S. Butler and D. F. R. Gilson, Spectrochim. Acta A, 47 (1991) 909-913.

[20] D. M. Adams, P. W. Ruff and D. R. Russell, J. Chem. Soc. Faraday Trans., 87 (1991) 1831-1836.

[21] Y. Huang, I. S. Butler, D. F. R. Gilson and D. Lafleur, Inog. Chem., 30 (1991) 117-120.

[22] (a) D. M. Adams, P. D. Hatton, A. C. Shaw and T-K. Tan, J. Chem. Soc., Chem. Comm., (1981) 226-227; (b) D. M. Adams, P. D. Hatton and A. C. Shaw, J. Phys., Condens. Matter, 3 (1991) 6145-6158.

[23] D. M. Adams and I. O. C. Ekejiuba, J. Chem. Phys., 78 (1983) 5408-5412.

[24] Y. Huang, I. S. Butler and D. F. R. Gilson, Inorg. Chem., 30 (1991) 1098-1102.

[25] Y. Huang, I. S. Butler and D. F. R. Gilson, Inorg. Chem., 31 (1992) 4762-4765.

[26] Y. Huang, I. S. Butler and D. F. R. Gilson, Inorg. Chem., 31 (1992) 303-305.

[27] D. Lesage, Honours Project Research Report, McGill University, 1994.

[28] H. Li and I.S. Butler, Inorg. Chem., 34 (1995) 1193-1197.

[29] D. M. Adams and P. A. Fletcher, Spectrochim. Acta A, 44 (1988) 437-443.

[30] J. A. Baldwin, I. S. Butler and D. F. R. Gilson, in preparation.

[31] J. L. Coffer, J. R. Shapley and H. G. Drickamer, Inorg. Chem., 29 (1990) 3900-3901.

---

[32] K. L. Bray, H. G. Drickamer, D. Michael, P. Mingos, M. J. Watson and J. R. Shapley, Inorg. Chem., 30 (1991) 864-866.

[33] H. G Drickamer and K. L. Bray, Acc. Chem. Res., 23 (1990) 55-61.

[34] K. L. Bray, H. G. Drickamer, E. A. Schmitt and D. N. Hendrickson, J. Am. Chem. Soc., 111 (1989) 2849-2856.

[35] K. L. Bray and H. G. Drickamer, J. Phys. Chem., 93 (1989) 7604-7609.

[36] K. L. Bray and H. G. Drickamer, J. Phys. Chem., 95 (1991) 559-562.

[37] K. L. Bray and H. G. Drickamer, J. Phys. Chem., 94 (1990) 2154-2159.

[38] For example, (a) G. L. Kubas, C. J. Unkefer, B. I. Swanson and E. Fukushima, J. Am. Chem. Soc., 108 (1986) 7000-7009; (b) L. Wisniewski, M. Mediati, C. M. Jensen and K. W. Zilm, J. Am. Chem. Soc., 115 (1993) 7533-7534.

[39] R. D. Markwell, I. S. Butler, C. M. Edwards, D. H. Burns, A. Fafara, C. Bianchini and M. Peruzzini, J. Am. Chem. Soc., (1998) submitted.

[40] T. L. Carroll, J. R. Shapley and H. G. Drickamer, J. Am. Chem. Soc., 107 (1985) 5802-5803.

[41] T. L. Carroll, J. R. Shapley and H. G. Drickamer, J. Chem. Phys., 85 (1986) 6787-6791.

[42] J. R. Shapley and H. G. Drickamer, J. Clust. Sci., 5 (1994) 145-155.

[43] (a) D. E. Morris, C. D. Tait, R. B. Dyer, J. R. Schoonover, M. D. Hopkins, A. P. Sattelberger and W. H. Woodruff, Inorg. Chem., 29 (1990) 3447-3452; (b) D. E. Morris, A. P. Sattelberger and W. H. Woodruff, J. Am. Chem. Soc., 108 (1986) 8270-8271.

[44] T. L. Carroll, J. R. Shapley and H. G. Drickamer, Chem. Phys. Lett., 119 (1985) 340-343.

[45] R. T. Roginski, T. L. Carroll, A. Moroz, B. R. Whittlesey, J. R. Shapley and H. G. Drickamer, Inorg. Chem., 27 (1988) 3701-3709.

[46] J. L. Coffer, H. G. Drickamer, J. T. Park, R. T. Roginski and J. R. Shapley, J. Phys. Chem., 94 (1990) 1981-1985.

[47] J. L. Coffer, H. G. Drickamer and J. R. Shapley, J. Phys. Chem., 94 (1990) 5208-5210.

[48] R. Chevrel, M. Hirrien and M. Sergent, Polyhedron 5 (1986) 87-94.

[49] J. L. Coffer, J. R. Shapley and H. G. Drickamer, Polyhedron, 8 (1989) 801-804.

[50] D. M. Adams and M. Pogson, J. Phys. C: Solid State Phys., 21 (1988) 1065-1079.

[51] H. den Adel, H. B. Brom, D. J. Ligthelm and R. A. Wind, Physica B, 111 (1981) 171-182, and references therein.

[52] D. M. Adams and J. Haines, J. Chem. Soc., Faraday Trans., 88 (1992) 3587-3589.

[53] D. M. Adams and J. Haines, Spectrochim. Acta A, 49 (1993) 237-248.

[54] M. Pagannone and H. G. Drickamer, J. Chem. Phys., 43 (1965) 4064-4066.

[55] J. Eckert and R. Youngblood, Solid State Commun., 44 (1982) 1393-1396.

[56] D. M. Adams and S. J. Payne, Inorg. Chim. Acta, 19 (1976) L49-L50.

[57] D. M. Adams and J. Haines , J. Phys Chem. 95 (1991) 7068-7071.

[58] (a) I. J. Hyaus and A. Ron, J. Chem. Phys., 59 (1973) 3027-3030; (b) I. J. Hyaus, J. Chem. Phys. Lett., 18 (1973) 399-401.

[59] D. M. Adams and A. D. Williams, J. Phys. Chem. Solids, 41 (1980) 1073-1078.

[60] R. T. Roginski, A. Moroz and H. G. Drickamer, Chem. Phys. Lett., 143 (1988) 577-579.

[61] R. T Roginski, J. R. Shapley and H. G. Drickamer, J. Phys. Chem., 92 (1988) 4316-4319.

[62] R. T. Roginski, A. Moroz, D. N. Hendrickson and H. G. Drickamer, J. Phys. Chem., 92 (1988) 4319-4323.

[63] L. V. Interrante, K. W. Browall and F. P. Bundy, Inorg. Chem., 13 (1974) 1158-1162.

[64] N. Matsushita and N. Kuroda, Mol. Cryst. Liq. Cryst., 256 (1994) 867-872.

[65] N. Kuroda, M. Sakai, Y. Nishina and K. Sasaki, Phys. Rev. Lett., 68 (1992) 3056-3059.

[66] G. S. Kanner, J. Tinka Gammel, S. P. Love, S. R. Johnson, B. Scott and B. I. Swanson, Phys. Rev. B, 50 (1994) 18682-18685.

[67] H. Tanino, N. Koshizuka, K. Kobayashi, M. Yamashita and K. Hoh, J. Phys. Soc. Japan, 54 (1985) 483-486.

[68] M. A. Stroud, H. G. Drickamer, M. Heinrichs Zeitlow, H. B. Gray and B. I. Swanson, J. Am. Chem. Soc., 111 (1989) 66-72.

[69] J. L. Coffer, J. R. Shapley and H. G. Drickamer, Chem. Phys. Lett., 149 (1988) 487-490.

[70] B. Renker, L. Bernard, C. Vettier, R. Comes and B. P. Schweiss, Solid State Commun., 41 (1982) 935-937.

[71] H. Kobayashi, A. Kobayashi, K. Asaumi and S. Minonura, Solid State Commun., 35 (1980) 293-296.

[72] Y. Hara, I. Shirotani and A. Onodera, Solid State Commun., 17 (1975) 827-830.

[73] L. V. Interrante and F. P. Bundy, Inorg. Chem., 10 (1971) 1169-1174.

[74] J. C. Zahner and H. G. Drickamer, J. Chem. Phys., 33 (1990) 1625-1628.

[75] Y. Hara, I. Shirotani and A. Onodera, Solid. State. Commun., 19 (1976) 171-175.

[76] Y. Hara and M. F. Nicol, Bull. Chem. Soc. Jpn., 51 (1982) 1982-1984.

[77] M. Tkacz and H. G. Drickamer, J. Chem. Phys., 85 (1986) 1184-1189.

[78] U. Sinha, M. D. Lowery, W. W. Ley, H. G. Drickamer and D. N. Hendrickson, J. Am. Chem. Soc., 110 (1988), 2471-2477.

[79] U. Sinha, M. D. Lowery, W. S. Hammack, D. N. Hendrickson, and H. G. Drickamer, J. Am. Chem. Soc., 109 (1987), 7340-7345.

[80] T. M. Bockman, H. R. Chang, H. G. Drickamer and J. K. Kochi, J. Phys. Chem., 94 (1990) 8483-8493.

[81] W. S. Hammack, H. G. Drickamer and D. N. Hendrickson, Chem. Phys. Lett., 151 (1988) 469-473.

[82] J. M. Lang, Z. A. Dreger and H. G. Drickamer, Chem. Phys. Lett., 192 (1992) 299-302.

[83] J. M. Lang, Z. A. Dreger and H. G. Drickamer, J. Phys. Chem., 97 (1993) 2289-2294.

[84] I. S. Butler, N. T. Kawai, Y. Huang, M. Louloudi and N. Hadjiliadis, Inorg. Chim. Acta, 196 (1992) 119-122.

[85] S. M. Barnet, I. S. Butler, S. Top and G. Jaouen, Vib. Spectrosc., 8 (1995) 263-277.

[86] S. F. Agnew, J. R. Schoonover, B. I. Swanson and W. H. Woodruff, J. Am. Chem. Soc., 107 (1985) 6716-6718.

[87] S. D. Hamann, Aust. J. Chem., 32 (1978) 11-18, and references therein.

[88] J. Xu, D. F. R. Gilson, I. S. Butler and I. Stangel, J. Biomed. Mater. Res., 30 (1996) 239-244.

[89] M. J. Arce, A. L. Viado, Y.-Z. An, S. I. Khan and Y. Rubin, J. Am. Chem. Soc., 118 (1996) 3775-3776.

[90] S. D. Warner, I. S. Butler and I. Wharf, Coord. Chem. Rev., (1998) submitted.

[91] R. D. Markwell and I. S. Butler, unpublished results.

Chapter 2

Theory and Experiment

2.1 Vibrational Spectroscopy

2.1.1 The Effect of Pressure on Vibrations in Solids [1]

High-pressure infrared and Raman experiments involve the monitoring of the effects, at a molecular level, of changes in the intra- and intermolecular distances that are produced by pressure. The most noticeable effect is pressure-induced frequency shifts. In a completely harmonic approximation, where the force constant operating between two masses is truly a constant and independent of the distance between the masses, the application of pressure would cause no observed frequency shift at all. Therefore, the study of pressure-induced frequency shifts can be considered to be the study of the anharmonicity of atomic and/or molecular interactions.

The frequency, bandshape and intensity of a normal mode of vibration is governed by the masses of the moving nuclei, the magnitudes of the restoring forces as they are displaced along the normal coordinate, the distortion of the electron clouds that accompany the nuclear displacement, and the anharmonic coupling to other vibrational modes. Under compression, the equilibrium spacing between the nuclei changes, which distorts the electron cloud and the restoring forces, while the nuclear masses are not affected. Isotopic substitution experiments, in which the mass changes but everything else remains unaltered, are the complement to the pressure experiment.

The frequency shifts caused by the application of modest, hydrostatic pressures do not usually significantly affect the form of the normal coordinate. As the nature of the vibration is not changed and the mass remains the same, then it is only the force constant change that causes the frequency shift. Many studies focus on the change in effective force constant that comes from the change in internuclear spacing coupled with the anharmonic nature of interatomic, and inter- and intramolecular interactions.

It has been shown that, for both internal and external modes of vibration, the pressure-induced frequency shifts follow directly from the anharmonicity of the bonds coupled with the changes in internuclear spacing caused by the pressure.

The general effect can be seen in terms of an equilibrium spacing, r_e, that results from the balance between one composite attractive potential, V_A, and one composite repulsive potential, V_R, which can be adequately described by

$$V_A = -A - B(r_e + x)^{-n} \tag{2.1}$$

and

$$V_R = C + D(r_e + x)^{-m} \tag{2.2}$$

for sufficiently small deviations, x, from the equilibrium spacing. The total potential energy, V, is

$$V = V_A + V_R \tag{2.3}$$

At equilibrium,

$$\left(\frac{\partial V}{\partial x}\right)_{x=0} = 0 \tag{2.4}$$

It is the force constant d^2V/dx^2 and its dependence on small displacements, x, from the equilibrium position that are of interest. When x is zero, this gives the equilibrium force constant, k_o, and a general expression for d^2V/dx^2 written in terms of k_o:

$$\frac{d^2V}{dx^2} = k_o\left[1 - (n + m + 3)\, x/r_e\right] \tag{2.5}$$

This gives a completely general statement about the anharmonicity close to equilibrium in a force constant that comes from a potential function that can be adequately described as the sum of attractive and repulsive contributions. When this expression is expressed as the percent change in force constant in terms of the percent change in distance,

$$\frac{\Delta k}{k_o} \times 100 = -100(n + m + 3)\, x/r_e \tag{2.6}$$

the anharmonicity of the force constant is clear. If n = 6 and m = 12, as in the Lennard-Jones potential function, and $x = 0.01r_e$, i.e., a 1% deviation from r_e,

$$\frac{\Delta k}{k_o} \times 100 = -(6 + 12 + 3) = -21\% \tag{2.7}$$

Thus, the initial rate of change of force constant for a Lennard-Jones potential function can be expressed as -21% for a 1% change in spacing. For strong covalent bonds, an anharmonicity of -6% for a 1% change in lattice spacing has been calculated and determined by experiment.

These results indicate that weak interactions are more anharmonic than are strong chemical bonds. However, even the strongest bonds, whether in small molecules or in hard crystals, still show an anharmonicity of about -6% per 1% change in spacing. This general statement for bond stretching vibrations can be extended to bending vibrations and both internal and external vibrational modes. The order of frequency shifts with pressure is 1-3 cm^{-1} $kbar^{-1}$ for external modes. For internal bond stretching modes the range is 0.3-1 cm^{-1} $kbar^{-1}$. Bond-bending modes are less affected and are of the order of 0.1-0.3 cm^{-1} $kbar^{-1}$. Any deviations from these values usually arise because of the particular nature of the bonding interactions, e.g. π-backbonding interactions in organometallic complexes, or intra- and inter-molecular interactions, e.g., in hydrogen-bonding.

The volume dependence of a vibrational frequency is contained in the Grüneisen parameter [2,3]. For a vibrational mode of frequency ν_i, as a function of volume V, occupied by the unit mass of a crystal, the corresponding Grüneisen parameter γ_i, can be written as

$$\gamma_i = \frac{-V d\nu_i}{\nu_i dv} = \frac{-d(\ln \nu_i)}{d(\ln v)} \tag{2.8}$$

This relation can be more conveniently written as

$$\gamma_i = -\frac{1}{\kappa_s}\frac{d \ln \nu_i}{dp} \tag{2.9}$$

where κ_s is the isothermal compressibility of the crystal

$$\kappa_s = -\frac{1}{V_S}\left(\frac{\delta V_S}{\delta p}\right)_T \tag{2.10}$$

Values of γ_i for IR and Raman bands of molecular crystals are typically 0.03 to 3.

2.1.2 The effect of pressure on electronic transitions [4]

The initial effect of compression is to stabilize a bonding orbital relative to its antibonding combination, for a given molecular bond. For a transition from the bonding to the antibonding orbital, the energy of the transition increases (blue shift) as the pressure increases. However, in this simple model, the intermolecular interactions experienced by the molecules in the crystal lattice or in solution are not taken into account. The primary intermolecular interaction, for larger molecular ions, is an attractive van der Waals force, which can be expressed as:

$$E \sim -(\alpha_1 \alpha_2 / R^6) \qquad (2.11)$$

where R is the distance between the interacting species, α_1 is the polarizability of the molecule or bond, and α_2 is the polarizability of the medium as seen by the electron cloud of the molecule. In general, although not always, the molecule is more polarizable when the electron is in the antibonding orbital since it is less tightly bound when in the excited state. The contribution of the intermolecular interaction to the pressure shift of an electronic transition is a red-shift, i.e. to lower energy. Many of the examples of pressure-tuning electronic absorption spectroscopy reveal the different degrees of balance between the intramolecular and intermolecular forces.

2.1.3 Phase transitions

It is particularly interesting when the application of pressure induces a phase transition from one crystalline form to another. Phase transitions can be first-order or second-order. The Gibbs free energy, G, is defined for a given mass of material by

$$G = U - TS + PV \qquad (2.12)$$

For two phases to be in thermodynamic equilibrium at a particular pressure and temperature, the Gibbs free energy must be the same for the material in either phase. A transition is referred to as 'first-order' if the first derivative of the free energy is discontinuous at the phase change, e.g., if there is a volume discontinuity, then this indicates a first-order transition because $V = (\delta G/\delta P)_T$. However, if there is no discontinuity in the first derivative of G, but there is a discontinuity in the second derivative, then the transition is termed 'second-order' or continuous. Thus, if the volume changes continuously, but the compressibility shows a discontinuity, then this is a second-order transition and $K = -(1/V)(\delta V/\delta P)_T = -(1/V)(\delta^2G/\delta^2P)$. Plots of frequency *vs.* pressure reveal discontinuities in the slope of the graph at the pressure where a phase transition occurs.

Vibrational soft modes are often associated with a phase transition. A soft mode is a vibrational mode, the frequency of which goes to zero as the temperature or pressure approaches the phase transition temperature or pressure. Structural phase transitions are generally accompanied by crystal distortions or displacements of ions and molecules, the mean value of such a displacement corresponding to an order parameter.

2.1.4 Bandshape and intensities as a function of pressure

There is no single straightforward hypothesis which can be used to treat intensity and bandshape changes as a function of pressure in the way that the frequencies were treated in terms of bond anharmonicities. For a given vibration, that is both the IR and Raman active, the frequency shift with pressure will be the same. However, the band shape can be quite different and changes in a different way. Intensities are complementary, but both may increase, decrease, or change in opposite senses on the application of pressure. In most cases, any bandshape or intensity changes observed are small. Any significant changes are generally associated with a phase change, Fermi resonance, soft modes, hindered rotations, or, uni-axial pressure, for example.

2.1.5 Experimental Procedure

All the high pressure experiments reported in this thesis were performed using a diamond-anvil cell from High Pressure Optics, Tucson, Arizona, which was equipped with two type IIa diamonds. The sample was held within a centrally drilled 300-μm hole of a 260-μm thick stainless-steel gasket. The gasket was held in place over one diamond anvil using plasticine. With the second diamond in place, pressure was applied by simply turning the screw by hand (Fig. 2.1).

The FT-Raman spectra were recorded on a Bruker IFS-88 spectrometer equipped with a Bruker FRA-106 Raman attachment coupled to Nikon Optiphot-2 microscope, with a 4× long-range objective to focus laser illumination and to collect the backscattered radiation. A NIR Nd^{3+}:YAG laser at 1064.1 nm was employed. Typical laser powers were of the order of 50-250 mW. The infrared spectra were measured on a Bruker IFS-48 spectrometer equipped with an A-590 microscope (15× objective), a Sony colour video system and a liquid nitrogen-cooled MCT detector.

The antisymmetric ν(NO) mode of the NO_3^{2-} ion of $NaNO_3$ in a NaBr matrix (0.2-0.4%) was used as the internal pressure calibrant for the FT-IR studies [5]. Pressure calibration in the FT-Raman spectra was by-way-of the diamond t_{2g} phonon line, at 1332.4 cm^{-1} at ambient pressure [6]. Further details regarding the methods of pressure calibration can be found in Chapter 1, Section 1.3. For the pressure calibration in the IR and FT-Raman, errors of ± 1.2 kbar and ± 2 kbar, respectively, are estimated.

Spectral manipulations were made using the Bruker OPUS® software. Peak-fit routines using the Levenberg-Marquardt iteration technique were used determine accurate peak positions, particularly for overlapping peaks. Linear least-squares analyses were used to determine the pressure dependence, dν/dp. Values for dν/dp are quoted to 2 significant figures when the correlation coefficient, r^2, > 0.95. When $0.8 < r^2 > 0.95$, values for dν/dp are quoted to 1 significant figure. If $r^2 < 0.80$, values for dν/dp are quoted only if there are 10 or more data points.

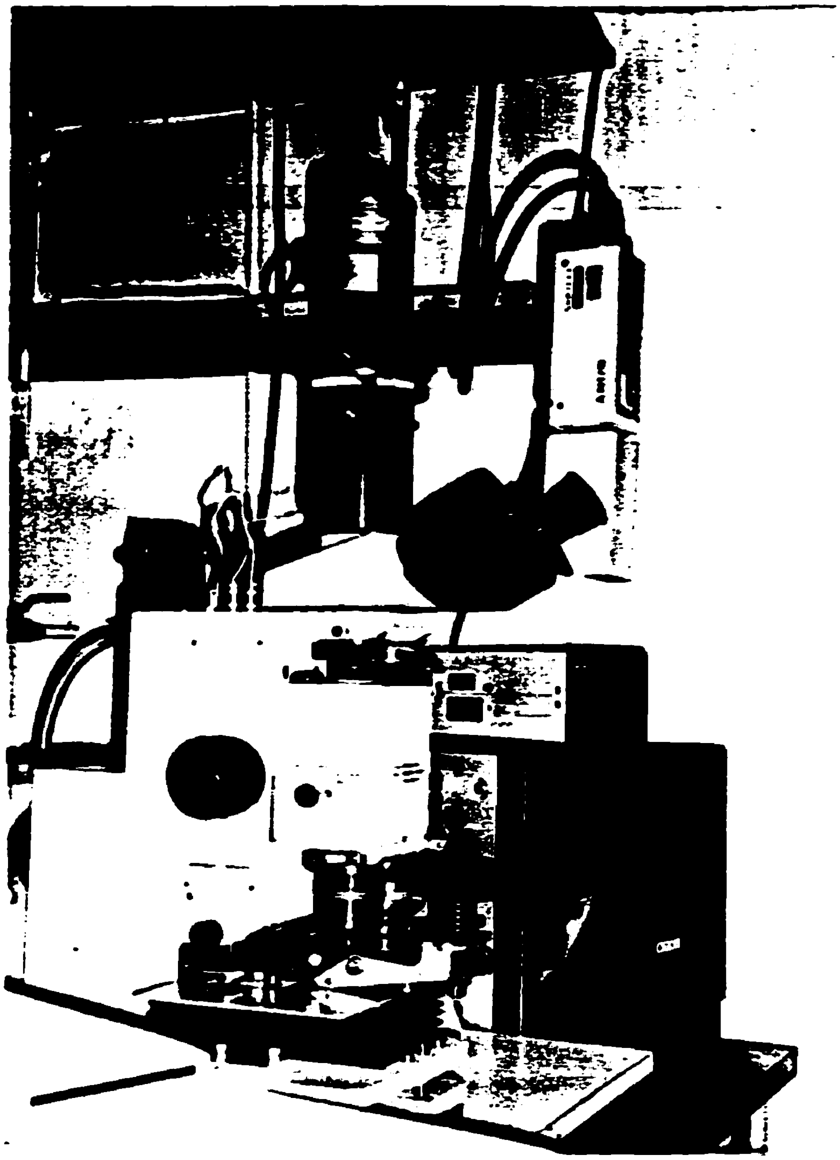

Figure 2.1. The FT-IR microscope and diamond-anvil cell.

2.2 Powder X-ray Diffraction

2.2.1 The Bragg Law

X-rays have a high penetrating power that is ideal for studying solids. A regular array of atoms is analogous to an optical experiment involving a diffraction grating. A grating has a series of parallel lines, evenly spaced, which reflect the incident beam resulting in a cooperative effect, with the interference patterns for each pair of lines adding together to give an extended series of minima and maxima. A two-dimensional grating will give a more complicated pattern, from which the spacing between the two planes can be derived. The crystal is a three-dimensional lattice and thus produces an even more complicated pattern, but this can be simplified by considering the reflecting planes in the crystal. Many descriptions of x-ray diffraction can be found in the literature, see for example reference [7].

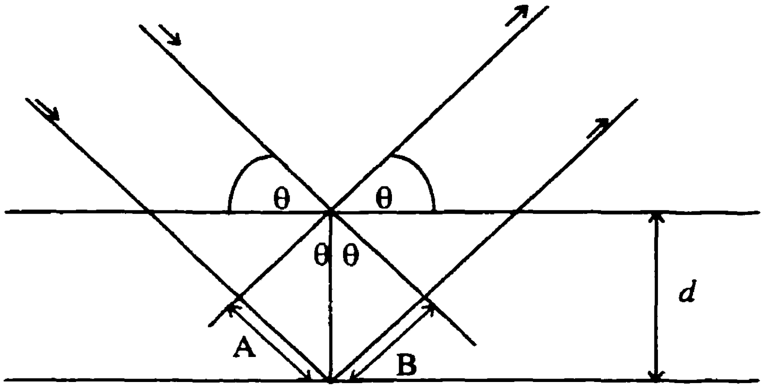

Scheme 2.1. The Bragg Law for parallel planes.

In a 2-D array of atoms, as in Scheme 2.1, the incident beam is reflected, partly from the top row and partly from the second. For constructive interference to occur, the path difference must be a multiple of the wavelength of the incident beam, as expressed by Bragg's Law

$$n\lambda = 2d\sin\theta \qquad (2.13)$$

where d is the distance between the planes, λ is the wavelength in Å of the incident beam and n is an integral. The diagram shows only two scattering planes, but implicit here is the presence of many sets of parallel identical planes, each of which is separated form its adjacent neighbour by the spacing *d*. The locations of the planes are defined by a periodic function whose "wavelength" is related to the dimensions of the unit cell and the orientation of the plane, *hkl*, the Bragg law defining the conditions for constructive interference. The pattern produced depends on the orientation of the crystal with respect to the incident beam but, by changing the orientation, it should be possible to observe all the reflections in turn. Single crystals do not contain just one type of atom, and each atom will have a repeating pattern in the lattice, giving rise to the same set of reflections at the same angle. But because the patterns for various types of atoms do not coincide exactly, the diffracted beams are not in phase. The total intensity of the reflection depends on how far apart the various lattices are, i.e., on the positions of the atoms in the lattice.

In a powder, there are many small crystals, randomly orientated, each capable of diffracting in the normal way. Thus, there can be many reflections. Each plane, at angle θ to the beam, produces a diffracted beam lying on a cone of half-angle 2θ. In principle, each set of (*hkl*) lines will give rise to a diffraction cone. The angle θ can be measured from the location of the diffraction intensity and, if the value of (*hkl*) is known, the value of d_{hkl} can be deduced from the Bragg reflection:

$$(2\sin\theta/\lambda) = h^2a^{*\,2} + k^2b^{*2} + l^2c^{*2} + 2hk\mathbf{a}^*\cdot\mathbf{b}^* + 2hl\mathbf{a}^*\cdot\mathbf{c}^* + 2hl\mathbf{b}^*\cdot\mathbf{c}^* \quad (2.14)$$

Similarly, the position of the reflections can be used to obtain accurate cell dimensions. However, there is a loss of information as each reflection is now described by only one angle and intensity. Reflections may be superimposed or at least unresolved and so indexing can be mostly trial and error.

As well as the collection and interpretation of high-pressure X-ray diffraction patterns for a wide variety of materials, a large part of the research focuses on the development and improvement of the techniques and data processing. Structure determination of low-symmetry materials can be problematic because of many overlapping bands, which can lead to ambiguous indexing schemes or spacegroup determinations. The presence of variable atomic coordinates also creates a degree of structural ambiguity. Another commonly occurring problem in high-pressure diffraction studies is that of preferred orientation, a consequence of the extreme conditions.

One development has been the collection of full 2-D Debye-Scherrer (DS) patterns [8] on an appropriate area detector, such as an image plate. Integration of the complete 2-D diffraction pattern, i.e., the intensities for every point of the same 2θ are averaged to yield the conventional 1-D diffraction pattern, improves the signal/noise ratio of the integrated profile and enhances the accuracy of the peak intensities. The ability to be able to measure very low-angle reflections more accurately greatly improves the accuracy of indexing. Furthermore, space group determination often depends on establishing which reflections are absent. The extent to which one can be confident that a reflection is, or is not, absent is greatly improved by achieving the greatest possible signal/noise ratio. Important information on preferred orientation and effects like deviatoric stress (due to stresses within the sample) can be obtained form the full 2-D image prior to integration. Other developments include using angular-dispersive diffraction techniques and synchrotron radiation.

In the preparation of powder samples for X-ray diffraction, it is important that the crystallites have a "good size", and that there is a random orientation of these micro-crystals. The micro-crystal size is known to influence the intensity of the diffraction peaks. Furthermore, it has been shown that for a pressure-induced phase transformation of ZrO_2, the size of the crystallites determined the pressure of the phase transition [9]. As the crystallite size decreased, higher pressures were required to induce the phase transition. The crystallite size had been selected from 29.3 nm to >100 nm, while the threshold pressure for the phase transition was found to vary from 6.1 to 3.4 GPa, respectively.

2.2.2 The High-pressure Powder X-ray Diffraction Experiment

The powder X-ray diffraction measurements under high pressure were performed using a diamond-anvil cell (DAC) with 500-μm diameter anvil flats. Finely ground potassium chromate, K_2CrO_4 (Strem Chemicals), was placed in a 150-μm drilled hole of an inconel (Ni) gasket, pre-indented to a thickness of 120 microns. A 4:1 methanol-ethanol mixture was employed as a pressure-transmitting medium in one run, whereas in a second run no pressure-transmitting medium was added. Ruby powder was added along with the sample to measure the pressure. About 5 % w/w titanium carbide, TiC, was added to absorb Nd^{3+}-YAG laser radiation. Laser heating was performed at 40 GPa using a 50-W Nd^{3+}-YAG laser in order to attempt to induce a phase transition.

The powder X-ray diffraction experiments were performed in the angular-dispersive mode using zirconium-filtered, molybdenum radiation ($\lambda_{K\alpha}$ = 0.71073 Å) from a fine focus tube. An X-ray capillary optic was used to obtain a 100-nm diameter beam at the sample. The X-ray capillary optic was recently installed in the laboratory and offers several improvements to the high-pressure experiment (Fig. 2.2a). The X-ray beam was quasi-monochromatic, with the K_β intensity at about 3% of that of the K_α radiation. Since the diameter of the beam was focused onto the sample, the possibility of diffraction from the gasket was much reduced. The quality of the diffraction pattern was significantly improved as a result. The rear diamond of the DAC was mounted over a slit allowing access to $2\theta = \pm 40°$. The diffraction patterns were collected on image plates placed at either 83.84 or 147.25 mm from the sample (Fig. 2.2b). Exposure times were of the order of 24 to 60 h. The image plate contains small crystals of BaFBr doped with Eu^{2+}. When a diffracted beam hits the plate an electron in the conduction band is excited and Eu^{2+} is oxidized. In the "read" process, a laser (PhosphorImager) is rastered across the surface of the plate. This causes the electron to fall back into the conduction band and $Eu^{3+} \rightarrow Eu^{2+}$. The

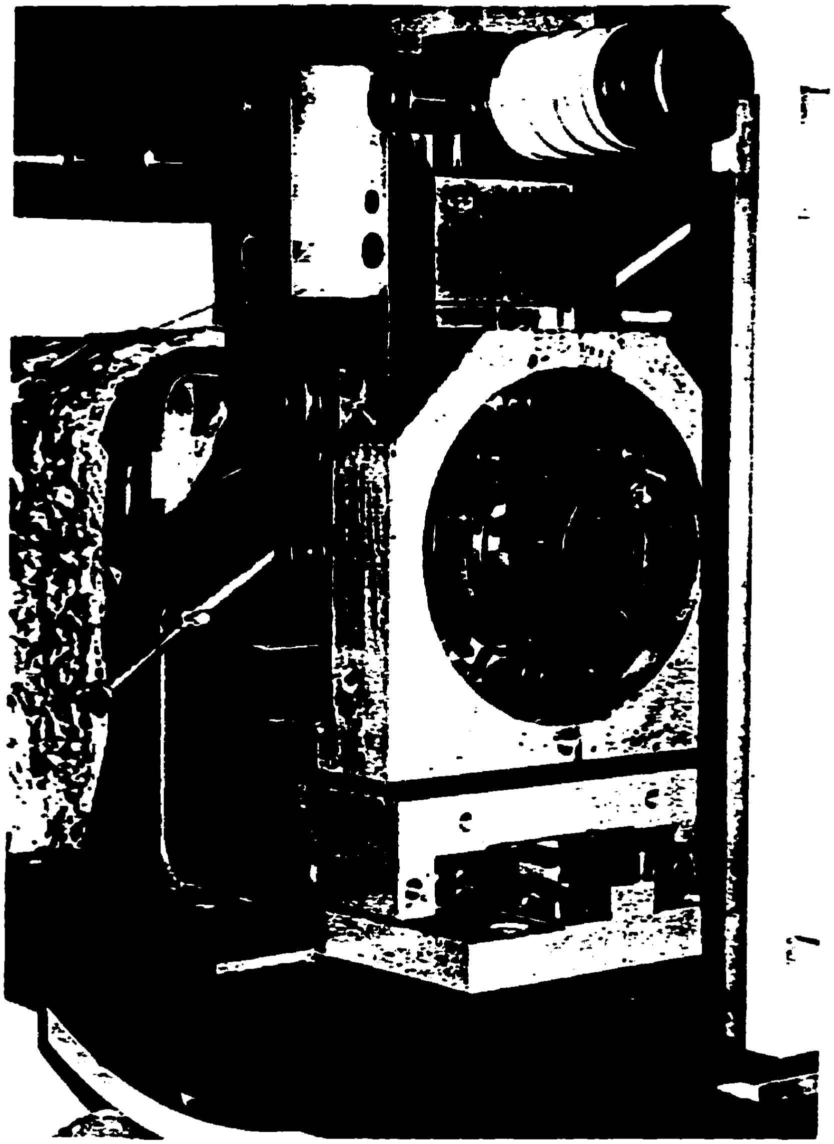

Figure 2.2. (a) The diamond-anvil cell used in the high-pressure powder X-ray diffraction experiments is a lever-arm design. The mount allows precise allignment of the cell in the x, y and z directions.

Figure 2.2. (b) The X-ray capillary optic and image plate.

intensity of the luminescence emitted is proportional to the intensity of the diffracted beam, which originally fell on the plate.

The coordinates of the diamond diffraction spots, and other intense spots due to micro-crystallites in the sample, were located in the 2-D pattern using "Image Quant", and were subsequently removed prior to integration. The program Peak-fit was used to measure the background and peak positions, from which approximate cell constants were calculated. The diffraction patterns were analyzed using whole-pattern fitting and Reitveld refinement methods.

2.2.3 Reitveld Refinement and Whole-pattern Fitting [7]

In whole-pattern fitting, the overall profile is analyzed without reference to any structural model, i.e., set of atomic positions, but approximate cell parameters are required. The observed intensity y_i, at every step *i* of the profile is modeled by a calculated intensity

$$y_{ci} = y_{bi} + \sum_{k=k_1}^{k_2} I_k . \Omega_{ik} \qquad (2.15)$$

where y_{bi} is the background intensity at step i; Ω_{ik} describes the line shape of line k with Bragg angle θ_k; I_k is the integrated intensity of the kth line of the pattern contributing to step i. The line positions are constrained by the cell parameters, but the intensities are free variables. This is a convenient procedure to extract maximum information from patterns of samples with known cell constants but an unknown atomic arrangement. First, a set of lines within the angular range of interest are generated from the approximate cell parameters then the Reitveld formula is used to calculate by iteration the integrated intensities starting from estimated intensities. The main limitation with this method is that if two peaks overlap completely, either accidentally for low lattice symmetry or exactly in the case of a high symmetry lattice, they cannot be separated.

Profile fitting structure refinement, i.e., Reitveld refinement, is the most efficient procedure of powder data analysis when the structure of the sample is at least approximately known. The Reitveld algorithm fits the observed data using as variables the instrumental characterization and the structural parameters of the sample material (cell constants, atomic and displacement parameters).

The refinement minimizes the function

$$M = \Sigma w_i (y_i - y_{ci})^2 \qquad (2.16)$$

where w_i is the weight assigned to each individual step, and y_i and y_{ci} are the observed and calculated intensity at the i^{th} step, respectively. The calculated intensities are determined by summing the contributions of the overlapping Bragg reflections plus the background:

$$y_{ci} = y_{bi} + \sum_{\phi=1}^{phases} S\phi \sum_{k=k_1} j_{\phi k} . Lp_{\phi k} . O_{\phi k} . \left| F_{\phi k} \right|^2 \qquad (2.17)$$

y_{bi} = the background intensity at position 2θ; S is a scale factor, proportional to the volume fraction of the phase; j_k = multiplicity of the k^{th} reflection; Lp_k = Lorentz factor; O_k describes the effects of preferred orientation; $|F_k|$ is a structure factor, including a thermal vibration contribution; Ω_{ik} describes the peak profile function, which approximates the effects of both instrumental and possibly sample parameters.

2.3 References

1. W. F. Sherman and G. R. Wilkinson, in Advances in Infrared and Raman Spectroscopy, Vol. 6, R. J. H. Clark and R. E. Hester, eds., Heydon and Son, London 1980.
2. R. Zallen, Phys. Rev. B: Solid State, B9 (1974) 4485-4496.
3. R. Zallen and M. L. Slade, Phys. Rev. B: Condens. Matter, B18 (1978) 5775-5798
4. H. G. Drickamer, Acc. Chem. Res., (1986) 329-334.
5. D. D. Klug and E. Whalley, Rev. Sci. Instrum., 54 (1983) 1205-1208.
6. R. D. Markwell and I. S. Butler, Can. J. Chem., 73 (1995) 1019-1022; I. S. Butler, C. M. Edwards and R. D. Markwell, Spectrochim. Acta A, 53 (1998) 2253-2259.
7. In "Modern Powder Diffraction", D. L. Bish and J. E. Post (eds.), Rev. Mineral, 20, 1989.
8. For example, M. I. McMahon, R. J. Nelmes, H. Liu and S. A. Belmonte, High Press. Res., 14 (1996) 277-286.
9. S. Kawasaki, T. Yamanaka, S. Kume and T. Ashida, Solid State Commun., 76 (1990) 527-530.

Chapter 3

High-Pressure Vibrational Study of (η^6-arene)Cr(CO)$_2$(CX) Complexes (X = O, S): π-Backbonding to CX Ligands and the Effect of Variation in the Arene Ligand[1]

3.1 Introduction

The thiocarbonyl ligand, CS, is isoelectronic with the carbonyl ligand, CO. However, because the LUMO of the CS ligand is lower in energy and the HOMO is higher in energy than are the corresponding molecular orbitals of the CO ligand, the thiocarbonyl ligand is expected to be both a better σ-donor and π-acceptor ligand. Therefore, one would predict stronger M-CS bonds compared to M-CO bonding interactions for analogous complexes, and the thiocarbonyl complexes should be more thermodynamically stable. However, the number of known transition metal thiocarbonyl complexes belies the prediction. The aim of the present study was to investigate the effects of applied, external pressure on the vibrations of a typical Cr(0) thiocarbonyl complex of the general formula (η^6-arene)Cr(CO)$_2$(CS), and to compare the observed pressure behaviour to that of the parent tricarbonyl complex, (η^6-arene)Cr(CO)$_3$, in order to probe further the nature of the M-CO and M-CS interactions.

The frequencies of the ν(CO) and ν(CS) modes and their behaviour under pressure can tell us a great deal about the extent of π-backbonding from the chromium metal to the CO and CS ligands. Adams and Ekejiueba [1] were the first to report that, under pressure, the amount of π-backbonding from a metal to the π*-orbitals on CO can increase, resulting in a shift of the ν(CO) modes to lower wavenumbers. However, the pressure dependences of these modes are not due simply to one effect, but the result of several competing effects. There are two main effects of pressure on

---

[1] C. M. Edwards, I. S. Butler and R. J. Moore, in preparation.

the complex, with special reference to carbonyls. First, compression of the crystal lattice leads to a shortening of the intramolecular distances and, consequently, to an increase in the vibrational wavenumbers of all the internal modes, including ν(CO). Secondly, increasing the pressure augments the π-backbonding from the metal to the π*-orbitals of the CO groups, resulting in a reduction of the CO bond order and a concomitant decrease in ν(CO). Small positive, or negative dν/dp values for the ν(CO) modes are a good indication of increased π-backbonding to the CO ligand. The extent of π-backbonding is dependent on several other factors, including metal oxidation state and the nature of the other ligands coordinated to the metal center.

3.2 Experimental

The two chromium(0) complexes, $(\eta^6\text{-}C_6H_5CO_2CH_3)Cr(CO)_3$ [2] and $(\eta^6\text{-}C_6H_5CO_2CH_3)Cr(CO)_2(CS)$ [3], were synthesized according to the literature methods. Further details on the high-pressure experiments can be found in Chapter 2, Section 2.1.5.

3.3 Results and Discussion

The $(\eta^6\text{-}C_6H_5CO_2CH_3)Cr(CO)_2(CS)$ complex crystallizes in the triclinic P1 space group and, since there is only the identity symmetry element, the molecule belongs to the point group C_1 [4]. Group theory predicts 69 normal vibrations of symmetry *a*, all of which are both IR and Raman active. For the purpose of determining the number of expected bands in the ν(CO) and ν(CS) region, however, it is sufficient to consider just the local symmetry of the $Cr(CO)_2(CX)$ fragment. The parent $Cr(CO)_3$ fragment has C_{3v} symmetry for which group theory predicts two ν(CO) bands, $a_1 + e$, both being IR and Raman active. For the thiocarbonyl complex, the $Cr(CO)_2(CS)$ fragment has C_s symmetry and so two bands, $a' + a''$, are expected for the ν(CO) modes and one band, a′, for the ν(CS) mode. For the tricarbonyl complex, three bands are seen in the Raman spectrum of the solid powder, which are assigned to ν(CO), at 1970.4 *w*, 1898.6 *s*, and 1870.0 *s* cm^{-1} (Fig. 3.1, bottom). The presence of more peaks than predicted by group theory is as a result of factor group splitting. The high frequency peak at 1970.4 cm^{-1} is assigned to the a_1 mode and the two strong peaks at 1898.6 and 1870.0 cm^{-1} have been assigned to the e mode, which has been split. Two peaks observed in the thiocarbonyl spectrum at 1962.9 *m* and 1912.4 *s* cm^{-1} have been assigned to the ν(CO) stretches (Fig 3.1, top), and the ν(CS) mode is found at 1205.1 *m* cm^{-1}, this band having a distinct shoulder on the low wavenumber side at 1197.5 cm^{-1}. The frequencies and relative intensities were in good agreement with those reported previously in the literature [5]. The solution (benzene) FT-IR spectrum showed two peaks for the ν(CO) modes for $(\eta^6\text{-}C_6H_5CO_2CH_3)Cr(CO)_3$, at 1990 *m* and 1927 *s* cm^{-1}. Two bands at 1984 *m* and 1944 *m* cm^{-1} in the solution (benzene) FT-IR spectrum of the thiocarbonyl complex were assigned to the ν(CO) modes. The ν(CS) band was located at 1216 cm^{-1} (Nujol mull). The frequencies of the ν(CO) modes can sometimes differ by as much as 20 cm^{-1} from the Raman to the infrared [5]. It was not possible to determine the peak positions in the solid-state IR spectra for these complexes as the peaks in the 2000-1700 cm^{-1} region were very broad and overlapping.

Vibrational assignments and pressure dependences for the observed Raman peaks of $(\eta^6\text{-}C_6H_5CO_2CH_3)Cr(CO)_3$ and $(\eta^6\text{-}C_6H_5CO_2CH_3)Cr(CO)_2(CS)$ are presented in Tables 3.1 and 3.2, respectively. Discontinuities in the wavenumber *vs.* pressure plots (Fig. 3.2) were found for all the modes examined over a range of pressures from 10-15 kbar. These discontinuities provide evidence for a pressure-induced structural change. The appearance of new peaks at pressures above 10 kbar affords further evidence of a structural change. Since the spectra in both phases are quite similar and the changes in the pressure dependences are gradual, occurring over a 10-15 kbar range, this transition is most likely second-order and the structure of both phases are quite similar. In the high-pressure phase, the crystal is more densely packed and the intermolecular interactions that couple the vibrational motions between the molecules

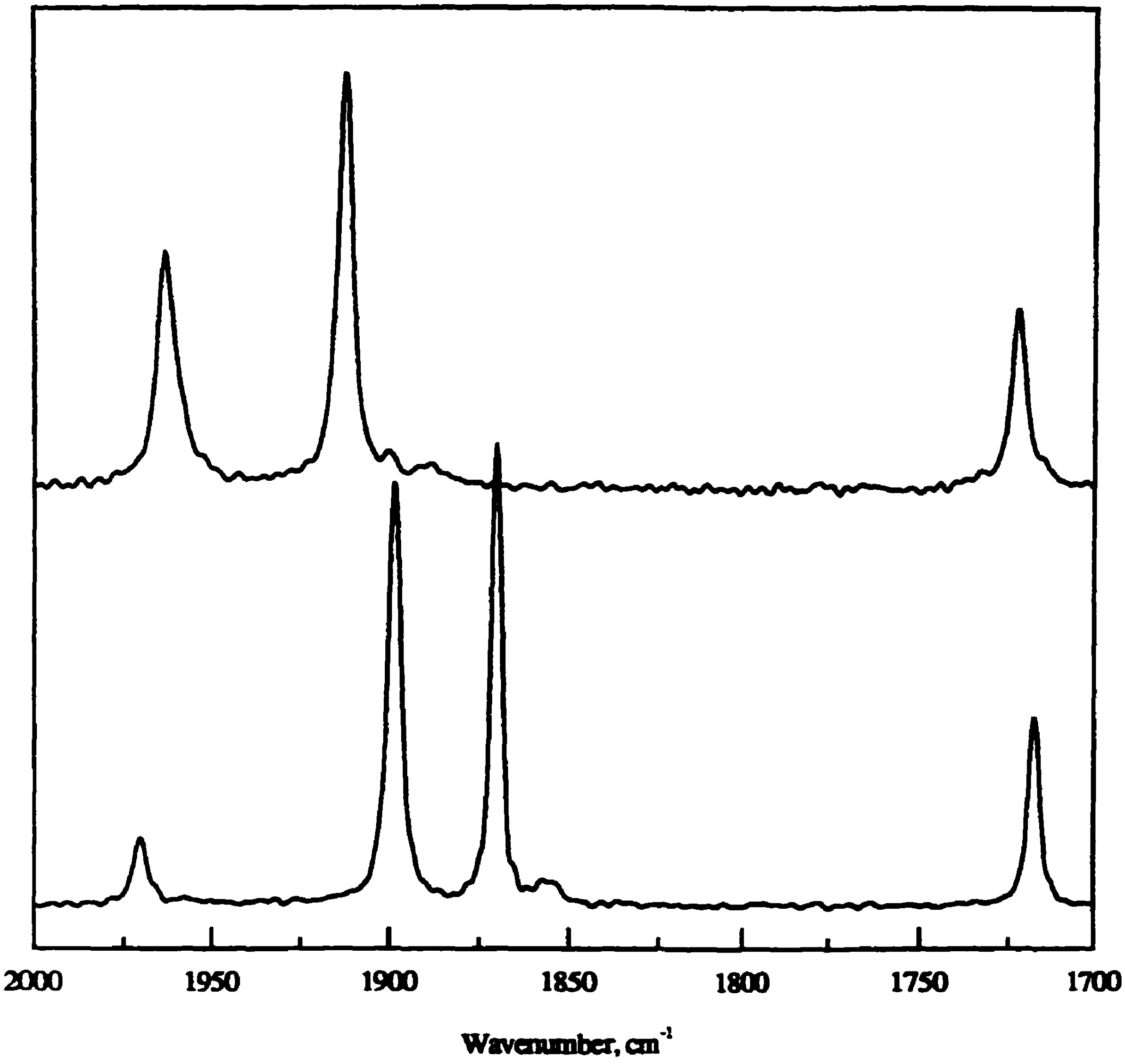

Figure 3.1. FT-Raman spectra in ν(CO) region for powdered (η^6-$C_6H_5CO_2CH_3$)Cr(CO)$_2$(CS) (top) and powdered (η^6-$C_6H_5CO_2CH_3$)Cr(CO)$_3$ (bottom). The band at ~1720 cm^{-1} in each case is the ν(C=O) mode of the methylbenzoate ligand. The very weak features are due to ^{13}CO-satellite modes (in natural abundance).

Table 3.1. Raman modes and their pressure dependence for $(\eta^6$-$C_6H_5CO_2CH_3)Cr(CO)_3$.

ν, cm^{-1}	$d\nu/dp$, cm^{-1} $kbar^{-1}$ low-pressure phase	high-pressure phase	Assignments [5]
3118.4	0.03	1.69	
3115.1	n.o	1.66	$\nu(CH)$
3106.6	0	1.23	
3100.8	n.o	1.51	
3090.7	n.o	1.78	$\nu(CH)$
3085.5	-0.01	0.55	
2962.1	0.07	0.97	$\nu(CH_3)_{asym}$
1970.4	0.03	0.27	$\nu(CO)$
1898.6	0.05	0.19	
1870.0	-0.03	-0.07	$\nu(CO)$
1855.7	0.08	n.o	
1717.4	0.04	0.06	$\nu(C{=}O)_{ester}$
1523.8	0	0.32	ν_{8a}
1507.3	0.12	n.o	ν_{8b}
1456.5			ν_{10b}
1439.3			$\delta(CH_3)_{asym}$
1416.4			ν_{19a}
1299.7	n.o.	0.06	$\nu(C\text{-}OMe)$
1276.1	0.04	0.27	ν_{13}
1157.5	-0.04	0.24	ν_{15}
1150.2	-0.12	0.36	ν_{9a}
1015.2	-0.08	0.24	ν_{18a}
998.5	-0.06	0.42	ν_{12}
979.7	0.03	0.36	ν_5
953.6	0.08	0.59	
882.0	0.03	0.52	ν_{17b}
818.2	0	0.28	ν_1
773.2	0.27	0.13	$\pi(CH)$
678.5	0.02	0.3	$\delta(OCO)$
663.5	0.04	0.46	$\delta(CrCO)$
647.9	0.10	n.b	$\pi(CCC)$
632.5	0.05	n.b	$\delta(CrCO)$
623.6			$\delta(CrCO)$
537.4			

Table 3.1 cont'd.

486.3			
480.3	0	0.69	ν(Cr-CO)
474.4	n.o	0.34	ν(Cr-CO)
451.9	0	0.54	
388.5	0.07	0.40	δ(COMe)
348.2	0	0.92	ν(Cr-R)$_{\mathrm{sym}}$
324.8	0.02	0.82	ν(Cr-R)$_{\mathrm{asym}}$
311.2	0.03	0.31	
298.4	0.06	1.89	
139.1	0.2	0.77	δ(OC-Cr-CO)
120.1	0.03	0.1	
108.7	0	0.63	
95.3	0.03	0.85	lattice modes
92.7			

n.o Not observed. n.b No break in slope.

Table 3.2. Raman modes and their pressure dependence for (η^6-$C_6H_5CO_2CH_3$)-$Cr(CO)_2(CS)$.

ν, cm^{-1}	dν/dp, cm^{-1} kbar^{-1}		Assignments [5]
	low-pressure phase	high-pressure phase	
3104.7	0.01	2.3	
3096.3	0	0.12	
3083.7	0.02	0.64	$\nu(CH)_{cycle}$
3069.2	0.09.	n.o	
2959.7	0	0.71	$\nu_s(CH_3)$
2951.6	0	0.68	
1962.9	0.01	0.17	$\nu_s(CO)$
1912.4	-0.03	-0.34	$\nu_a(CO)$
1722.3	-0.03	-0.04	$\nu(CO)_{ester}$
1279.9	0.02	0.36	$\nu(CO)$
1300.2	0.04	0.49	ν_3
1205.1	0.02	0.63	$\nu(CS)$
1197.5			
1155.6	-0.03	n.b	$\rho(CH_3)$
1144.8	0	n.b	ν_{15}
1015.4	0.04	0.22	ν_{18a}
997.5	0.03	0.37	ν_1, ν_{12}
982.0	0	0.22	ν_5
953.4	0	0.44	ν_{17b}
883.9	0.05	0.19	ν_{10a}
830.7	0.02	0.26	ν_{10b}
817.3	0.03	0.18	$\delta(OCO)$, $\nu(CO)$
770.9	0.04	0.11	ν_{11}
678.0	0.27	0.13	$\gamma(C{=}O)$
622.5	0.04	0.23	ν_{6b}
640.8	0.04	0.32	$\delta_a(CrCO)$
592.3	-0.55	n.b	$\delta(CrCS)$
524.3	-0.16	0.26	$\delta(CrCS)$
500.1	0.02	0.23	ν_{16a}
452.1	0.02	0.61	$\nu_s(Cr\text{-}CO)$
429.4	0.04	0.29	$\nu(Cr\text{-}CS)$
385.8	0.05	0.21	$\nu(C_I\text{-}C_E)$
366.9	0.02	0.16	r(OCO)
342.4	0	0.62	$\delta(COMe)$

Table 3.2 cont'd.

318.9	0.03	0.79	ν_a(Cr-R)
298.1	0.03	0.69	$\delta(C_I-C_E)$
280.9	0	0.82	ν_s(Cr-R)
275.9	0	0.57	
136.5	1.8	n.b.	δ(OC-Cr-CO)
107.2	0.01	0.82	
93.2	0	0.76	lattice modes
76.5	0.03	1.17	

n.o Not observed. n.b No break in slope.

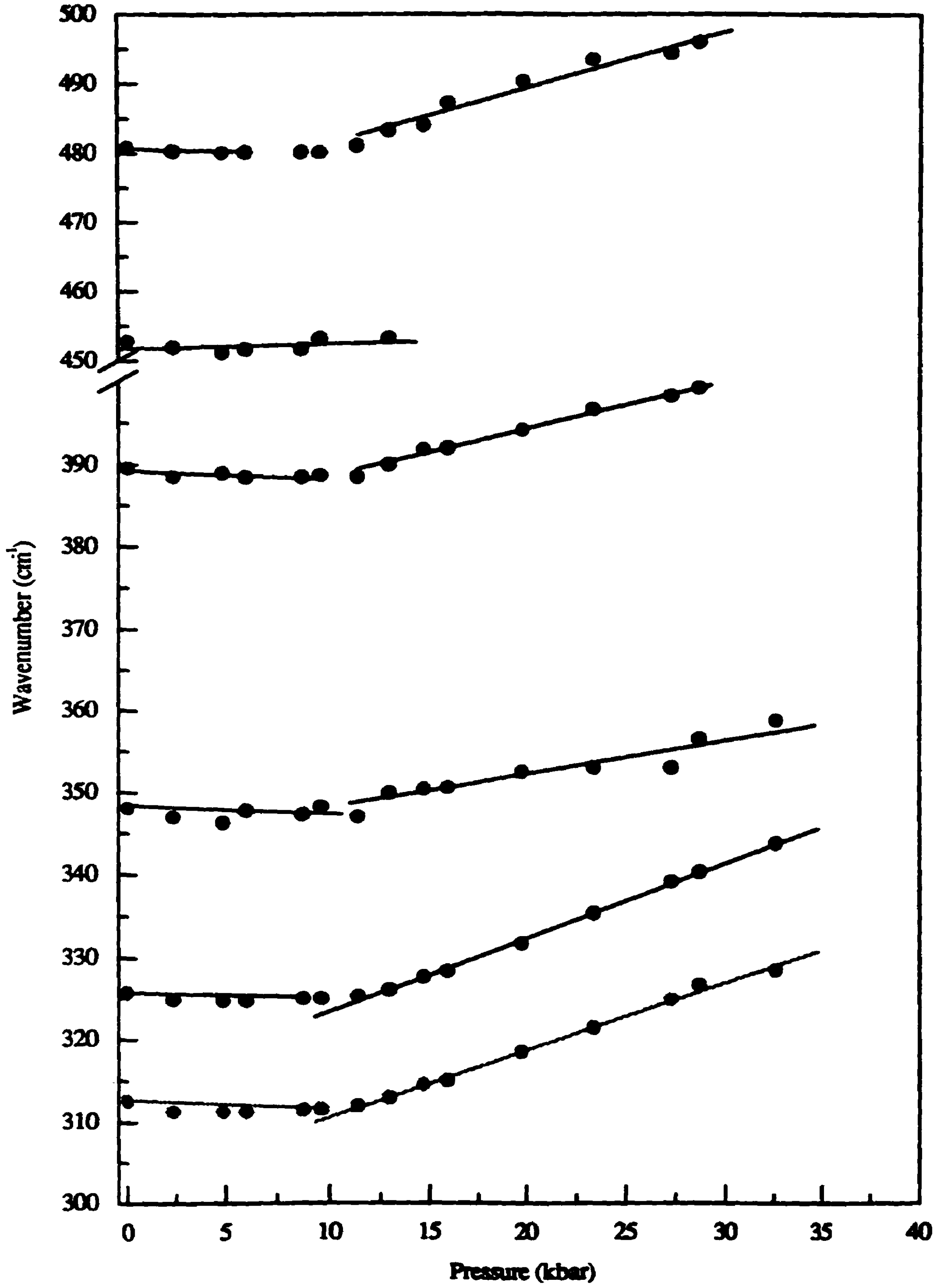
500
490
480
470
460
450
390
380
370
360
350
340
330
320
310
300
Wavenumber (cm⁻¹)
0
5
10
15
20
25
30
35
40
Pressure (kbar)

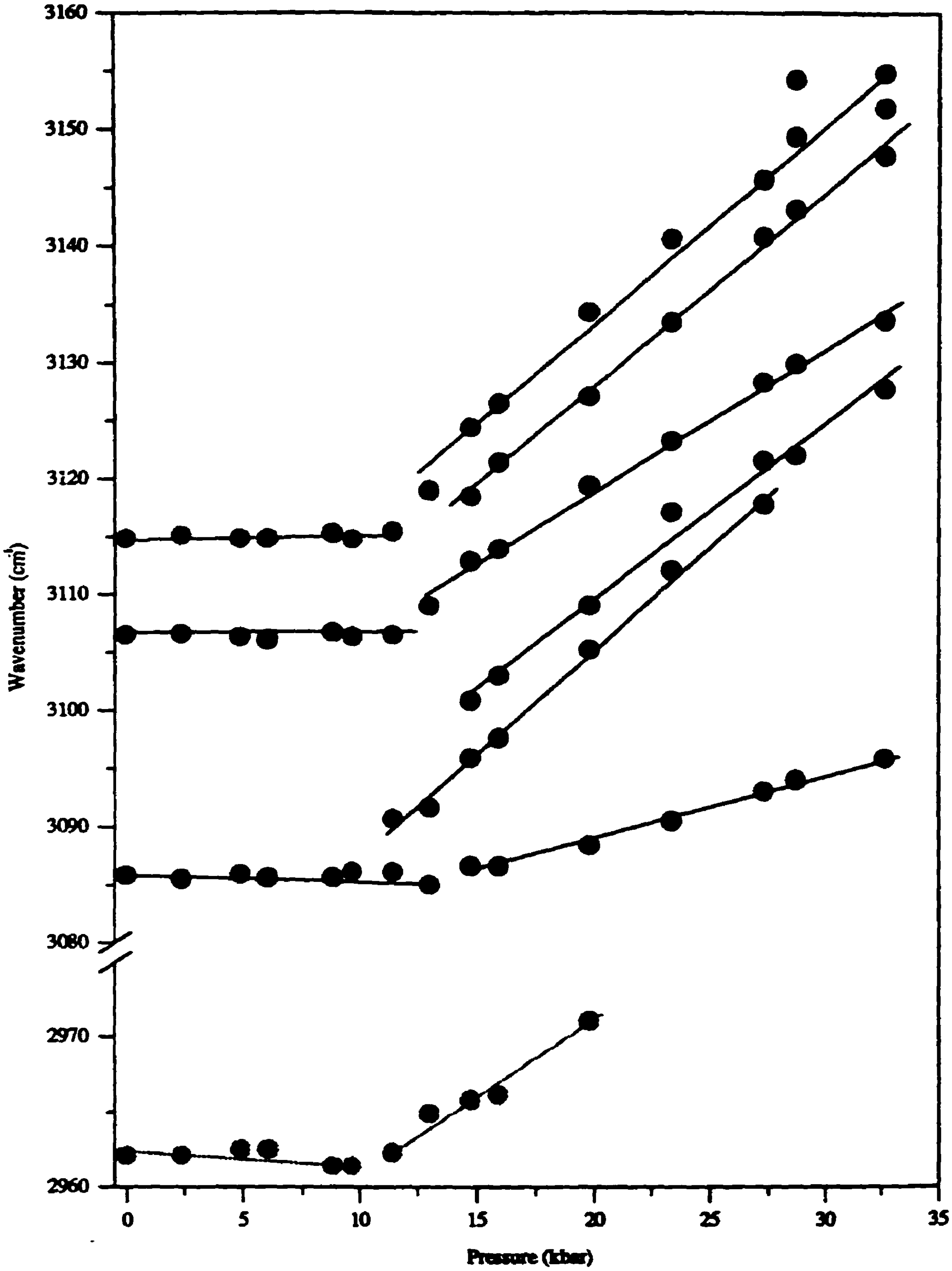

Figure 3.2. Wavenumber vs. Pressure plots for selected Raman vibrational bands of (η^6-$C_6H_5CO_2CH_3$)$Cr(CO)_3$.

in the primitive cell are all strongly enhanced. As a result, factor group splitting becomes more important in the high-pressure phase. The pressure dependences of many of the vibrational modes increase dramatically after the phase change. The ν(CS) and the symmetric and antisymmetric ν(Cr-ring) modes are particularly sensitive in the high-pressure phase, dν/dp = 0.6-0.9 cm^{-1} $kbar^{-1}$, as are the lattice modes. Several bending modes of both complexes show particularly high pressure shifts; for the δ(OC-Cr-CO) bending modes at 139.1 and 136.5 cm^{-1} for the tricarbonyl and thiocarbonyl, respectively, dν/dp = 1.89 and 1.8 cm^{-1} $kbar^{-1}$. Bending modes are generally expected to have a pressure shift of the order of 0.1-0.3 cm^{-1} $kbar^{-1}$ [6].

The determination of the pressure dependences of the IR modes was more difficult. First, the calibration peak was often obscured by other bands associated with the methylbenzoate ligand. Secondly, the ν(CO) bands are not observed in the DAC because of a broad absorption for the diamond window in the 2300-1900 cm^{-1} region. Peak positions of the ν(CO) fundamentals can often be estimated from the overtone region, but this region contained many overlapping, broad peaks.

3.3.1 ν(CO) and ν(CS) modes

Figure 3.3 shows the ν(CO) Raman modes for the chromium tricarbonyl complex with increasing pressure. The bands, originally at 1970.4 and 1898.6 cm^{-1}, show positive pressure dependences both before and after the discontinuity, with dν/dp = 0.03 and 0.27 cm^{-1} $kbar^{-1}$, and 0.05 and 0.19 cm^{-1} $kbar^{-1}$, respectively. The band at 1870.0 cm^{-1}, however, shows a negative pressure dependence and dν/dp = -0.03 and -0.07 cm^{-1} $kbar^{-1}$. Closer inspection of the spectra in this case reveals that above 30 kbar the pressure dependence changes again and becomes positive, but because there is only one data point, it was still possible to fit a good straight line through the data points above 15 kbar, with good fit. The 1855.7 cm^{-1} band shows a very small, positive pressure dependence up to 13 kbar, but becomes too weak in intensity to follow at higher pressures. The small and negative pressure dependences

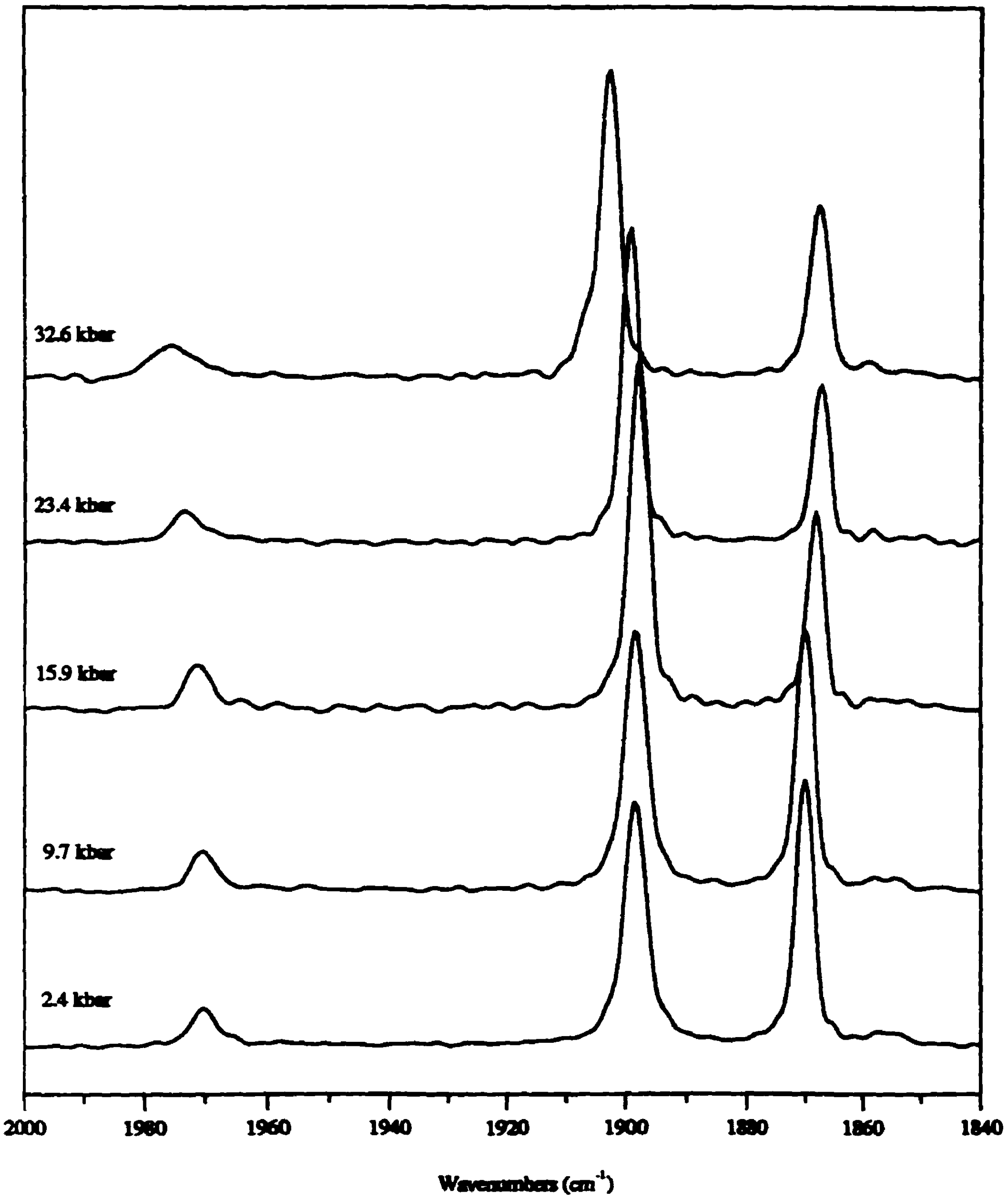

Figure 3.3. FT-Raman spectra of ν(CO) modes for (η^6-$C_6H_5CO_2CH_3$)$Cr(CO)_3$ (powder) with increasing pressure.

suggest that an increase in the Cr → CO π-backbonding is occurring under high pressure.

Although it appears that there is little change in the four ν(CO) Raman bands up to ~11 kbar, subtle changes in band shape and relative intensity are in fact occurring. The relative intensities of the two strong peaks at 1898.6 and 1870.0 cm^{-1} change as the pressure increases. When the 1870.0 cm^{-1} peak is kept at constant intensity, an increase to maximum intensity of the 1898.6 cm^{-1} peak was observed, followed by a decrease in intensity as the pressure was further increased to ~32 kbar. Closer inspection of the band shape of this peak reveals a shoulder on the high wavenumber side, which increases slightly in intensity as the pressure increases, although it never becomes a well resolved peak, or a distinct shoulder. It is known that the Raman intensity can be affected by pressure [6], but no one, simple model has been proposed to account for the changes. The 1970.4 cm^{-1} band is derived from the totally symmetric a_1 mode and involves a much larger volume change than does the antisymmetric vibration, and so this mode can be expected to have a larger, positive pressure dependence, which will additionally compensate for the negative contribution from the π-ackbonding effect.

For $(\eta^6\text{-}C_6H_5CO_2CH_3)Cr(CO)_2(CS)$, the a'' ν(CO) mode at 1912.4 cm^{-1} showed a negative pressure dependence before and after the structural change where dν/dp = -0.03 and -0.34 cm^{-1} $kbar^{-1}$, respectively, and the a' mode at 1962.9 cm^{-1} showed a positive pressure dependence, dν/dp = 0.01 and 0.17 cm^{-1} $kbar^{-1}$ (Fig. 3.4). The ν(CS) mode at 1205.1 cm^{-1} was initially insensitive to pressure but, above 14 kbar, showed a large and positive pressure shift of 0.63 cm^{-1} $kbar^{-1}$. The pressure dependence of the shoulder on the low wavenumber side was hard to determine as it was often difficult to locate the true position of the band.

The pressure dependences of the ν(CO) modes of the $Cr(CO)_2(CS)$ moiety show more negative or slightly smaller, positive pressure dependences compared to those for the tricarbonyl analogue. These results suggest that, upon exchange of a carbonyl ligand for a thiocarbonyl ligand, the π-backbonding effect dominates over the

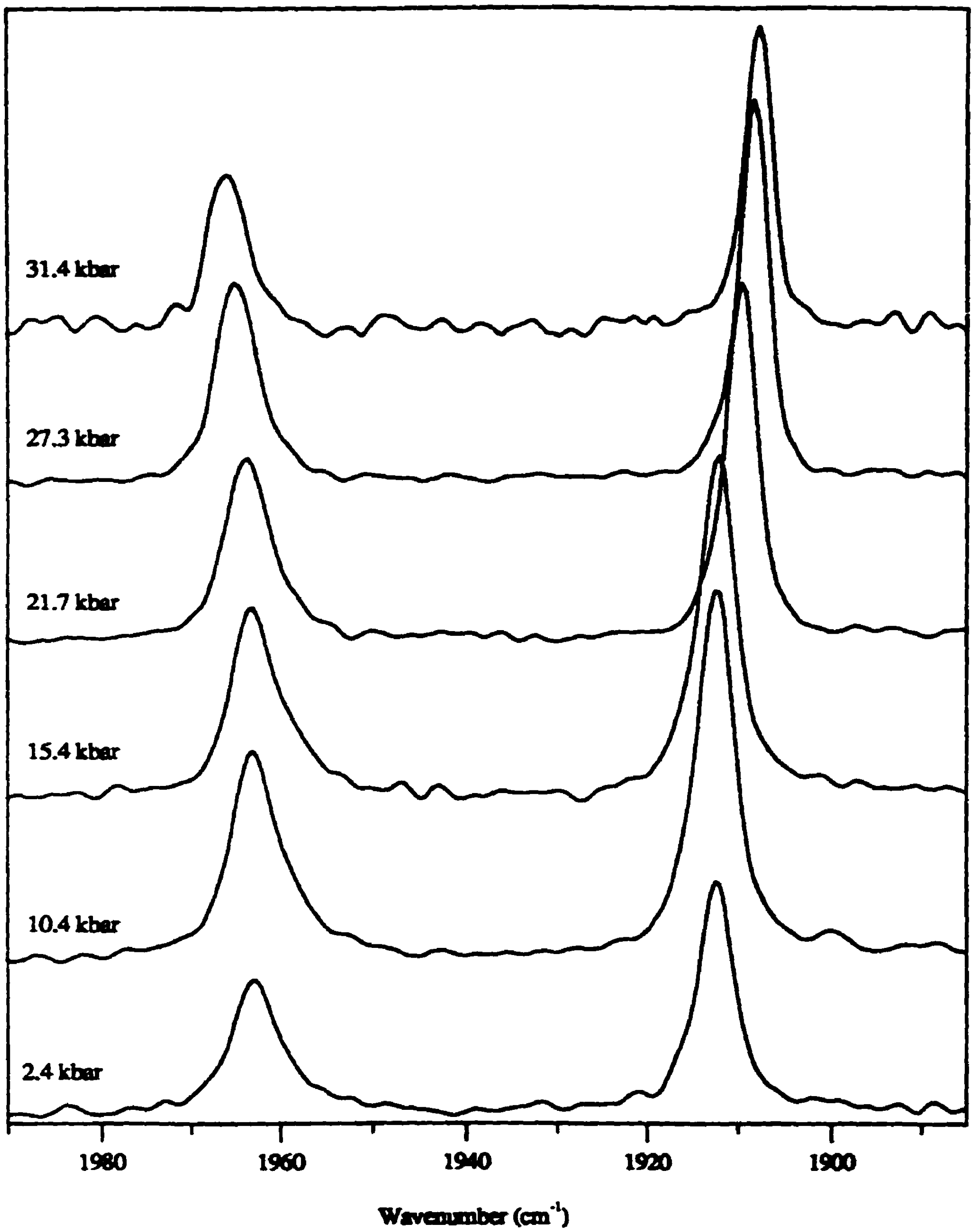

Figure 3.4. FT-Raman spectra of ν(CO) modes for (η^6-$C_6H_5CO_2CH_3$)$Cr(CO)_2(CS)$ (powder) with increasing pressure.

compression effect, and π-backbonding from the chromium to the remaining carbonyls increases to a greater extent. Although π-backbonding is expected to be greater to the thiocarbonyl ligand at ambient pressure, under pressure it is π-backbonding to the carbonyl ligand that occurs to a greater extent, at least based solely on dv/dp values. This suggestion means there is a limit to the amount of electron density that can be accepted into the π*-orbitals of CS. This same result has been observed for the related complexes $CpRe(CO)_3$ and $Cp^*Re(CO)_3$ (Cp = cyclopentadiene and Cp* = pentamethylcyclopentediene) [7].

Unlike the ν(CO) modes, the pressure sensitivities of the ν(CS) modes are not simply the result of the competition between lattice compression and the π-backbonding effects. Since there is appreciable mixing of the ν(CS) mode with the low-energy ν(Cr-CS) mode, as a result of their same symmetry, the large positive value for this latter mode would be expected to contribute positively to the overall pressure sensitivity of ν(CS). Consequently, a small positive or negative pressure dependence for the ν(CS) mode could indicate that the π-backbonding effect was dominant.

3.3.2 ν(CrC) and δ(CrC) modes

It is now appropriate to look at the ν(Cr-CO) and ν(Cr-CS) modes in the 700-300 cm^{-1} region, since, if under pressure the amount of π-backbonding to the CO and CS ligands is changing, related changes should be seen in the pressure dependences of these vibrational modes. For the tricarbonyl and thiocarbonyl complexes, these regions of the Raman spectrum are quite different (Fig. 3.5). The two ν(Cr-CO) modes of the tricarbonyl complex have been assigned to the relatively strong peak at 480.3 cm^{-1} and the weak shoulder at 474.4 cm^{-1}. The bending δ(CrCO) modes are assigned to weak features in the 700-600 cm^{-1} region: 663.5, 632.5 and 623.6 cm^{-1}. The strong ν(Cr-CO) mode at 480.3 cm^{-1} has a large pressure sensitivity above ~14 kbar, with dν/dp = 0.69 cm^{-1} kbar^{-1}. The weak shoulder at 474.4 cm^{-1} becomes more prominent as the pressure is increased and dν/dp = 0.34 cm^{-1} kbar^{-1}, from ~13 kbar (Fig. 3.6). Up to this pressure, the shoulder was too weak to discern with any confidence. The bending modes at lower wavenumbers were too weak to determine their positions accurately, but the peak at 663.5 cm^{-1} was a little stronger and dν/dp = 0.46 cm^{-1} kbar^{-1}, above ~14 kbar. An increase in π-backbonding will have the effect of increasing the strength of the chromium-carbon bond, which adds onto the effect of lattice compression. Therefore, large, positive values of dν/dp for the ν(CrCO) modes are expected and observed.

For the $Cr(CO)_2(CS)$ moiety, the ν(Cr-CO) mode is a medium intense peak at 452.1 cm^{-1}, a weaker peak at 429.4 cm^{-1} being attributed to the ν(Cr-CS) mode (Fig. 3.5). The δ(CrCS) bending modes are very weak peaks at 524.3 and 500.1 cm^{-1}. The δ(CrCO) modes appear at 640.8 and 622.5 cm^{-1}. As the pressure increases, the ν(Cr-CO) and ν(Cr-CS) bands shift to higher wavenumbers with dν/dp = 0.02 and 0.61 cm^{-1} kbar^{-1}, and 0.04 and 0.29 cm^{-1} kbar^{-1}, respectively (Fig. 3.7). Above ~25 kbar, the ν(Cr-CO) band at 454 cm^{-1} splits into a doublet. The ν_a(Cr-CO) mode, at ~500 cm^{-1}, overlaps with other peaks in the region and was not observed at increased pressures.

A comparison of the frequencies of the observed ν(Cr-CO) modes at 480 and 452 cm^{-1} for the carbonyl complex and thiocarbonyl complex, respectively, indicate a longer, weaker bond between the chromium and the carbonyl ligands when one carbonyl ligand is substituted for a thiocarbonyl ligand. This clearly shows that the CS ligand is a better π-acceptor at ambient pressure, compared to CO. The pressure sensitivities of the ν(Cr-CO) modes in the tricarbonyl and the thiocarbonyl complexes were comparable.

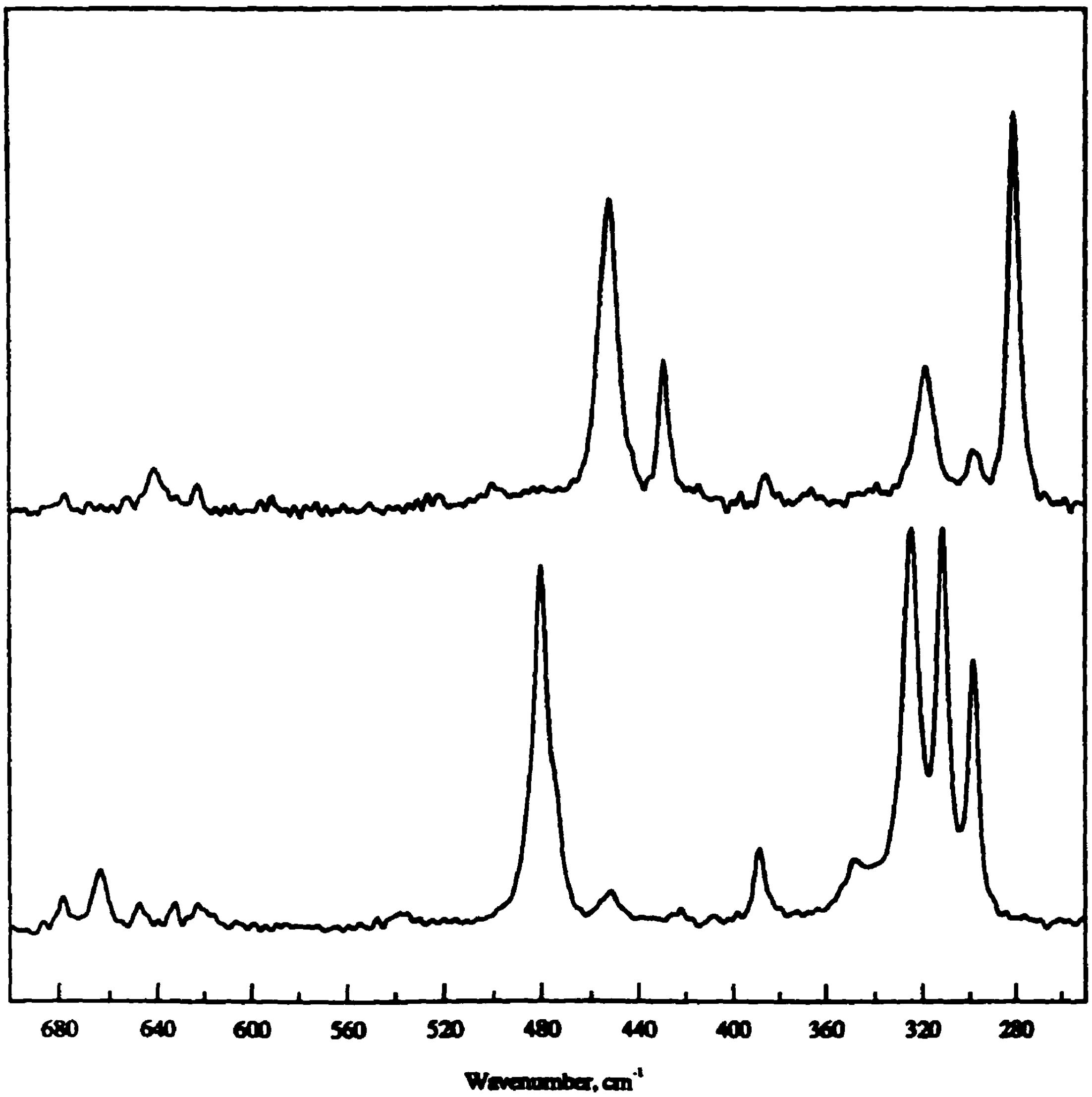

Figure 3.5. FT-Raman spectra of ν(Cr-CX), δ(CrCX) and ν(Cr-Ring) modes for powdered (η^6-$C_6H_5CO_2CH_3$)Cr(CO)$_2$(CS) (top) and (η^6-$C_6H_5CO_2CH_3$)Cr(CO)$_3$ (bottom).

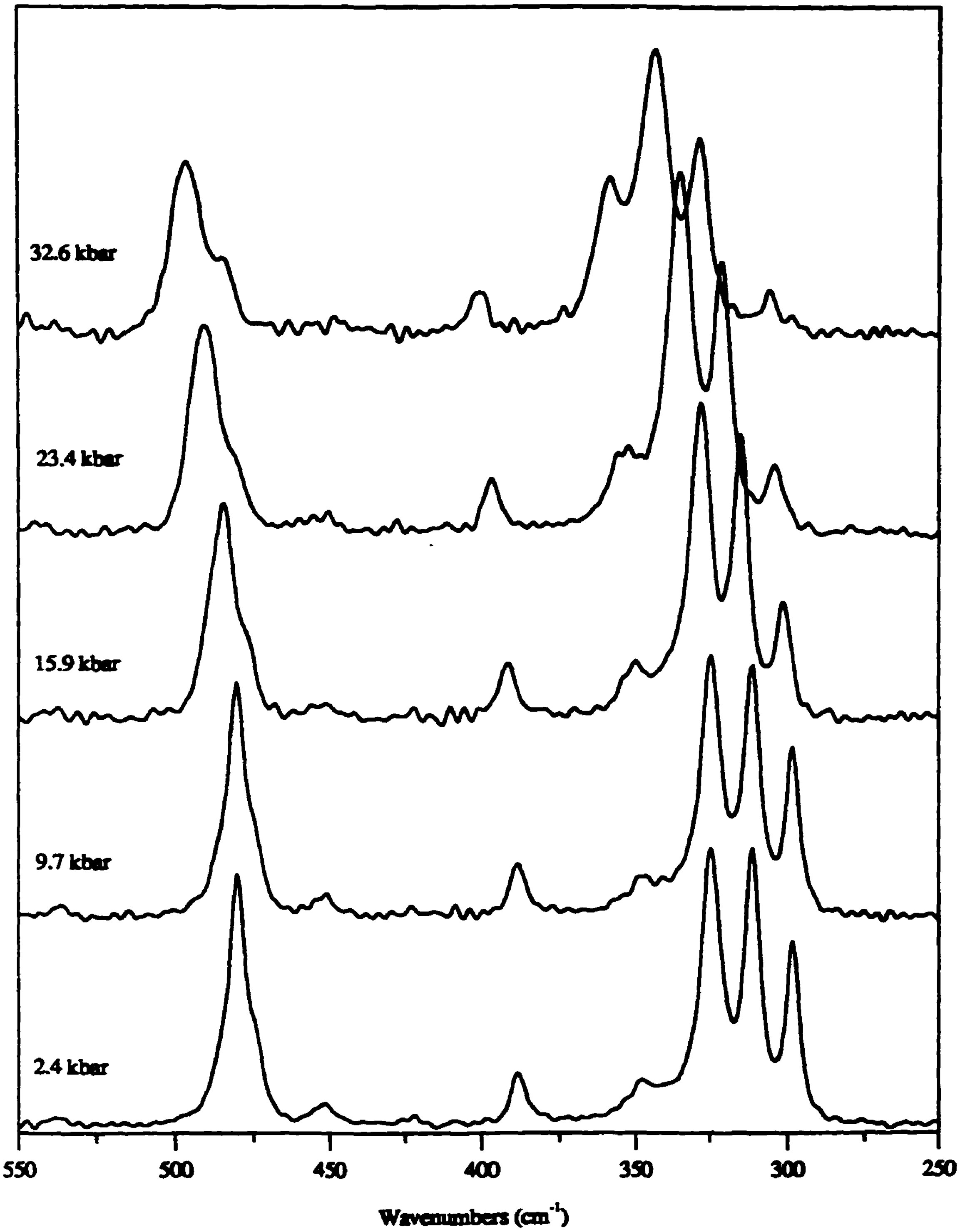

Figure 3.6. FT-Raman spectra of ν(Cr-CO) and ν(Cr-Ring) modes for powdered (η^6-$C_6H_5CO_2CH_3$)Cr(CO)$_3$ with increasing pressure.

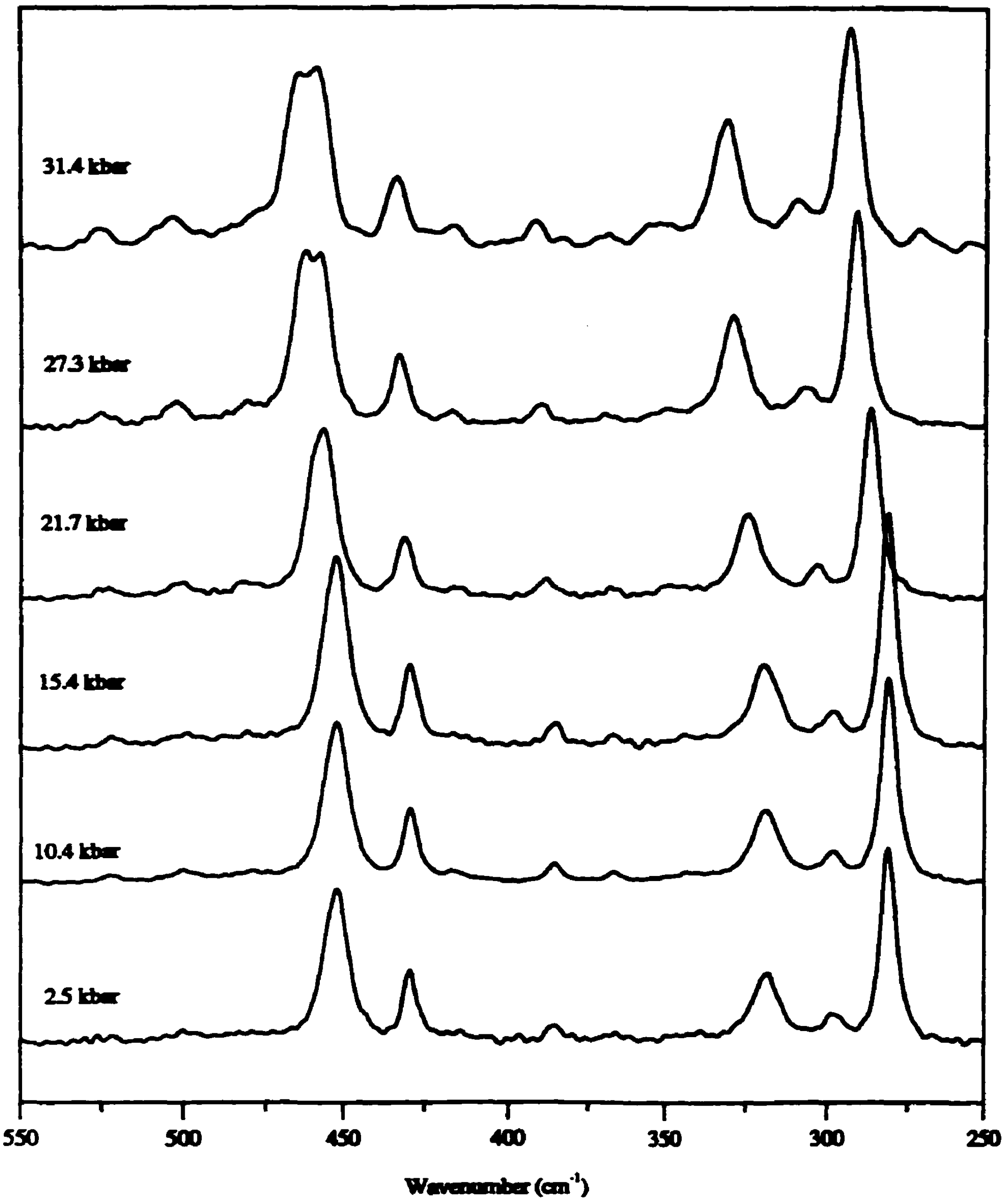

Figure 3.7. FT-Raman spectra of ν(Cr-CX) and ν(Cr-Ring) modes for powdered (η^6-$C_6H_5CO_2CH_3$)Cr(CO)$_2$(CS) with increasing pressure.

3.3.3 ν(M-Ring) modes

The majority of the remaining peaks in the vibrational spectrum are assigned to modes associated with the fourth ligand, η^6-methylbenzoate, and to lattice modes. One interesting region is that just below 350 cm^{-1}, where both the carbonyl and thiocarbonyl complexes have a series of relatively strong Raman peaks. These bands are assigned to $\nu(Cr\text{-}R)_{sym}$ and $\nu(Cr\text{-}R)_{asym}$, or the ring tilt modes (Fig. 3.5). For the triocarbonyl complex, two bands of similar intensity, at 324.8 and 311.2 cm^{-1}, are assigned to ν_{sym}(Cr-Ring) and ν_{asym}(Cr-Ring), respectively. Above 15 kbar, these bands showed large pressure sensitivities of 0.92 and 0.82 cm^{-1} kbar^{-1}, respectively (Fig. 3.6). As the pressure was increased, the low wavenumber band at 311.2 cm^{-1}, exhibited a continuous decrease in intensity relative to the band at 324.8 cm^{-1}. Band assignments were made after determining the pressure sensitivity. Since symmetric vibrations involve a much greater volume change than do antisymmetric modes, the former are expected to be more sensitive to compression of the crystal lattice and hence exhibit higher dv/dp values. Although the differences in dv/dp values are small, it would seem reasonable to suggest that the high wavenumber band is derived from the symmetric ring tilt mode (larger dv/dp) and that the lower wavenumber band is derived from the antisymmetric mode (smaller dv/dp). Adams and Squire [5(b)] have reported the Raman spectrum for (η^6-C_6H_6)$Cr(CO)_3$ and assigned three strong bands at 323, 311 and 299 cm^{-1} as the Cr-Ring symmetric and antisymmetric modes, these modes having a strong interaction and so sharing intensity.

A weak band at 348.2 cm^{-1} steadily gains intensity as the pressure increases to become a moderately strong peak at the highest pressure, while a peak of medium intensity at 298.4 cm^{-1} loses intensity at a similar rate. These bands also have comparable pressure dependences – 0.31 and 0.40 cm^{-1} kbar^{-1} for the 298.4 cm^{-1} and 348.2 cm^{-1} bands, respectively. The fact that their Raman intensities are obviously connected under pressure indicates that they are derived from the same mode. The 348.2 cm^{-1} band was assigned to the δ(COMe) bending mode.

The symmetric and antisymmetric ring tilt modes in the thiocarbonyl spectrum give rise to two bands at 318.9 *w* and 280.9 *s* cm^{-1} (Fig. 3.5). The pressure dependences of these bands are 0.03 and 0.79 cm^{-1} $kbar^{-1}$, and 0 and 0.82 cm^{-1} $kbar^{-1}$, respectively (Fig. 3.7). The weaker band at 318.9 cm^{-1} appears to gain some intensity from ambient pressure. Again, tentative assignments were made based on their pressure dependences. From these assignments, upon substitution of a CO for a CS ligand, there is a switch in the relative energies of the symmetric and antisymmetric ring tilt modes. For the tricarbonyl ν_s(Cr-R) > ν_a(Cr-R) and for the thiocarbonyl, ν_s(Cr-R) < ν_a(Cr-R).

For the $(\eta^6\text{-}C_6H_6)Cr(CO)_2(CS)$ complex [8], the ν_a(Cr-R) mode was attributed to a medium intense peak at 315 cm^{-1}, while the ν_s(Cr-R) mode was assigned to a medium intense peak at 280 cm^{-1}. For the analogous methybenzoate complex, the two bands at 314 and 272 cm^{-1} were assigned to the metal-ring stretching modes [5(c)].

Although the CS ligand is isoelectronic with the CO ligand, substitution of CO for CS is not straightforward. Lichtenberger and Fenske [9] have shown through theoretical and experimental studies, that in order to understand the physical properties of transition metal thiocarbonyl complexes, it is necessary to consider the molecule as a whole and not just the isolated ligands and the metal. Although, in the first instance the CS ligand can be considered to be a better σ-donor and π-acceptor than is CO, filled 2π-$d\pi$ orbital interactions are possible, which effectively deplete electron density from the metal center. Because of the lower electronegativity of sulfur, additional charge is placed on the carbon of CS, which leads to a destabilization of the HOMO 7σ of CS. The reduced interaction between the C and S *pπ* orbitals leads to more stabilized π*-orbitals on CS, compared to those on CO. Ultimately, this leads to an increased electron-accepting capability of the CS ligand. Furthermore, the CS 2π-orbitals, predominantly sulfur in character but also containing appreciable C character, are significantly destabilized and as a result are now more likely to interact with a filled metal *d*-orbital, of the correct symmetry, in the complex (Fig. 3.8). As a result, the metal *d*-electron density in the bonding combination is less

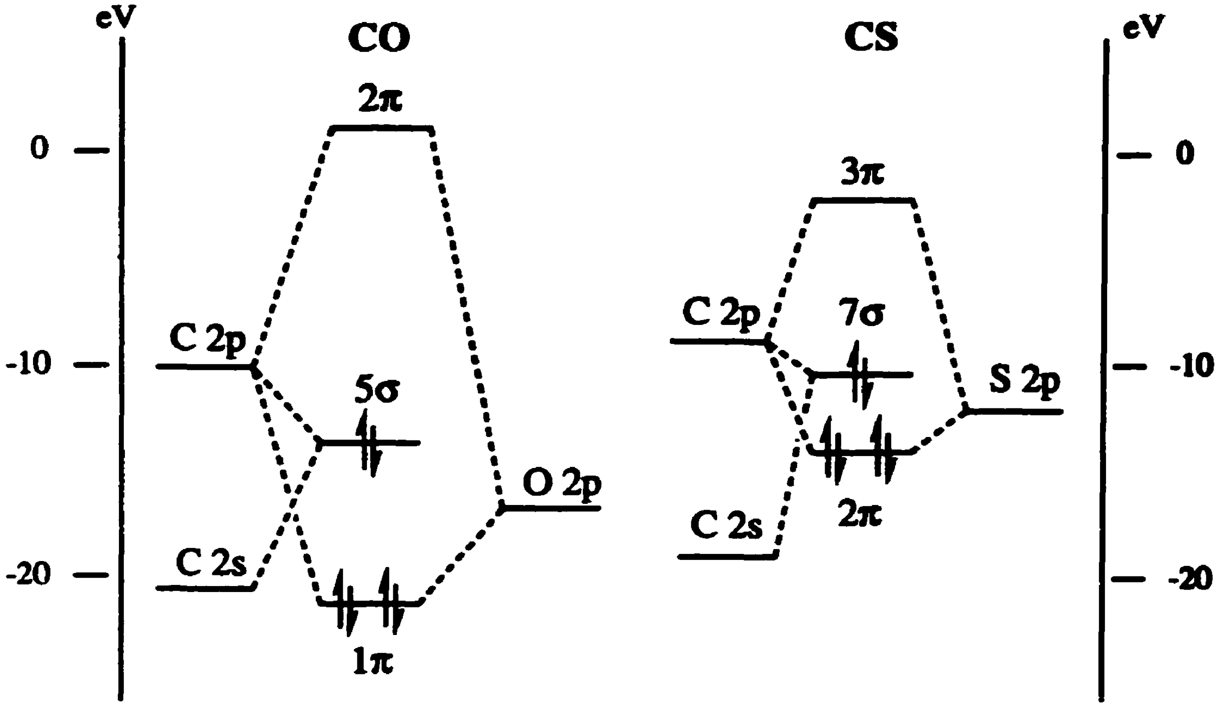

Figure 3.8. (a) Molecular orbital diagram for CO and CS (adapted from ref. 9).

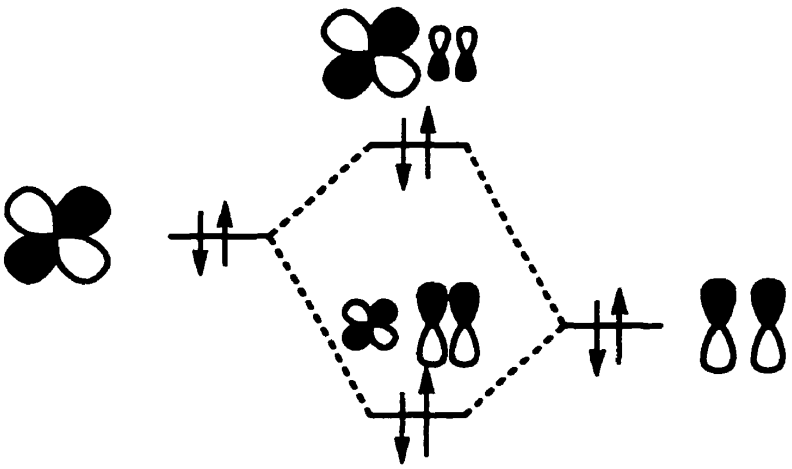

Figure 3.8. (b) Schematic diagram of the orbital energies and characters resulting form a filled ligand π-orbital interacting with a filled M *d* orbital.

accessible for π-backbonding because of the stability of the bonding molecular orbital. The antibonding orbital is now at a more favorable energy for backbonding, compared to the unperturbed metal orbitals but, because of partial delocalization onto the ligand, there is again less electron density available at the metal center.

3.4 Comparison of pressure effects on (η^6-arene)$Cr(CO)_2(CX)$ complexes and $Cr(CO)_5(CS)$

The synthesis of thiocarbonyl complexes is often facilitated through the use of organic ligands such as arenes with a high ratio of σ-donor to π-acceptor ability. The CO_2CH_3 group is electron withdrawing and has been shown to facilitate the synthesis of (η^6-$C_6H_5CO_2CH_3$)$Cr(CO)_2(CS)$. However, the presence of an electron-withdrawing group on the arene may cause a decrease in the σ-donor capability of the arene ligand. Comparison of the pressure dependences of the vibrational modes may reveal the effect, if any, on the presence of this electron-withdrawing group.

A high-pressure IR study was performed earlier on (η^6-C_6H_6)$Cr(CO)_2(CS)$ [10]. The pressure dependences of the observed IR bands for the $Cr(CO)_2(CS)$ moiety were reported. Because of the strong diamond absorption in the region of the spectra where the ν(CO) modes are located, the positions and pressure dependences of the ν(CO) modes were estimated from the binary combination and overtone region (~4000 cm^{-1}). Data comparison must therefore be treated with caution, since it is known that the frequencies of the ν(CO) modes can differ by up to 20 cm^{-1} on going from Raman to infrared [5], and those given for the benzene complex are estimated values only.

Table 3.3 shows the frequency and pressure dependences for the ν(CO), ν(Cr-CX), δ(CrCX) and ν(Cr-R) modes, where R represents the arene ring, for $Cr(CO)_5(CS)$ [11], (η^6-C_6H_6)$Cr(CO)_2(CS)$ [10], (η^6-$C_6H_5CO_2CH_3$)$Cr(CO)_2(CS)$ and (η^6-$C_6H_5CO_2CH_3$)$Cr(CO)_3$. Their comparison allows us to observe the effect of substitution of three carbonyl ligands for the benzene ligand, and for the

Table 3.3. Pressure dependences of selected Raman-active modes. [a]Ref. 11; [b]Ref. 10; [c]This work; [d]A phase transition was observed in the 10-15 kbar range; the pressure dependences are given for the low-pressure phase and the high-pressure phase.

$Cr(CO)_5(CS)$[a]		(η^6-C_6H_6)-$Cr(CO)_2(CS)$[b]		(η^6-$C_6H_5CO_2CH_3$)-$Cr(CO)_2(CS)$[c]		(η^6-$C_6H_5CO_2CH_3$)-$Cr(CO)_3$[c]		Assignment
ν, cm^{-1}	d ν/dp, cm^{-1} $kbar^{-1}$	ν, cm^{-1}	d ν/dp, cm^{-1} $kbar^{-1}$	ν, cm^{-1}	d ν/dp,[d] cm^{-1} $kbar^{-1}$	ν, cm^{-1}	d ν/dp,[d] cm^{-1} $kbar^{-1}$	
2088^{eq}	0.18	1962	0.37	1962	0.01, 0.17	1970	0.03, 0.27	
2017^{eq}	0.22	1943	-0.59			1898	0.05, 0.19	ν(CO)
2017^{ax}	-0.18	1908	0.59	1912	-0.03, -0.34	1870	-0.03, -0.07	ν(CO)
1989^{eq}	-0.53	1856	-0.54			1855	0.08, n.o.	
1289	-0.25	1211	0.85	1205	0.02, 0.63			ν(CS)
1260	-0.09	1192	0.37	1197	1.12			
427^{eq}	0.73	452	0.80	452.1	0.02, 0.61	480	0, 0.69	
422^{ax}	0.82					474	n.o. , 0.34	ν(CrCO)
381^{eq}	0.78							
352	0.70	432	0.41	429	0.04, 0.3			ν(CrCS)
636	-0.46	646	0.17			663	0.04, 0.46	
512	0.16	611	0.33	640	0.04, 0.32	632	0.05, n.o.	δ(CrCO)
487	0.21	600	0.12			623	n.o.	
340	n.o.	521	0.21	592	-0.55, n.o.			δ(CrCS)
		502	0.28	524	-0.16, 0.26			

n.o., Not observed.

methylbenzoate ligand, as well as substitution for a thiocarbonyl ligand in an arene complex. In the literature, several references have considered how these ligand substitutions influence the force constants of various vibrations [8,11,12].

Substitution for a benzene ligand results in a significant shift to lower frequencies for the ν(CO) modes and further substitution of a methylbenzoate ligand results in a smaller shift to higher wavenumbers; note, there is a difference of ~20 cm^{-1} between the IR and Raman frequencies, the latter being lower. The pressure dependences of these modes, however, are comparable. The ν(CO) modes are slightly more sensitive in $(\eta^6\text{-}C_6H_6)Cr(CO)_2(CS)$ than in $Cr(CO)_5(CS)$, but slightly smaller in $(\eta^6\text{-}C_6H_5CO_2CH_3)Cr(CO)_2(CS)$. These results indicate an increase in the amount of π-backbonding to the remaining CO ligands when an benzene or methylbenzoate is substituted into $Cr(CO)_5(CS)$. The presence of the electron-withdrawing group, however, does appear to have some influence on the amount of π-backbonding to the carbonyls and their pressure sensitivity. The pressure dependences also reflect the competing π-backbonding and compression effects, which result in negative and positive pressure shifts, respectively.

If we consider the CS ligand, a dramatic shift in the frequency of the ν(CS) stretching mode from 1289 to 1211 and 1205 cm^{-1} for the pentacarbonyl, benzene and methylbenzoate complexes, respectively, is observed. This is the same trend as observed for the CO ligand. Since there is less competition in the arene ring for π-backbonding from the Cr dπ-electrons, there is an increase in π-backbonding to the π*-orbitals of the remaining CO and CS ligands. In contrast to the CO ligand, the pressure dependence of the ν(CS) stretching mode also changes quite significantly upon substitution of the arene ligand. For $(\eta^6\text{-}C_6H_6)Cr(CO)_5(CS)$, the ν(CS) mode shows a negative pressure shift, whereas in the arene complexes the pressure dependences are large and positive. This could indicate an increased coupling of the ν(CS) and ν(Cr-CS) modes for the latter. Calculations indicate a larger mixing of the ν(CS) and ν(Cr-CS) modes, compared to that of metal-carbonyl modes [12]. From vibrational force constant calculations, it was also noted that the effect of substitution on the Cr-CS group was greater than its effect on the Cr-CO group [12]. It has been suggested previously that the thiocarbonyl ligand is capable of acting as a 'charge-buffer ligand' [13]. This means that for various complexes the π-acceptor/σ-donor ratio for coordinated CS can be larger or smaller than that for coordinated CO, implying a greater adaptability of CS to its environment. The similar pressure dependences for the CO modes in the different complexes, but varying pressure sensitivities of the CS modes could be a result of this charge-buffering effect.

The ν(Cr-CO) and ν(Cr-CS) modes show positive shifts in frequency as the π-backbonding increases into the π^*-orbitals, with concomitant increases in the Cr-C bond strengths. The pressure dependences of the ν(Cr-CO) modes are similar for all the complexes, although there is a small decrease from $(\eta^6\text{-}C_6H_6)Cr(CO)_2(CS)$ to $(\eta^6\text{-}C_6H_5CO_2CH_3)Cr(CO)_2(CS)$. The frequency of the ν(Cr-CS) mode increases from 352 to 432 cm^{-1} on substitution for a benzene ring and the pressure dependence decreases from 0.70 to 0.41 cm^{-1} kbar^{-1}, i.e., ν(Cr-CS) is less pressure sensitive in $(\eta^6\text{-}C_6H_6)Cr(CO)_2(CS)$.

The presence of the CO_2CH_3 substituent on the benzene ring appears to have a small effect on all of the ν(CO), ν(Cr-CO) and ν(Cr-CS) stretching vibrations. The pressure shifts with the methylbenzoate ligand are smaller for some modes, notably the ν(Cr-CO) and ν(CS) modes. As mentioned previously, the methylbenzoate ligand was used since it favors formation of the thiocarbonyl ligand. From force field calculations, it was indicated that although there is minimal mixing of Cr-C and Cr-R modes, the bending δ(CrCO) modes are highly mixed with ν(Cr-C) and ν(Cr-R) [12]. Comparison of the δ(CrCO) and δ(CrCS) modes and their pressure dependences may provide some information. The δ(CrCO) and δ(CrCS) modes show the expected shift to higher wavenumbers on substitution for an arene ligand. Upon substitution of C_6H_6 or $C_6H_5CO_2CH_3$ into $Cr(CO)_5(CS)$ there is a dramatic increase in the frequency of the bending δ(CrCS) mode, by ~200 cm^{-1}. Since the extent of π-backbonding has increased to give a stronger Cr-CO bond, an increase in the rigidity of the Cr-CX group results. The range of pressure dependences for the δ(CrCO) and δ(CrCS) modes show significant variations from one complex to the next. Often these bands are relatively weak, however, which makes measurement difficult with increasing pressure. No data for the pressure dependence of the δ(CrCS) vibrations are available for the $Cr(CO)_5(CS)$ complex. For the benzene complex, the pressure dependences of this mode were 0.21 and 0.28 cm^{-1} $kbar^{-1}$. For the methylbenzoate complex, the initial pressure dependence were -0.55 and -0.16 cm^{-1} $kbar^{-1}$. Above 15 kbar, the pressure dependence became positive (dν/dp = 0.26 cm^{-1} $kbar^{-1}$).

The final two columns of Table 3.3 compare $(\eta^6\text{-}C_6H_5CO_2CH_3)Cr(CO)_3$ and $(\eta^6\text{-}C_6H_5CO_2CH_3)Cr(CO)_2(CS)$. The pressure dependences for the ν(CO) and ν(CS) modes, and the ν(Cr-CO) and ν(Cr-CS) modes, indicate an increase in π-backbonding to the CO ligand under applied pressure, but little, if any, increase in π-backbonding to the CS ligand. The smaller dν/dp value for ν(Cr-CS) compared to ν(Cr-CO) suggests that the shift in the former is simply due to compression. For ν(Cr-CO), the negative pressure shift due to the increase in π-backbonding, and the positive pressure shift induced by compression, are combined.

3.5 Conclusions

The pressure dependences of the Raman-active modes of $(\eta^6\text{-}C_6H_5CO_2CH_3)Cr(CO)_3$ and $(\eta^6\text{-}C_6H_5CO_2CH_3)Cr(CO)_2(CS)$ revealed the presence of a second-order phase transition between 10 and 15 kbar. Although the new phases were not identified, the Raman modes were particularly sensitive above the phase transition pressure. The ν(CS) mode and the symmetric and antisymmetric ν(Cr-R) modes were highly responsive in the high-pressure phase, as were the lattice modes. Several bending modes were also very pressure sensitive, most notably the δ(OC-Cr-CO) modes. The larger negative pressure shifts for the ν(CO) modes, compared to the ν(CS) modes, in the thiocarbonyl complex indicated a greater increase in π-backbonding to the remaining CO ligands than to the CS ligand. Substitution of a CS ligand for CO ligand in $(\eta^6\text{-}C_6H_5CO_2CH_3)Cr(CO)_3$ appears to influence the relative energies of the ν_s(Cr-R) and ν_a(Cr-R) modes; $\nu_s(\text{Cr-R}) > \nu_a(\text{Cr-R})$ for the tricarbonyl, but $\nu_s(\text{Cr-R}) < \nu_a(\text{Cr-R})$ for the thiocarbonyl complex.

On comparison with $(\eta^6\text{-}C_6H_6)Cr(CO)_3$, we have shown that the arene ligand does influence the Cr-CO and Cr-CS bonding interactions. The electron-withdrawing group of the methylbenzoate ligand leads to less π-backbonding to CO and CS. This is likely to be due to less σ-donation form the arene ring to Cr. The frequency and pressure dependence of the δ(CrCS) mode are dramatically changed from $(\eta^6\text{-}C_6H_6)Cr(CO)_2(CS)$ to $(\eta^6\text{-}C_6H_5CO_2CH_3)Cr(CO)_2(CS)$, possibly as a result of increased mixing of the δ(CrCS) and ν(Cr-R) modes and/or CS π - Cr d-orbital interactions. The ability of the CS ligand to tailor its σ-donor/π-acceptor ratio is strongly reflected from the $d\nu/dp$ values of the ν(CS) mode. This may have implications in the reactivity of monothiocarbonyl complexes and substitution reactions to form dithiocarbonyl complexes and further.

Since, under compression, it is generally easier to reduce the weaker intermolecular interactions, many high-pressure studies do just that. In many compounds, hydrogen bonding is often responsible for the rigid strucutre observed. Many pressure-tuning studies have been made and theoretical models proposed. The following chapter discusses the use of pressure-tuning IR spectroscopy to study the intermolecular interactions in Magnus' green salt, $[Pt(NH_3)_4][PtCl_4]$. Although the N-H···Cl distance determined from the crystal strucutre was considered too long for hydrogen bonds to be present, the IR evidence was contradictory.

3.6 References

---

[1] D. M. Adams and I. O. C. Ekejiuba, J. Chem. Phys., 77 (1982) 4793-4795.

[2] C. A. L. Mahaffy and P. L. Pauson, Inorg. Synth., 19 (1979) 154-158.

[3] M. D. Rausch, G. A. Moser, E. J. Zaiko and A. L. Lipman, Jr., J. Organomet. Chem., 23 (1970) 185-192.

[4] J. Y. Saillard, G. Le Bourgne and D. Grandjean, J. Organomet. Chem., 94 (1975) 409-416.

[5] (a) P. Caillet and G. Jaouen, J. Organomet. Chem., 91 (1975) C53-C56; (b) D. M. Adams and A. Squire, J. Chem. Soc., Dalton, (1974) 558-565; (c) P. Caillet, J. Organomet. Chem., 102 (1975) 481-490.

[6] J. R. Ferraro, Vibrational Spectroscopy at High External pressures: The Diamond-anvil Cell, Wiley 1984.

[7] For example, (a) Y. Huang, I. S. Butler and D. F. R. Gilson, Inorg. Chem., 30 (1991) 1098-1102; (b) Y. Huang, I. S. Butler and D. F. R. Gilson, Inorg. Chem., 31 (1992) 4762-4765.

[8] A. M. English , K. R. Plowman and I. S. Butler, Inorg. Chem., 21 (1982) 338-347.

[9] D. L. Lichtenberger and R. F. Fenske, Inorg. Chem,. 15 (1976) 2015-2022.

[10] Y. Huang, I. S. Butler and D. F. R. Gilson, Inorg. Chem., 31 (1992) 303-305.

[11] A. M. English, K. R. Plowman and I. S. Butler, Inorg. Chem., 20 (1981) 2553-2565.

[12] I. S. Butler, A. Garcia-Rodriguez, K. R. Plowman and C. Frank Shaw III, Inorg. Chem., 15 (1976) 2602-2608.

[13] M. A. Andrews, Inorg. Chem., 16 (1977) 496-499.

Chapter 4

Pressure-Tuning FT-IR Spectroscopy of Magnus' Green Salt and its Derivatives[1]

4.1 Introduction

The vibrational frequency of the hydrogenic group is often used as a guide to determine the presence and strength of hydrogen bonding in organic compounds, ionic salts and transition metal complexes [1]. The application of high pressures has been shown to provide interesting information regarding the nature and strength of the hydrogen bonding present in various complexes [2].

Lippincott and Schroeder [3] proposed a one-dimensional model of the hydrogen bond, which was later incorporated into aother model in order to describe the effect of applied pressures on the hydrogen bond [4]. Unlike other models, that of Lippincott and Schroeder introduces a hydrogen-oxygen repulsive force into the empirical potential energy function for hydrogen bonds. This addition gives a more quantitative result in the pressure model, particularly in the case of stronger hydrogen bonds or at very high pressures.

Magnus'' green salt, $[Pt(NH_3)_4][PtCl_4]$ (MGS), contains planar units of $[Pt(NH_3)_4]^{2+}$ and $[PtCl_4]^{2-}$ ions which stack parallel to the c-axis of the unit cell. The Pt atoms form direct bonding interactions, forming a chain with d(Pt-Pt) = $c/2$ = 3.25 Å. This results in a structure with two sets of Pt atoms at $z = 0$ and $^1/_2$, Fig 4.1. From this figure, it can also be seen that the structure is not organized simply as layers of $[Pt(NH_3)_4]^{2+}$ ions alternating with layers of $[PtCl_4]^{2-}$ ions. The crystal structure was reported by Atoji *et al.* in 1950 [5]. Although the hydrogens were not located, the N···Cl distance was reported to be 3.45 Å and considered long enough that hydrogen bonds were not present in MGS. Infrared peaks for the ν(NH) mode in MGS were observed by Atoji *et al.* at 3277 and 3182 cm^{-1}, while for free NH_3, ν(NH) is at 3414 and 3337 cm^{-1}.

---

[1] C. M. Edwards and I. S. Butler, in preparation.

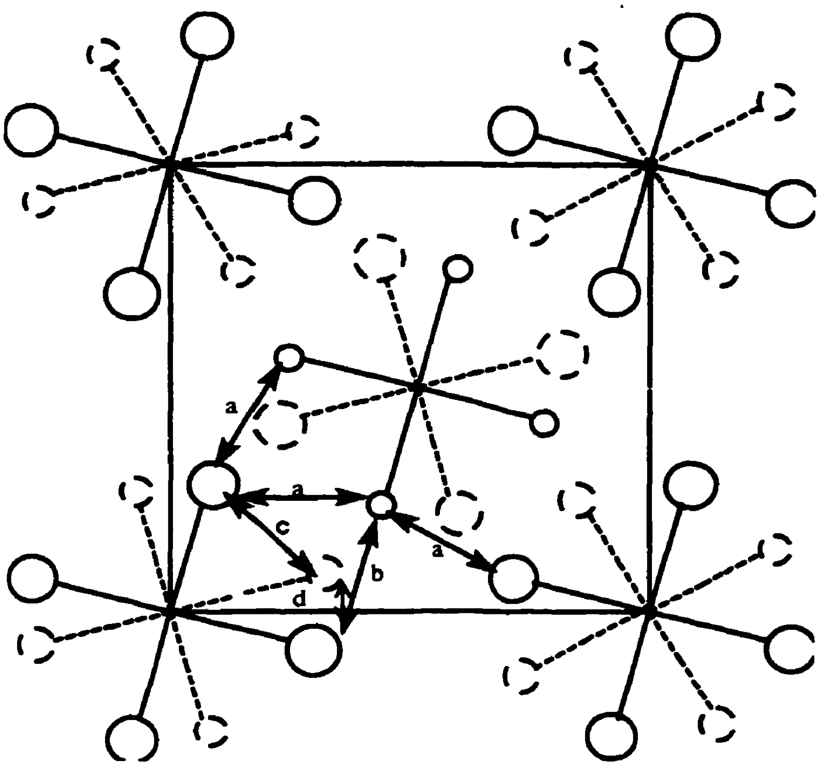

Figure 4.1. Atomic arrangement of Magnus' green salt. (Not to scale.) Large circles represent chlorine atoms and small circles nitrogens. Solid and broken lines indicate $z = 0$ and $^1/_2$ respectively. Platinum atoms are at the centers of square ions. $a = 3.45$ Å, $b = 3.47$ Å, $c = 3.96$ Å, and $d = 3.43$ Å. From ref. 5.

For a linear hydrogen-bond of the form N-H⋯Cl, as the distance R between the N and Cl atoms is reduced by compression, the electrostatic attraction between the proton and the chloride increases. The length of the N-H bond increases as a result, and its restoring forces and stretching frequency decrease. For linear hydrogen bonds, this model also accounts for the increase in frequency of the deformation modes under compression, since the increased H⋯Cl attraction makes it more difficult for the proton to move away from the N⋯Cl line and so increasing the restoring force for the bending vibration. Under compression, the stretching modes show negative pressure shifts and the bending modes positive pressure shifts. In the situation where the distance R is very small, as is the case for strong hydrogen bonds or at very high pressures, the N-H and H⋯Cl repulsive forces are an important part of the total forces and, under these circumstances, it might be expected that the trends discussed above would be reduced or even reversed.

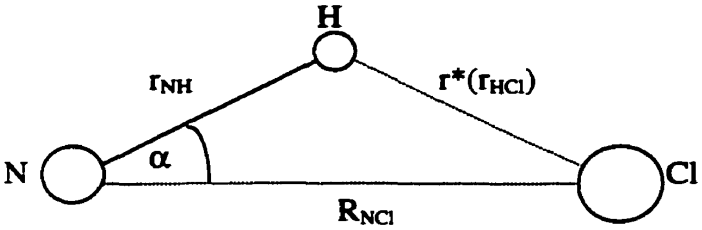

Scheme 4.1

The empirical function described by Lippincott and Shroeder can be used to interpret nonlinear hydrogen bonds under compression. The potential energy function for the ν(NH) stretching mode can be described by the following equations, using Scheme 4.1 above to describe the geometry:

$$r^* = (R^2 + r^2 - 2Rr\cos\alpha)^{1/2} \quad (4.1)$$

$$V_1 = D_0(1 - \exp\{-n(r-r_0)^2/2r\}) \quad (4.2)$$

$$V_2 = -D_0^*\exp(-n^*(r^*-r_0)^2/2r) \quad (4.3)$$

$$V = V_1 + V_2 + E(R) \quad (4.4)$$

where r_0 is the equilibrium N-H distance in the absence of hydrogen bonding and D and D* are the N-H and H$\cdots$Cl dissociation energies, respectively. The term E(R) consists of contributions arising from the van der Waals repulsion and Coulomb potential energies between N and Cl, which are independent of r. Plots of the potential, [V-E(R)]/D, as a function of r_{NH} for a range of R or α produces a series of potential curves. If the curvature of the bottom of the potential well increases with increasing R and/or α, then this means that there will be an increase in the force constant, k_H, since

$$k_H = (\delta^2V/\delta r^2)_{eq} \qquad (4.5)$$

We have undertaken a high-pressure IR study of MGS and two derivatives, $[Pt(ND_3)_4][PtCl_4]$ (MGS-D) and $[Pt(NH_3)_4][PtBr_4]$ (MGS-Br), from ambient pressure to ~40 kbar, in order to examine the possibility of weak hydrogen bonding of the type N-H$\cdots$Cl in these complexes. The structure of MGS and the derivatives MGS-Br and MGS-D possess the same space group, P4/*mnc*, and have similar unit cells. Substitution of methylamine for ammine in the salts has been shown to have no effect on the length of the c-axis [6], indicating that the methyl groups are held in the Pt-N planes and that the structure is strong enough to prevent rotation about the Pt-N bonds. Hydrogen bonding could be responsible for this rigid structure.

4.2 Experimental

The syntheses of MGS and the two derivatives were performed according to literature methods [7]. Hexachloroplatinic(II) acid, H_2PtCl_6 (Aldrich), was reduced with sulfurous acid (>6% SO_2), under acidic conditions. The reduction product, H_2PtCl_4, was reacted with aqueous ammonia to yield $[Pt(NH_3)_4]Cl_2$. The addition of $[Pt(NH_3)_4]Cl_2$ to an aqueous solution of H_2PtCl_4 resulted in the immediate precipitation of MGS, $[Pt(NH_3)_4][PtCl_4]$. The bromine derivative was prepared in the same manner, using H_2PtBr_6. For the deuterated derivative, $[Pt(NH_3)_4]Cl_2$ was dissolved in D_2O, followed by rapid evaporation to dryness. This was repeated three times. The resulting $[Pt(ND_3)_4]Cl_2$ was mixed with H_2PtCl_4 in D_2O-solution, the product $[Pt(ND_3)_4][PtCl_4]$ precipitating immediately. Further details on the high pressure experiment can be found in Chapter 2, Section 2.1.5.

4.3 Results

The vibrational modes in the mid-IR (4000-600 cm^{-1}) region of the spectra of MGS, MGS-D and MGS-Br are the internal modes of the NH_3 or ND_3 moiety coordinated to Pt(II) (Fig. 4.2). The $\nu_s(NH)$ and $\nu_{as}(NH)$ modes are located above 3100 cm^{-1} for MGS and MGS-Br. For the deuterated complex, the $\nu_s(ND)$ and $\nu_{as}(ND)$ modes lie between 2470 and 2300 cm^{-1}. The isotopic shift was found to be of the order of 1.37 and 1.34 for the symmetric and antisymmetric NH stretch, respectively. These bands were typically broad and asymmetric in shape, suggesting a splitting of the bands.

The symmetric and degenerate deformation modes are located between 1700 and 1300 cm^{-1}. The $\delta_s(NH_3)$ mode is assigned to a strong band at 1313.6 cm^{-1} in MGS, 1315 cm^{-1} in MGS-Br and 1013.9 cm^{-1} in MGS-D. The deuterium isotopic shift was 1.29. This strong band has a shoulder on the low wavenumber side for all complexes, but is stronger for MGS than for MGS-Br and MGS-D. The $\delta_d(NH_3)$ mode of MGS is split into two bands at 1546.1 and 1631.8 cm^{-1}. A similar splitting was observed for MGS-Br. For MGS-D, the $\delta_d(NH_3)$ mode was assigned to a band at 1152.9 cm^{-1}, with a shoulder at 1143 cm^{-1}. The resultant isotopic shift was 1.38. The bands at 824.5, 821.8 and 636 cm^{-1} for MGS, MGS-Br and MGS-D, respectively, are assigned to the rocking $\rho(NH_3)$ mode. A shoulder on the high wavenumber side is clearer in MGS than in the other derivatives. The larger splitting of the bands in MGS suggests a greater reduction in symmetry and/or a larger factor group splitting, compared to the two derivatives. The frequencies and relative intensities of the bands in each spectrum were in good agreement with literature [6b].

Figures 4.3-5 show selected regions of the IR spectra for increasing pressures. Plots of wavenumber vs. pressure show more clearly the negative pressure shift of the

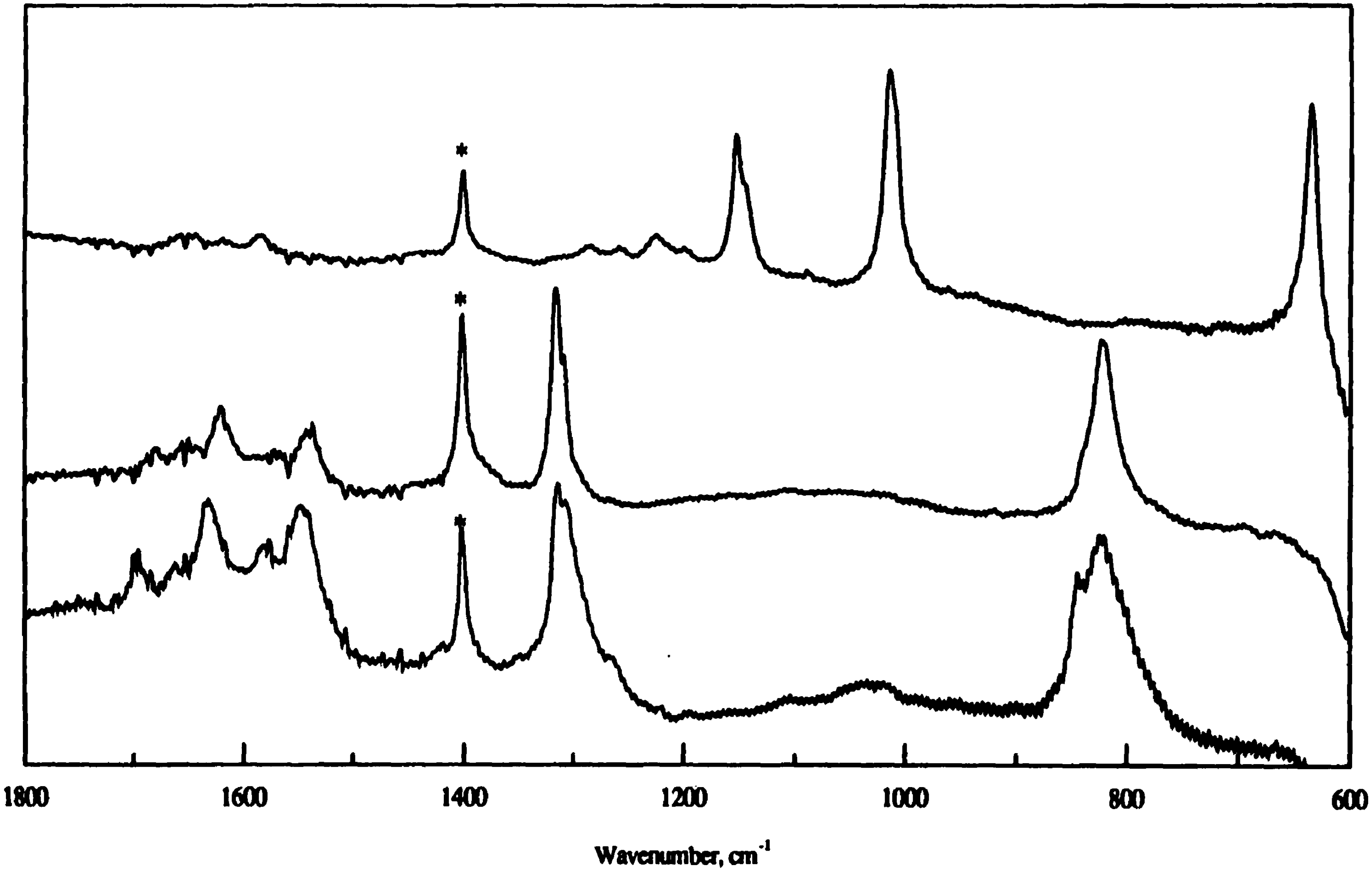

Figure 4.2. Ambient pressure mid-IR spectra of MGS (bottom), MGS-Br (middle) and MGS-D (top). *marks the antisymmetric NO stretch of the sodium nitrate calibrant.

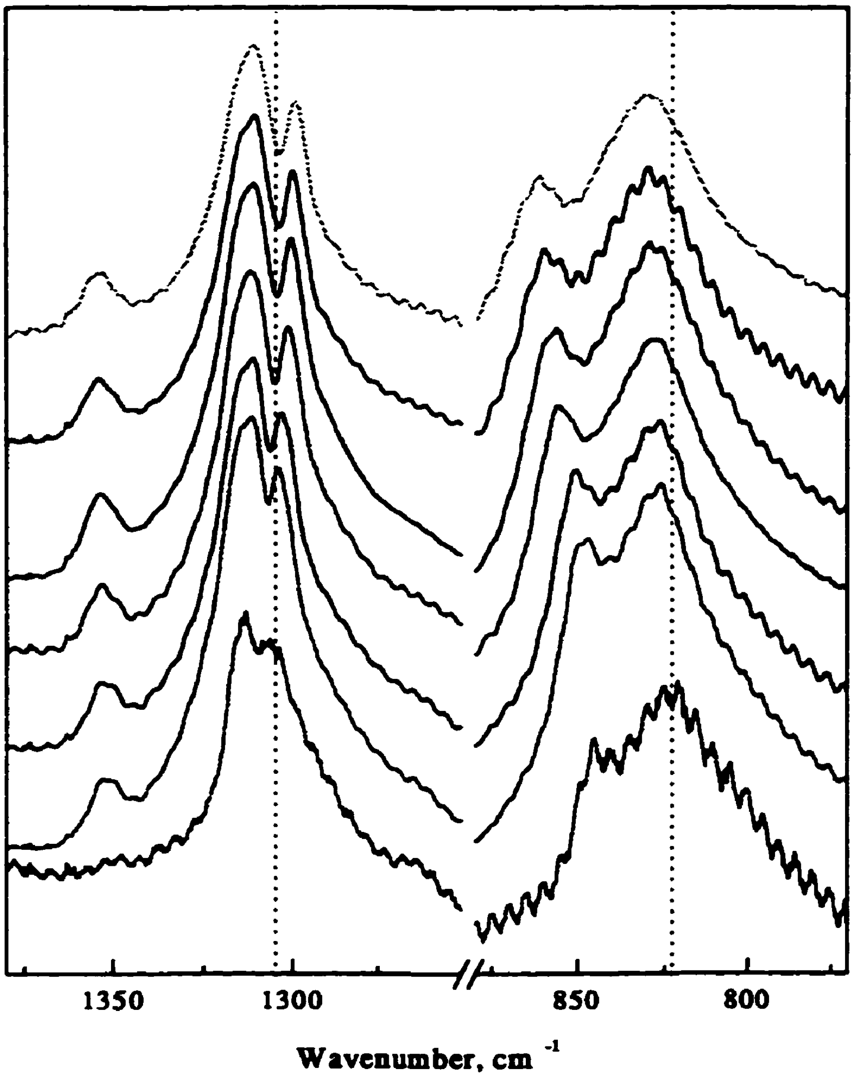

Figure 4.3. (a) The $\delta_s(NH_3)$ (1375-1200 cm^{-1}) modes and $\rho(NH_3)$ modes (850-775 cm^{-1}) of MGS as a function of pressure, from ambient pressure (bottom) to ~ 40 kbar (top).

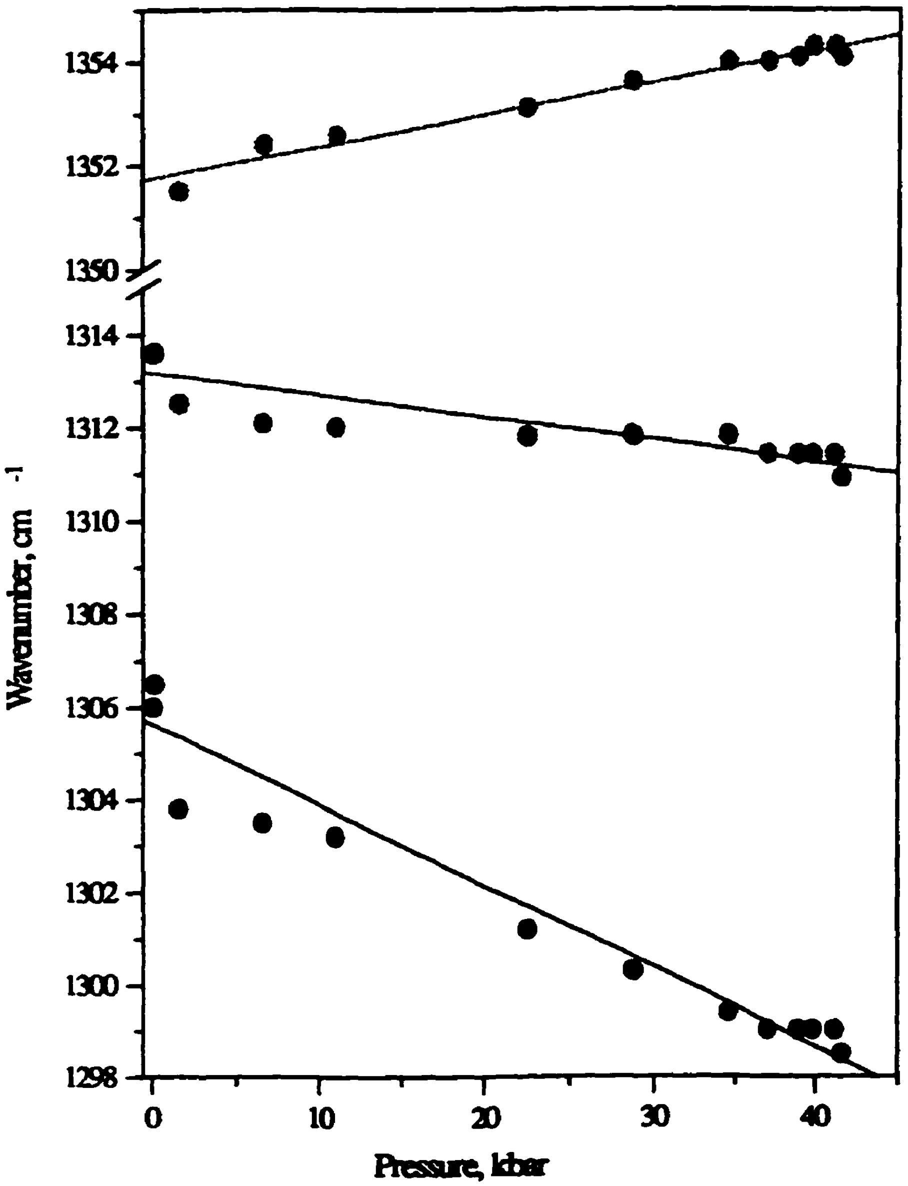

Figure 4.3. (b) Pressure dependences of the IR-active $\delta_s(NH_3)$ modes of MGS.

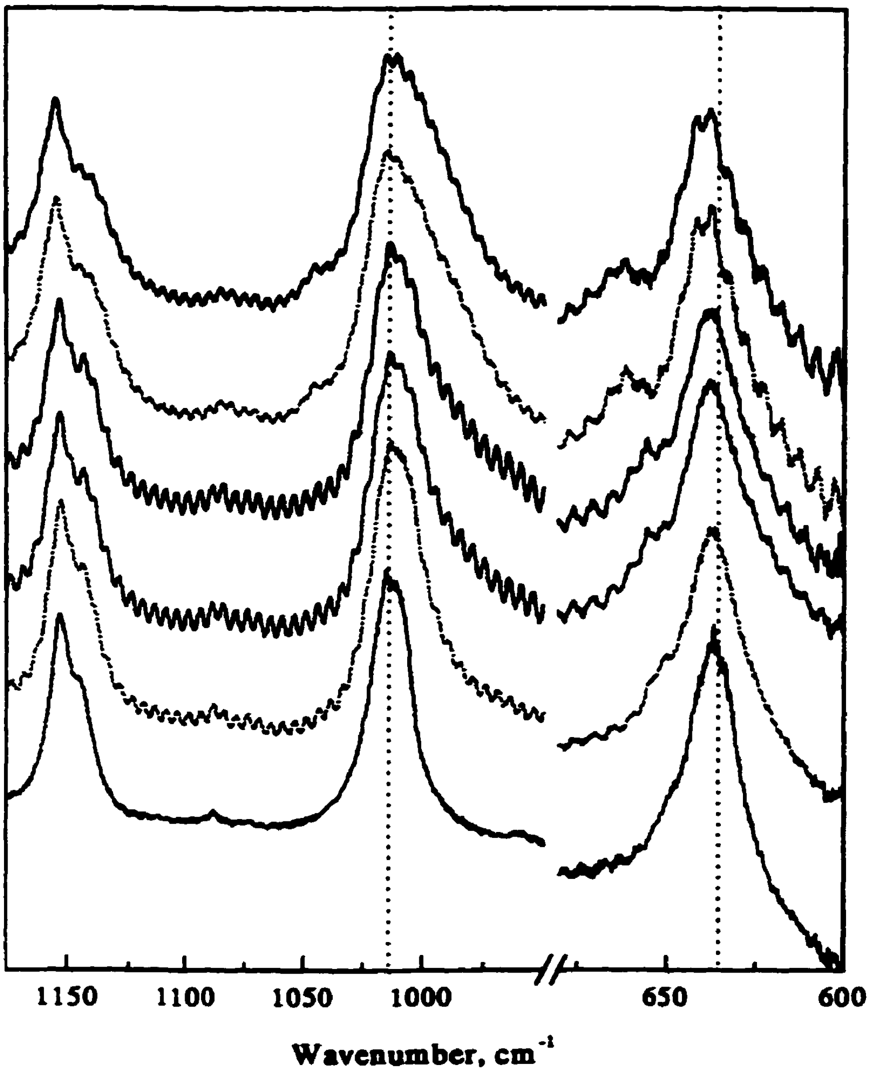

Figure 4.4. (a) The $\delta_s(NH_3)$ modes (1150 cm^{-1}), $\delta_d(NH_3)$ modes (1050-975 cm^{-1}) and $\rho(NH_3)$ modes (650-600 cm^{-1}) of MGS-D as a function of pressure, from ambient pressure (bottom) to ~40 kbar (top).

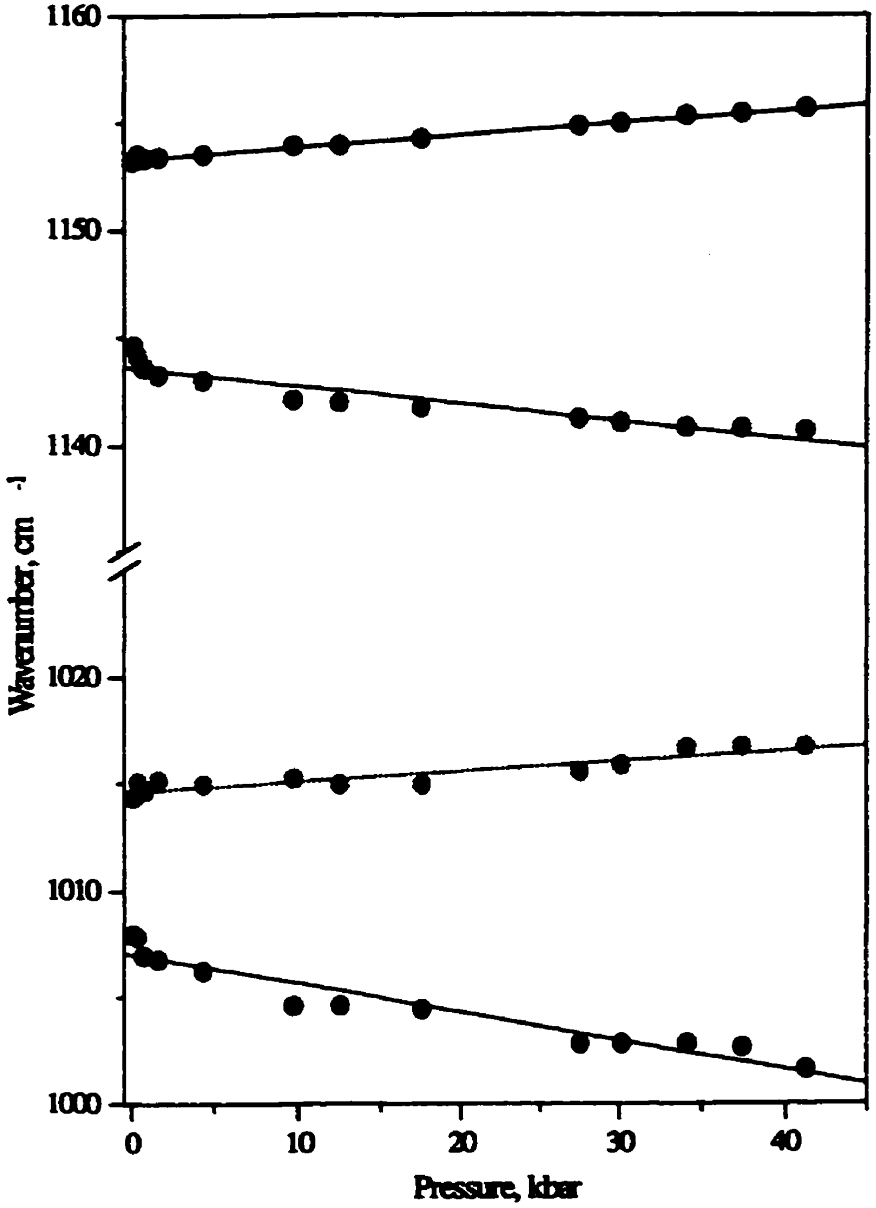

Figure 4.4. (b) Pressure dependences of the IR-active $\delta_d(NH_3)$ and $\delta_s(NH_3)$ modes of MGS-D.

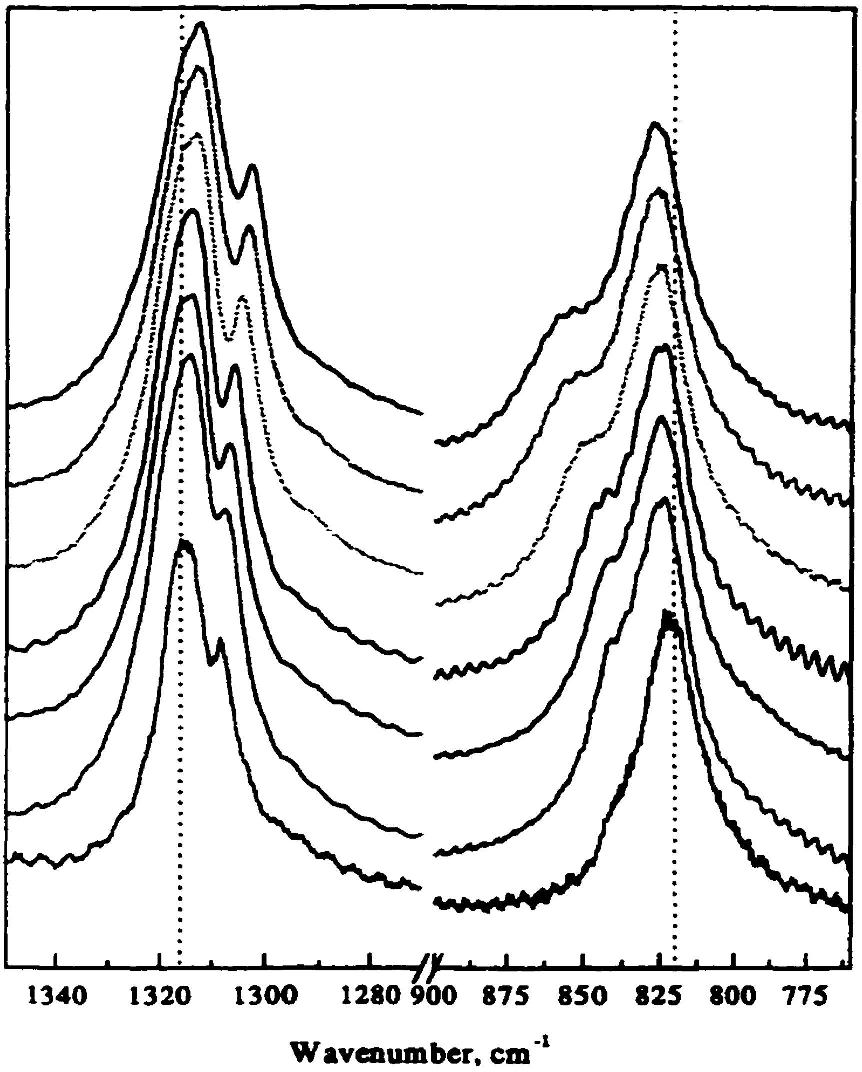

Figure 4.5. (a) The $\delta_s(NH_3)$ modes (1340-1300 cm^{-1}) and the $\rho(NH_3)$ modes (850-800 cm^{-1}) of MGS-Br as a function of pressure, from ambient pressure (bottom) to ~40 kbar (top).

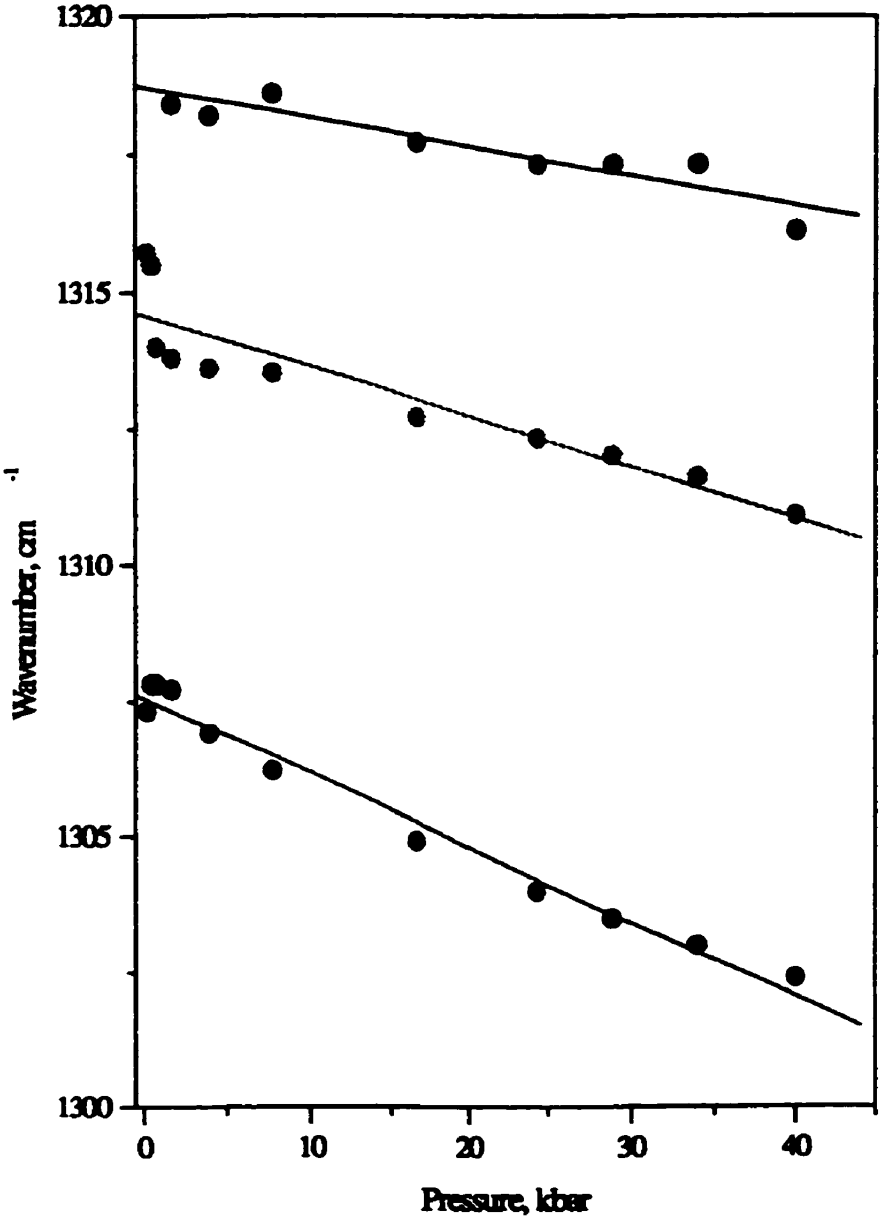

Figure 4.5. (b) Pressure dependences of the IR-active $\delta_s(NH_3)$ modes of MGS-Br.

$\delta_s(NH_3)$ modes and the positive pressure shift of all other modes. One exception is the $\nu_{as}(NH_3)$ mode of MGS-Br, which shows a negative pressure shift. The pressure dependences of all of the observed IR-active modes of MGS, MGS-Br and MGS-D are presented in Table 4.1. All the vibrational modes exhibited a continuous change in frequency over the pressure range studied, although some bands, for example the $\delta_s(NH_3)$ modes of MGS, did show slight curvature in the wavenumber *vs.* prssure plots at low pressures. A least-squares fit, however, gave $r^2 > 0.9$ for all bands. The band assigned to $\nu_{as}(NH_3)$ in MGS-D exhibited a greater curvature and two values for dv/dp are reported.

The $\rho(NH_3)$ mode in all three complexes shows a small, positive pressure shift, while the shoulder on the high wavenumber side has a larger dv/dp value and, as a result, becomes more distinct at higher pressures. The dv/dp values for the $\rho(NH_3)$ mode were comparable for all the complexes. The bending $\delta_d(NH_3)$ modes shift to higher wavenumbers with increasing pressures, these modes being more sensitive in MGS and least sensitive for MGS-D. The symmetric and antisymmetric stretching modes showed positive pressure dependences, the dv/dp values being notably smaller than are those observed for the other modes. The pressure dependences of the $\nu_s(ND_3)$ modes are somewhat greater than are those for $\nu_{as}(ND_3)$; for the $\nu_s(ND_3)$ mode at 2316.4 cm^{-1}, $dv/dp = 0.76\ cm^{-1}\ kbar^{-1}$. At higher pressures, the slope appears to level. The dv/dp values for the $\nu_{as}(NH_3)$ and $\nu_{as}(ND_3)$ modes in MGS and MGS-D are comparable. The $\nu_{as}(NH_3)$ mode in MGS-Br is the exception, shifting to lower wavenumbers with increasing pressures.

The effect of compression was reversible for all three complexes, although sluggish on decompression producing some hysterisis. Compression also resulted in piezochromism - the colour changed from green to orange-red. The transition pressure was close to 16 kbar, but it was difficult to determine any trend for the transition pressure from MGS to MGS-D to MGS-Br. Under compression the decrease in the Pt-Pt distance leads to an increase overlap of the d_{z^2} orbitals on

Table 4.1. FT-IR vibrational modes, their pressure dependences and assignments, for $[Pt(NH_3)_4][PtCl_4]$ (MGS), $[Pt(ND_3)_4][PtCl_4]$ (MGS-D) and $[Pt(NH_3)_4][PtBr_4]$ (MGS-Br).

MGS		MGS-D		MGS-Br		Assignment
cm^{-1}	dν/dp, cm^{-1} kar^{-1}	cm^{-1}	dν/dp, cm^{-1} kar^{-1}	cm^{-1}	dν/dp, cm^{-1} kar^{-1}	
824.5	0.062	636	0.072	821.8	0.067	$\rho(NH_3)$
846.2	0.41	650	0.3	840.5	0.44	
1306.0	-0.17	1006	-0.12	1307.3	-0.14	
1313.6	-0.048	1013.9	0.05	1315.7	-0.073	$\delta_s(NH_3)$
1351.5	0.061			1323.0	-0.053	
*1541.0	0.05	1143	-0.082			
1546.1	0.27	1152.9	0.06	1538.5	0.20	$\delta_d(NH_3)$
1580.0	0.45					
1631.8	0.46			1619.8	0.40	$\delta_d(NH_3)$
*1661.1	0.94					
3184.0	0.11	2316.4	0.76, 0.11	3176.2	0.26	$\nu_s(NH_3)$
3223.8	0.21	2343.0	0.12	3212.2	0.32	
3269.1	0.15	2444.6	0.15	3272.2	-0.15	
3298.5	0.09	2466.5	0.06	3290.2	-0.070	$\nu_a(NH_3)$
				*3304.4	-0.33	

* Indicates a band not present in the ambient pressure spectrum.

adjacent platinums. The colour change is a consequence of the a shift to lower energies of the electronic transitions, in the visible region [8].

4.4 Discussion

The obvious splitting of the vibrational modes in the FT-IR spectra of MGS, MGS-Br and MGS-D is the first indication of hindered rotation of the NH_3 group about the Pt-N bond. Several spectroscopic criteria have been proposed as evidence of specific hydrogen bonds in salts, with particular reference to ammonium salts. Dunsmuir and Lane [9] proposed that the presence of both the combination bands ($\nu_4 + \nu_6$) and ($\nu_2 + \nu_6$), a broadening of the lattice modes in the far-IR (ca. 200 cm^{-1}) and a shift of the ν_4 mode to progressively higher frequencies above 1400 cm^{-1} are a good indication to the presence of hydrogen bonds. The ν_4, ν_2 and ν_6 modes are the symmetric HNH bend, the antisymmetric HNH bend and the NH_4^+ torsion, respectively. The torsional mode results from restricted rotation of the ammonium ion. Waddington also attributed the loss of the degeneracy of the ν_3 N-H stretch and ν_4 deformation modes in ammonium salts to reduced rotation of the NH_4^+ ion because of hydrogen bonds [10]. A single, sharp band was observed for those salts in which the NH_4^+ ion was freely rotating.

For weak hydrogen bonding, the above model shows that dv/dp will be negative for the $\nu(NH_3)$ modes and positive for the $\delta(NH_3)$ modes. Nakamoto *et al.* [1] were of the opinion that, if this model interprets the behaviour of straight hydrogen bonds, then for bent and bifurcated hydrogen bonds, the $\nu(NH_3)$ and $\delta(NH_3)$ modes should show high and low frequency shifts, respectively. Any hydrogen bonds in MGS will be bent; the calculated N-H-Cl angle is 95° if the N-H bond length and H-N-H bond angle are the same as for NH_3. It is also possible that each chloride ion forms a hydrogen bond to each of the protons of the adjacent NH_3 group. The presence of strong interactions, even after substitution for a methylamine which lies in the Pt-N···Cl plane, indicates the presence of strong interactions of this plane. In the first instance, the high pressure results could be an indication of weak, bent hydrogen bonds in MGS and its derivatives MGS-D and MGS-Br, which increase in strength under compression.

Several studies, however, have shown that even in the case of bent and bifurcated hydrogen bonds, the model proposed by Lippincott and Shroeder is still valid and in some cases bent hydrogen bonds have been found to be stronger than straight hydrogen bonds in the same material. In hydroxylammonium chloride, NH_3OHCl, the NHCl angle is 153-157° and *d*(N-Cl) = 3.2 Å. A neutron diffraction study revealed that each proton forms a hydrogen bond with a chloride in the neighbouring molecule [11]. Under compression, dv/dp for ν(NH) = -0.25 cm^{-1} $kbar^{-1}$ and dv/dp for $\delta(NH_3)$ and $\rho(NH_3)$ = 0.12 cm^{-1} $kbar^{-1}$ [12].

In contrast, many ammonium compounds have been identified in which, under compression, the N-H stretches and the bending modes of hydrogen-bonded NH_4^+ ions shift anomalously to higher and lower frequencies, respectively [2]. In $(NH_3)_4Pb(SO_4)_2$, the ammonium ions are all equivalent and in sites of C_{3v} symmetry, with one straight hydrogen bond on the threefold axis and nine further oxygens forming three triangles, related by the three-fold axis containing the nitrogen, **1**. The closest oxygen-to-nitrogen distance is that with the oxygen on the three-fold axis. From the frequency of the $\nu(NH_3D^+)$ mode in a partially deuterated salt, Oxton and coworkers [13] showed that it was the hydrogen bonds formed by the off-axis protons which formed the strongest hydrogen bonds. For the related salt $(NH_3)_2SiF_6$, dv/dp for the antisymmetric N-H stretch and bending modes are 1.0 and 0.04 cm^{-1} $kbar^{-1}$, respectively [2]. These salts behave as though they have very strong hydrogen bonds, instead of the weak hydrogen bonds as interpreted from bond distances and vibrational frequencies. The observed pressure shifts could be a result of anisotropy of the compressibility of the salts, causing bending and subsequent weakening of the hydrogen bonds. Alternatively, strong electrostatic forces could be superimposed on the hydrogen bonding forces, and in their response to compression, many of the salts behave as if they had strong rather than weak hydrogen bonds.

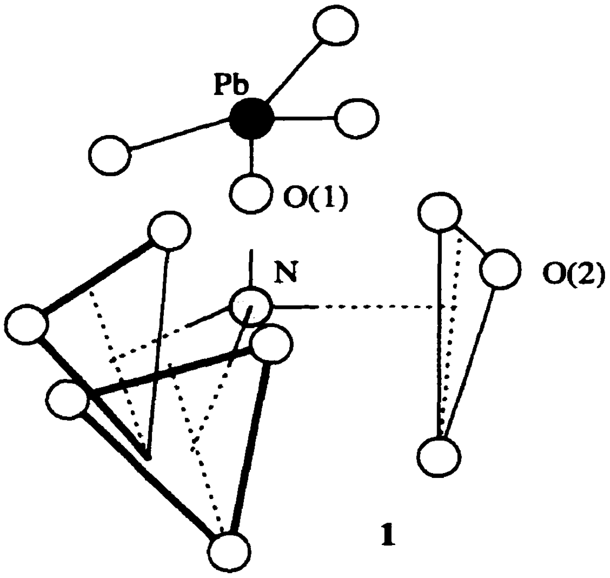

1

A high-pressure study of hexaamminenickel(II) halides, $[Ni(NH_3)_6]X$, (X = Cl, Br I), up to ~100 kbar, revealed a phase transition at 51 kbar for X = Cl and Br and at 23 kbar for X = I [14]. A splitting of the vibrational modes at the transition pressure showed that the phase transition involved a reduction in symmetry and an ordering of the NH_3 groups. Under ambient conditions, the NH_3 groups have considerable rotational freedom. Furthermore, under compression, the $\delta_s(NH_3)$ and $\delta_d(NH_3)$ modes showed a negative pressure shift. For the $\delta_s(NH_3)$ mode, dv/dp = -0.83 (X = Cl), -0.75 (X = Br) and -0.90 (X = I) cm^{-1} $kbar^{-1}$. The large, negative shift of the $\delta_s(NH_3)$ mode was attributed to a coupling of this mode to a soft mode associated with the phase transition. The v(NH) modes showed positive pressure dependences, dv/dp = 0.55, 0.48 and 0.24 cm^{-1} $kbar^{-1}$ for X = Cl, Br and I, respectively, for phase I. Above the phase transition pressure, dv/dp = 0.13, 0.21 and 0.07 cm^{-1} $kbar^{-1}$ for X = Cl, Br, I, respectively.

4.5 Conclusions

The similarity of the results for $[Ni(NH_3)_6]X_2$ with those observed for MGS and its derivatives, and the increased splitting uder compression, confirm that there is restricted rotation of the NH_3 moiety about the Pt-N bond in MGS, MGS-D and MGS-Br. The cause of this restricted rotation cannot be conclusively attributed to the presence of hydrogen bonding of the type Pt-N$\cdots$Cl, but neither can it be ruled out. The form of the symmetric deformation $\delta_s(NH_3)$ mode results in a decrease of the Pt-N-H bond angle for all the three protons. Under compression, the N$\cdots$Cl distance decreases, but also during the vibration the N-H-Cl becomes less bent and the strength of a hydrogen bond will increase. Thus, the presence of increasing strength hydrogen bonds will reduce the restoring forces of the vibrational mode and lower the frequency of the vibration. This could explain the negative pressure dependence of the symmetric deformation $\delta_s(NH_3)$ mode. Bromine is less electronegative and so less likely to form hydrogen bonds than is chlorine. The differences in the pressure dependences of the vibrational modes are relatively small on going from MGS to MGS-Br, with the exception of the antisymmetric $\nu_{as}(NH_3)$ mode. It is not understood as yet why this mode shows a negative pressure shift.

If, under compression, the delicate balance of the competing molecular forces (cation-anion interactions, van der Waals forces and hydrogen-bonding) are disrupted and, if a second configuration of comparable stability exists, solid-state isomerization can be induced. Examples of isomerization in metal clusters and piezochromic transitions of the Cu(II) complexes were discussed in Chapter 1, Section 1.4.2. The dihydride-dihydrogen interconversion in $[(PP_3)Co(H)_2]BPh_4$, $[PP_3 = P(C_2H_4PPh_2)_3]$ was also described in the introduction. In a continuation of the study of these compounds, Chapter 5 decribes the high-pressure IR study of $ReH_7(dppe)$.

4.6 References

1. K. Nakamoto, M. Morgoshes and R. E. Rundle, J. Am. Chem. Soc., 77 (1955) 6480-6486.
2. S. D. Hamann, Aust. J., Chem., 31 (1978) 11-18, and references therein.
3. E. R. Lippincott and R. Schroeder, J. Chem. Phys., 23 (1955) 1099-1106.
4. S. D. Hamann and M. Linton, Aust. J. Chem., 28 (1975) 2567-2578.
5. M. Atoji, J. W. Richardson and R. E. Rundle, J. Am. Chem. Soc., 79 (1957) 3017-3020.
6. J. R. Miller, J. Chem. Soc., (1961) 4452-4457.
7. (a) R. N. Keller, Inorg. Synth., 2 (1946) 250-253; (b) J. R. Hall and D. A. Hirons, Inorg. Chim. Acta, 34 (1979) L277-L279.
8. L. V. Interrante and F. P. Bundy, Inorg. Chem., 10 (1971) 1169-1180.
9. J. T. R. Dunsmuir and A. P. Lane, Spectrochim. Acta A, 28 (1972) 45-50.
10. T. C. Waddington., J. Chem. Soc., (1958) 4340-4344.
11. U. M. Padmanabhan H. G. Smith and S. W. Peterson, Acta Cryst., 22 (1967) 928-930.
12. S. D. Hamann and M. Linton, Aust. J. Chem., 29 (1976) 1641-1647.
13. I. A. Oxton, O. Knop and M. Falk, Can. J. Chem., 53 (1975) 3394-3400.
14. D. M. Adams and J. Haines, J. Phys. Chem., 95 (1991) 7068-7071.

Chapter 5

Pressure-induced Solid-State Isomerisation: The Dihydride-Dihydrogen Interconversion[1]

5.1 Introduction

Hydride complexes formed by the cleavage of H_2 are known to play a key role in catalytic hydrogenation mechanisms of unsaturated organics and other compounds. Addition proceeds via an oxidative-addition pathway, the initial interaction of H_2 with a metal center being regarded only as a transient in hydride formation. The successful synthesis and characterization of the stable complex, $W(\eta^2\text{-}H_2)(CO)_3(PPr^i_3)_2$, containing a dihydrogen ligand by Kubas *et al.* in 1984 [1] paved the way for further work in this area. These dihydrogen complexes, along with polyhydride complexes, have become important model systems for investigating the nature of the bonding of molecular hydrogen to a metal and subsequent bond cleavage in catalytic processes.

The dihydrogen-dihydride interconversion is known for several complexes in solution, this interconversion being monitored by ^{1}H-NMR spectroscopy [2]. The barrier to interconversion in $IrCl(H)_2(H_2)(PPr^i_3)_2$ is below 3 kcal/mol. We have recently shown for the first time that dihydride to dihydrogen isomerization can be induced in the solid state under compression at room temperature [3]. Under modest pressures of just 6-10 kbar, the pale yellow dihydride complex, $[(PP_3)Co(H)_2]BPh_4$, $[PP_3 = P(C_2H_4PPh_2)_3]$ is transformed to the red dihydrogen complex, $[PP_3Co(\eta^2\text{-}H_2)]BPh_4$. The disappearance of the ν(Co-H) stretching mode, and the ν(Co-D) stretching mode in the deuterated analogue $[(PP_3)Co(D)_2]BPh_4$, was observed at the transition pressure.

In this paper, we present the results of a high-pressure vibrational study on the neutral rhenium heptahydride complex, $ReH_7(dppe)$ (**1**) (dppe = ethylene-1,2-bisdiphenylphosphine), which indicates that, on application of hydrostatic pressure, at

---

[1] C. M. Edwards and I. S. Butler, Inorg. Chem., in preparation.

pressures above 5 kbar a hydrogen-hydrogen interaction is formed. This interaction increases as the pressure is further increased up to 40 kbar. There was no evidence for a pressure-induced interconversion in the analogous triphenylphosphine complex, $ReH_7(PPh_3)_2$ (**2**).

5.2 Experimental

The rhenium(VII) complex **1** was prepared according to literature methods, i.e., $ReOCl_3(dppe)$ [4] was first prepared by the addition of concentrated HCl to $NaReO_4$ in boiling ethanol. The blue-green complex, which is precipitated as the addition proceeds, was reduced with $Li[AlH_4]$ in THF under reflux (90 min) [5]. The resulting solution was evaporated and the crude residue was extracted with THF. Concentration of the solution and cooling to -20°C afforded crystals of the desired product, **1**. The analogous deuterated complex was prepared following the same method, the reduction step being performed with $Li[AlD_4]$. Further details of the high pressure experiment can be found in Chapter 2, Section 2.1.5.

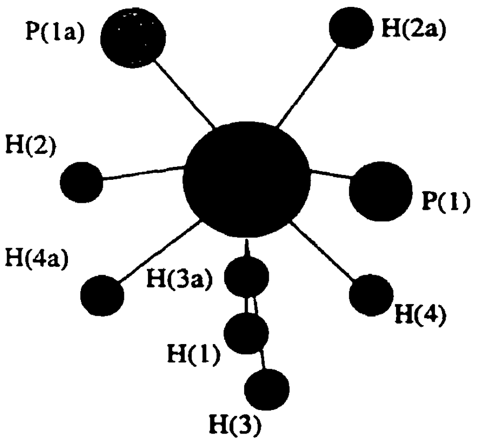

1

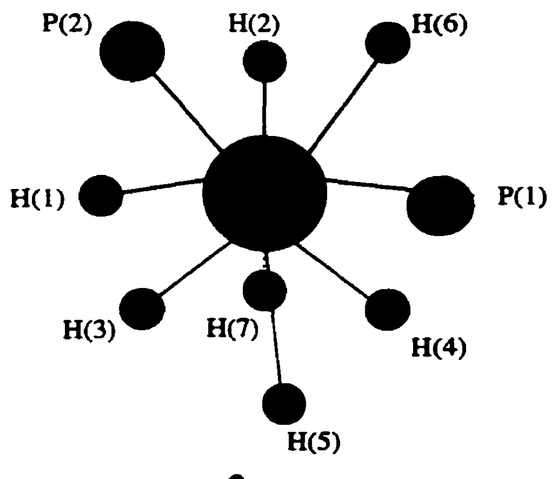

2

5.3 Results

Complex **1**, $ReH_7(dppe)$, has been described as a classical polyhydride with seven discrete hydride ligands. Single-crystal neutron diffraction studies of $ReH_7(dppe).2THF$ [6] have revealed that the structure is a monocapped, square antiprism with H(1) in the capping position and the diphosphine occupying diagonal positions on the square uncapped face. The shortest intramolecular H...H separation is 1.77 Å [H(1)...H(4)]. Complex **2**, $ReH_7(PPh_3)_2$, is thought to deviate from the classical polyhydride structure, having a structure in which one H...H separation is much shorter than is the average H...H separation for classical non-bonded hydrides of about 1.6 Å, yet not as close as the typical values of 0.8 Å for coordinated dihydrogen ligands $[M(\eta^2\text{-}H_2)]$. This shorter H...H distance presumably indicates a significant H...H bonding interaction. The structure of the **2** is not available, but $ReH_7\{P(p\text{-}tolyl)_3\}_2]$ [7] has also been described as having a monocapped, square antiprismatic geometry, the two phosphine ligands occupying diametrically opposed positions on the capped, square face P(1)-H(1)-P(2)-H(6), the uncapped face being defined by four hydrogen atoms arranged as a trapezoid, H(3)-H(5)-H(4)-H(7). The H(3)-H(5) separation is the shortest at 1.357(7) Å.

In solid-state IR spectrum of $ReH_7(dppe)$, three bands at ~1977, 1900 and 1824 cm^{-1} were assigned to the ν(Re-H) modes. For $ReH_7(PPh_3)_2$, the ν(Re-H) modes were located at 1965 and 1896 cm^{-1}. For the deuterated analogue, the ν(Re-D) modes shifted to ~1411 and ~1369 cm^{-1}, respectively. These bands were typically broad, although for the hydride complexes, the higher frequency band was often relatively strong in intensity. The peak frequencies are in agreement with those reported in the literature [5]. Some residual hydride species always remained in the deuterate.

The IR spectra of $ReH_7(dppe)$ with increasing pressure are shown in Figure 5.1. The band assignments [8] and pressure dependences for the observed modes are reported in Table 5.1. The pressure dependences are reported for two pressure regions, a low-pressure phase and a high-pressure phase, where appropriate.

Figure 5.1. IR spectra in the 1600-950 cm^{-1} region of ReH$_7$(dppe) with increasing pressure. The sharp peak indicated by * in each spectrum is the antisymmetric ν(NO) mode of the NO$_3^{2-}$ ion of NaNO$_3$, the internal pressure calibrant.

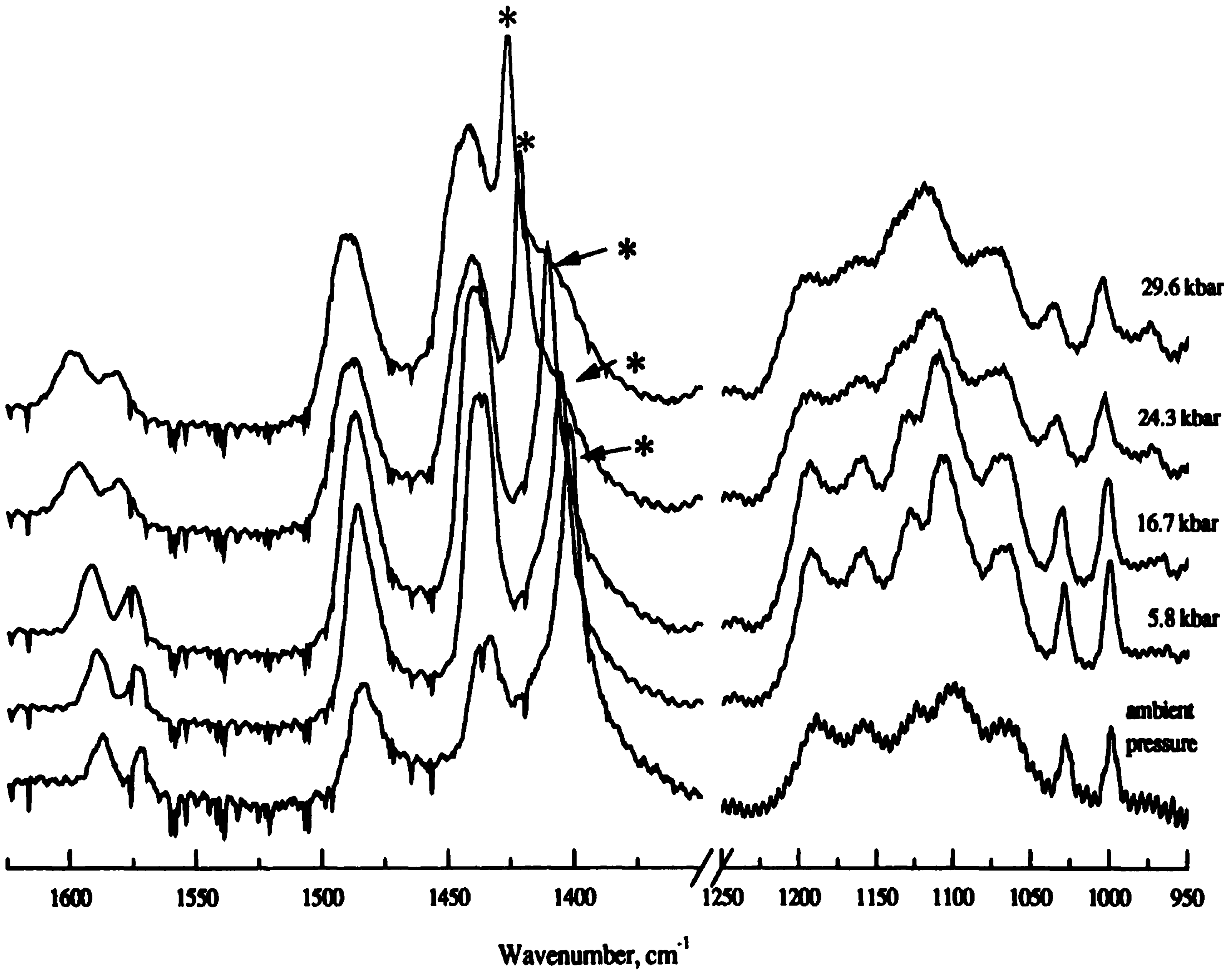
*
*
*
*
*
29.6 kbar
24.3 kbar
16.7 kbar
5.8 kbar
ambient pressure
1600
1550
1500
1450
1400
1250
1200
1150
1100
1050
1000
950
Wavenumber, cm^{-1}

Table 5.1. Pressure dependences of the IR bands of $ReH_7(dppe)$.

ν, cm^{-1}	$d\nu/dp$, cm^{-1} kbar^{-1}		Assignments
	low pressure phase	high pressure phase	
783.6 *ms*	0.07[a]	-0.08	δ(ReH)
796.4 *w*	0.11[a]	0.1	
811.3 *m*	0.53[b]	0.26	
896.4 *vs*	0.9[b]		
918.3 *sh*	0.43	n. b.	γ(CH), i
969.9 *w*		0.25[c]	
998.8 *m*	0.17	n. b.	ring breath, p
1006.4		0.3[c]	
1028.8 *m*	0.19	n. b.	β(CH), b
1036.1 *sh, w*		0.3[b]	
1060.6 *ms*	0.2[c]		β(CH), d
1106 *s*	0.5[b]		q X-sensitive
1158.9 *m*	0.01	n. b.	β(CH), c
1190.3 *ms*	0.18	n. b.	β(CH), a
1276.7 *w*	0.5	n. b.	CH$_2$-wag + e
1312.5 *m*	0.22	n. b.	o ν(CC)
1335.1 *m*	0.22	n. b.	
1402.7 *sh, w*	0.6[d]		p + w
1406.9 *s*	0.5[e]		i + y
1435.9 *vs*	0.25	n. b.	δ(CH)
1475.4 *vs*	0.5[b]	0.1	n, m
1484.4 *vs*	0.4[b]	0.3	
1572.2 *m*	0.36[e]	0.2	l, k
1587.1 *m*	0.39[c]		
2636.7 *vw,br*	0.24[a]	0.34	ν(HH)
2849.0 *s*	0.4[b]	0.27	
2868.2 *s*	0.4[b]	0.49	ν_s(CH)
2897.6 *sh, m*	0.4	n. b.	
2914.8 *sh, m*		0.4[d]	
2930.3 *s*		0.5[d]	ν_{as}(CH)
2964.0 *s*	0.36	n. b.	
2990.2 *sh, m*	0.44	n. b.	
3023.3 *m*	0.57	n. b.	
3056.3 *s*	0.54	n. b.	ν(CH) ring
3078.1 *sh,m*	0.6[a]		

[a] Up to or from 23.2 kbar; [b] Up to or from 16.7 kbar; [c] Up to 29.6 kbar; [d] From 9.2 kbar; [e] Up to 27.7 kbar; n.b., No break in slope.

However, from the wavenumber vs. pressure plots, up to three pressure phases were observed for some modes. Several of the vibrational modes, e.g., Fig. 5.2, showed small positive shifts with initial increases in pressure and then, from 16.7 kbar, showed much greater pressure dependences, leveling off again above 29.6 kbar. The pressure dependences given in Table 5.1 show the initial pressure response, below 16.7 kbar, or 23.4 kbar for those curves where the increase was smaller. In contrast, the ν(CC) modes at 1475.4 and 1484.4 cm^{-1}, for example, had a larger initial response to pressure, between 16.7 and 29.6 kbar the pressure shift was much smaller, and then above 29.4 kbar the pressure dependence increased again (Fig. 5.3). The band at 1276 cm^{-1}, assigned to the CH_2-wag + e mode, shows a different response to applied pressure, increasing to a maximum with increasing pressure (Fig. 5.3). The pressure dependence reported in Table 5.1 for this band is based on the initial pressure shift. Other modes exhibit almost linear pressure shifts up to 40 kbar. Furthermore, as the pressure increases, several peaks lose intensity and are not observed at higher pressure, e.g., those at 1060.6 and 1406.9 cm^{-1}, while three peaks at 969.9, 1006.4 and 1036.1 cm^{-1} only appear at higher pressures. These observations suggest that, over the 16.7-29.6 kbar range, the complex undergoes a phase change, during which several modes become more or less pressure sensitive. Other modes are practically insensitive to the phase change.

The IR spectrum of the deuterate ReD_7(dppe) proved to be more complicated to interpret, due to overlapping bands and the inability to observe clearly the calibration peak in the spectrum. Furthermore, the regions between 1250 and 1000 cm^{-1} and below 950 cm^{-1} were a continuous, broad absorption band, most likely due to the presence of THF, from which the crystals are recrystallized.

As the pressure was increased above ~5 kbar, a broad, weak peak appeared at ~2636 cm^{-1} in the IR spectrum of ReH_7(dppe) (Fig. 5.4). Because of interference fringes in the spectra and the broadness of the band, it was difficult to follow with increasing pressure. However, the results do suggest a positive shift of this band with increasing pressure. No such band was observed for ReD_7(dppe). Based on observations made by Kubas and others [2(a), 9,10], the new peak at ~2636 cm^{-1} has

Figure 5.2. Wavenumber *vs*. pressure plot for the ν_s(CH) and ν_{as}(CH) modes of ReH_7(dppe).

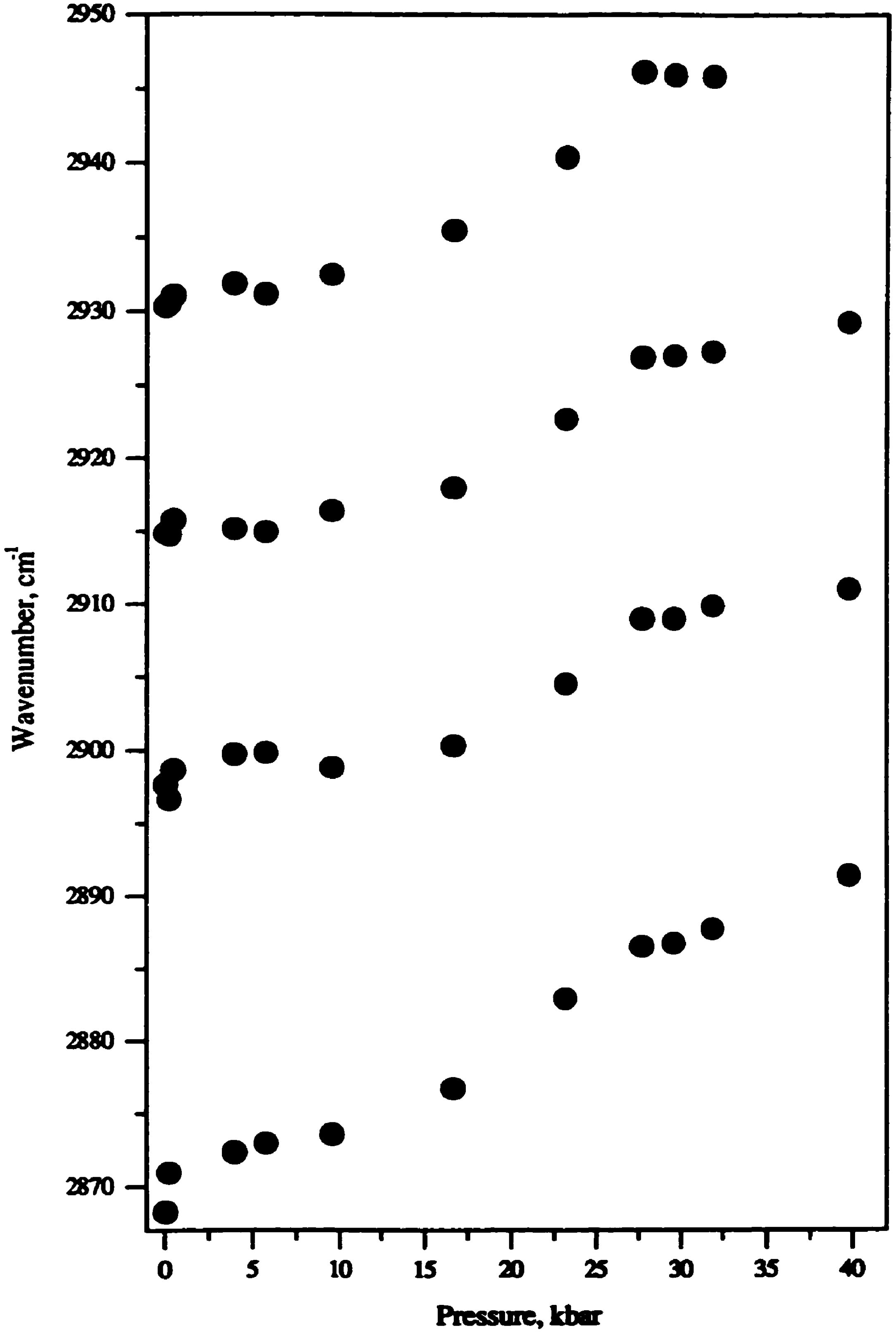
2950
2940
2930
2920
2910
2900
2890
2880
2870
Wavenumber, cm^{-1}
0
5
10
15
20
25
30
35
40
Pressure, kbar

Figure 5.3. Wavenumber *vs.* pressure plot for selected vibrations between 1490 and 1270 cm^{-1} of ReH$_7$(dppe).

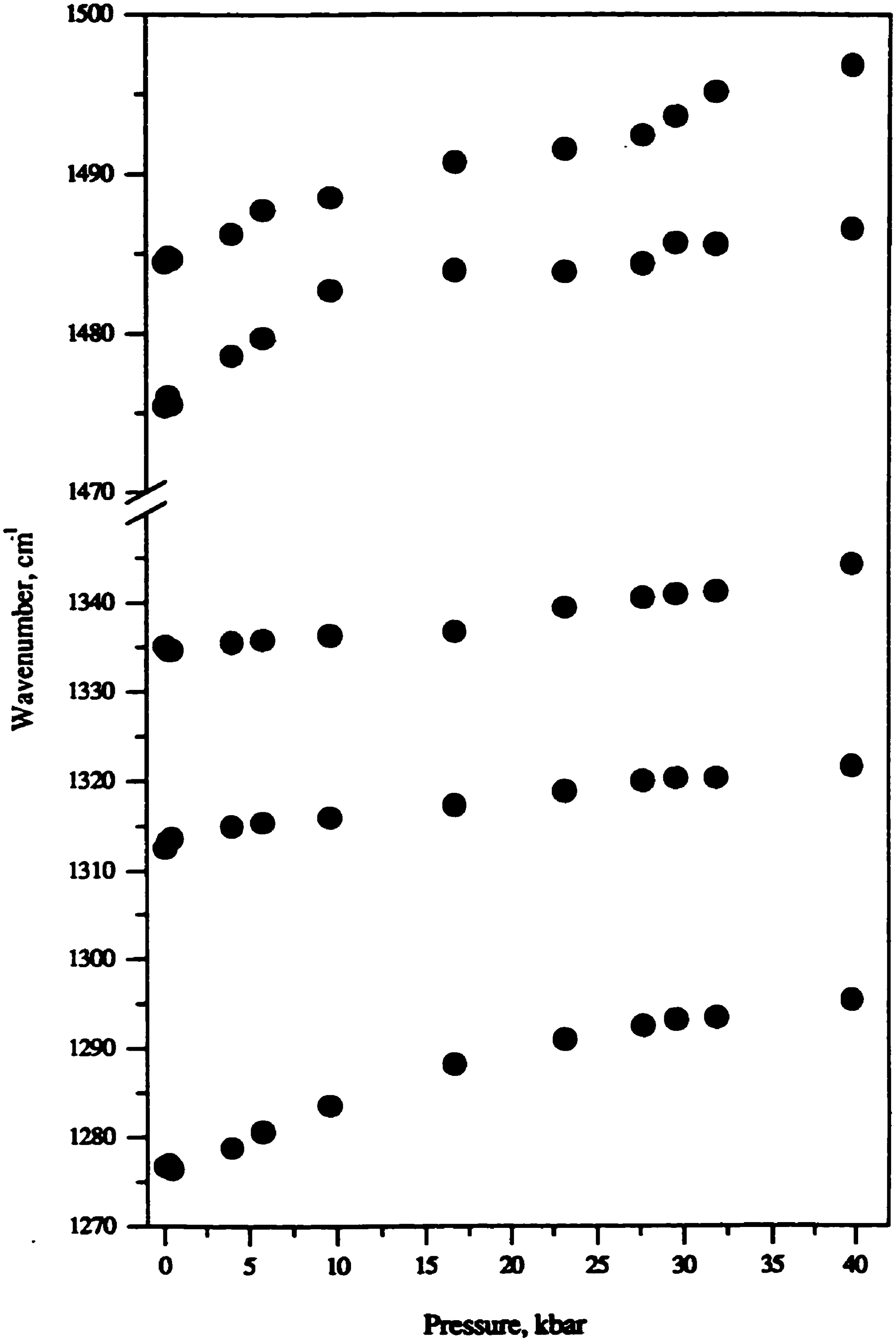
1500
1490
1480
1470
1340
1330
1320
1310
1300
1290
1280
1270
Wavenumber, cm^{-1}
0
5
10
15
20
25
30
35
40
Pressure, kbar

Figure 5.4. IR spectra of $ReH_7(dppe)$ at three pressures, showing the growth of a broad band centered at ~1236 cm^{-1} from 5.8 kbar.

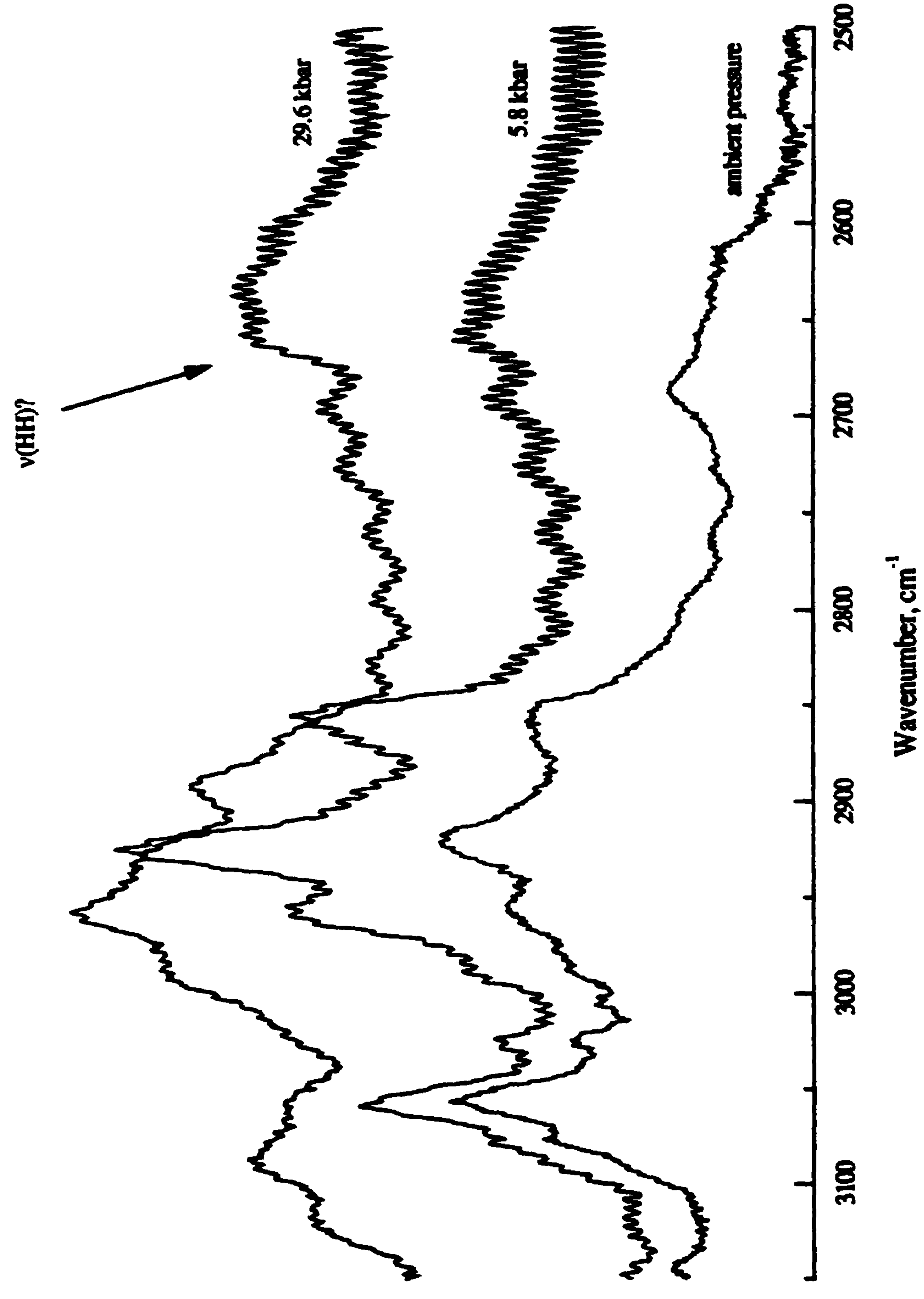
ν(HH)?
29.6 kbar
5.8 kbar
ambient pressure
2500
2600
2700
2800
2900
3000
3100
Wavenumber, cm^{-1}

been assigned to ν(HH) of a Re(η^2-H_2) moiety. The application of pressure to ReH_7(dppe) appears to cause a decrease in one H...H intramolecular separation and an increase in their bonding interaction. On the basis of this assignment, this band should shift to ~1900 cm^{-1} for ν(DD) in ReD_7(dppe). However, the broad absorption due to the diamond would obscure any new bands appearing in this region.

5.4 Discussion

The initial frequency of this new peak (~2636 cm^{-1}) is lower than is that reported for any coordinated dihydrogen stretching frequency in the literature. The closest H...H separation in ReH_7(dppe) is 1.77 Å, between H(1) and H(4), and it seems reasonable to suggest that it is between these particular hydrogens that the pressure-induced interaction occurs. A bonding scheme proposed for metal-dihydrogen complexes is analogous to the Dewar-Chatt-Duncanson model for M-olefin π-bonding, in which there is a transfer of electrons from the H_2 σ-orbital into a vacant metal *d*-orbital, plus transfer of electrons from an occupied metal *d*-orbital to the σ*-antibonding orbital of H_2 [9]. H_2 binding and eventual cleavage of the H-H bond is thus aided by backdonation of electrons from the metal to the H_2 σ*-orbital. The stability of the dihydrogen *vs.* dihydride ligand is, therefore, a balance between σ-donation to the metal and π-backbonding from the metal to the H_2 ligand. Cleavage of the dihydrogen ligand to form the two hydride ligands can be thought of as either by a gradual lengthening of the H-H bond as more electrons are put into the σ*-antibonding orbital, or, as progression along the reaction coordinate from dihydrogen to dihydride is made, there is little change in the H-H bond length until such a situation is reached when no more π-backbonding can be tolerated and the bond breaks. Complexes of the type $Mo(CO)(\eta^2\text{-}H_2)(Ph_2PC_2H_4PPh_2)_2$ [10] and $[Fe(\eta^2\text{-}H_2)(H)(Ph_2PC_2H_4PPh_2)_2]BPh_4$ [11] contain dihydrogen ligands in which the H-H distance remains practically constant along the reaction coordinate, from dihydrogen to dihydride, until bond breaking is imminent. In comparison, $[Re(\eta^2\text{-}H_2)H_4(Cyttp)]SbF_6$ [12] features a surprisingly long H-H bond and follows a smooth gradation in structure as it progresses along the reaction coordinate from dihydrogen to dihydride.

The magnitudes of the pressure shift of the ν(HH) mode of the dihydrogen ligand, dν/dp = 0.24 and 0.34 cm^{-1} $kbar^{-1}$, are relatively small compared to values normally seen for vibrations involving hydrogens. Since vibrations involving hydrogens are particularly anharmonic, they can be expected to have large pressure shifts of over 1.0 cm^{-1} $kbar^{-1}$. The initial effect of compression is a decrease of the inter- and intramolecular interactions, which results in a positive pressure shift for most vibrational modes. If the amount of π-backbonding from the metal increases, a negative shift of the frequency of the ν(HH) mode would be observed. Under compression, these two effects could combine and the result is a smaller pressure shift. The small, positive pressure shifts observed could be an indication of an increasing π-backbonding.

Although there is one H-H distance shorter than the others in the single crystal at ambient pressure, the results do not tell us if there is just one H-H interaction forming between these two particular hydrogens, or some other situation. It has been suggested that, in polyhydrides, a delocalized σ-bonding analogous to the π-system of allyls is possible [9]. Coordination of this type has been used to explain long H-H bond lengths, but X-ray and neutron diffraction studies have shown that in some cases an asymmetric or even an end-on H_2 coordination is more likely the cause of the longer H-H bond distances. The low frequency of the observed ν(HH) mode at ~2636 cm^{-1}, however, seems to indicate that a relatively short H-H bond is formed directly upon forming the interaction. For the complex $Mo(CO)(\eta^2\text{-}H_2)(dppe)_2$ [10], where *d*(HH) = 0.8-0.85 Å, ν(HH) = 2650 cm^{-1} and in $W(\eta^2\text{-}H_2)(CO)_3(PPr^i_3)_2$ [1], *d*(HH) = 0.82(1) Å, and ν(HH) = 2695 cm^{-1}, based on the D_2 complex. It is possible that a complex of the type $Re(\eta^2\text{-}H_2)(H)_5(dppe)$ resembles the aforementioned Mo and Fe complexes, which show a relatively flat reaction coordinates from $M\text{-}(\eta^2\text{-}H_2) \rightarrow M\text{-}(H)_2$. Many Re-dihydrogen complexes, however, contain elongated H-H bonds and/or asymmetric coordination of the H_2 ligand [13].

Preliminary results from pressure-tuning FT-IR studies of $ReH_7(PPh_3)$ and its deuterate show no indication of a pressure-induced coordinated dihydrogen formation, in spite of the closest hydrogen-hydrogen distance being smaller than in ReH_7(dppe). Consideration of the electronic effects alone would lead one to believe that pressure-induced dihydrogen formation would be more likely for $ReH_7(PPh_3)_2$ than for ReH_7(dppe). For a series of compounds of general formula $Mo(CO)(H_2)(R_2PC_2H_4PR_2)_2$ [9], when R = Ph, the dihydrogen ligand is stable. However, when R = Et, the H-H bond breaks and a complex with discrete hydride ligands is more stable. This change from Ph to Et represents just a small increase in the electron density at the metal center, but sufficient to cause an increase in the π-backbonding from the metal to the H_2 ligand. Aside from the obvious difference in the number of phenyl rings on the phosphine, the most noticeable difference in their structure is the P-Re-P angle, reported as 83° and 151.3(1)°, for ReH_7(dppe) and $ReH_7\{P(p\text{-tolyl})_3\}_2]$, respectively. The larger P-Re-P angles and symmetrical geometry of the phosphine ligands in $ReCl(\eta^2\text{-}H_2)(PMePh_2)_4$ (P-Re-P = ~168.8 and ~164.3°) [12(b)] were considered sufficient to stabilize the dihydrogen, as the distortion and closing-up of the P-Re-P angle to accommodate the two dihydride ligands is too great.

It is most likely that the phase change that occurs in ReH_7(dppe) between 16.1 and 29.6 kbar involves rotation of the phenyl rings, possibly in order to accommodate the formation of $(\eta^2\text{-}H_2)$. Phenyl ring rotation under pressure has been recognized in triphenylphosphine (PPh_3) [14] and in the coordination complexes Ph_4M (M = Si, Ge, Pb, Sn) [15].

5.5 Conclusions

The effect of applied pressure on the neutral, classical heptahydride complex, $ReH_7(dppe)$, is the formation of a η^2-H_2 ligand. The low frequency of the ν(HH) mode at ~2640 cm^{-1} suggests a short H-H bond distance, significantly smaller than the closest ambient pressure separation of 1.7 Å. Bond distances of the order 0.8-0.9 Å are normally associated with ν(HH) frequencies of ~2650-2700 cm^{-1}. An asymmetrically coordinated dihydrogen cannot be ruled out. The lack of pressure-induced η^2-H_2 formation in $ReH_7(PPh_3)_2$ is possibly due to geometric rather than electronic factors, the latter being normally considered as the most important factor governing the $M(\eta^2\text{-}H_2) \leftrightarrow M(H)_2$ interconversion. Rotation of the phenyl rings may assist in the dihydride-dihydrogen interconversion.

The combination of high-pressure and high-temperature has been successful in creating new materials. The solid-state polymerization of acetylene at ~142 kbar, and the synthesis of sp^2-bonded carbon nitrides, were achieved in a diamond-anvil cell. Since the discovery of C_{60} and higher fullerenes, the formation of endohedral fullerenes has been the subject of many publications. A novel route to the formation of endohedral fullerenes has been proposed which involves insertion of an atom into the vacant cavity of the C_{60} fullerene *via* formation of a temporary hole within the fullerene cage while the sample is subjected to high temperatures and pressures. This approach has already proved successful for $^3He@C_{60}$, as well as Ne, Ar, Kr and even Xe. The following chapter describes initial experiments in which the application of high-pressure has been used in an attempt to insert a cobalt atom into the cage of a modified fullerene.

5.6 References

[1] G. J. Kubas, R. R. Ryan, B. I. Swanson, P. J. Vergamini and H. J. Wasserman, J. Am. Chem. Soc., 106 (1984) 451-452.

[2] e.g. (a) G. L. Kubas, C. J. Unkefer, B. I. Swanson and E. Fukushima, J. Am. Chem. Soc., 108 (1996) 7000-7009; (b) L. Wisniewski, M. Mediati, C. M. Jensen and K. W. Zilm, J. Am. Chem. Soc., 115 (1993) 7533-7534.

[3] R. D. Markwell, I. S. Butler, C. M. Edwards, D. H. Burns, A. Fafara, C. Bianchini and M. Peruzzini, J. Am. Chem. Soc., (1998) in preparation.

[4] G. W. Parshall, Inorg. Synth., 17 (1977) 110-111.

[5] J. Chatt and R. S. Coffey, J. Chem. Soc., (1969) 1962-1972.

[6] J. A. K. Howard, S. A. Mason, O. Johnson, I. C. Diamond, S. Crennell, P. A. Keller and J. L. Spencer, J. Chem. Soc., Chem. Commun., (1988) 1502-1503.

[7] L. Brammer, J. A. K. Howard, O. Johnson, T. F. Koetzle, J. L. Spencer, A. M. Stringer, J. Chem. Soc., Chem. Commun., (1991) 241-243.

[8] (a) D. H. Whiffen, J. Chem. Soc., (1955) 1350-1356; (b) R. J. H. Clark, C. D. Flint and A. J. Hempleman, Spectrochim. Acta, 43A (1987) 805-816.

[9] G. J. Kubas, Acc. Chem. Res., 21 (1988) 120-128.

[10] G. J. Kubas, C. J. Burns, J. Eckert, S. W. Johnson, A. C. Larson, P. J. Vergamini, C. J. Unkefer, G. R. K. Khalsa, S. A. Jackson, and O. Eisenstein., J. Am. Chem. Soc., 115 (1995) 569-581.

[11] J. S. Ricci, T. F. Koetzle, M. T. Bautista, T. M. Hofstede, R. H. Morris and J. F. Sawyer, J. Am. Chem. Soc., 111 (1989) 8823-8827.

[12] Y. Kim, H. Deng, D. W, Meek and A. Wojcicki, J. Am. Chem. Soc., 112 (1990) 2798-2800.

[13] (a) D. Michos, X. L. Luo, J. A. K. Howard and R. H. Crabtree, Inorg. Chem., 31 (1992) 3194-3196; (b) F. A. Cotton and R. L. Luck, Inorg. Chem., 30 (1991) 767-774.

[14] R. D. Markwell and I. S. Butler, unpublished results.

[15] S. D. Warner, I. S. Butler and I. Wharf, Coord. Chem. Rev., (1998) submitted.

Chapter 6

Pressure-Tuning Vibrational Spectroscopic Study of $(\eta^5\text{-}C_5H_5)Co(C_{64}H_4)$: Can Endohedral Fullerenes Be Formed Under Pressure?[1]

6.1 Introduction

A novel route to the formation of endohedral fullerenes has been proposed which involves insertion of an atom into the vacant cavity of the C_{60} fullerene *via* formation of a temporary hole within the fullerene cage while the sample is subjected to high temperatures and pressures. This approach has already proved successful for $^3He@C_{60}$, as well as Ne, Ar, Kr and even Xe [1]. To allow insertion of a larger metal atom, however, a larger hole must first be cut in the C_{60} framework. Rubin and co-workers have recently succeeded in producing a 15-membered hole by the consecutive triple scission of a six-membered ring on the C_{60} surface *via* consecutive pericyclic reactions [2]. Subsequent oxidative cobalt insertion affords the Co(III) organometallic complex **1**, $CpCo(C_{64}H_4)$ ($Cp = \eta^5\text{-}C_5H_5$), in which an ethylene bridge acts as a η^2-handle to the metal (Scheme 6.1). The carbon-carbon distance in the ethylene bridge [1.329(14) Å] of **1** is approximately the same as that calculated for the bis-fulleroid **2** (1.336 Å). The bond distances between the ethylene bridge carbons and the cobalt(III) of **1** are 2.119(9) and 2.112(10) Å, i.e., somewhat longer than those observed in CpCo(COD) [2.010-2.025 Å; COD = 1,2-cyclooctadiene] [3].

The application of pressure in a diamond-anvil cell (DAC) causes a decrease in sample volume and concomitant decreases in the intermolecular and intramolecular distances [4]. Consequently, we felt that it would be interesting to ascertain whether, upon application of sufficient external pressures to $CpCo(C_{64}H_4)$, the cobalt atom might be encouraged to slip inside the fullerene cage through an 11-membered ring, in which the ethylene bridge and the two methine carbons form part of the ring. For such an event to occur, the Cp-Co bond would also have to be broken. We report here the results of an

---

[1] C. M. Edwards, I. S. Butler, W. Qian and Y. Rubin, J. Mol. Struct., 1997, in press.

investigation of the IR and Raman spectra of CpCo($C_{64}H_4$) in a DAC as a function of pressure during which it was hoped that an endohedral fullerene would be produced.

6.2 Experimental

Compounds **1** (containing one molecule of toluene per unit cell) and **2** were obtained as reported previously [2]. None of the bands expected for solid toluene were observed to any significant extent in the vibrational spectra of compound **1** (*vide infra*). The high-pressure experiment is described in Chapter 2 Section 2.1.5.

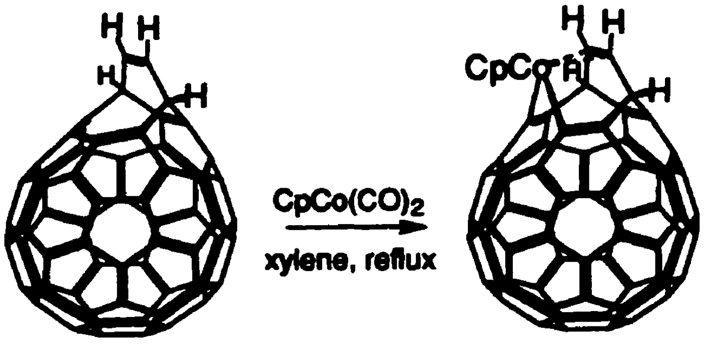

2 **1**

Scheme 6.1.

6.3 Results

There are numerous overlapping bands observed in the IR spectra of both the bis-fulleroid, $C_{64}H_4$, and the organometallic complex, CpCo($C_{64}H_4$), which broaden considerably with increasing pressure thereby making measurement of their positions difficult. In addition, the accurate determination of the applied pressure in the IR measurements proved particularly difficult because the band due to the symmetric N-O stretch of the internal $NaNO_3$ calibrant (1401.3 cm^{-1}, at ambient pressure) becomes overlapped with several other bands at higher pressures. With the aid of band-fitting procedures, however, good estimates of the applied pressures could eventually be obtained. These band-fitting procedures also permitted assignment of several of the bands by comparison of the IR spectra of $C_{64}H_4$ and CpCo($C_{64}H_4$). For instance, the two weak bands observed in the IR spectrum of $C_{64}H_4$ at 1669 and 1678 cm^{-1} disappear upon complexation of the Cp-Co moiety to the $C_{64}H_4$ fulleroid unit and a new, strong band develops at 1525 cm^{-1}. The two original weak bands are assigned to the ν(C=C) stretching modes of the ethylene bridge which, as expected [5], are shifted to lower energies by ~150 cm^{-1} upon complexation. There is another identifiable band of CpCo($C_{64}H_4$) at 1327 cm^{-1}, which is typical for a δ(CH) mode of the Cp ring [5]. The medium-intense band at 1493 cm^{-1}, at ambient pressure, is common to both the fulleroid and the complex and is attributed to a ν(CC) mode of the carbon skeleton. All of the bands mentioned above exhibit positive pressure dependences.

Contrary to the IR, it was easy to monitor the effect of pressure on the FT-Raman bands of CpCo($C_{64}H_4$) because, unlike those of the bis-fulleroid $C_{64}H_4$, they are not obscured by a strong fluorescence background. The pressure dependence of several bands and their tentative assignments are given in Table 6.1. For all the observed Raman bands of CpCo($C_{64}H_4$), there is a discontinuity in the slopes of the wavenumber *vs.* pressure plots between 8.8 and 13.1 kbar, as shown in Figure 6.1. The Raman bands located at ~1455 cm^{-1} are the most intense and have been assigned to the "pentagonal pinch" mode in which opposite-sided pentagons of the fullerene cage contract. In the case of C_{60}, this pentagonal pinch mode appears at 1469 cm^{-1} [6] while, for $C_{64}H_4$, the strongest Raman features are at 1450 and 1458 cm^{-1}. For the latter compound, only five data points were available on going from ambient pressure to ~43 kbar. The pressure dependences of the two bands in question are estimated as 0.3 and 0.2 cm^{-1} $kbar^{-1}$, respectively.

6.4 Discussion

The presence of a discontinuity in the slopes of the ν *vs.* P plots for the Raman bands of CpCo($C_{64}H_4$) between 8.8-13.1 kbar indicates the occurrence of a structural transition. Each of the bands at 546.0, 440.8, 314.1 and 266.9 cm^{-1} develops a shoulder on the high wavenumber side at pressures above 13 kbar (Fig. 6.2). These shoulders increase in intensity as the pressure is increased, providing additional evidence for a structural change.

Table 6.1. Pressure dependences for selected Raman modes of CpCo($C_{64}H_4$) between 13 and 47 kbar. (Below ~10 kbar, the pressure dependence of each band is essentially zero.)

Peak (cm^{-1})	dv/dp (cm^{-1} $kbar^{-1}$)	Tentative assignment
1585.8 *w*	0.37	ν(CC) “C_{60}”
1574.0 *w*	0.37	ν(CC) “C_{60}”
1566.8 *w*	0.32	
1520.0 *vw*	0.39	ν(CC), ethylene bridge
1459.7 *s*	0.58	“pentagonal pinch”
1452.4 *sh,m*	0.55	
1442.5 *sh,w*	0.32	ν(CC) Cp
1380.1 *w*	0.57	δ(CH)
1360.8 *w*	0.47	δ(CH)
1118.7 *w*	0.26	ν(CC) Cp
552.0, *sh*	0.10	
545.9 *m*	0.19	
474.7 *w*	0.20	antisym. ring tilt
440.9 *s*	0.33	ν(Co-Cp)
439.0, *sh*	0.19	ν(Co-Cp)
377.5 *w*	0.18	
341.1 *w*	0.22	
318.0, *sh*	0.39	
314.0 *w*	0.26	
269.7, *sh*	0.43	“C_{60}”
266.6 *ms*	0.31	“C_{60}”
257.7 *w*	0.5	
209.5 *ms*	0.16	
199.6 *ms*	0.26	
178.0 *ms*	0.11	

sh shoulder; *s* strong; *ms* medium strong; *m* medium; *w* weak and *vw* very weak.

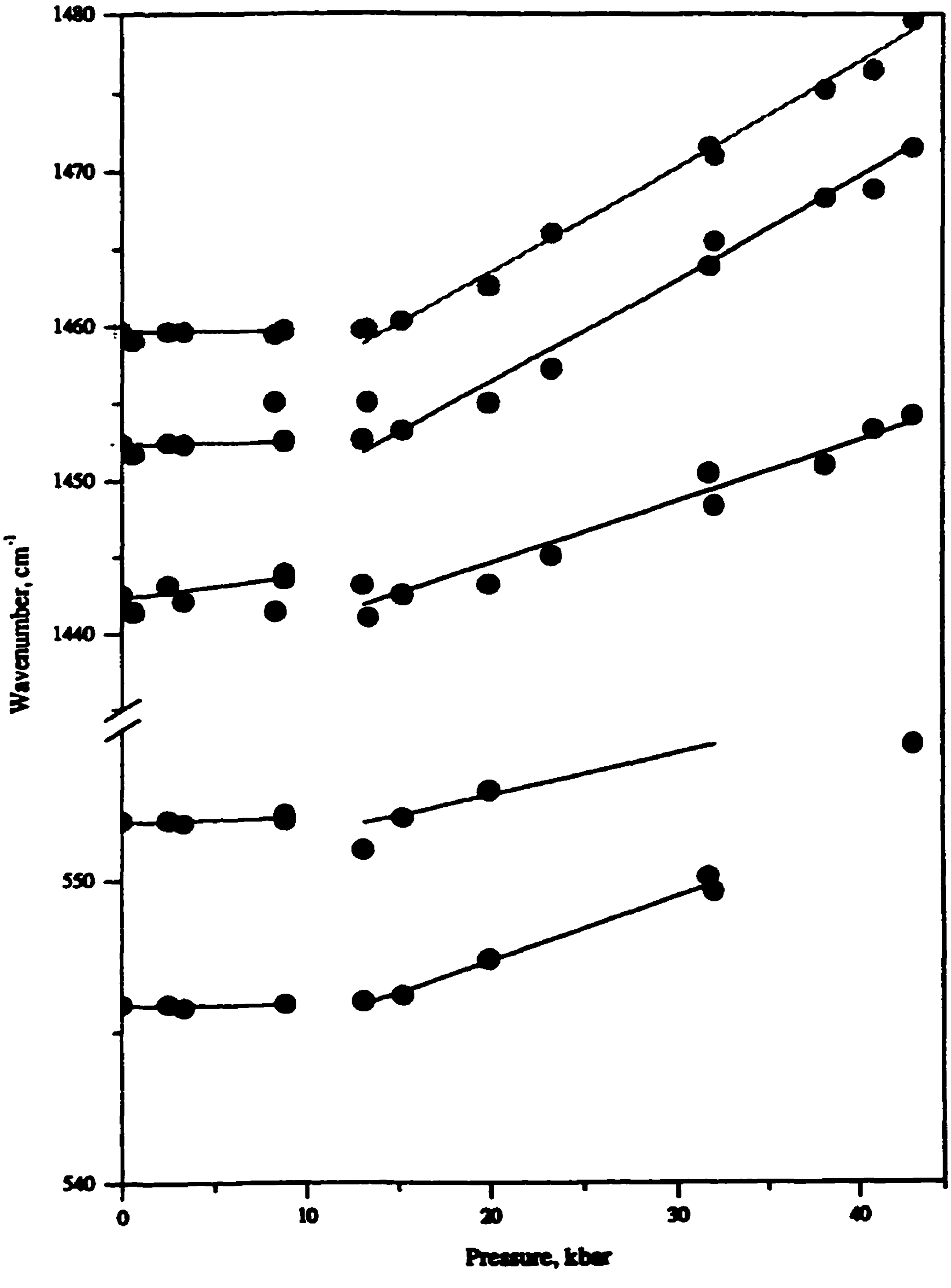

Figure 6.1. Pressure dependences of five of the Raman fundamentals of $CpCo(C_{64}H_4)$.

Although fewer data points are available for $C_{64}H_4$, it is evident that no structural change occurs even at pressures up to ~30 kbar. Moreover, on the basis of the pressure dependence of the pentagonal pinch mode at ~1455 cm^{-1}, $CpCo(C_{64}H_4)$ is more pressure sensitive than is $C_{64}H_4$, as shown in Figure 6.3. High-pressure X-ray diffraction studies on C_{60} have revealed that the weak van der Waals interactions decrease upon application of hydrostatic pressure to compensate for the decrease in volume and the intramolecular interactions remain essentially unchanged [7]. Coordination of the CpCo-moiety to the side of the fullerene cage renders the intramolecular interactions more pressure sensitive.

In the case of transition metal carbonyl [8] and alkene complexes [9], the π-backbonding interactions between the metals and the CO and alkene ligands are increased upon application of high external pressures. To increase the cobalt-fullerene interaction in $CpCo(C_{64}H_4)$, the strength of the cobalt-ethylene bridge interaction must be increased. Such a situation could be achieved by increasing the σ-donation from the ethylene bridge to the Co(III) center and/or by increasing the π-backdonation from the Co(III) center to the vacant π^*-orbitals of the ethylene bridge. The net effect of these interactions would be a decrease in the bond order of the C=C bond and consequently a decrease in the energy of the ν(C=C) mode. Therefore, if more π-backdonation does occur from the Co(III) center to the ethylene bridge under pressure, a negative pressure dependence should be observed for the ν(C=C) mode. The ν(C=C) mode of the ethylene bridge, however, shows a distinct positive pressure dependence (0.39 cm^{-1} $kbar^{-1}$).

For the Co atom to be pushed inside the fullerene cage, there must be a significant weakening of the Cp-Co bond such that it eventually ruptures altogether. A gradual lengthening of the Cp-Co bond would be expected, which would reveal itself as a gradual shift in the frequency of the ν(Cp-Co) stretching mode to lower wavenumbers with increasing pressure, until dissociation is complete when the mode would disappear completely. The ν(Cp-Co) mode is expected in the Raman spectrum in the 500-300 cm^{-1} region since, for Cp_2Co (cobaltacene) and $[Cp_2Co]^+$, this mode is located at 355 and 455 cm^{-1}, respectively [5]. While it is not possible to assign a specific Raman band to the

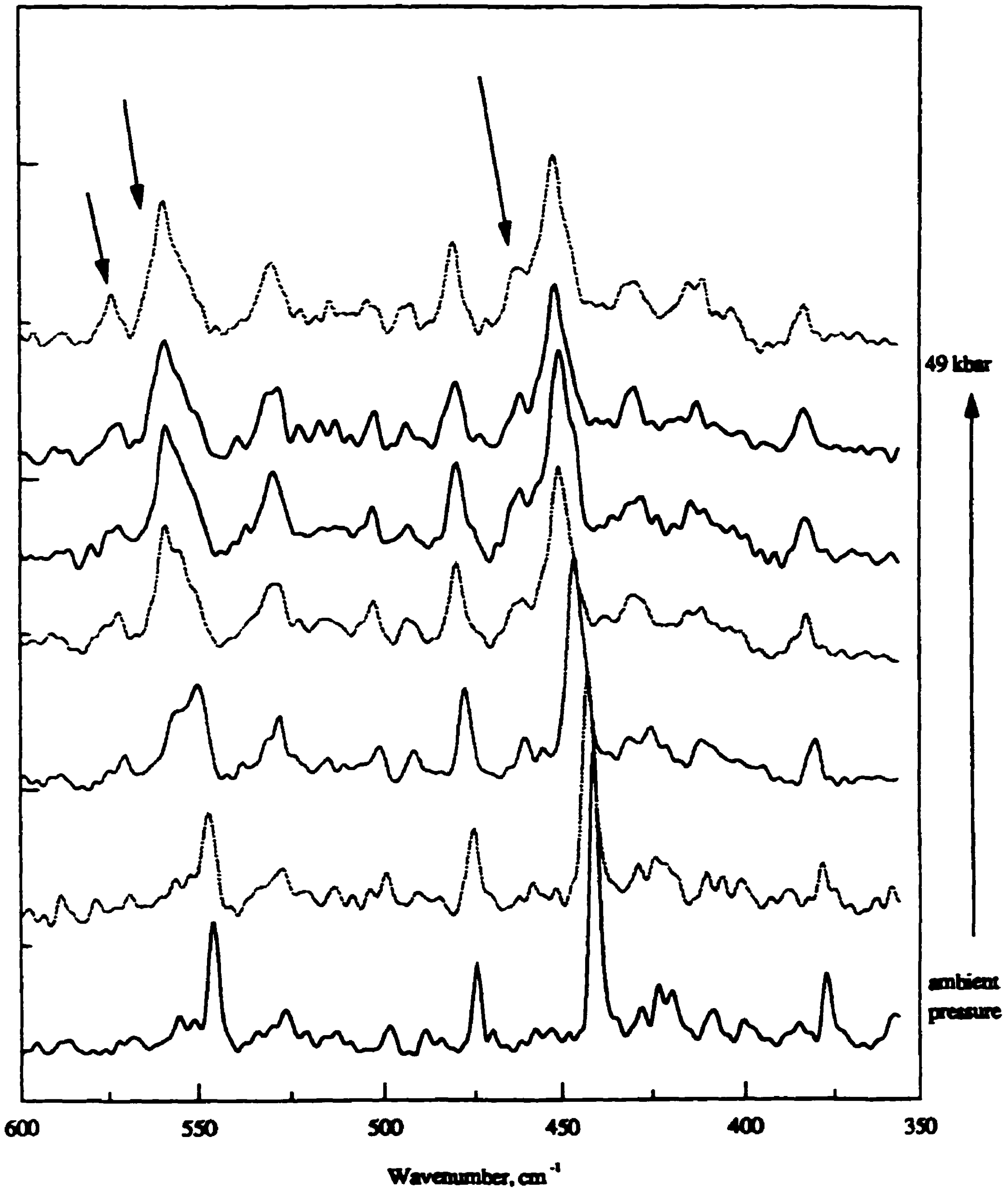

Figure 6.2. FT-Raman spectra in the ν(Co-Cp) region for CpCo($C_{64}H_4$), from ambient pressure to 49 kbar. The arrows indicate those bands which become increasingly more intense with increasing pressure.

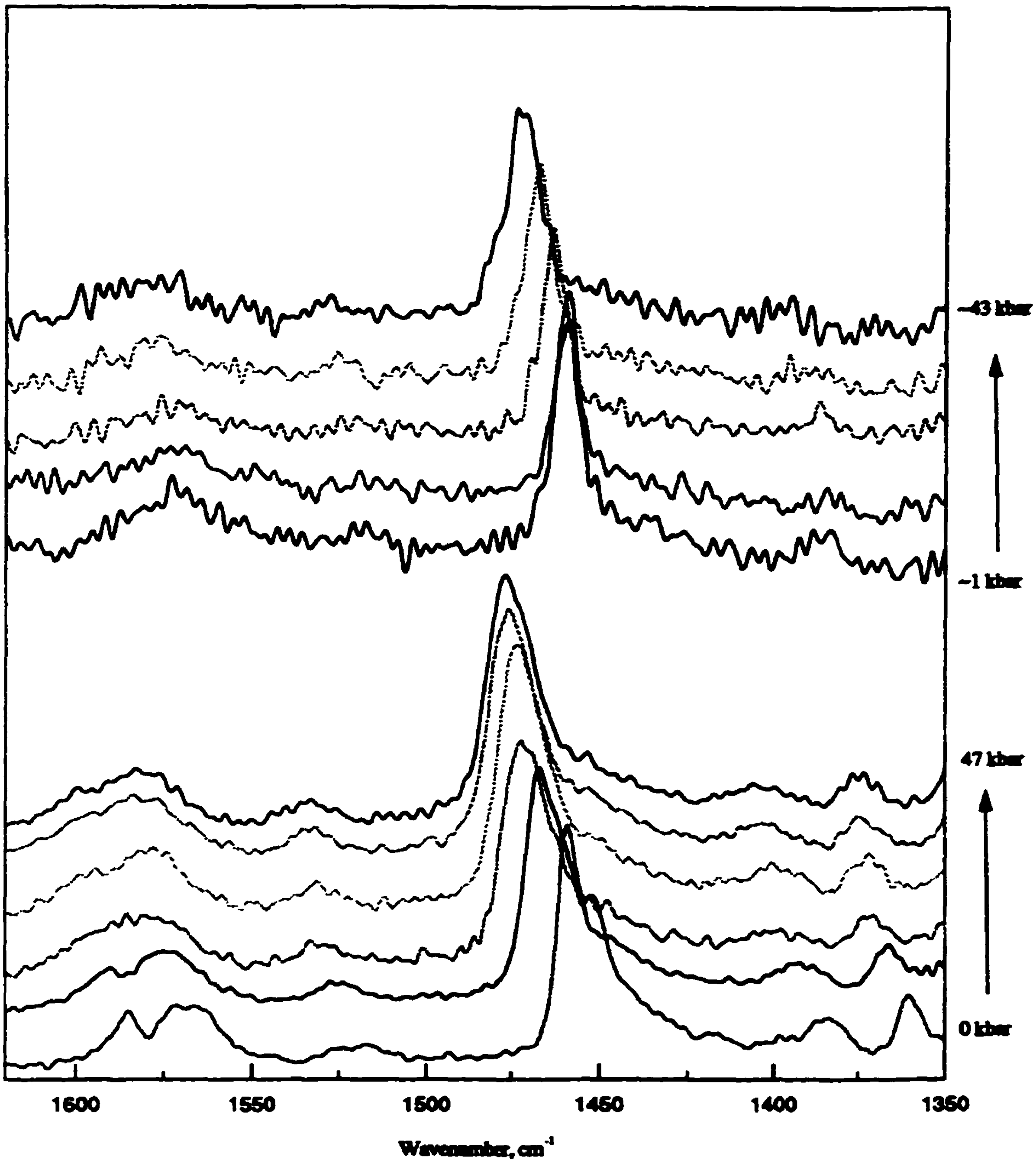

Figure 6.3. FT-Raman spectra in the region of the pentagonal pinch mode for CpCo($C_{64}H_4$) (bottom) and $C_{64}H_4$ (top) from ambient pressure to high pressure.

v(Cp-Co) mode, all the Raman bands in the 500-300 cm^{-1} region do show positive pressure dependences throughout the pressure range investigated.

6.5 Conclusions

The application of high external pressures (up to ~40 kbar) on the Co(III) fullerene complex, CpCo($C_{64}H_4$), does not increase the metal-fullerene interaction sufficiently for insertion of the metal atom into the fullerene cage to occur. There is, however, evidence for a structural change at 8.8-13.1 kbar, most probably due to the rotation of the Cp ligand about the Cp-Co bond similar to that seen in ferrocene under high pressure [10] and at low temperature [11]. For ferrocene, under high-pressure there is a phase transition at about 11.5 kbar. The Cp-Co bond is too strong to be broken by the pressures applied in the present work but replacement of the Cp ring with a more electron-withdrawing ligand, such as pentafluorocyclopentadiene (C_5F_5), or a more labile ligand such as indenyl, might lead to the desired result.

Up until now, the high-pressure experiments have been exclusively IR and Raman techniques. While much information can be obtained from such experiments, often more detailed information regarding the structure of a compound is needed. In collaboration with the CNRS Laboratoire de Physico-Chimie des Matériaux, Meudon, France, we have carried out some initial high-pressure powder X-ray diffraction experiments on potassium chromate, K_2CrO_4. In much the same way as powder X-ray diffraction data is interpreted in regular ambient pressure measurements, the powder patterns with increasing pressure are interpreted to give detailed structural information.

6.6 References

---

[1] (a) M. Saunders, H. A. Jiménez-Vázquez, S. Mroczkowski, M. L. Gross, D. E. Giblin and R. J. Poreda, J. Am. Chem. Soc., 116 (1994) 2193-2194; (b) B. A. Dicamillo, R. L. Hettich, G. Guiochon, R. N. Compton, M.Saunders, H. A. Jiménez-Vázquez, A. Khong and R. J. Cross, J. Phys. Chem., 100 (1996) 9197-9201; (c) M. Saunders, R. J. Cross, H. A. Jiménez-Vázquez, R. Shimshi and A. Khong, Science, 271 (1996) 1693-1697; (d) R. Shimshi, A. Khong, H. A. Jiménez-Vázquez, R. J. Cross and M. Saunders, Tetrahedron, 52 (1996), 5143-5148.

[2] M. J. Arce, A. L. Viado, Y.-Z. An, S. I. Khan and Y. Rubin, J. Am. Chem. Soc., 118 (1996) 3775-3776.

[3] J. Ondracek, V. Schehlmann, J. Maixner and B. Kratochvil, Collect. Czech. Chem. Commun., 55 (1990) 2447-2452.

[4] W. F. Sherman and G. R. Wilkinson, in R. J. H. Clark and R. E. Hester (Eds.), Advances in Infrared and Raman Spectroscopy, Wiley-Interscience, (1990) Chapter 4.

[5] D. M. Adams, in "Metal-Ligand and Related Vibrations", Edward Arnold Publ., London, U.K., (1967) Chapter 4.

[6] W. Brockner and F. Menzel, J. Mol. Struct., 378 (1996) 147-163.

[7] (a) J. E. Fischer, P. A. Heiney, A. R. McGhie, W. J. Romanow, A. M. Denenstein, J. P. McCauley and A. B. Smith, Science, 252 (1991) 1288-1290; (b) S. J. Duclos, K. Brister, R. C. Haddon, A. R. Kortan and F. A. Thiel, Nature, 351 (1991) 380-382.

[8] For example, see (a) D. M. Adams and I. O. C. Ekejiuba, J. Chem. Phys., 77 (1982) 4793-4797; (b) Y. Huang, I. S. Butler, D. F. R. Gilson and D. Lafleur, Inorg. Chem., 30 (1991) 117-121.

[9] (a) J. Baldwin, M.Sc. Thesis, McGill University, Montreal, Quebec, Canada, 1992; (b) J. Baldwin , I. S. Butler and D. F. R. Gilson in Proceedings of 27th Annual Meeting of the Microbeam Analysis Society, eds. G. W. Bailey, J. Bentley and J.

A. Small, San Francisco Press, Inc., San Francisco, California, U.S.A. (1992) 1536-1537.

[10] D. M. Adams and A. D. Williams, J. Phys. Chem. Solids, 41 (1980) 1073-1078.

[11] (a) P. G. Calvarin and J. F. Berar, J. Appl. Cryst., 8 (1975) 380-385; (b) F. Rocquet, L. Berreby and J. P. Marsault, Spectrochim. Acta A, 20 (1972) 1101-1107.

Chapter 7

High-Pressure X-ray Diffraction Study of Potassium Chromate: Pressure-induced Orientational Disorder and its Implications for Amorphization in A_2BX_4 Compounds[1]

7.1 Introduction

The need to understand the structures and transformation mechanisms of minerals under high pressures is important in our understanding of many geophysical phenomena such as ocean floor spreading, the earth's magnetic field and deep-focus earthquakes. These and other phenomena are determined, at least in part, by the properties of the materials that compose the earth's interior [1]. The mantle and crust are composed predominantly of silicate minerals. Perhaps, the most extensively studied of these minerals is the magnesium-iron olivine, $(Mg,Fe)_2SiO_4$, in which the SiO_4^{2-} tetrahedra are isolated. The 400-km seismic discontinuity between the upper mantle and the transition zone was long proposed to be caused by transformations in the olivine phase of $(Mg,Fe)_2SiO_4$ to a denser phase. The α (olivine)-to-β (spinelloid) transformation has been shown to be consistent in terms of pressure (depth) with this discontinuity [2]. The α (olivine)-to-β (spinelloid)-to-γ (spinel) phase transformations are also connected with the origins of deep-focus earthquakes [2].

The structurally related silicate, Ca_2SiO_4, in which the SiO_4^{2-} tetrahedra are also isolated, is an important constituent of Portland cement clinker and appears in refractories. Ca_2SiO_4 exists in several polymorphs [3] and their temperature- and pressure-induced transformations have been studied extensively by powder X-ray diffraction [4,5] and Raman spectroscopy [6]. The orthorhombic γ-Ca_2SiO_4, which is stable under ambient conditions, is in fact isostructural with olivine. The above disilicates are examples of A_2BX_4 compounds, which have been extensively studied in

---

[1] C. M. Edwards, J. Haines, I. S. Butler and J. M. Léger, J. Chem. Phys. Solids, in preparation.

relation to their high-pressure, low-temperature phases, and mechanisms of transformation. Potassium chromate, K_2CrO_4, is another A_2BX_4 compound, with isolated CrO_4^{2-} tetrahedra and is isostructural with the high-temperature, orthorhombic, α'_H form of Ca_2SiO_4 [4]. The high-pressure β-Ca_2SiO_4 polymorph has a closely-related monoclinic structure. With the exception of a solitary Raman study up to ~5 GPa [7], no previous high-pressure work on K_2CrO_4 has been undertaken.

Other A_2BX_4 compounds that have been investigated at high pressures include Cs_2MoS_4 [8], Na_2MoO_4 and Na_2WO_4 [9], and K_2ZnCl_4 and Rb_2ZnCl_4 [10]. Many A_2BX_4 compounds undergo pressure-induced amorphization. The relation between crystalline and amorphous phases is of interest because the transition from crystalline to amorphous involves only small displacements of the atoms in the crystal. Whether there is a size criterion for amorphization has been the subject of several studies [9,11]. For a series of A_2BX_4 compounds it was found that the $r(BX_4)/r(A)$ ratio could be used to determine the effect of compression on the material.

Interestingly, both Ca_2SiO_4 and K_2CrO_4 can be considered as oxygen-stuffed analogues of AX_2 compounds. For example, in γ-Ca_2SiO_4, the Ca_2Si sub-lattice has a Ni_2In-type structure and the K_2Cr sub-lattice of K_2CrO_4 has a Co_2Si-type structure, Fig. 7.1. γ-Ca_2SiO_4 transforms to β-Ca_2SiO_4 under compression and at the transition the Ca_2Si sub-lattice changes from a Ni_2In-type to a distorted Co_2Si-type. High pressure studies on AX_2 compounds with the $PbCl_2$ structure type, for example BaX_2 (X = Cl, Br, I) [12], PbF_2, $PbCl_2$ and $SnCl_2$ [13] and BaF_2 [14], show that high-pressure transformations involve increases in cation coordination number beyond 9. BaF_2 transforms to a Ni_2In-type structure in which the Ba-coordination increases to eleven, the highest value observed in AX_2 compounds, whereas the other dihalides transform to Co_2Si-related structures, in which the coordination number is ten.

In this paper, we present the results of a high-pressure, powder X-ray diffraction study of K_2CrO_4 up to 52 GPa. The results reveal a pressure-induced disordering which has implications on the amorphization mechanisms of A_2BX_4 compounds.

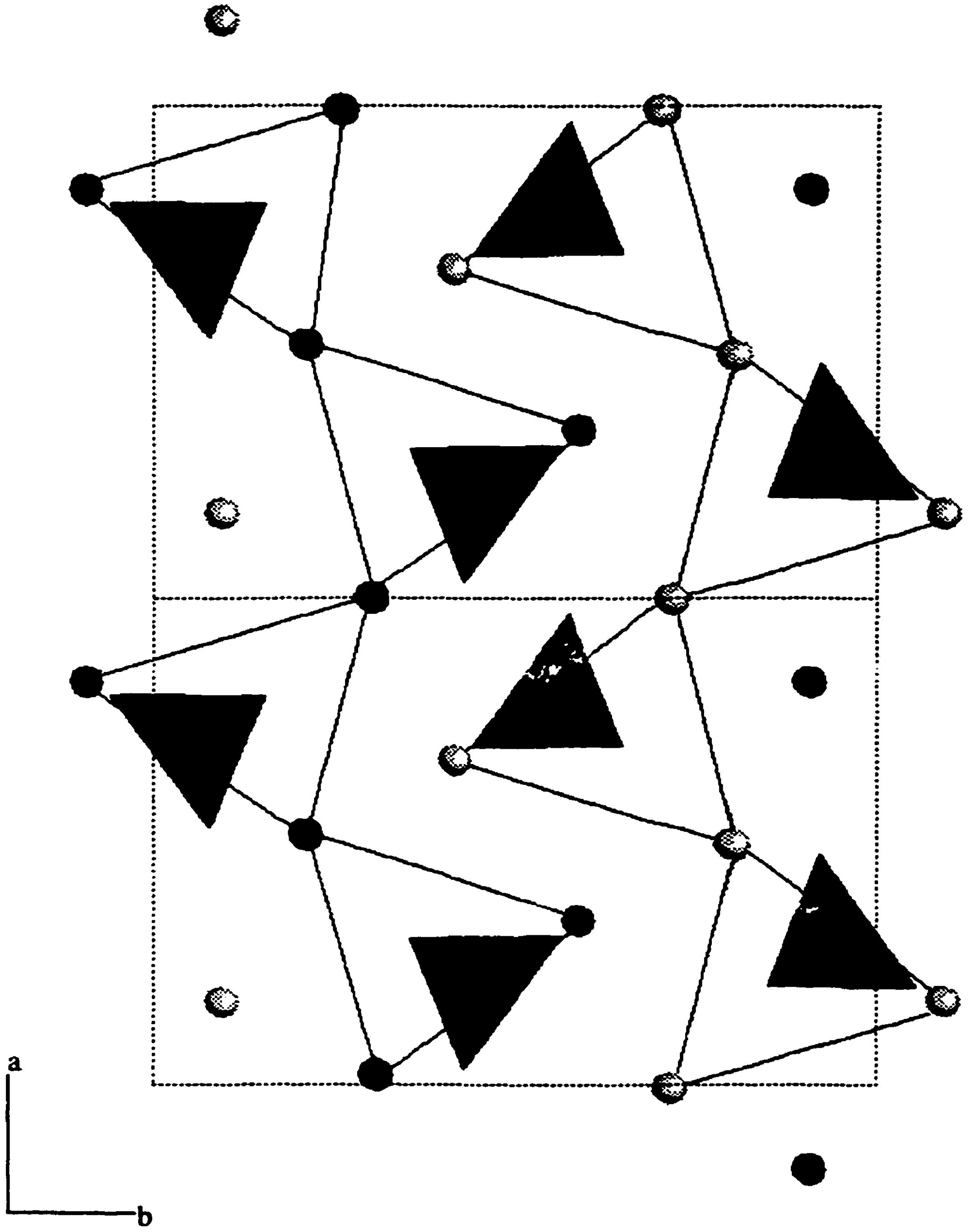

Figure 7.1. Schematic representation of the K_2CrO_4 structure. The broken line outlines the orthorhombic unit cell. The CrO_4^{2-} tetrahedron is represented by a polyhedron. (Dark symbols $z = {}^1/_4$, light symbols $z = {}^3/_4$.)

7.2 Experimental

Full details on the high-pressure X-ray diffraction procedure are presented in Chapter 2, Section 2.2.2.

7.3 Results

Powder X-ray diffraction patterns of orthorhombic K_2CrO_4 (P*nam*, D_{2h}^{16}, Z = 4) [15,16], were recorded from ambient pressure to 52 GPa. Diffraction patterns upon decompression were also recorded. All the powder patterns were analyzed using whole-pattern fitting; the cell parameters were initially estimated from the 2θ values of the [200], [020] and [002] lines in the powder pattern. Rietveld refinement of the crystal structure, Fig. 7.2, Table 7.1, was possible up to 15 GPa, above which pressure-induced line broadening and a lowering of intensity prevented further refinements. Due to the large number of refinable oxygen positional parameters, slack constraints were placed on the tetrahedral Cr-O distances assuming a polyhedral bulk modulus of 500 GPa; this is of the same order of magnitude as the polyhedral bulk modulus of the SiO_4 tetrahedra in quartz [17], which are approximately the same size (Si-O = 1.610 Å, Cr-O = 1.646 Å). Cell constants for pressures greater than 15 GPa were obtained by whole-pattern fitting.

As the pressure was increased certain diffraction lines broadened and split as a result of anisotropic changes in the unit cell dimensions. Most strikingly, the overall intensity gradually falls with increasing pressure, beginning at close to 16.2 GPa. This is most noticeable for the 020, 011, 111, 200, 210 and 121 lines, below 12° at ambient pressure, which, in addition, show a decrease in relative intensity with increasing pressure from ~16.2 GPa. The 310 line, initially at 16.48°, also loses intensity from 16.2 GPa. At 16.2 GPa, the two strongest TiC (5 % w/w in the sample) lines at 16.62° and 19.21° appeared clearly in the diffraction pattern. The lines of K_2CrO_4 continued to decrease in intensity with further compression up to 52 GPa, at which

Figure 7.2. Experimental (+) and calculated (solid line) diagrams from the Reitveld refinement of K_2CrO_4 at 7.5 GPa ($R_B = 6.4$, $R_P = 10.7$, $R_{wp} = 9.9$). The intensity is in arbitrary units, with the difference profile on the same scale. The vertical bars indicate the calculated positions of diffraction lines ($K\alpha_1$).

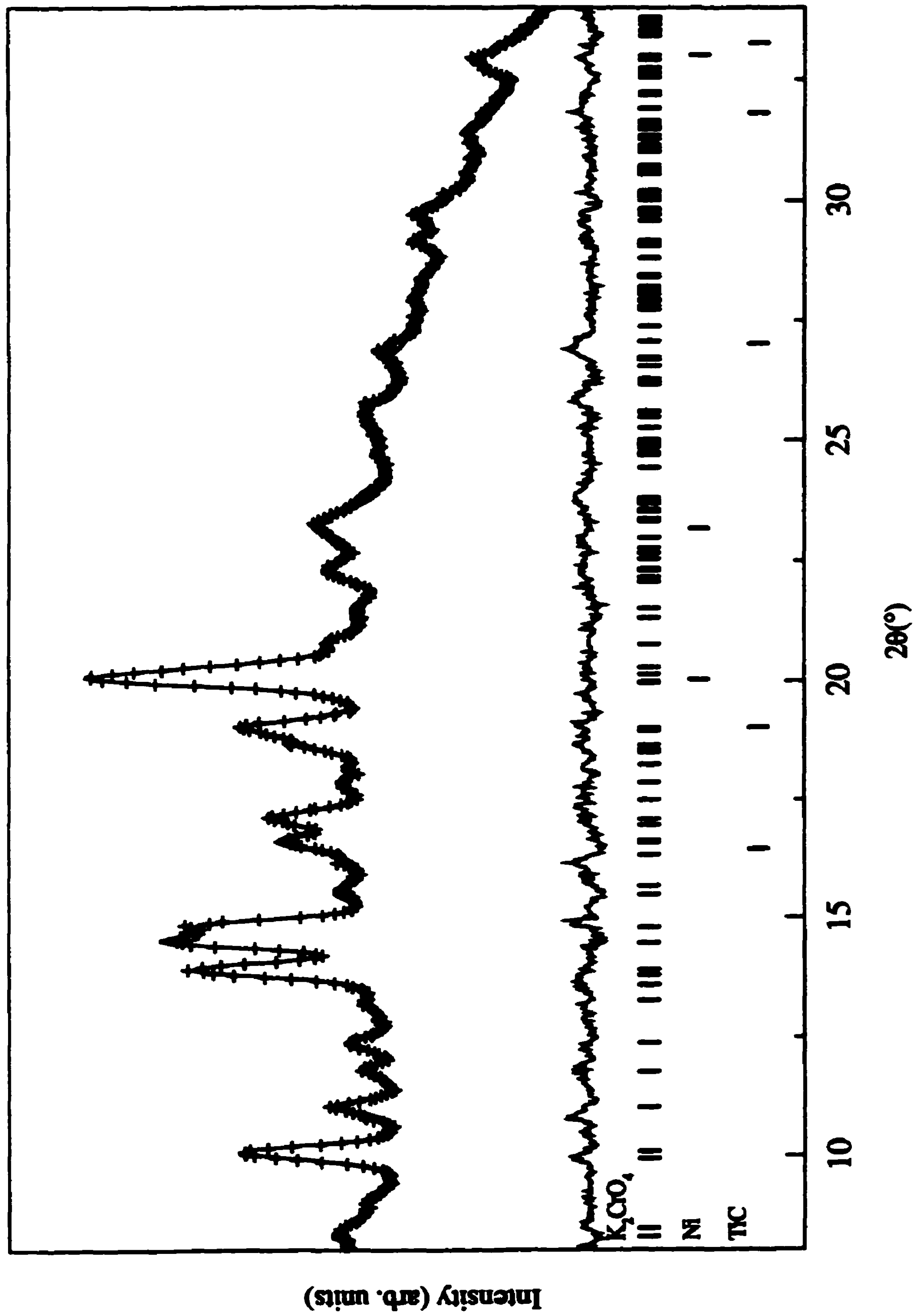
Intensity (arb. units)
2θ(°)
10
15
20
25
30
K_2CrO_4
Ni
TiC

Table 7.1. Structural data for K_2CrO_4 (space group P*nam*, Z = 4). [a]Values from ref. 16.

P	0.1 MPa[a]	7.4 GPa
a	7.662 Å	7.380(1) Å
b	10.391 Å	9.830(1) Å
c	5.919 Å	5.509(1) Å
Cr (x,y,z)	0.22911, 0.42061, 0.25	0.2391(3), 0.4241(3), 0.25
K1 (x,y,z)	0.66568, 0.41434, 0.25	0.6658(8), 0.3901(8), 0.25
K2 (x,y,z)	-0.01099, 0.69989, 0.25	-0.021(1), 0.6877(6), 0.25
O1 (x,y,z)	0.01549, 0.42001, 0.25	0.0173(4), 0.432(2), 0.25
O2 (x,y,z)	0.30187, 0.57044, 0.255	0.308(3), 0.5827(7), 0.25
O3 (x,y,z)	0.30294, 0.34716, 0.47750	0.311(2), 0.359(1), 0.505(1)

pressure they were weaker than the most intense lines of the titanium carbide. Diffraction patterns of the recovered samples in the gasket are identical to those of the starting material, indicating the reversible nature of the pressure-induced changes. Since all the diffraction patterns could be interpreted in terms of the orthorhombic phase any structural changes induced under pressure do not involve a transition to a different crystal structure. The sample colour changed from transparent yellow to red with increasing pressure due to a shift in the optical absorption bands.

In a second high-pressure experiment the sample was heated at 40 GPa using a Nd:YAG laser for 30 minutes. The temperature was not measured; however, visible emission from the sample was observed indicationg a temperature of above 1000°C. The sample colour changed from transparent red, to a dark, opaque red. No changes in the X-ray diffraction patterns were observed after heating thus confirming the absence of a transition to a new crystalline phase. In addition, the diffraction lines did not sharpen and there were no changes in intensity.

7.4 Discussion

7.4.1 Compression of K_2CrO_4 and Comparison with The High-pressure Behaviour of AX_2 Compounds

In K_2CrO_4, edge-sharing columns of trigonal-prisms of K^+ ions form a network of corrugated layers, the axis of the prisms lying parallel to **c**. The chromate tetrahedra are surrounded by eleven potassium ions in a penta-capped trigonal prism, Fig. 7.1.

Figure 7.3 shows the changes in the lattice parameters as a function of pressure. Up to 16.2 GPa the *a* lattice parameter is observed to decrease by 5.2%, whereas *b* and *c* decrease by 8.4 and 8.5%, respectively. Hence, compression along the chain direction, i.e. along the **a** direction, is more difficult than is that parallel to the prism axis (**c**) or between the layers (**b**). A plot of the relative volume as a

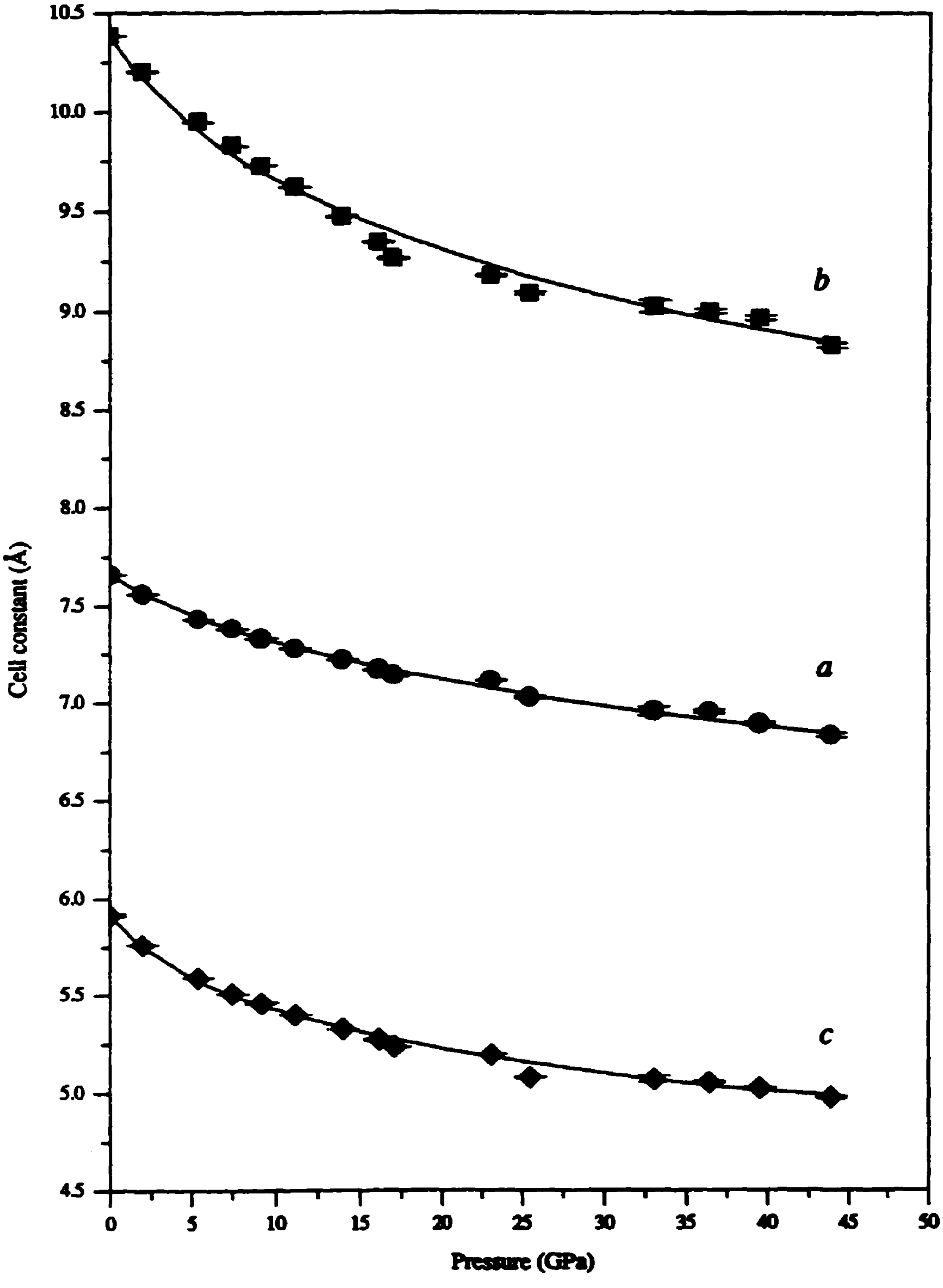

Figure 7.3. Lattice parameters of K_2CrO_4 in 4:1 methanol:ethanol, as a function of pressure. At ambient pressure, *a* (●) = 7.6597(7) Å, *b* (■) = 10.387(1) Å and *c* (◆) = 5.9188(5) Å. Solid lines represent non-linear least-squares fits to the data.

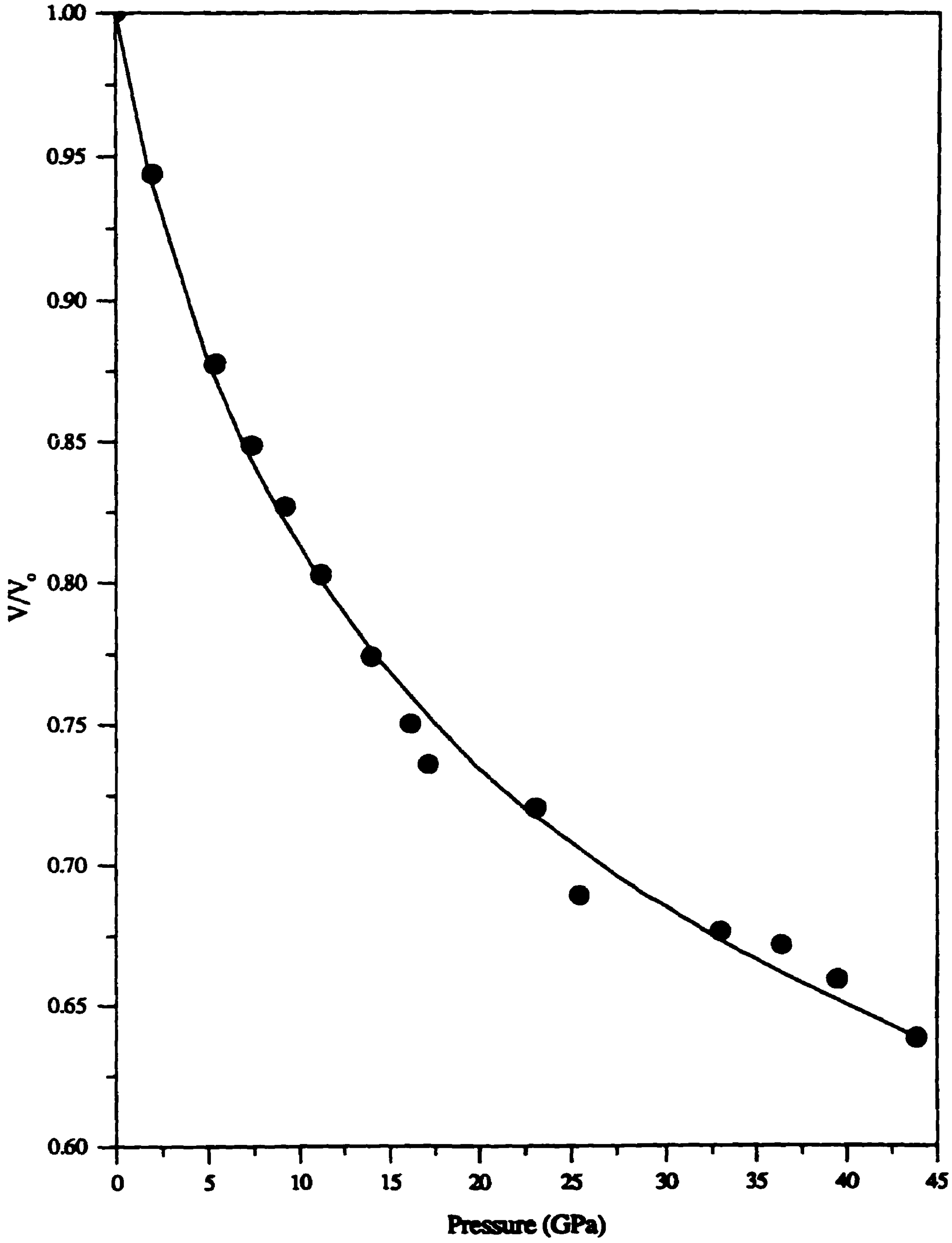

Figure 7.4. Relative volume of K_2CrO_4 in 4:1 methanol:ethanol as a function of pressure. At ambient pressure, V_o = 470.911(2) Å^3. The solid line represents a Birch-Murighan equation of state using the parameters obtained in the study.

function of pressure shows that K_2CrO_4 is highly compressible (Fig. 7.4). The Birch-Muraghan (BM) equation-of-state [18] (EOS) $P = (3/2)B_o(x^{-7}-x^{-5})[1-a(x^{-2}-1)]$ was used to fit the pressure-volume data, from ambient pressure to 44 GPa, whereby $x = (V/V_o)^{1/3}$, $a = (3/4)(4-B'_o)$, V is the volume, B is the isothermal modulus and B′ its first derivative. The subscript zero indicates ambient conditions. The values obtained from the fit are $B_o = 26(2)$ GPa and $B'_o = 6.0(5)$.

The high-pressure behavior of K_2CrO_4 is similar to that of β-Ca_2SiO_4 with respect to the *a*/*b* and (*a*+*b*)/*c* cell constant ratios. Potassium chromate has a higher *a*/*b* ratio at ambient pressure compared to β-Ca_2SiO_4 (Co_2Si-type) (Fig. 7.5). Under increasing pressure, the overall changes in the *a*/*b* and (*a*+*b*)/*c* ratios are similar, but more marked in K_2CrO_4 due to its greater compressibility. In both cases, the *a*/*b* (the trigonal prisms lie parallel to **b**) and (*a*+*b*)/*c* ratios increase with pressure, since the *c* lattice parameter decreases at the same rate as does the *b* parameter. This is opposite to what is observed in the AX_2 compounds such as BaF_2 and $BaCl_2$, which are anti-types of the A_2B sub-structures in the A_2BX_4 compounds. These compounds have *a*/*b* and (*a*+*b*)/*c* ratios of 0.85 and 3.61, and 0.83 and 3.66, respectively, at ambient pressure. Under applied pressure, BaF_2 transforms to the Ni_2In structure, while $BaCl_2$ transforms to the Co_2Si-related, postcotunnite structure [12]. Both transitions involve a significant decrease in both the *a*/*b* and (*a*+*b*)/*c* ratios, since under pressure the a parameter decreases more rapidly than do the *b* or *c* parameter.

$PbCl_2$, Co_2Si and Ni_2In-type structures all have a structure made up of corrugated layers of trigonal prisms directed along **a** sharing an edge parallel to the short c direction. In the Ni_2In structure (*Pnam* setting), the prisms are aligned exactly along the **a** direction (Fig. 7.6c), while in the cotunnite ($PbCl_2$) structure the prisms form corrugated layers with a tilt angle of 25°, (Fig. 7.6a). In Co_2Si, the tilt angle is 7°, (Fig. 7.6b). The coordination number increases from 9 to 10 to 11 for the $PbCl_2$-to-Co_2Si-to-Ni_2In structures [19]. A logical path for transformation under the application of pressure would be from the $PbCl_2$ to Co_2Si to Ni_2In-type structure. In fact, $PbCl_2$, with coordination number 9, transforms to the post-cotunnite structure

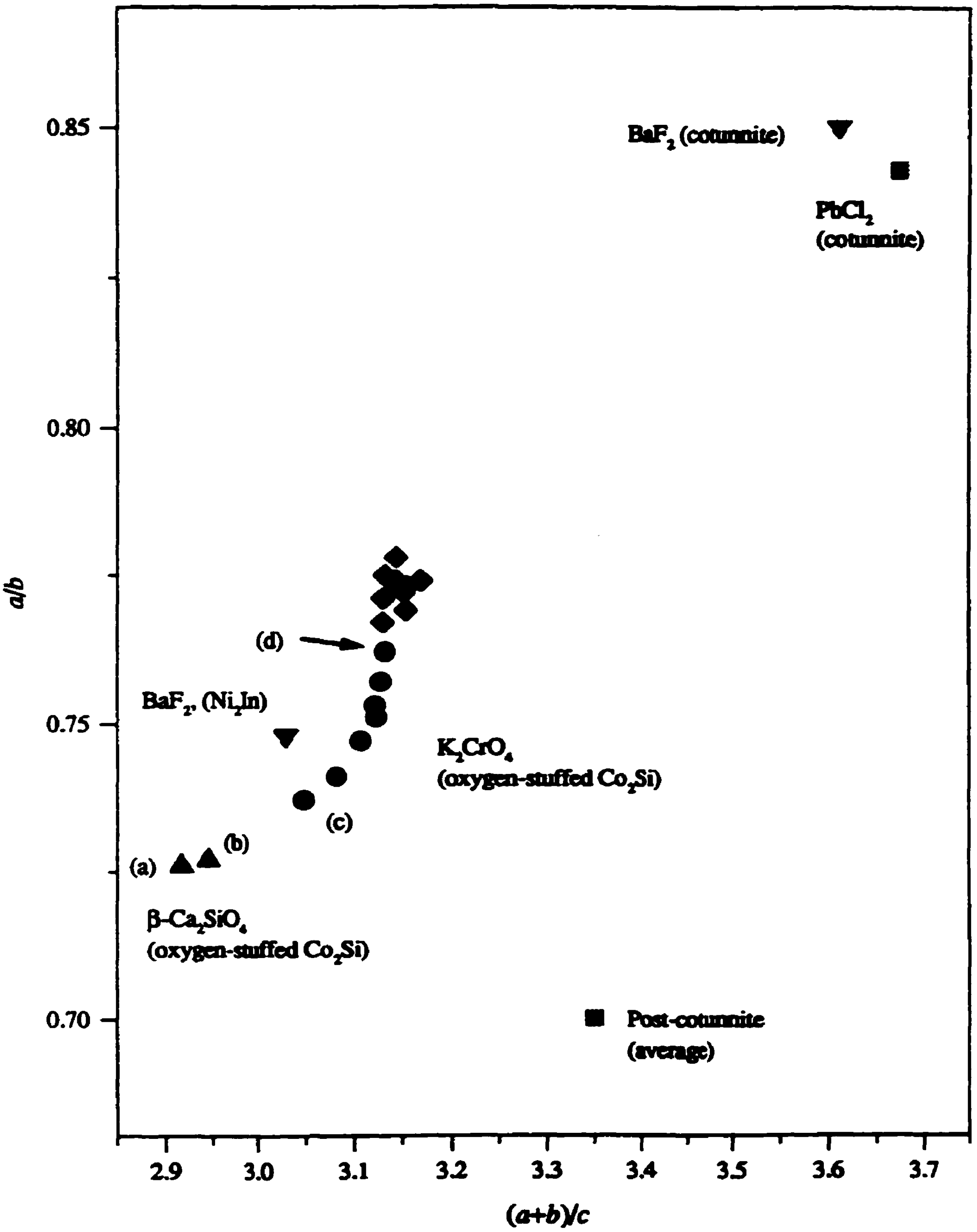

Figure 7.5. Cell constant ratios: *a/b vs.* (*a*+*b*)/*c* of selected A_2BX_4 and AX_2 compounds. β-Ca_2SiO_4 (▲) at (a) 0.1 MPa and (b) 14.7 GPa; K_2CrO_4 (●) at (c) ambient pressure to (d) 14.0 GPa. Points for K_2CrO_4 above 16 GPa up to 52 GPa are represented with diamonds (◆).

Figure 7.6. Schematic representation the $PbCl_2$-type structure (a), the Co_2Si-type structure (b), and Ni_2In-type structure (c). The broken lines outline orthorhombic unit cells; orthohexagonal in the case of Ni_2In. Open symbols $z = {}^1/_4$, filled symbols $z = {}^3/_4$.

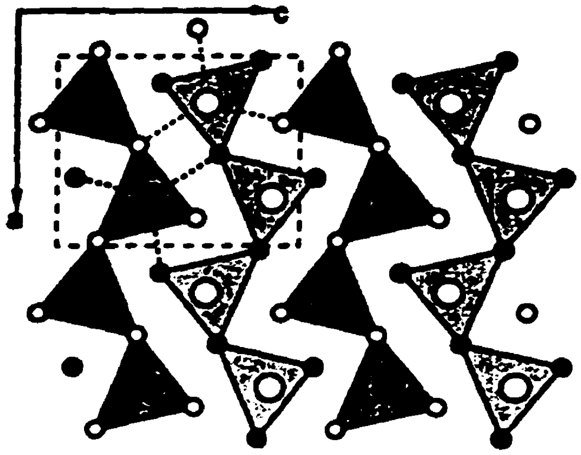
c
a

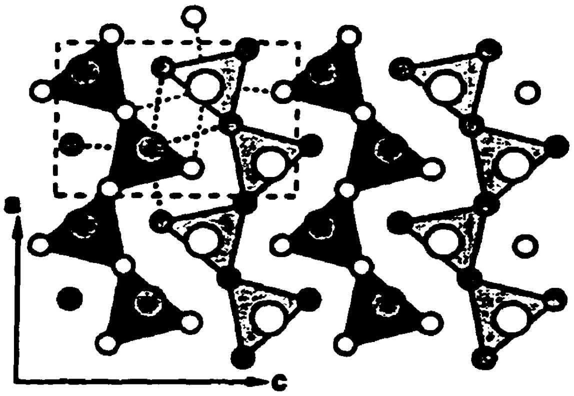
a
c

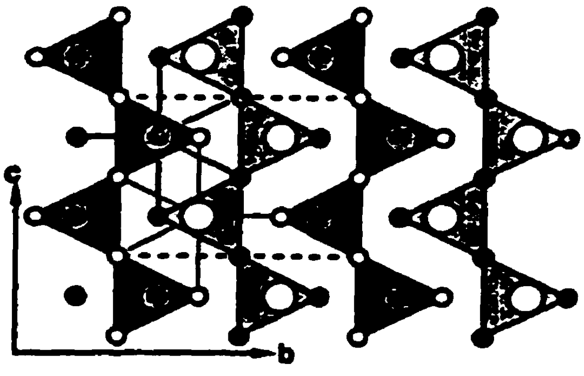
c
b

(Co_2Si-related) under pressure with a increase in coordination number of Pb to 10 [13]. Many other AX_2 compounds show a similar cotunnite to post-cotunnite transformation under compression at room temperature. $BaCl_2$ is one such example [12]. However, BaF_2 does not follow this pattern. BaF_2 has a cubic fluorite structure and under compression at room temperature [14], transforms to the $PbCl_2$-type structure and then a Ni_2In-type structure. In contrast to other AX_2 compounds, BaF_2 transforms to a structure where the coordination number increases to 11. The outer electrons of an anion are well shielded from the nucleus and are more sensitive to stress than are the electrons of the cation, which are more tightly bound. The consequence of this is that anions are more compressible than are cations, and the relative size of the cation increases with pressure. Therefore, in BaF_2, the relative size of the Ba^{2+} cation increases permitting an increased coordination. Since the F^- anion is smaller than is the Cl^- anion at ambient pressure, BaF_2 can transform to the Ni_2In-type structure with a coordination number of 11, whereas $BaCl_2$ increases its coordination number to 10 after the phase transition. In $PbCl_2$, the *a* parameter was found to decrease much more rapidly with pressure than do the *b* or *c* parameters [13], i.e., it was easier to induce compression along the chain direction. A similar result was observed for BaF_2 [14]. The cell constant ratio in $PbCl_2$-type phases of these AX_2 compounds thus tend towards . In contrast, for K_2CrO_4, the *a* parameter was the least compressible.

Obviously, when going from the AX_2 compounds to the "oxygen-stuffed" analogues the importance of the cation-to-anion ratio is changed. The packing is reversed from anions packed around cations in AX_2 compounds to cations (A^+ or A^{2+}) packed around anions (BX_4^{2-} or BX_4^{4-}) in the A_2BX_4 compounds. This situation can account for the different relative compressibilities of the *a*, *b* and *c* lattice parameters of the AX_2 and A_2BX_4 compounds, with the *a*/*b* and (*a*+*b*)/*c* ratios increasing with pressure in the latter and decreasing in the former. The effect of pressure on A_2BX_4 compounds is thus the inverse of that on AX_2 compounds.

7.4.2 Pressure-induced Disorder

A possible explanation for the decrease in diffracted intensity would be that K_2CrO_4 begins to amorphize under applied pressure, (Fig. 7.7a). The powder X-ray diffraction patterns of a series of A_2BX_4 compounds, K_2ZnCl_4, Rb_2ZnCl_4, Rb_2ZnBr_4, Cs_2ZnBr_4, Cs_2ZnCl_4 and K_2SeO_4, were recorded under pressures of up to 60 GPa [9]. It was found that the first three compounds listed became amorphous under pressure and showed no phase transition to another crystal phase. The latter two compounds showed a crystal-crystal phase transition and Cs_2ZnBr_4 was an intermediate case. In an attempt to address the question as to what is the basic structural feature of a crystal which dictates its tendency to amorphize under compression, these authors examined the relation between this behavior and the $r(BX_4)/r(A)$ ratio; $r(BX_4)$ is the average B-X distance of the tetrahedra and $r(A)$ is the cationic radius. Table 7.2 shows the $r(BX_4)/r(A)$ ratio for a series of A_2BX_4 compounds studied. Potassium chromate falls into the group between Cs_2ZnCl_4 and K_2SeO_4, and, if it does indeed fit into the observed trend, it would not be expected to amorphize under compression. Interestingly, γ-Ca_2SiO_4, which has a crystal structure related to that of potassium chromate, has a $r(BX_4)/r(A)$ ratio of 1.651 and therefore would be expected to amorphize under pressure. However, between 2.1 and 5.1 GPa, γ-Ca_2SiO_4 undergoes a displacive transition to β-Ca_2SiO_4, which remains the stable pressure phase up to 14 GPa [6]. The rBX_4/rA ratio for β-Ca_2SiO_4 is 1.653. A further transition to a tetragonal K_2NiF_4-type structure has been reported to occur between 22 and 26 GPa, at 1000 °C [5]. This structure is composed of SiO_6 octahedra and not tetrahedra, as in the lower pressure forms. It is not known whether, at room temperature, β-Ca_2SiO_4 may amorphize at higher pressures due to the absence of the thermal activation required for the silicon coordination to increase from four to six. Potassium chromate does not undergo a crystal phase transition under applied pressures of up to 50 GPa, even when heated. The atom coordinates for chromium, potassium-1 and potassium-2 as a function of pressure (Fig. 7.8) indicate that the K_2Cr sub-lattice remains fairly constant under compression. Disordering of cation-centered tetrahedra

Figure 7.7. Experimental X-ray diffraction patterns of K_2CrO_4 (a) at 7.5 GPa (bottom) and 52.0 GPa (top). (b) Experimental pattern (bottom) and the calculated pattern with zero oxygen occupancy (top), at 0.1 MPa. (Note the important decrease in the intensity of the 111 reflection in both cases.)

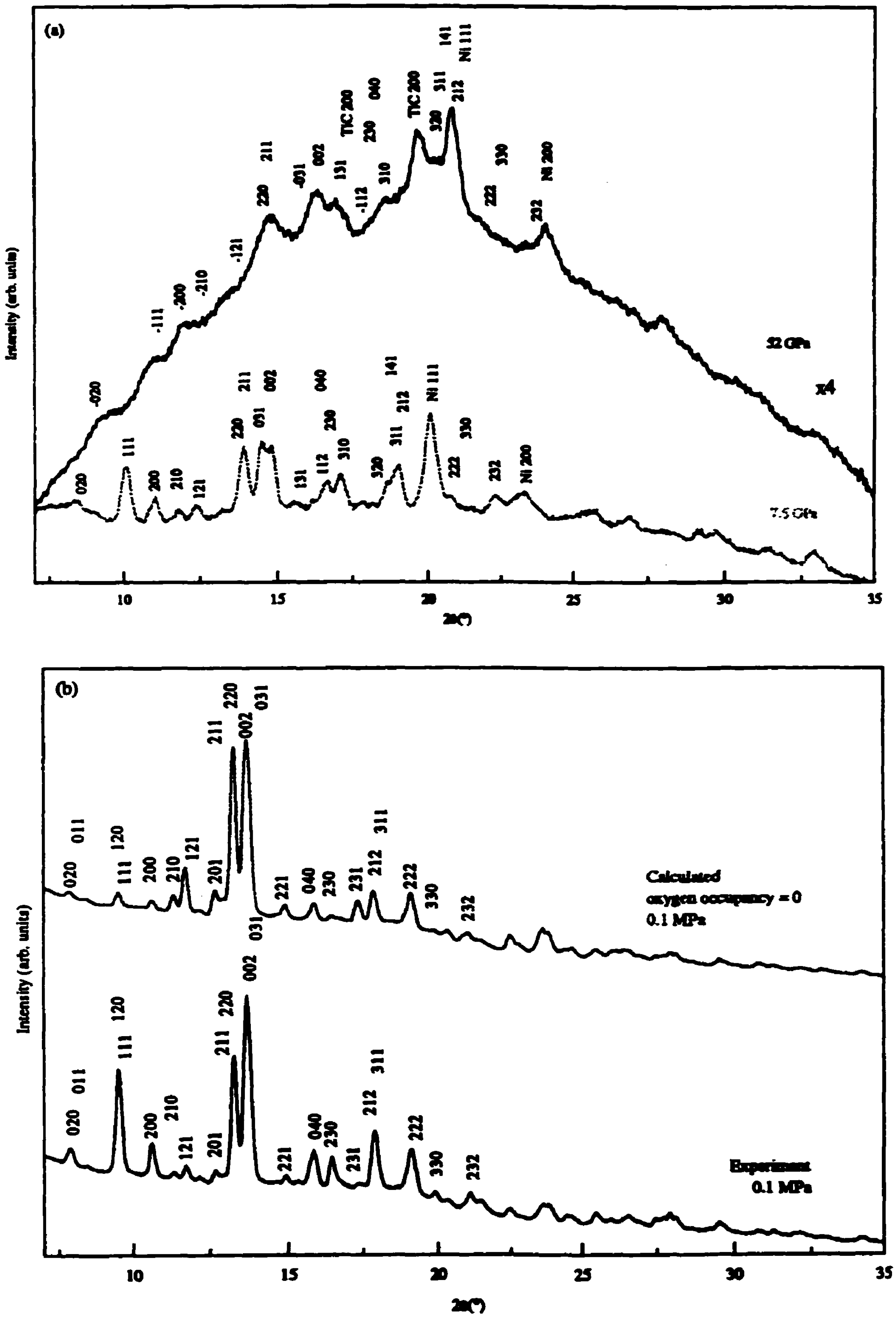
(a)
Intensity (arb. units)
-020
-111
-200
-210
-121
220
211
-031
002
131
TiC 200
-112
230
040
310
TiC 200
320
311
212
141
Ni 111
222
330
232
Ni 200
52 GPa
x4
020
111
200
210
121
220
211
031
002
131
112
230
040
310
320
311
212
141
Ni 111
222
330
232
Ni 200
7.5 GPa
10
15
20
25
30
35
2θ(°)
(b)
Intensity (arb. units)
020
011
111
120
200
210
121
201
211
220
002
031
221
040
230
231
212
311
222
330
232
Calculated
oxygen occupancy = 0
0.1 MPa
Experiment
0.1 MPa
10
15
20
25
30
35
2θ(°)

Table 7.2. High-pressure amorphization in isostrucutral A_2BX_4 compounds as a function of the ratio $r(BX_4)/r(A)$, where $r(BX_4)$ is the radius of the tetrahedra, which is equal to the average B-X distance, and $r(A)$ is the cationic radius, in Å (ref. 9).

A_2BX_4	$r(BX_4)$ / $r(A)$	Complete Amorphisation below 60 GPa
K_2ZnCl_4	1.691	Yes
β-Ca_2SiO_4	1.653	No[a]
Rb_2ZnBr_4	1.616	Yes
Rb_2ZnCl_4	1.521	Yes
Cs_2ZnBr_4	1.431	No
Cs_2ZnCl_4	1.347	No
K_2CrO_4	1.236	No?
K_2SeO_4	1.225	No

[a] Reconstructive transformation to a K_2NiF_4 structure.

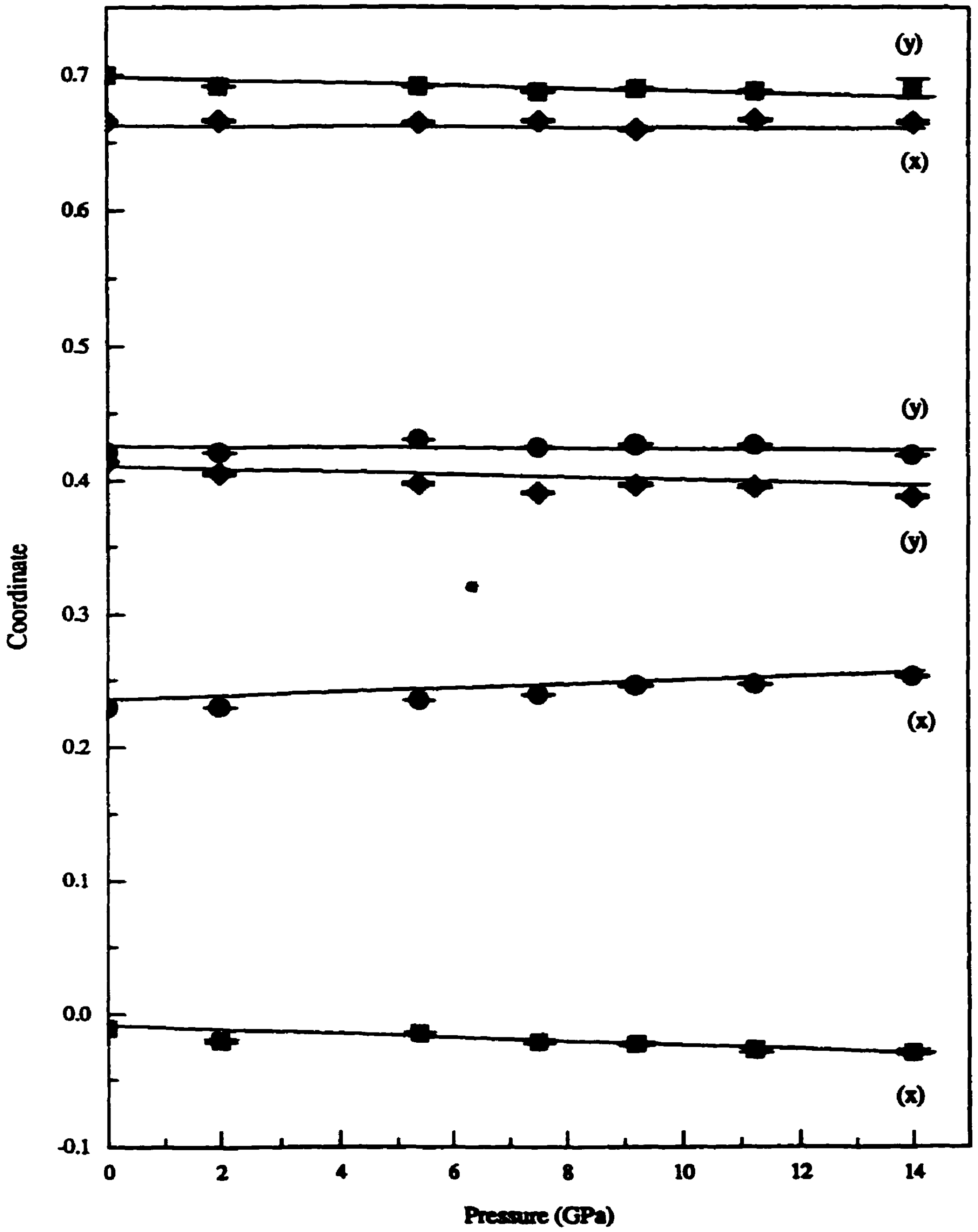

Figure 7.8. (x,y) coordinates for Cr (●), K1 (◆) and K2 (■) in K_2CrO_4 from ambient pressure to 15 GPa.

at high pressures is commonly encountered in many systems and such a process could be responsible for the observed changes in intensity. This hypothesis has been tested by calculating diffraction patterns for the K_2Cr sub-lattice, i.e., with the oxygen occupancy set to zero. By setting the oxygen occupancy to zero and calculating the powder pattern, we are able to ascertain to which peaks the oxygen atoms contribute by observing which lines show changes in intensity. The result is shown in Figure 7.7(b). A decrease in the relative intensity of several lines, including the 020, 011, 120, 111, 200, 210, and 310 lines, is observed. These lines, which decrease in intensity when the oxygen occupancy is set to zero, are those same lines which showed a decrease in relative intensity in the recorded powder patterns for increasing pressure. Figure 7.7(a) shows the recorded powder patterns at 7.5 (bottom) and 52 GPa(top). Aside from the decrease in overall diffracted intensity, other significant changes are the considerable relative decrease in the intensities of the 020, 011, 120, 111, 200, 230 and 212 lines. These results indicate that while a significant degree of order is reained in the K_2Cr sub-lattice, the tetrahedra begin to adopt various orientations (static orientational disorder) and thus long range periodicity is lost in the oxygen sub-lattice, hence the changes in relative intensity. The decrease in overall intensity is an indication of the beginning of amorphization, which could be expected to reach completion at a pressure well above 52 GPa. The disordering of the chromate tetrahedra is thus the first step in the pressure-induced amorphization process.

The K_2Cr sub-lattice of K_2CrO_4 has a Co_2Si-type structure. Under pressure there is a pressure-induced disordering in which the CrO_4^{2-} tetrahedra adopt various orientations. No phase change or complete amorphization is observed up to 52 GPa or with laser heating at 40 GPa. Under pressure, the size of the potassium atom increases relative to the chromate tetrahedron. Steric and repulsive interactions will increase, which can initially be accommodated by rotation of the chromate tetrahedra without significant changes in the cation positions because the initial cation-to-tetrahedral radius ratio is high.

Similar pressure-induced disorder has also been observed in a series of related compounds. In sodium potassium sulfate, $NaKSO_4$, and sodium potassium chromate,

$NaKCrO_4$, the SO_4^{2-} and CrO_4^{2-} tetrahedra become disordered without a significant change in the structural arrangement of the cations, possibly due to an impeded ferroelastic transition [20]. A crystallographically related crystal, $LiKSO_4$, has been studied extensively with variations in temperature and pressure [21]. The experimental studies of its high-pressure response show that a ferroelastic transition occurs at room temperature as the crystal is compressed. Raman measurements reveal that orientational disorder of the SO_4^{2-} tetrahedra occurs at high pressure. It should be noted that in olivine, the tetrahedra share edges with adjacent $(Mg,Fe)O_6$ octahedra and thus the above disordering mechanism is unavailable. At high pressure, a crystal-crystal transformation to spinel is observed.

Evidence for similar (sub-lattice) amorphization in $Co(OH)_2$ was recently reported [22]. A broadening of the infrared and Raman band for the OH stretching mode indicated a disordering of the crystalline $Co(OH)_2$ under compression, at ~11.2 GPa. This disorder was found to be reversible and involving only the H sub-lattice. The X-ray diffraction patterns showed that the Co-O sublattice remained ordered between ambient pressure and 30 GPa. In $Ca(OH)_2$, as a result of the larger cation size, amorphization is induced under compression at ~12 GPa. For the intermediate case, $Mg(OH)_2$, there was no evidence for pressure-induced amorphization below 80 GPa. These results also indicate the existence of a size criterion for pressure-induced amorphization or disorder.

Even though the radius ratio criteria predict that K_2CrO_4 should remain crystalline under compression, the present results indicate that the CrO_4^{2-} anions become orientationally disordered. It is highly probable that similar disordering occurs in a large number of A_2BX_4 compounds. In the case of K_2CrO_4, the tetrahedra are small and disordering can occur without major disruption of the A_2B sublattice. This is the first step in the amorphization process. For compounds with larger tetrahedra, this disordering greatly affects the cation sublattice as the anion site is too small and the compound rapidly undergoes complete amorphization.

7.5 Conclusions

The pseudoscheelite salt K_2CrO_4 has been studied by angle-dispersive, powder X-ray diffraction as a function of pressure in a diamond anvil cell. No phase transition to a new crystalline phase was induced by pressures up to 52 GPa or by laser-heating at 40 GPa. However, the relative intensity of several diffraction peaks in the powder pattern decreased gradually above ~16.2 GPa, which is consistent with a pressure-induced disordering of the CrO_4^{2-} tetrahedra. This has been checked by calculating the diffraction pattern for zero oxygen occupancy. The lines, which decrease the most in intensity when the oxygen occupancy is set to zero, are those same peaks which showed a decrease in relative intensity in the recorded powder patterns for increasing pressure. These results indicate that while a significant degree of order is retained in the K_2Cr sub-lattice, the tetrahedra begin to adopt various orientations (static orientational disorder) and thus long-range periodicity is lost in the oxygen sub-lattice, hence the changes in the relative intensity. For $r(BX_4)/rA$ ratios of less than ~1.4, disordering of the tetrahedra can occur initially without disrupting the A_2B sub-lattice, whereas for larger values this disordering rapidly leads to complete amorphization if no reconstructive phase transition intervenes. Pressure-induced disordering of tetrahedral units in A_2BX_4 compounds is the first step in the amorphization process.

K_2CrO_4 is an oxygen-stuffed analogue of the Co_2Si-type structure. The effect of pressure on the a/b and $(a+b)/c$ cell constant ratios in A_2BX_4 compounds is the opposite of that observed for AX_2 compounds. This is due to differences in the nature of the constituent ions.

7.6 References

---

1. For example, High-pressure Research: Application to Earth and Planetary Science, Geophysical Monograph 67, *Min. Phys.* **2**, (Edited by M. H. Manghnani and Y. Syono), Terra Scientific Publishing Company, Tokyo, and American Geophysical Union, Washington DC (1992).
2. Akaogi M., Ito E. and Navrotsky A., J. Geophys. Res. 94 15671 (1989); Katsura T. and Ito E., *J. Geophys. Res.* **94** 15663 (1989).
3. Barbier J. and Hyde B. G., *Acta. Cryst.* **B41** 383 (1985).
4. Remy C., Andrault D. and Madon M., *J. Am. Ceram. Soc.* **80** 851 (1997).
5. Liu L. G., *Phys. Chem. Minerals* **3** 291 (1978).
6. Remy C., Reynard B. and Madon M., *J. Am. Ceram. Soc.* **80** 413 (1997).
7. Huang Y. and Butler I. S., *Appl. Spectrosc.* **44** 1326 (1990).
8. Lorenz B., Orgzall I., Dorhout P. K., Raymond C. C., Brister K., Weishaupt K., D'Adamo R. and Hochheimer H. D., *Phys. Rev. B* **55** 2800 (1997).
9. Breitinger D. K., Emmert L. and Kress W., *J. Mol. Struct.* **61** 195 (1980).
10. Serghiou G., Reichmann H.-J. and Boehler R., *Phys. Rev. B* **55** 14765 (1997).
11. For example, Winters R. R., Serghiou G. C. and Hammack W. S., *Phys. Rev. B* **46** 2792 (1992); Robeson, J. R., Winters, R. R. and Hammack W. S., *Phys. Rev. Lett.* **73** 1644 (1994); Serghiou G. C., Winters, R. R. and Hammack W. S., *Phys. Rev. Lett.* **68** 3311 (1992); Serghiou G. C. and Hammack W. S., *J. Chem. Phys.* **96** 6911 (1992).
12. Léger J. M., Haines J., and Atouf A., *J. Appl. Cryst.* **28** 416 (1995); Léger J. M., Haines, J. and Atuof A., *Phys. Rev. B.* **51** 390 (1995); Haines J., Léger J. M. and Schulte O., *Phys. Rev. B.*, in press.
13. Léger J. M., Haines J. and Atouf A., *J. Phys. Chem. Solids* **57** 7 (1996).
14. Léger J. M., Haines J., Atouf A., Schulte O. and Hull S., *Phys. Rev. B* **52** 13247 (1995).
15. Zachariasen W. H. and Zeigler G. E., *Z. Krist.* **80** 164 (1931).
16. Toriumi K. and Saito Y., *Acta Cryst. B* **34** 3149 (1978).

17. Hazen R. M. and Finger L., *Comparative Crystal Chemistry*, Wiley, New York (1982).

18. Birch F., *Phys. Rev. B* **2** 4194 (1947).

19. Hyde B. G., O'Keeffe M., Lyttle W. M. and Brese N. E., *Acta Chem. Scand.* **46** 216 (1992).

20. Bernadin III F. E. and Hammack W. S., *Phys. Rev. B*, **54** 7026 (1996).

21. Savenko B.N., Sangaa D., Smirnov L.S., Ivanov A.N. and Moroz B., *Bull. Russian Acad. Sci.* **56** 66 (1992); Chaplot S.L. and Sikka S.K., *Phys. Rev. B* **47** 5710 (1993).

22. Nguyen J. H., Kruger M. B. and Jeanloz R., *Phys. Rev. Lett.*, **78** 1936 (1997).

Chapter 8

8.1 Summary

The introductory Chapter 1 of this thesis is a review article of pressure-tuning spectroscopy of inorganic materials over the past 15 years, highlighting some of the areas in which high-pressure research using the diamond-anvil cell has provided interesting results on metal-ligand bonding interactions, pressure-induced isomerization and piezochromism, one-dimensional structures and intermolecular interactions, such as hydrogen bonding. The remainder of the thesis presented new work, covering several of the areas described in the introduction.

Chapter 3 of this thesis discussed the high-pressure study of the transition-metal carbonyl and thiocarbonyl complexes $(\eta^6\text{-}C_6H_5CO_2CH_3)Cr(CO)_3$ and $(\eta^6\text{-}C_6H_5CO_2CH_3)Cr(CO)_2(CS)$. The pressure dependences of the Raman-active modes of $(\eta^6\text{-}C_6H_5CO_2CH_3)Cr(CO)_3$ and $(\eta^6\text{-}C_6H_5CO_2CH_3)Cr(CO)_2(CS)$ revealed a phase transition between 10 and 15 kbar, the Raman modes being particularly sensitive above the phase-transition pressure. The sign and magnitudes of the pressure-induced shifts of the $\nu(CO)$, $\nu(CS)$, $\nu(Cr\text{-}CO)$ and $\nu(Cr\text{-}CS)$ modes indicated an increase in π-backbonding to the CO and CS ligands. The larger negative pressure shifts of the $\nu(CO)$ modes in the thiocarbonyl complex indicated that the increase in π-backbonding to the remaining CO ligands was greater than to the CS ligand. Substitution of a CS ligand for CO ligand in $(\eta^6\text{-}C_6H_5CO_2CH_3)Cr(CO)_3$ also affects the relative energies of the $\nu_s(Cr\text{-}R)$ and $\nu_a(Cr\text{-}R)$ modes; $\nu_s(Cr\text{-}R) > \nu_a(Cr\text{-}R)$ for the tricarbonyl, but $\nu_s(Cr\text{-}R) < \nu_a(Cr\text{-}R)$ for the thiocarbonyl complex. Comparison with the benzene analogue $(\eta^6\text{-}C_6H_6)Cr(CO)_2(CS)$ and with $Cr(CO)_5(CS)$, showed that the presence of the electron-withdrawing group of the methylbenzoate ligand resulted in less π-backbonding to CO and CS, due to reduced σ-donation form the arene ring to the Cr center. The frequency and pressure dependences of the $\delta(CrCS)$ modes were particularly sensitive to the nature of the arene ring; $d\nu/dp = 0.25$ and -0.16 to -0.55

cm^{-1} $kbar^{-1}$ for $(\eta^6\text{-}C_6H_6)Cr(CO)_2(CS)$ and $(\eta^6\text{-}C_6H_5CO_2CH_3)Cr(CO)_2(CS)$, respectively. Increased mixing of the δ(CrCS) and ν(Cr-R) modes and/or CS π - Cr d-orbital interactions has been suggested following force constant calculations. The large variation in dν/dp observed for the ν(CS) modes of the complexes studied points to the ability of the CS ligand to tailor its σ-donor/π-acceptor ratio.

The nature of intermolecular interactions in Magnus' green salt $[Pt(NH_3)_4][PtCl_4]$ (MGS), and the two derivatives, $[Pt(ND_3)_4][PtCl_4]$ (MGS-D) and $[Pt(NH_3)_4][PtBr_4]$ (MGS-Br), were discussed in Chapter 4. The similarity of the results from a pressure-tuning IR study of $[Ni(NH_3)_6]X_2$ with those observed for MGS and its derivatives confirms that there is restricted rotation of the NH_3 moiety about the Pt-N bond in MGS, MGS-D and MGS-Br. This restricted rotation cannot be conclusively attributed to the presence of hydrogen bonding of the type Pt-N⁻⁻Cl, but neither can hydrogen-bonding be ruled out. The form of the symmetric deformation $\delta_s(NH_3)$ mode results in a decrease of the Pt-N-H bond angle, for all three hydrogens. A decrease in the N⁻⁻Cl distance under compression, coupled with a change in the N-H-Cl angle to a more linear geometry, could lead to an increased strength of a hydrogen bond. A concomitant reduction in the restoring forces of the bending $\delta_s(NH_3)$ mode could explain the observed negative pressure dependence of this mode. Bromine, being less electronegative, is less likely to form hydrogen bonds than is chlorine. The differences in the pressure dependences of the vibrational modes are relatively small from MGS to MGS-Br, with the exception of the antisymmetric $\nu_{as}(NH_3)$ mode, which shows a negative pressure shift, dν/dp = -0.15, -0.07 and -0.33 cm^{-1} $kbar^{-1}$. The reason for these differences is not fully understood.

The pressure-induced dihydride-dihydrogen interconversion in the neutral rhenium hydride complex, $ReH_7(dppe)$ (dppe = ethylene-1,2-bisdiphenylphosphine), is discussed in Chapter 5. As the pressure was increased above ~5 kbar, a broad, weak peak appeared at ~2636 cm^{-1} in its IR spectrum. This band was assigned to a ν(HH) mode of a $Re(\eta^2\text{-}H_2)$ moiety. The low frequency of the ν(HH) mode suggests a short H-H bond distance, smaller than the closest hydride-hydride distance at ambient pressure of 1.7 Å. Bond distances of the order 0.8-0.9 Å are normally associated with ν(HH) frequencies of ~2650-2700 cm^{-1}. Preliminary studies have been made on a second rhenium heptahydride complex $ReH_7(PPh_3)_2$. The non-linear shift of the IR modes with increasing pressure suggested that rotation of the phenyl rings was occurring under compression. This rotation may assist in the dihydride-dihydrogen interconversion, suggesting that, in this case, geometric rather than electronic factors, the latter being normally considered as the most important factor governing the $M\text{-}(\eta^2\text{-}H_2) \leftrightarrow M\text{-}(H)_2$ interconversion, play a key role in the pressure-induced dihydride-dihydrogen interconversion.

Chapter 6 looks at the effect of applied pressure on a fullerene derivative, $CpCo(C_{64}H_4)$, a novel fulleride complex, in which the cobalt metal is coordinated to an opening on the "C_{60}" surface, an ethylene bridge acting as an η^2-handle to the metal. This complex has been subjected to high, external pressures up to 40 kbar, to ascertain whether, upon application of sufficient pressure, the cobalt atom might be encouraged to slip inside the fullerene cage. No indication of an increased Co(III)-fullerene interaction was observed form the high-pressure Raman spectra. There is, however, evidence for a structural change between 8-13 kbar, most probably due to rotation of the Cp ligand about the Cp-Co bond, similar to that observed for ferrocene under compression.

The final chapter, Chapter 7, is concerned with a high-pressure powder X-ray diffraction experiment, in which the effect of applied pressures up to 52 GPa, (520 kbar) on potassium chromate K_2CrO_4, was examined in an attempt to look more closely at the pressure-induced amorphization in A_2BX_4 compounds and the mechanism of amorphization. No phase transition to a new crystallographic phase was induced by pressures up to 52 GPa or by laser-heating at 40 GPa. However, a gradual decrease in the intensity of several diffraction peaks in the powder pattern from ~16 GPa, and the relative stability of the K_2Cr sub-lattice, was consistent with a pressure-induced disordering of the CrO_4^{2-} tetrahedra. K_2CrO_4 is an oxygen-stuffed analogue of the Co_2Si-type structure. Under pressure, the AX_2 compounds show a tendency towards a highly coordinated Ni_2In-type structure, whereas the A_2BX_4 compounds tend towards the analogue of the Co_2Si structure. The effect of pressure on A_2BX_4 compounds is thus the opposite of that on AX_2 compounds, due to differences in the relative compresibilities of the constituent ions. For BX_4/A ratios of less than ~1.4, disordering of the tetrahedra can occur without disrupting the A_2B sub-lattice, whereas for larger values this disordering leads to amorphization if no reconstructive phase transition intervenes. Pressure-induced disordering of tetrahedral units in A_2BX_4 compounds is a likely first step in the amorphization process.

8.2 Contributions to Original Knowledge

1. We have further demonstrated the use of pressure-tuning IR in the study of M-CO and M-CS π-backbonding interactions. We have shown that, under compression, π-backbonding increases preferentially to CO rather than CS, in spite of the lower energy of the HOMO and LUMO of the CS ligand. Comparison with the high-pressure data of several $(\eta^6\text{-arene})Cr(CO)_2(CX)$ complexes and $Cr(CO)_5(CS)$ shows that the nature of the arene ring influences the extent of π-backbonding. The dv/dp values for ν(CS) indicate the ability of CS to tailor its σ-donor/π-acceptor ratio, as suggested in the literature.

2. The study on MGS and its derivatives demonstrates the use of pressure-tuning spectroscopy to examine the nature of intermolecular interactions, such as hydrogen-bonding. The stability of the structure of MGS is most likely due to weak hydrogen bonds of the form $N\text{-}H\cdots Cl$, which restrict rotation of the NH_3 group about the Pt-N bond.

3. We have demonstrated that a dihydride-dihydrogen isomerization can be induced in a neutral rhenium complex, $ReH_7(dppe)$. The isomerization was observed n the IR spectrum, through the appearance of a broad band at ~2636 cm^{-1}, above 5.6 kbar, this band being assigned to ν(HH) of $Re(\eta^2\text{-}H_2)$. The non-linear pressure-

induced shifts of the IR vibrational bands suggested that rotation of the phenyl rings was occurring, possibly assisting in the dihydride-dihydrogen isomerization.

4. Initial pressure experiments to insert the Co into the "C_{60}" cage of the cobalt-fulleride $CpCo(C_{64}H_4)$ were unsuccessful. Discontinuities in the wavenumber *vs.* pressure plots indicate a phase transition between 8-13 kbar, probably involving rotation of the Cp ligand. If the cyclopentadienyl ring is too strongly coordinated to the Co metal, its loss and subsequent Co insertion would be impossible.

5. We have shown that the application of pressures up to 52 GPa to K_2CrO_4 results in disordering of the CrO_4^{2-} tetrahedra, as seen from a decrease in the intensity of several lines in the powder X-ray diffraction patterns. K_2CrO_4 is highly compressible and the observed decreases in the lattice parameters are shown to be the reverse of that observed for AX_2 materials. K_2CrO_4 can be considered as an oxygen-stuffed analogue of AX_2 materials; the different compressibilities result from the different constituent ions. These results have implications on the mechanism of amorphization in A_2BX_4 materials.

8.3 Suggestions for Future Work

It is always of interest to expand the number of high-pressure studies made to a larger range of complexes. Changing the metal centre and/or the ancillary ligands can produce interesting results. More specific examples of future studies are outlined below. As well as these, one development will be in the area of high-pressure powder X-ray diffraction experiments. Along with this, expanding the pressure range attainable for Raman studies under high-pressures is also of interest.

1. The complex $(\eta^6\text{-}C_6H_6)Cr(CO)_3$ has not been previously studied under high-pressure. Pressure-tuning vibrational studies are of interest since this complex completes the series studied in Chapter 3.

2. The high-pressure Raman spectra of MGS and its derivatives may provide further evidence for hydrogen-bonding, from the pressure dependence of the ν(Pt-Cl) and ν(Pt-N) stretching modes. Initial FT-Raman studies were unsuccessful since the compounds burn in the laser. When the sample is studied as a pressed pellet (KBr or KCl) sample burning is reduced. It would be of interest to incorporate this sample preparation for use in the diamond-anvil cell.

3. One of the main features of the $CpCo(C_{64}H_4)$ complex thought to prevent cobalt insertion is the Cp ligand, it being too strongly coordinated to the Co. Rubin *et al.*, have recently prepared an indenyl (Ind) complex, $(Ind)Co(C_{64}H_4)$. From the DSC and TGA curves, $^1/_2$ and 1 equivalent indenyl molecules are lost at ~250° and ~550°, respectively. These results indicate that the indenyl ligand is much more weakly bound compared to Cp in $CpCo(C_{64}H_4)$. We intend to undertake further high-pressure studies, as well as high-temperature studies, on the complex $(Ind)Co(C_{64}H_4)$, in an attempt to form endohedral fullerenes.

4. The Raman spectra of K_2CrO_4 can provide information on the disordering of the chromate tetrahdra. In the powder X-ray diffraction patterns, this occurred above 16 GPa (160 kbar). Currently, the maximum pressure we can acheive is ~60 kbar. There exist several other A_2BX_4 materials, for example K_2WO_4, which would be of interest to study in a similar way.

8.4 Publications

1. "Pressure-tuning FT-Raman Spectroscopic Study of The T_{2g} Phonon Mode of a Diamond-anvil Cell."
   R. D. Markwell, C. M. Edwards and I. S. Butler, *Spectrochim. Acta,* 53A (1997) 2253.

2. "Pressure-tuning IR Spectroscopy of Bacteriorhodopsin."
   S. M. Barnett, C. M. Edwards, I. S. Butler and I. W. Levin, *J. Phys Chem. B.* 101 (1997) 9421.

3. Pressure-tuning Vibrational Spectroscopy Study of (η^5-C_5H_5)Co($C_{64}H_4$): Can Endohedral Fullerenes be Formed Under Pressure?
   C. M. Edwards, I. S.Butler, Y. Rubin and W, *J. Mol. Struct.* (1997) accepted.

4. "Pressure-tuning Spectroscopy of Inorganic Compounds: A Summary of The Last 15 years."
   C. M. Edwards and I. S. Butler, Coord. Chem. Rev., in preparation.

5. "High-pressure X-ray Diffraction Study of Potassium Chromate: Pressure-induced Orientational Disorder and its Implications for Amorphization in A_2BX4 Compounds."
   C. M. Edwards, J. Haines, I. S. Butler and J. M. Leger, J. Phys. Chem. Solids., in preparation.

6. "Pressure-induced Solid-State Isomerisation: The Dihydride-Dihydrogen Interconversion."
   C. M. Edwards and I. S. Butler, Inorg. Chem., in preparation.

7. "Pressure-Tuning FT-IR Spectroscopy of Magnus' Green Salt and its Derivatives."
   C. M. Edwards and I. S. Butler, in preparation.

8. "High-Pressure Vibrational Study of (η^6-arene)Cr(CO)$_2$(CX) Complexes (X = O, S); π-Backbonding to CX Ligands and the Effect of Variation in the Arene Ligand."
   C. M. Edwards and I. S. Butler, in preparation.

9. "Pressure-induced Isomerisation of Solid Transition Metal Complexes."
   R. D. Markwell, C. M. Edwards, I. S. Butler, C. Bianchini, D. Burns and A. Fafara, J. Am. Chem. Soc., in preparation .

8.5 Conferences

The work presented in this thesis, and other high pressure studies, have been presented at several conferences.

1. 28th Inorganic Discussion Weekend, University of Western Ontario, London, Ontario, November 3-5, 1995.
   "Pressure-induced Isomerisation of Solid Transition Metal Complexes: Conversion of a Rhenium Dihydride Complex in to its Molecular Dihydrogen Analogue at ~ 10 kbar."
   C. M. Edwards, R. D. Markwell and I. S. Butler (oral presentation).

2. SACIQ, Symposium Annuel de Chimie Inorganique du Québec, Bishops University, Lennoxville, Quebec, August 2-3 1996.
   "High-Pressure Vibrational Study of Cr-CO and Cr-CS Interactions."
   C. M. Edwards, R. Moore and I. S. Butler (oral presentation).

3. 29th Inorganic Discussion Weekend, McGill University, Montreal, Quebec, November 1-3, 1996.
   "Pressure-Tuning Study of Magnus' Green Salt."
   C. M. Edwards and I. S. Butler (poster presentation).

4. Deuxième Colloque franco-québécois en Chimie Inorganique et Organométallique: Castres, France, May 11-14, 1997.
   "Polymorphisme dans Le Ligand DIPHOS Induit par La Haute Pression."
   C. M. Edwards et I. S. Butler (poster presentation).

   "L'effet de Haute Pression sur Les Spectres Infrarouges du Complexe de Magnus et Ses Dérivés."
   C. M. Edwards et I. S. Butler (poster presentation).

5. 80th Canadian Society for Chemistry Conference, Windsor, Ontario, Canada, June 1-4, 1997.
   "Pressure-tuning FT-IR and FT-Raman study of CpCo($C_{64}H_4$); Can endohedral fullerenes be formed under pressure?"
   I. S. Butler and C. M. Edwards (oral presentation).

6. 43rd International Conference on Analytical Sciences and Spectroscopy, McGill University, Montreal, Quebec, August 10-13, 1997.
   "A High-Pressure X-ray Powder Diffraction Study of Potassium Chromate, K_2CrO_4."
   C. M. Edwards, J. Haines, I. S. Butler and J. M. Léger (poster presentation).

7. 30th Inorganic Discussion Weekend, University of Toronto, Toronto, Ontario, October 24-26, 1997.
"High-Pressure X-ray Diffraction Study of Potassium Chromate: Pressure-Induced Orientational Disorder and its Implications for Amorphization in A_2BX_4 Compounds.
C. M. Edwards, J. Haines, I. S. Butler and J. M. Léger (poster presentation).

Appendix

Copies of journal and/or author signed permissions for reuse of figures (Chapter 1) and/or text (co-authors for Chapters 3, 6 and 7) in the thesis.